UNIVERSIDADE ESTADUAL DE CAMPINAS

INSTITUTO DE QUÍMICA

JULIA HELENA BORMIO NUNES

INVESTIGATION OF THE ANTICANCER ACTIVITIES AND MECHANISMS OF ACTION OF METAL COMPLEXES WITH BIOACTIVE LIGANDS

INVESTIGAÇÃO DA ATIVIDADE ANTICÂNCER E DOS MECANISMOS DE AÇÃO DE COMPLEXOS METÁLICOS COM LIGANTES BIOLOGICAMENTE ATIVOS

CAMPINAS
2019

JULIA HELENA BORMIO NUNES

INVESTIGATION OF THE ANTICANCER ACTIVITIES AND MECHANISMS OF ACTION OF METAL COMPLEXES WITH BIOACTIVE LIGANDS

INVESTIGAÇÃO DA ATIVIDADE ANTICÂNCER E DOS MECANISMOS DE AÇÃO DE COMPLEXOS METÁLICOS COM LIGANTES BIOLOGICAMENTE ATIVOS

Tese de Doutorado apresentada ao Instituto de Química da Universidade Estadual de Campinas como parte dos requisitos exigidos para a obtenção do título de Doutora em Ciências

Doctor's Thesis presented to the Institute of Chemistry of the University of Campinas as part of the requirements to obtain the title of Doctor in Sciences.

Supervisor: Prof. Dr. Pedro Paulo Corbi

O arquivo digital corresponde à versão final da Tese defendida pela aluna Julia Helena Bormio Nunes e orientada pelo Prof. Dr. Pedro Paulo Corbi.

CAMPINAS
2019

Ficha catalográfica
Universidade Estadual de Campinas
Biblioteca do Instituto de Química
Camila Barleta Fullin - CRB 8462

N922i

Nunes, Julia Helena Bormio, 1991-
Investigation of the anticancer activities and mechanisms of action of metal complexes with bioactive ligands / Julia Helena Bormio Nunes. – Campinas, SP : [s.n.], 2019.

Orientador: Pedro Paulo Corbi.
Tese (doutorado) – Universidade Estadual de Campinas, Instituto de Química.

1. Câncer. 2. Complexos metálicos. 3. Citotoxicidade. 4. Atividade antiproliferativa. I. Corbi, Pedro Paulo. II. Universidade Estadual de Campinas. Instituto de Química. III. Título.

Informações para Biblioteca Digital

Título em outro idioma: Investigação da atividade anticâncer e dos mecanismos de ação de complexos metálicos com ligantes biologicamente ativos
Palavras-chave em inglês:
Cancer
Metal complexes
Cytotoxicity
Antiproliferative assay
Área de concentração: Química Inorgânica
Titulação: Doutora em Ciências
Banca examinadora:
Pedro Paulo Corbi [Orientador]
Juliano Alves Bonacin
Paulo Cesar de Sousa Filho
Wilton Rogério Lustri
Márcia Regina Cominetti
Data de defesa: 13-09-2019
Programa de Pós-Graduação: Química

Identificação e informações acadêmicas do(a) aluno(a)
- ORCID do autor: https://orcid.org/0000-0001-8113-6679
- Currículo Lattes do autor: http://lattes.cnpq.br/5105696551185021

BANCA EXAMINADORA

Prof. Dr. Pedro Paulo Corbi (Orientador)

Prof. Dr. Juliano Alves Bonacin (IQ / UNICAMP)

Prof. Dr. Paulo Cesar de Sousa Filho (IQ / UNICAMP)

Prof. Dr. Wilton Rogério Lustri (Centro Universitário de Araraquara – UNIARA)

Profa. Dra. Márcia Regina Cominetti (Centro de Ciências Biológicas e de Saúde - UFSCar)

A Ata da defesa assinada pelos membros da Comissão Examinadora, consta no SIGA/Sistema de Fluxo de Dissertação/Tese e na Secretaria do Programa da Unidade.

Este exemplar corresponde à redação final da Tese de Doutorado defendida pela aluna **Julia Helena Bormio Nunes**, aprovada pela Comissão Julgadora em 13 de setembro de 2019.

Essa Tese é dedicada a todos que contribuem e que contribuíram nos estudos contra “O Imperador de Todos os Males”. A todos que sofrem e sofreram de câncer e a todos que são engajados na busca de soluções, com o objetivo de prover aos pacientes uma melhor qualidade de vida. Ao meu avô Edson, quem eu não tive a oportunidade de conhecer nesta vida, um dos muitos que lutou contra esta doença.

This Thesis is dedicated to all of those who contribute and have contributed in studies against “The Emperor of All Maladies”. To all of those who suffer and have suffered from cancer, and to those who are engaged in the search of solutions, in order to give patients a better life quality. To my grandpa Edson, who I did not have the opportunity to meet in this life, one of the many who fought against this disease.

Acknowledgements

First of all, I would like to thank the opportunity I had to do my doctoral studies and to work on this project, and all the consequences this has brought to me, especially all the people I had the opportunity to meet and work with.

I thank my family, Rafael and Lily, for all the love and company they provided during the last four years and before that. I thank my parents, Carlos and Cristina, and my brother, Vitor, for being very beloved, who have always believed in me and provided all the support I needed for conducting my studies. I thank my grandmas, Temes and Risa, the last one who used to call me a "doctor" even before the defense of this Thesis. I thank all my beloved family members, and those who are present only in memories.

I thank my supervisor Pedro Corbi, who always gave me the liberty to work on my own projects and for the trust that I would be able to succeed on my own and with my own timing. I thank my lab mates from LQBM and LQC for the nice working environment provided during the past four years. Fernando, Ana Thereza, Douglas, Enoque, Nina, Marcos Alberto, Carlos, and Anna Karla were my contemporary pos-graduate students in LQBM, thank you for the very nice group we composed. I thank my undergraduate student Laís, I had the opportunity to supervise her undergraduate project. She was an excellent student and a very sweet and competent person who I had the privilege to meet and work with. Also, I have to cite Marcos Ribeiro and Renan from LQC, very good friends who shared with me my daily basis, especially in the beginning of my PhD studies. I thank the technicians Cíntia and Diego, who helped with the organization of the lab. I thank the people I met in the lectures I took, as the students from the Sigoli Group, and the supervisors and students from my internships as "PED" in the disciplines of QI345, QI446 and QI145. I learned a lot from the disciplines, professors and students. I thank Deborah for the support and collaboration in crystal structure refinement (single X-ray diffraction). I thank all the technicians from the Chemistry Institute for the support in the characterization of the compounds.

I have to thank the opportunity I had to work in the Pharmcology and Toxicology Division (DFT) of CPQBA, in the group of Prof. João Ernesto de Carvalho, where I learned to do cell culture and met incredible people. Ana Lúcia was responsible for my supervision there, a very sweet person who contributed a lot with the work and ideas for the project. Paula Paiva (Paulinha) taught me to do cell culture, I will be forever thankful for everything I learned from her and the friendship we made, we became good friends and collaborators. Sica, the lab technician from DFT, an amazing person who always did more and worked more than she was supposed to, doing the cell culture maintenance and helping all the students with their projects. All the girls who were conducting their projects in DFT, Tuany, Adriana, Ellen, Lúcia, Mariana, Gisele, Patrícia, Lívia, Luciana, among others, all of them were very nice during my time in DFT.

I thank the opportunity I had to go to Austria and live again in Vienna, conducting nine months of my PhD research there. Delvina and her family received me as a daughter in Vienna and I am thankful to them, they made me feel like home. I thank OeAD for the Ernst Mach Grant scholarship and the nice workers form the Vienna regional office, Katharina, Karin, and Sandra. OeAD had nice events, where I met other scholarship holders, some who have become very nice friends. Maji and Ana Elena were the closest ones, Ana being the best friend I could have had in Vienna. She helped me survive through a different culture, reminding me of my roots and making me feel comfortable by speaking my own language with her.

I thank Prof. Keppler for accepting me in the Inorganic Chemistry Institute of the University of Vienna, and Christian Kowol, for the supervision and the trust on an unknown person working in his group. We had very nice and interesting discussions on Chemistry, I thank him very much for his attention and the nice environment he provided me for the time I spent there. My friends from the Kowol Group, Florian, Philipp, Alex, Marlene and Björn, we had great times and I thank them all for accepting me there and being so nice. Also, all the nice people form the Inorganic Chemistry Institute, as Guilherme, with whom I could speak Portuguese for some moments. From there I also thank Alex Roller and Natalie, Johannes Theiner, the people from NMR and mass spectrometry facilities, for the support with the characterization of my compounds.

I thank Petra Heffeter for her supervision by the Institute of Cancer Research of the Medical University of Vienna, and all the other people and students I met there, especially the ones from the Heffeter Group: Sonja (with whom I worked directly), Hemma, Diana, Isabella, Sabrina, Bianca, and Monika. Hugo was a Brazilian undergraduate internship student for two months in the Heffeter Group, I thank him for the nice moments we had, always reminding ourselves from Brazil.

At last, I thank all of those who were not cited here and have contributed to the time in which I did my PhD and wrote this Thesis, in a direct or indirect way.

I thank CAPES for the Brazilian scholarship. This study was financed in part by the Coordenação de Aperfeiçoamento de Pessoal de Nível Superior - Brasil (CAPES) - Finance Code 001.

“It is not about how much you do, but how much love you put into what you do that counts”

(Mother Theresa)

“Não é o quanto você faz, mas o quanto de amor que você coloca no que faz que importa”

(Madre Teresa)

Resumo

O câncer é a segunda causa de mortes no mundo, com mais de 18 milhões de novos casos registrados em 2018, com cerca de 9,5 milhões de mortes. A quimioterapia antineoplásica é o tipo de tratamento em que fármacos são utilizados para retardar ou impedir o crescimento de células cancerígenas, ou até mesmo matá-las. O uso de metalofármacos em quimioterapia começou com a descoberta das propriedades citotóxicas da cisplatina, que foi aprovada para uso em 1978. Desde então, a busca por outros metalofármacos tem sido um importante campo de investigação em Química Bioinorgânica e Medicinal.

Nesta Tese, complexos metálicos com ligantes bioativos foram sintetizados, caracterizados e investigados quanto às suas atividades antiproliferativas sobre um painel de células tumorais. Na primeira parte da Tese são apresentados cinco complexos metálicos de Ag(I), Au(I), Pd(II) e Pt(II) com derivados de uracila como ligantes: os complexos de prata, paládio e platina com 5-fluorouracil (Ag-5fu, Pd-5fu e Pt-5fu, respectivamente), o complexo de ouro com 2-tiouracil (Ph_3P-Au-tuH) e o complexo de prata com 2,4-ditiouracil ([Ag_2(dtu)]). O complexo Ag-5fu apresentou o melhor perfil antiproliferativo entre os complexos com 5-fluorouracil enquanto o complexo Ph_3P-Au-tuH foi o que apresentou os melhores resultados dentre os complexos metálicos com tiouracilas. Os complexos Ag-5fu e Ph_3P-Au-tuH tiveram seus mecanismos de morte celular investigados em linhagens celulares específicas, sendo capazes de promover a parada do ciclo celular na fase G1, inibir a formação de colônias e promover a morte celular programada.

A segunda parte desta Tese trata de tiossemicarbazonas, que são uma classe importante de agentes quelantes de metais também investigados como potenciais fármacos com ação sobre células tumorais. A COTI-2 é uma nova tiossemicarbazona desenvolvida pela *Cotinga Pharmaceuticals*, que está em ensaios clínicos de fase I. A COTI-2 e derivados da COTI-2, bem como os primeiros complexos metálicos de Fe(III), Cu(II) e Zn(II) com COTI-2 foram sintetizados e caracterizados por análises químicas e espectroscópicas. Todos os compostos tiveram suas atividades citotóxicas avaliadas *in vitro* sobre a linhagem tumoral SW480 (colorretal) e linhagens quimiorresistentes derivadas da SW480 (por exemplo a SW480/COTI que é resistente a COTI-2). A linhagem SW480/COTI foi sensível ao derivado N^4-terminal dimetilado (COTI-NMe_2) e o complexo de cobre(II) (Cu-COTI-2) apresentou os melhores resultados dentre os complexos metálicos, sendo mais ativo do que o ligante livre sobre as linhagens SW480 e SW480/COTI nas mesmas condições experimentais.

Abstract

Cancer is the second leading cause of deaths worldwide, with over 18 million new cases reported in 2018, with about 9.5 million deaths. Antineoplastic chemotherapy is the type of treatment in which drugs are used to slow or stop the growth of cancer cells, or even kill them. The use of metallodrugs in cancer chemotherapy began with the discovery of the cytotoxic properties of cisplatin, which was approved for use in 1978. Since then, the search for other metallodrugs has been an important field of investigation in Bioinorganic and Medicinal Chemistry.

In this Thesis, metal complexes with bioactive ligands were synthesized, characterized, and investigated concerning their antiproliferative activities over a panel of tumor cells. The first part of the Thesis presents five metal complexes of Ag(I), Au(I), Pd(II) and Pt(II) with uracil derivatives as ligands: the silver, palladium and platinum complexes with 5-fluorouracil (named Ag-5fu, Pd-5fu and Pt-5fu, respectively), the gold complex with 2-thiouracil (Ph_3P-Au-tuH) and the silver complex with 2,4-dithiouracil ([Ag_2(dtu)]). The Ag-5fu complex presented the best antiproliferative profile among the complexes with 5-fluorouracil, and the Ph_3P-Au-tuH complex presented the best results for the metal complexes with thiouracils. The Ag-5fu and Ph_3P-Au-tuH complexes had their cell death mechanisms investigated in specific cell lines, being able to promote G1 phase arrest of the cell cycle, to inhibit colony formation, and promoted regulated cell death.

The second part of this Thesis deals with thiosemicarbazones, which are an important class of metal chelating agents also investigated as potential drugs that can act on tumor cells. COTI-2 is a novel thiosemicarbazone developed by *Cotinga Pharmaceuticals*, which is currently in phase-I clinical trials. COTI-2 and COTI-derivatives, as well as the first metal complexes of Fe(III), Cu(II), and Zn(II) with COTI-2 were synthesized and characterized by chemical and spectroscopic techniques. All compounds had their cytotoxic activities evaluated *in vitro* over the SW480 (colorectal) tumor cell line, and SW480 chemoresistant lines (for example SW480/COTI, which is resistant to COTI-2). The SW480/COTI line was sensitive to the dimethylated N^4-terminal COTI-derivative (COTI-NMe_2), and the copper(II) complex presented the best results among the metal complexes, being more active than the free ligand over the SW480 and SW480/COTI lines under the same experimental conditions.

Abbreviations

$[Ag_2(dtu)]$ – Silver(I) complex with 2,4-dithiouracil

5fu or fuH_2 – 5-Fluorouracil

7-AAD – 7-Aminoactinomycin

ACN - Acetonitrile

Ag-5fu – Silver(I) complex with 5-fluorouracil

bp – Base pair

COTI-2 – 4-(pyridine-2-yl)-N-{[(8E)-5,6,7,8-tetrahydroquinolin-8-ylidene]amino}piperazine-1-carbothiamide

COTI-Nchexyl – N-cyclohexyl-2-(6,7-dihydroquinolin-8(5H)-ylidene)-N-methylhydrazine-1-carbothioamide

COTI-NH_2 – 2-(6,7-dihydroquinolin-8(5H)-ylidene)hydrazine-1-carbothioamide

COTI-NMe_2 – 2-(6,7-dihydroquinolin-8(5H)-ylidene)-N,N-dimethylhydrazine-1-carbothioamide

CP/MAS – Cross-polarization magic angle spinning

Cu-COTI-2 – Copper(II) complex with COTI-2

DCFH-DA – 2′,7′-Dichlorofluorescein diacetate

DMF – Dimethylformamide

DMSO - Dimethyl sulfoxide

DPBS – Dulbecco's phosphate buffered saline

dtu – 2,4-Dithiouracil with two deprotonated sites

$dtuH_2$ – 2,4-Dithiouracil

ESI-QTOF-MS – electrospray ionization quadrupole time-of-flight mass spectrometry

FBS – Fetal bovine serum

FDA – U.S. Food and Drug Administration

Fe-COTI-2 – Iron(III) complex with COTI-2

fu – 5-Fluorouracil with two deprotonated sites

fuH – Deprotonated 5-fluourouracil

GI_{50} – Concentration that inhibits 50% cell growth

GSH – Glutathione

HMG – High mobility group (protein)

IC_{50} – Half minimal inhibitory concentration (inhibition of a biological process or component by 50%)

IR – Infrared spectroscopy

MRP – Mismatch repair proteins

MS – Mass spectrometry

MTT – 3-(4,5-Dimethylthiazole-2-yl)-2,5-diphenyltetrazolium

NMR – Nuclear magnetic spectroscopy

Pd-5fu – Palladium(II) complex with 5-fluorouracil

PE – Platting efficiency

P-gp – P-glycoprotein

Ph_3P or PPh_3 – Triphenylphosphine

Ph_3P-Au-Cl – Chlorido(triphenylphosphine)gold(I) complex

Ph_3P-Au-tuH – Thiouracilato(triphenylphosphine)gold(I) or gold(I) complex with 2-thiouracil

pIRES – Internal ribosome entry site plasmid

PS – Phosphatidylserine

Pt-5fu – Platinum(II) complex with 5-fluorouracil

RA – Rheumatoid arthritis

Rh123 – Rhodamine-123

ROS – Reactive oxygen species

RPMI – Roswell Park Memorial Institute; medium for cell culture

RR – Ribonucleotide reductase

SD – Standard deviation

SI – Selectivity index

SYBR Green – Nucleic acid electrophoresis stain: N',N'-dimethyl-N-[4-[(E)-(3-methyl-1,3-benzothiazol-2-ylidene)methyl]-1-phenylquinolin-1-ium-2-yl]-N-propylpropane-1,3-diamine.

TGI – Total growth inhibition; concentration that inhibits 100% cell growth

TrxR – Thioredoxin reductase

TSC – α-(N)-Heterocyclic thiosemicarbazone

tuH – Deprotonated 2-thiouracil

tuH_2 – 2-Thiouracil

WHO – World Health Organization

Zn-COTI-2 – Zinc(II) complex with COTI-2

Human tumor cell lines:

U251 (glioma); MCF-7 (breast); NCI-ADR/RES (multidrug resistant ovarian); 786-0 (kidney); NCI-H460 (lung, non-small cells); PC-3 (prostate); OVCAR-3 (ovarian); OVCAR-8 (ovarian); HT29 (colon adenocarcinoma); K562 (chronic myeloid leukemia); SW480 (colorectal adenocarcinoma); SW480/tria (colorectal, Triapine resistant); SW480/COTI (colorectal, COTI-2 resistant)

Non-tumor human line:

HaCat (immortal keratinocyte)

Structures

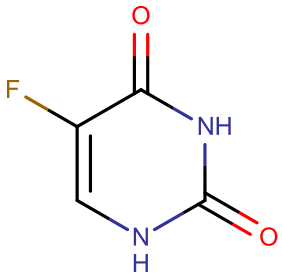

5fu or fuH_2

5-Fluorouracil

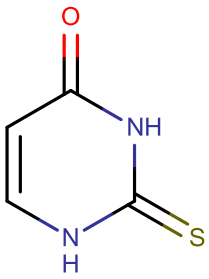

tuH_2

2-Thiouracil

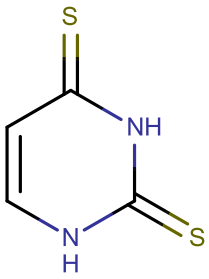

$dtuH_2$

2,4-Dithiouracil

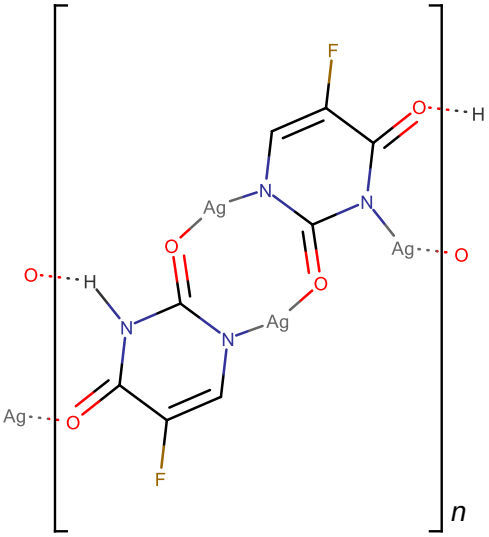

Ag-5fu

Silver(I) complex with 5-fluorouracil

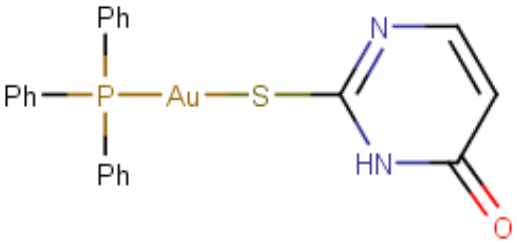

Ph_3P-Au-tuH

Thiouracilato(triphenylphosphine)gold(I) or gold(I) complex with 2-thiouracil

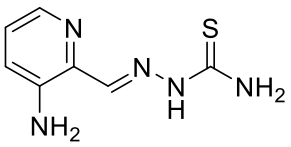

Triapine

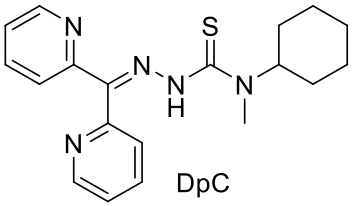

DpC

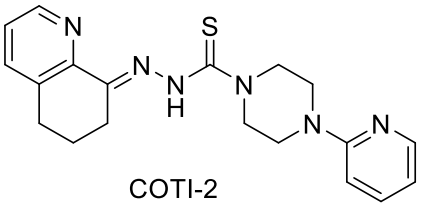

COTI-2

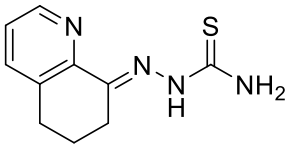

COTI-NH_2

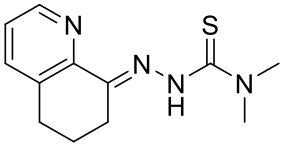

COTI-NMe_2

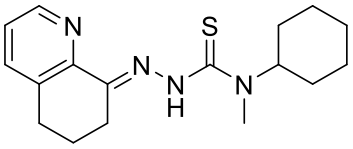

COTI-Nchexyl

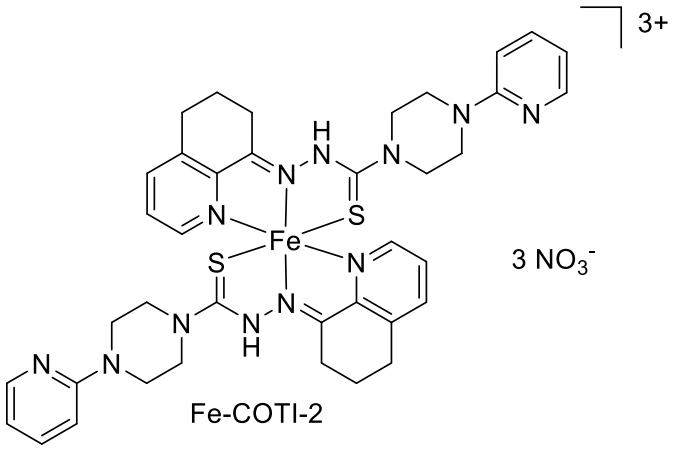

Fe-COTI-2

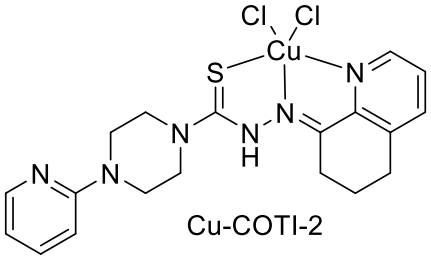

Cu-COTI-2

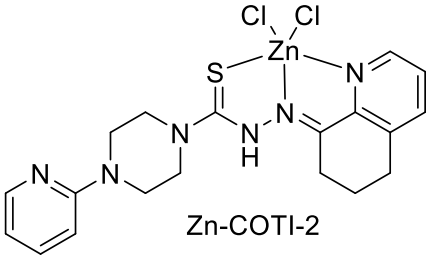

Zn-COTI-2

Summary

General Introduction

What is cancer?

Cancer is the name given to a series of diseases which have in common the rapid, abnormal, and uncontrolled growth of cells at any part of the body, which can spread into surrounding tissues [1]. Normally, cells grow and divide to form new cells in a controlled way, and when cells get old or damaged, they die, giving place to new cells. However, it can happen that cells become abnormal or damaged, and survive. Consequently, if these cells survive, they divide and create more abnormal or damaged cells that are not needed. This is the developing of cancer, and if these cells continue to multiplicate without stopping they form what is called a cancerous tumor [2]. Also, the different types of cancer can be differentiated by the tissue of origin of the cancerous cell, the multiplication speed of the cell, the capacity to invade surrounding tissues or to spread throughout the body (as known as metastasis), and the formation of solid tumors (which are masses of tissue) or not. For example, cancers of the blood (as leukemia) do not form solid tumors [1,2].

Causes of cancer and risk factors

Cancer is a genetic disease; it is caused by alterations in the genes (sequences of the DNA). More specifically, it is caused by the mutation (activation) of proto-oncogenes or by the mutation (inactivation) of tumor suppressor genes [3]. The development of the disease can have a hereditary factor involved or not, normally occurring due to ageing (because ageing means that cells have had more cell cycles, so the probability of a mutation is higher). However, there are many environmental exposures which can lead to cancer, which are called risk factors [2,4]. In fact, 80% to 90% of cancer cases are related to external causes rather than to heredity [5]. For example, tobacco smoke (even secondhand) [6], alcohol consumption, obesity, exposure to radiation (as ultra-violet radiation from sunlight [7]), and infectious agents (hepatitis, papillomaviruses, HIV [8,9]) are common risk factors.

Usually it is not possible to know the reason why some people develop cancer and others do not, however risk factors increase the chances of developing the disease [10], because the exposure to risk factors increases the chances of acquiring mutations in the genes. In this way, protective factors, that is, factors that are linked to a lower risk of cancer, as a healthy diet, being physically active, avoid smoking, among others, are ways of preventing cancer. However, it does not mean that one will not develop the disease, it just diminishes the risks. As an example, quitting smoking can avoid more than 60% of the risk of developing lung cancer [6].

Cancer statistics worldwide and in Brazil

In 2018 more than 18 million new cases were reported worldwide, with about 9.5 million deaths, according to the International Agency for Research on Cancer, from World Health Organization (WHO). Lung and breast cancers are the most diagnosed (about 2 million cases each), followed by colorectal (1.8 million cases), prostate (1.2 million cases), stomach (1 million cases) and liver (841 thousand cases). Lung cancer takes first place in mortality (1.7 million deaths), followed by colorectal (880 thousand deaths), stomach (762 thousand deaths), liver (781 thousand deaths) and breast (626 thousand deaths) cancers. Incidence and mortalities are higher in Asia and Europe, followed by North America, Latin America, Africa and Oceania [11].

In Brazil 559 thousand cancer cases were reported in 2018, with 243.5 thousand deaths (International Agency for Research on Cancer, WHO). Breast and prostate cancer represent 30% of new cases (about 85 thousand cases each), followed by colorectal, lung and thyroid cancers. In males, prostate cancer leads the number of new cases in 30.5%, followed by colorectal (8.9%), lung (6.9%), stomach (4.4%) and bladder (3.3%) cancers. For females breast cancer is in first place, representing 30.5% of new cases, followed by colorectal (9.6%), thyroid (6%), cervix uteri (5.8%) and lung (5.5%) cancers [12]. Considering mortality, for both genders lung cancer leads with 14.6% of deaths, followed by breast (8.4%) and prostate (7.7%) cancers. Data from Brazil's National Cancer Institute (2015) state that in males lung cancer is in first place of deaths (14.0%), followed by prostate (13.4%), colorectal (8.0%) and stomach (8.0%) cancers. For females breast cancer is in first place of deaths (16.1%), followed by lung (11.4%), colorectal (9.3%) and cervix uteri (6.2%) cancers [13].

History of cancer

The oldest description of what could be considered as cancer was discovered in Egypt, dating back to 3000 BC. It is part of an ancient Egyptian textbook, which describes tumors or ulcers of the breast that were removed by cauterization. The writing says that the disease had no treatment. Nevertheless, the origin of the word "cancer" was coined much latter, being credited to the Greek physician Hippocrates (460-370 BC). In Greek, the word *carcinos* and *carcinoma* refers to a crab, which was applied to describe the disease, because the finger-like spreading projections from the tumor reminded the shape of a crab. Afterwards, the Greek expressions were translated to *cancer*, the Latin word for crab [14].

There are many old theories about cancer. Hippocrates himself believed that the body contained different body fluids, and an imbalance of these fluids would result in disease. The excess of one of the fluids in a particular organ site was thought to cause cancer. This theory was standard through the Middle Ages for over 1300 years. As autopsies were forbidden for religious reasons, not much was known about

cancer by that time. Also, until the 18th century scientists believed that cancer was contagious [15]. By that time the first autopsies relating patient's illness to pathologic findings after death were done, what led to the foundation of scientific oncology, the study of cancer [16]. Also, with the development of anesthesia a century later, surgery was applied to "cure" cancer, and it was possible to correlate microscopic pathology (with the use of modern microscope) to illness [17]. It was only by the middle of the 20th century that scientists began to solve the complex problems of chemistry and biology behind cancer, and surgeons developed new methods for cancer treatment by combining surgery with chemotherapy and/or radiation [15]. The publication of Hanahan and Weinberg "The Hallmarks of Cancer" in the year 2000 was the breakthrough for a better understanding of the mechanisms of the disease [18,19].

Cancer treatment and chemotherapy

There are many kinds of cancer treatment, and each treatment depends on the type of cancer and on how advanced it is. In general, most ill people receive a combination of treatments. Common treatments are surgery, radiation therapy, chemotherapy, targeted-therapy and immunotherapy [20]. In this Thesis the focus will be on chemotherapy.

The term "chemotherapy" was coined by Paul Ehrlich by the 1900s and is defined as "the use of chemicals to treat diseases" [21]. Chemotherapy is the type of cancer treatment that uses drugs to slow or stop the growth of cancer cells, or even kill them. It is interesting that until the middle of the 20th century there was a lot of skepticism surrounding the clinical usefulness of chemotherapy for cancer treatment, because no one knew whether drugs caused more harm than good. It was only with combination therapy, that is, using more than one drug in treatment, that the concept of cure using chemotherapy in earlier stages of cancer was accepted [21].

Chemotherapeutic drugs can be administered orally, intravenously or topically. The first two delivery methods are systemic, that is, the drug goes through the bloodstream and throughout the body, while for the last method the drug is directed to a specific area of the body [22]. The first cures were obtained with systemic chemotherapy to treat leukemia, the cancer of the blood, by the 1960s [21,23].

Different types of chemotherapeutic agents

The idea of using toxic drugs for cancer therapy was inspired by the usage of nitrogen mustard during the World Wars [21,23]. Various DNA alkylating agents were then developed based on nitrogen mustard, however difficulty in administration and acute side effects such as nausea, vomiting and bone marrow suppression delayed the use of these drugs [24]. Folic acid antagonists were also synthesized by

the same time, based on experiments which showed that the administration of folic acid would accelerate tumor growth. Methrotrexate, a folate antagonist which is an anticancer drug used until nowadays in clinics was discovered by the 1950s [21,24]. After the first consistent successes of chemotherapy in the 1960s, several efforts were made to identify new treatments for cancer from 1970s onwards. In this way, several new classes of drugs were identified, such as anthracyclines, vinca alkaloids, and platinum drugs (which will be further explored in this Thesis) [24].

All cytotoxic chemotherapeutic agents exert their effect by disrupting the cell cycle by one or more processes. They cause cell death by apoptosis, either by directly interfering with DNA, or by targeting key proteins required for cell division. Unfortunately, they are also cytotoxic for normal cells, particularly to those with a high turnover, such as bone marrow and mucous membranes (mouth and intestine). Thus, chemotherapeutic drugs can be classified by their cell cycle effects, or by their biochemical properties. The ones which belong to the same biochemical class present a similar mechanism of action [25]. Table 1 shows the biochemical classification of chemotherapeutic drugs.

Table 1. Biochemical classification of chemotherapeutic drugs (adapted from the reference [25]).

Drug class	**Mechanism of action**	**Examples**
Alkylating agents	Impair cell function by forming covalent bonds in proteins, DNA, and RNA.	Platinum compounds (cisplatin, carboplatin, oxaliplatin); Nitrogen mustards (chlorambucil, melphalan); Oxazophosphorines (cyclophosphamide, ifosfamide).
Anti-metabolites	Structural analogues of metabolites involved in DNA and RNA synthesis. May substitute a metabolite that is normally incorporated into DNA or RNA, or compete for the catalytic site of an enzyme.	Pyridimide analogues (gemcitabine, 5-fluorouracil, capecitabine); Anti-folates (methotrexate, raltitrexed).
Anti-tumour antibiotics	Intercalate DNA at specific sequences, creating free radicals which cause strand breakage.	Anthracyclines* (doxorubicin, epirubicin), bleomycin, mitoxantrone.

Drug class	Mechanism of action	Examples
Topoisomerase inhibitors	Topoisomerase I and II are enzymes responsible for the uncoiling of DNA during replication. These enzymes are required for DNA synthesis to occur.	Irinotecan, topotecan (topoisomerase I inhibitors); Etoposide, teniposide (topoisomerase II inhibitor).
Tubulin-binding drugs	Prevent the formation of microtubule, which is important during mitosis, but also important for cell shape, and intracellular transport.	Vinca alkaloids (vincristine, vinorelbine, vinblastine); Taxanes** (paclitaxel, docetaxel).
Growth factor antagonists	Block signal transduction pathways implicated in proliferation and survival of tumor cells.	Gefitinib (tyrosine kinase inhibitor, targets the intracellular domain of the epidermal growth factor receptor - EGFR).
Monoclonal antibodies	Target specific proteins from tumors (targeted therapy).	Herceptin (targets Her-2/neu positive breast cancer); Bevacizumab (blocks VEGF***, inhibiting angiogenesis).

*Anthracyclines also have mechanism of action of topoisomerase I and II.

**Taxanes also prevent the disassembly of microtubules, inhibiting its normal functioning.

*** VEGF: Vascular Endothelial Growth Factor

Resistance to chemotherapeutic agents

Unfortunately, resistance to chemotherapy is one of the main reasons for treatment failure. After some chemotherapy sessions, the tumor cells can become resistant to drugs by a combination of different mechanisms, such as: (adapted from the reference [25])

1. Reduced delivery to the cell: as tumors grow they do not need much blood supply, so being further away from the blood stream they are exposed to lower concentrations of drug;

2. Decreased drug uptake: tumor cells can modify the structure or function of proteins involved in drug transport, affecting the amount of drug reaching the target. For example, a defective reduced folate carrier system confers resistance to methotrexate;

3. Decreased drug activation: many chemotherapeutic drugs require metabolic activation. For example, carboxylesterase is responsible for the conversion of irinotecan to its active metabolite SN-38, and reduced enzyme expression may cause resistance (the drug is not converted to its active form);

4. Increased drug efflux: presence of transport proteins that actively pump drugs out of cells. For example, MDR-1 (multi-drug resistance) gene, which codes for a trans-membrane P-glycoprotein that correlates with resistance when it is overexpressed;

5. Alteration in target protein: when a compound is designed to target a specific enzyme resistance can occur when the cell mutates the enzyme. It continues functioning; however, the drug has no affinity to the target;

6. Increased DNA repair: overexpression of genes involved in DNA repair can inactivate the effects of DNA binders, such as platinum compounds;

7. Inhibition of apoptosis, reducing cell kill;

8. Increased drug metabolism and detoxification.

Even though combination therapy reduces the chances of resistance by using compounds with different mechanisms of action, allowing additive of synergistic effects, toxicity plays a key role, and the absence of alternative results in the cessation of the therapy [25]. In this way, the search for new and improved chemotherapeutic compounds is of high interest. One recent example are targeted therapies, which can inhibit specific molecular targets implicated in cancer or single oncogenic drivers, rather than affecting cell division or DNA synthesis. Examples are small molecule inhibitors (as kinase inhibitors), monoclonal antibodies, and immunotherapeutics [26]. The last ones will not be discussed in detail here.

This work has its focus on anticancer compounds in Medicinal Inorganic Chemistry, which can be divided into two categories: (1) drugs that target metal ions in some form, and (2) metal-based drugs where the central metal ion is essential to the clinical application [27]. The first part of this Thesis will deal with the development of anticancer metal-based drugs, while the second part will be on novel anticancer drugs that target metal ions. Data from the first part of the Thesis was published in the following journals: Journal of Fluorine Chemistry 195 (2017) 93-101, Journal of Molecular Structure 1178 (2019) 169-178, and Toxicology In Vitro 60 (2019) 359-368.

PART 1: Metal complexes with uracil derivatives

Introduction

Metal compounds in cancer treatment

The vast majority of drugs in the market are organic (non-metal containing) substances, but there has been a great interest in the development of metal complexes as drugs or diagnostic agents. Based on the wide spectrum of coordination numbers and geometries, as well as kinetics properties, metal compounds offer mechanisms of drug action which cannot be achieved by organic compounds [28]. Also, therapeutic potentials of metal-based compounds date to ancient times. For example, arsenic trioxide was used as an antiseptic, in the treatment of rheumatoid diseases, syphilis and psoriasis by the Chinese, and was among the first compounds suggested for use in the treatment of leukemia during 18th and 19th centuries. Considering other therapeutic uses of metals, gold and copper were used by ancient Egyptians and Chinese in the treatment of syphilis [29], and copper was also used to sterilize water [30,31]. Silver was used by ancient Greeks and Romans to keep beverages pure for long periods [1], while in the middle ages it was applied in the treatment of skin wounds and burns [32].

Platinum compounds

Platinum complexes are widely used as anticancer compounds in the clinics. As a matter of fact, 50-70% of all chemotherapeutic treatments use a platinum compound [33,34], showing the importance of these metallodrugs in cancer chemotherapy. The discovery of the antiproliferative activities of cisplatin (*cis*-diamminedichloridoplatinum(II), $[PtCl_2(NH_3)_2]$, Figure 1a) by Rosenberg and co-workers can be considered the starting point of the use of metal complexes in cancer treatment [35]. Cisplatin was synthesized by Peyrone in 1844 and had its structure elucidated by Werner in 1893, however only in the 1960s its biological properties were observed [36]. While studying the effects of an electric field over *Escherichia coli* bacterial strain it was observed that the bacteria stopped to replicate. After investigating the reason of the replication cease it was found that platinum compounds were being generated by the platinum electrode and the ions in solution, and cisplatin was the main compound responsible for ceasing bacterial growth [37]. This led to the investigation of cisplatin in tumors (animal models) [38], which showed a great anticancer potential, and cisplatin was approved for clinical use by the FDA in 1978 [39].

Cisplatin exerts its mechanism of cytotoxic action by covalently binding to DNA. When intravenously administered cisplatin interacts with plasma proteins (human serum albumin, hemoglobin,

transferrin) and is widely distributed into body fluids and tissues. It enters the cell by passive transport or by active protein-mediated transport systems, such as copper transport proteins. In the cytoplasm cisplatin is hydrolyzed, losing the chlorido ligands, allowing the binding to DNA bases, especially to N7-guanidine residues of DNA [40]. Cisplatin, due to its *cis* conformation, forms mostly intrastrand adducts with DNA, causing torsions in the biomolecule's structure, what triggers programmed cell death by recognition of specific proteins as DNA-mismatch repair proteins (MRP) [41] and high-mobility group proteins (HMG) [42,43].

The *trans*-isomer, *trans*-diamminedichloridoplatinum(II) (transplatin), was also evaluated and appeared not to be therapeutically active. It forms mostly monofunctional adducts with DNA, which makes it easier to be deactivated by glutathione (GSH), for example, stressing the need for a *cis*-oriented geometry capable of bifunctional DNA binding and effective antitumor action. However, platinum compounds present many side effects, because platinum(II), being a soft Lewis acid, also binds to cysteine residues of proteins all over the body and, in special, glutathione and metallothionein inside the cell. Therefore, dosage is limited by general toxicity. Side effects include nausea, vomiting, loss of sensation in the extremities and nephrotoxicity [34].

Considering dosage limiting due to general toxicity of cisplatin and knowledge about ligand substitution in coordination chemistry, carboplatin was created. Carboplatin (*cis*-diammine(cyclobutane-1,1-dicarboxylate-O,O')platinum(II), $[Pt(C_6H_6O_4)(NH_3)_2]$, Figure 1b) is considered a second generation of cisplatin, in which the chlorido ligands are replaced by the 1,1-cyclobutanedicarboxylato anion, a bidentate ligand. The hypothesis was that a more kinetically stable leaving group would lower the toxicity without affecting the antitumor efficacy, what turned out to be correct. Carboplatin is less toxic to the gastrointestinal tract, less neurotoxic and does not cause nephrotoxicity. However, other side effects as myelosuppression occur [44]. Even though, higher doses can be administered when compared to cisplatin.

Although carboplatin is less toxic than cisplatin because of differences in ligand exchange kinetics, both cause the same torsion to the DNA molecule [45], therefore having the same mechanism of action and presenting the same resistance patterns, because of the same cellular recognition. Examples of resistance factors would include efflux pumps, DNA repair systems, anti-apoptotic factors, deficient drug uptake, among others [46]. The resistance factors are cell line dependent; for example, cells that are deficient in DNA repair systems are more sensitive to cisplatin [47]. Also, cells deficient in MRP (*mismatch repair proteins*) and HMG (*high mobility group*) proteins are resistant to cisplatin, because the DNA torsion is not recognized and cell death is not triggered [48,49]. In this way, a hypothesis would be that different DNA torsions would cause different cell recognition and, therefore, different cellular responses. Oxaliplatin ([(1R,2R)-Cyclohexane-1,2-diamine](ethanedioato-O,O')platinum(II), $[Pt(C_2O_4)(C_6H_{14}N_2)]$, Figure 1c) is the third generation of cisplatin, in which the amino ligands are substituted by a diaminocyclohexane (DACH) and the chlorido ligands are substituted by an oxalato

anion. Interestingly, oxaliplatin showed a different pattern of sensitivity to that of cisplatin and carboplatin in *in vitro* tests. Moreover, the cellular accumulation seems to be less dependent on copper transporters and MRP do not recognize oxaliplatin-induced DNA adducts. This showed that the differences in the DNA intrastrand crosslinks formed by oxaliplatin retains its activity over some cancer cells with acquired resistance to cisplatin [44,49].

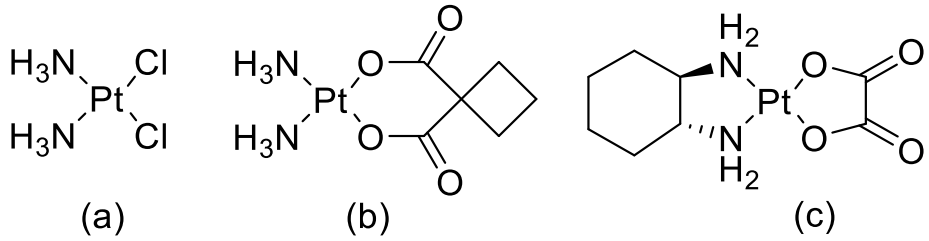

Figure 1. Structures of (a) cisplatin, (b) carboplatin, and (c) oxaliplatin.

The understanding of the mechanisms of action of these compounds and the structure-activity relationships led to the development of many platinum(II) compounds for the treatment of cancer. However, only cisplatin, carboplatin and oxaliplatin are the ones approved worldwide for clinical use. Nedaplatin, heptaplatin, and lobaplatin are approved for use only in Japan, South Korea, and China, respectively. Many other platinum(II) compounds have been evaluated considering other strategies, as *trans*-geometry complexes with bulky ligands, which form mostly monoadducts with DNA and avoid deactivation by metallothioneins and GSH [50–52]. In addition, polynuclear platinum(II) complexes were developed, which present different DNA-adduct formation [53–55], therefore resulting in different cellular responses and differentiated cytotoxicity. Platinum(IV) compounds were developed as pro-drugs, in which the intracellular reduction leads to the counter platinum(II) complex, which presents the known mechanisms of action. Nevertheless, platinum(IV) compounds are more lipophilic, what enhances the drug uptake, and they also suffer less deactivation by GSH and metallothioneins [56–58]. Also, these compounds can have linkers to target cancer cells, or bioactive linkers which can be intracellularly released and have an additive effect to the platinum(II) compound [59,60].

Other metals envisaged for cancer treatment

Cisplatin is the center of metal-based compounds as anticancer drugs in the modern era [29]. However, the acquired or intrinsic resistance of some tumors and the side effects of platinum compounds are major drawbacks. There is a need for new approaches to circumvent these drawbacks [61]. In this way, other metal ions have been explored, considering that metal centers display various oxidation states and coordination numbers, as well as geometry diversity, kinetics and thermodynamics features that lead to multi-target agents [62]. For platinum compounds DNA is the main target, and other metal-based

compounds are known to present novel modes of DNA binding, which are considered “classical non-platinum metal compounds”. On the other hand, other metal-based compounds can have proteins and enzymes as targets, which are considered “non-classical metal compounds” [61]. Other metal ions, some used in this work, and others that are very important considering Medicinal Inorganic Chemistry, in spite of platinum(II), are described next.

Palladium

Due to geometric similarities between Pt(II) and Pd(II) coordination compounds, palladium(II) complexes have been studied as anticancer drugs, although the chemistry concerning both metals is quite different. The aquation and ligand-exchange rates of palladium(II) complexes are about 10^5 times faster when compared to the platinum(II) counterparts, and the first present in general a better solubility. Most of the palladium-based compounds can be considered as classical non-platinum, because, in general, they have the DNA as the main target. Therefore, some palladium(II) complexes may have potential for cancer therapy [63], by tuning the substitution lability using steric and electronic effects of ligands [64]. In general, higher activity can be achieved using bulkier ligands (as bipyridine or phenanthroline, for example) that hand in a lower reactivity towards GSH, also being able to cause a greater distortion in DNA as consequence of palladium-DNA binding [65,66].

Nevertheless, there are also palladium(II) candidates which can be considered as non-classical metal compounds. As for an example of a palladium(II) compound evaluated in clinical trials, padeliporfin (Figure 2) is a photosensitizer based on a Pd(II) center, evaluated for photodynamic therapy of prostate cancer [67]. It is a water-soluble compound which is activated locally by the use of low-power laser light, causing the induction of reactive oxygen species (ROS) [68].

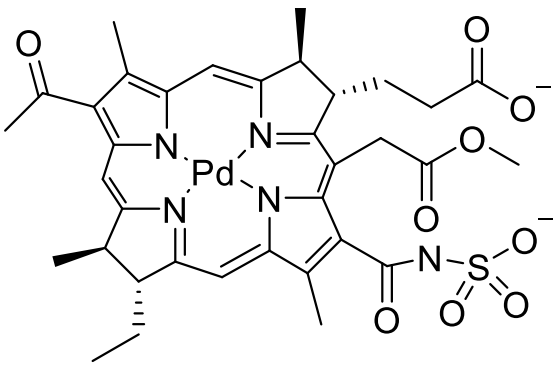

Figure 2. Structure of padeliporfin.

Ruthenium

Although not explored in this work, ruthenium compounds were the first non-platinum candidates to reach clinical trials and, therefore, it is important to cite them here. The biological activity of ruthenium ions was first examined by Dwyer *et al.* in the 1950s [69]. Ruthenium complexes are among the most studied non-platinum metal compounds with anticancer activities [70], and NAMI-A (imidazolium *trans*-tetrachlorido-(dimethylsulfoxide)imidazole-ruthenate(III), Figure 3a) was the first non-platinum candidate to reach clinical trials [71], followed by KP1019 (*trans*-tetrachloridobis-(1H-indazole)ruthenate(III), Figure 3b) and its sodium salt KP1339 (Figure 3c) [72]. When compared to platinum drugs, these ruthenium(III) compounds present fewer and less side effects. The reduced toxicity is attributed, in part, to the ability of Ru(III) to mimic iron binding to serum protein, so these compounds possess high affinity to cancer cells with transferrin receptors, increasing the amount that reaches cancer cells when compared to healthy cells [29,34]. Also, these compounds do not target primarily the DNA, although they present DNA interactions. KP1019, for example, reacts with DNA and induces apoptosis *via* the intrinsic mitochondrial pathway, being accumulated mainly in cell nucleus [40].

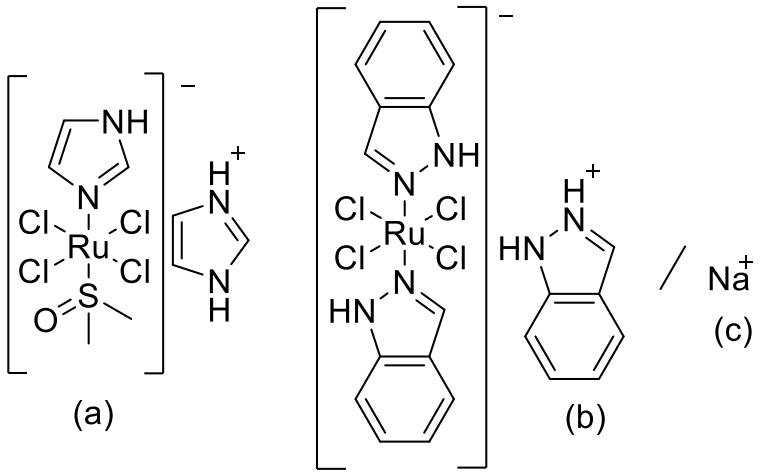

Figure 3. Structures of (a) NAMI-A, (b) KP1019, and (c) KP1339.

The activity of these ruthenium(III) compounds is based on the principle "activation by reduction", that is, Ru(III) can be reduced to Ru(II) and then re-oxidized in the cellular environment [70]. This leads to the disturbance of redox homeostasis, leading to the generation of ROS. Also, the reaction with GSH can induce depletion of the intracellular GSH pools, which renders cells more susceptible to endogenous and exogenous oxidative stress [73]. Therefore, both DNA and protein interactions are discussed to be responsible for the anticancer activity of ruthenium drugs [74].

Gold

About 3500 years ago gold was used in a variety of medicines in Arabia and China, however more as a result of its precious nature than of known medicinal properties [75]. The rational use of gold in medicine started in the end of the 19th century, when Robert Koch first described the antimicrobial activity of $K[Au(CN)_2]$ against tuberculosis [76]. Nevertheless, due the severe toxicities of gold cyanide compounds, Jacques Forestier identified the biological activities of thiolate gold compounds, which were further applied in the treatment of rheumatoid arthritis (RA) [70]. One of the most representative drugs of this type is auranofin (Figure 4), an orally administered thiolate phosphine gold(I) coordination compound [77]. Auranofin presents a two-coordination linear geometry. Gold(I) compounds can also form trigonal three-coordination and tetrahedral four-coordinated complexes [78].

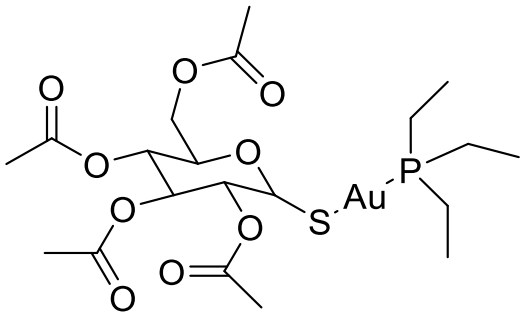

Figure 4. Structure of auranofin.

Gold compounds were considered to be used as antitumor agents since RA patients treated with auranofin showed unexpectedly low rates of malignancies [40,70]. The mechanism of antitumor action of auranofin is not primarily based on DNA interactions, but on the interaction with cellular redox processes by targeting mitochondria [70]. One of the major impacts of Au(I) compounds is the inhibition of redox enzymes, such as the seleno-enzyme thioredoxin reductase (TrxR). Such enzymes are essential to many cellular processes, particularly in maintaining the ROS levels [79]. Elevated concentrations of TrxR have been found in human tumor cells and they have been associated with tumor proliferation, and the inhibition of TrxR induces mitochondria-dependent apoptosis [40]. Thus, TrxR inhibition and disturbance of mitochondrial respiration lead to an increase in the production of ROS, mitochondrial swelling, and a decrease in mitochondrial membrane potential, what leads to apoptosis [70]. This dissimilar mechanism of action of auranofin, when compared to cisplatin, concedes auranofin a contrasted scope of activity, for example by inducing apoptosis in some cisplatin-resistant cell lines [80]. This shows that a different mechanism of action can overcome tumor-resistance to some well-established drugs.

Because of the context of auranofin, gold(I) phosphine compounds have been evaluated as potential anticancer agents [77,81–84]. For example, studies have shown that larger and more lipophilic substituents of the phosphine enhance the cytotoxicity of the gold compounds [85], while the thiosugar moiety, present in auranofin, is not mandatory for its pharmacological action [86]. As mentioned before, gold(I) phosphine compounds have mitochondria as the main target [87,88].

Last but not least, gold(III) compounds have also been evaluated as anticancer drugs. Gold(III) is isoelectronic and isostructural to Pt(II), forming square-planar four-coordinate complexes, so it is expected that the mechanism of action of gold(III) compounds is also based on DNA interactions. Indeed, there is a greater affinity of Au(III) when compared to Au(I) to the DNA, and binding can be both electrostatic and covalent [70]. However, gold(III) complexes rapidly react and reduce to gold(I) under physiological conditions, so the use of multidentate *N,N*- or *N,N,N*- donor ligands, such as ethylenediamine (en), diethylenediamine (dien), phenathroline (phen), or terpyridine (terpy) are applied for stabilization against ligand exchange and reduction [89].

Silver

Silver has been extensively employed as an antimicrobial compound in medicinal chemistry. As an example, silver-sulfadiazine (Figure 5) is a coordination compound used in the treatment of burns, in order to avoid bacterial infections [90,91]. As an antibacterial agent, Ag(I) ions have been shown to interact with DNA, to impair essential enzymes, cause cell wall disruption, induce ROS formation and cause mitochondrial dysfunctions [92,93]. These interactions with different cellular components show that silver(I) compounds could also be evaluated as anticancer agents [94], and could result in multi-targeted drugs [62]. In fact, silver(I) compounds have been evaluated as anticancer agents in the past years, which exhibit interesting cytotoxic activities, as well as a diversity of coordination geometries, with *O*-, *N*-, *S*- and *P*- donor ligands [95–98].

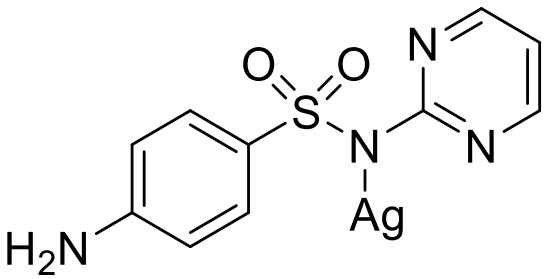

Figure 5. Structure of silver-sulfadiazine.

An advantage of the use of silver in comparison to other metals is its low toxicity towards humans, that is, the human body can tolerate the presence of silver in low doses without any toxic effects [96]. Also, a phenomenon termed “the zombie effect” was observed in silver-killed bacteria, in which the dead bacteria were able to induce death in viable bacteria. The killed bacteria acted as a reservoir of silver ions, and when in contact to viable bacteria the ions diffused or migrated towards the new target [96,99]. In principle, this could also occur for tumor cells [96], but no studies regarding this phenomenon have been reported for cancer cells so far. In fact, very little is reported regarding the mechanism of antitumor action of silver compounds, when compared to other metals, such as platinum and gold. Most reports on silver compounds focus on the cytotoxicity, and few really dig into the mechanism of action, specially comparing the roles of metal and ligand in the biological activity of the complex. It is known that the anticancer action of silver compounds differ from that of platinum derivatives in terms of DNA interactions. It seems that silver(I) compounds have a mechanism of action more likely to gold(I), having mitochondria as target [96,100].

One disadvantage of the use of silver compounds is the bioavailability, since Ag(I) ions are rapidly precipitated as AgCl or sequestered as Ag-protein complexes. In this way, encapsulation and drug delivery of silver compounds is necessary, especially considering that few is reported about *in vivo* testing, what is necessary for the developing of new pre-clinical silver agents [96,101].

Ligands

Despite the metal ion, ligands play a very important role in the biological activity of metal coordination compounds. Ligands (from the Latin word *ligare*, which means “to bind”) are metal-binding molecules [102]. The concept of Lewis acid/base can be applied, in which the metal ion is a Lewis acid, and the ligand is a Lewis base. Ligands are, most often in Medicinal Inorganic Chemistry, organic compounds that can tune physical properties of the complex. For example, in the case of platinum(II) compounds, carboplatin has a slower ligand exchange rate than cisplatin, what confers the first a higher kinetic stability due to the chelating ligand. As another example, considering the use of silver(I) compounds in burns, Ag(I) ions are slowly released to the skin when silver-sulfadiazine is used, differently from silver nitrate, which results in lower side effects from the first when compared to the second. Sulfadiazine in this case acts as a carrier, despite being a sulfonamide with antibacterial activities as well. So, in general, ligands can modify reactivity and lipophilicity, stabilize oxidation states, and contribute to substitution inertness [102].

One strategy in the development of metal-based anticancer drugs is the combination of a metal ion with a biologically active ligand, in which the ligand itself presents some biological activity. This strategy is employed in order to enhance the activities of free metal and free ligand, pursuing an additive

or synergistic effect. In this way, uracil derivatives were chosen as ligands in this work: 5-fluorouracil, 2-thiouracil and 2,4-dithiouracil.

5-Fluorouracil

5-Fluorouracil (5fu or fuH_2, $C_4H_3FN_2O_2$, Figure 6) is a fluoropyrimidine analogue to uracil and an important fluorine anticancer agent [103]. It acts by misincorporating itself into RNA and DNA, and also inhibiting the nucleotide synthetic enzyme thymidylate synthase, leading to DNA damage [104–106]. Fluorination of nucleosides is an interesting feature, and it is suggested that the fluorine atom in 5fu may mimic a hydrogen atom and then turn the substrate (uracil) into an inhibitor (5-fluorouracil) [107]. 5-Fluorouracil is widely used in the treatment of cancer, particularly for colorectal, breast, and aerodigestive tract tumors [104]. In the viewpoint of coordination chemistry, 5-fluorouracil is a versatile ligand and its coordination to metal ions may provide interesting effects among the antiproliferative activities of the metal ion and the free drug. The first silver(I), palladium(II) and platinum(II) complexes with 5-fluorouracil were reported in the literature in the 1970's [108–110]. At that time, only the synthetic route and elemental and potentiometric studies of the obtained complexes were presented. No spectroscopic, structural or biological studies were discussed so far. Considering the cited circumstances, these compounds were revisited, and the synthesis, characterization, and antiproliferative assays of a silver(I) complex, a palladium(II) complex, and a platinum(II) complex with 5-fluorouracil are presented [111,112]. Besides, insights into the mechanism of cell death caused by the silver(I) complex over ovarian resistant tumor cells are presented as well.

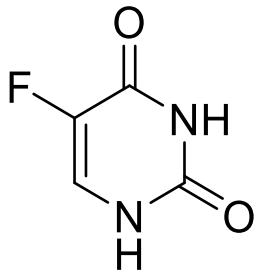

Figure 6. Structure of 5-fluorouracil.

2-Thiouracil and 2,4-Dithiouracil

2-Thiouracil (tuH_2, $C_4H_4N_2OS$) is an uracil analog that presents a sulfur atom bound to carbon C2 instead of an oxygen atom (Figure 7a). 2-Thiouracil and its analogs are used in the treatment of hyperthyroidism [113]. Furthermore, 2,4-dithiouracil ($dtuH_2$, $C_4H_4N_2S_2$) is an analog to 2-thiouracil, with a sulfur bound to carbon C4 instead of an oxygen atom (Figure 7b). Uracil derivatives, in general, present remarkable biological properties [104], and many metal complexes with these ligands are reported in the literature [114–118]. However, despite few cases [119,120], no biological studies were studied in deep so far. Here, a gold(I) complex with 2-thiouracil and triphenylphosphine and a silver(I) complex with 2,4-dithiouracil are presented, besides the evaluation for the first time of these compounds as antiproliferative agents. At last, preliminary studies of the cell death mechanism of the gold(I) complex with 2-thiouracil over lung tumor cells was also investigated.

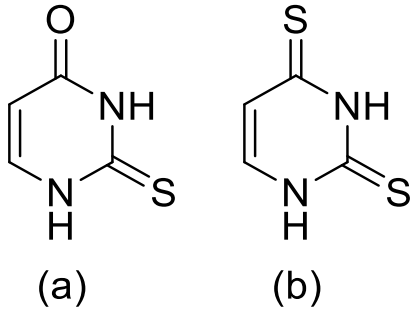

Figure 7. Structures of (a) 2-thiouracil and (b) 2,4-dithiouracil.

Objectives

The objective of the first part of this Thesis was the synthesis, characterization and evaluation of the antiproliferative activities of Ag(I), Au(I), Pd(II), and Pt(II) metal complexes with uracil derivatives over a panel of tumor cells. The evaluation of the cell death mechanism of some compounds over selected cell lines was also envisaged.

Materials and Methods

Starting Materials

5-Fluorouracil (fuH_2 or 5fu), 2-thiouracil (tuH_2), 2,4-dithiouracil ($dtuH_2$), silver nitrate ($AgNO_3$), potassium tetrachloropalladate(II) ($K_2[PdCl_4]$), potassium tetrachloroplatinate(II) ($K_2[PtCl_4]$), potassium tetrachloroaurate(III) ($K[AuCl_4]$), triphenylphosphine (Ph_3P), potassium hydroxide (KOH), SYBR green (nucleic acid gel stain) 2′,7′-dichlorofluorescein diacetate and rhodamine-123 were purchased from Sigma-Aldrich Laboratories (purity >98%). The 1 Kb Plus DNA Ladder (1.0 μg μL^{-1}) was purchased from Invitrogen (Thermo Fischer Scientific). All reagents were used without further purification.

Culture medium RPMI 1640 and fetal bovine serum (FBS) were purchased from Gibco (Grand Island, New York, USA). Penicillin/streptomycin (1000 U/mL:1000 l g/mL) and trypsin-EDTA 0.25% were purchased from Vitrocell (Campinas, São Paulo, Brazil). Guava Nexin Reagent, Guava Multicaspase kit (Caspase Reagent Working Solution, Apoptosis Wash Buffer and Caspase 7-AAD Reagent Working Solution) and Guava Cell Cycle Reagent were purchased from Merck-Millipore.

Synthesis of the silver(I) complex with 5-fluorouracil

The complex was prepared by the reaction of $AgNO_3$ (1.0 mmol, 0.17 g, 1 eq.) with fuH_2 (1.0 mmol, 0.13 g, 1 eq.) and KOH (1.0 mmol, 0.057 g, 1 eq.) in aqueous solution. The final volume of the synthesis was 10 mL. After 2 h of vigorous stirring at room temperature, a gelatinous white precipitate was obtained. The compound was vacuum filtered and washed with water. The final product was dried in desiccator with P_2O_5. Elemental analysis: Calcd. for $[Ag_3(C_4HFN_2O_2)(C_4H_2FN_2O_2)]$ (%): C, 16.5 ; H, 0.52 ; N, 9.6. Found (%): C, 16.8 ; H, 0.38 ; N, 9.6. The complex is slighlty soluble in dimethyl sulfoxide (DMSO). It is insoluble in water and in other common organic solvents. This complex will be further referred to as Ag-5fu.

Synthesis of the palladium(II) complex with 5-fluorouracil

This complex was prepared by the reaction of $K_2[PdCl_4]$ (0.25 mmol, 0.082 g, 1 eq.) with fuH_2 (0.50 mmol, 0.065 g, 2 eq.) and KOH (0.50 mmol, 0.028 g, 2 eq.) in aqueous solution. The final volume of the synthesis was 5 mL. After 3 h of stirring at room temperature, a yellow to orange precipitate was obtained. The compound was vacuum filtered and washed with water, ethanol and diethyl ether. The final product was dried in desiccator with P_2O_5 and under low pressure. Elemental analysis, flame atomic spectroscopy and ICP-OES: Calcd. For $K[PdCl(C_4H_2FN_2O_2)_2]\cdot H_2O$ (%): C, 21.0 ; H, 1.32 ; N, 12.3 ;

Pd, 23.3 ; K, 8.5. Found (%): C, 20.7 ; H, 1.39 ; N, 12.8 ; Pd, 22.3 ; K, 6.6. The complex is soluble in DMSO and dimethylformamide (DMF), however it decomposes in these solvents. It is slightly soluble in methanol. It is insoluble in water and in other common organic solvents. This complex will be further referred to as Pd-5fu.

Synthesis of the platinum(II) complex with 5-fluorouracil

This complex was prepared by the reaction of $K_2[PtCl_4]$ (0.125 mmol, 0.052 g, 1 eq.) with fuH_2 (0.25 mmol, 0.034 g, 2 eq.) and KOH (0.25 mmol, 0.014 g, 2 eq.) in aqueous solution. The final volume of the synthesis was 3 mL. After 2 h of stirring in a water bath (70 °C), a cold mixture of ethanol/ethylic ether 1:1 was added to the reaction solution, until the formation of a brownish precipitate. The solid was separated by centrifugation and washed with the same ethanol/ethylic ether solvent mixture. The final product was dried in desiccator under low pressure. Elemental analysis, flame atomic spectroscopy and ICP-OES: Calcd. for $K_2[PtCl_2(C_4H_2FN_2O_2)_2]$ (%): C, 15.9 ; H, 0.67 ; N, 9.3 ; Pt, 32.4 ; K, 13.0. Found (%): C, 15.9 ; H, 0.69 ; N, 9.0 ; Pt, 30.7 ; K, 10.7. The complex is soluble in water and DMSO, however it decomposes in these solvents. It is insoluble in other common organic solvents. This complex will be further referred to as Pt-5fu.

Synthesis of the silver(I) complex of 2,4-dithiouracil

The complex was prepared by the reaction of $AgNO_3$ (0.60 mmol, 0.10 g, 2 eq.) with $dtuH_2$ (0.30 mmol, 0.044 g, 1 eq.) and KOH (1.0 mmol, 0.045 g, 3.3 eq.) in aqueous solution. The final volume of the synthesis was 6 mL. After 1 h of stirring at room temperature, an orange precipitate was obtained. The compound was vacuum filtered and washed with water. The final product was dried in desiccator with P_2O_5. Elemental analysis and ICP-OES: Calcd. for $[Ag_2(C_4H_2N_2S_2)]$ (%): C, 13.4 ; H, 0.56 ; N, 7.8. Found (%): C, 13.6 ; H, 0.47 ; N, 7.6. The complex is insoluble in water and in common organic solvents, such as methanol, ethanol, acetone, acetonitrile (ACN), dichloromethane, chloroform, DMF and DMSO. This complex will be further referred to as $[Ag_2(dtu)]$.

Synthesis of the gold(I) complex with 2-thiouracil

First, the chlorido(triphenylphosphine)gold(I) complex (Ph_3P-Au-Cl) was prepared by adding a solution of PPh_3 (1.0 mmol, 0.26 g, 2 eq.) in chloroform (1.0 mL) to a solution of $K[AuCl_4]$ (0.50 mmol, 0.19 g, 1 eq.) in ethanol/acetone 1:1 (1.0 mL). After 30 min, the Ph_3P-Au-Cl was isolated by filtration in a Büchner funnel and washed with ethanol. Further, Ph_3P-Au-Cl (0.10 mmol, 0.49 g, 1 eq.) dissolved in chloroform (1.0 mL) was added to $AgNO_3$ (0.10 mmol, 0.017 g, 1 eq.) in methanol (1.0 mL),

producing AgCl, which was centrifuged and discarded. The (triphenylphosphine)gold(I) supernatant was reserved for posterior use as the precursor for the synthesis of the 2-thiouracilato(triphenylphosphine)gold(I) complex.

Proceeding with the preparation, tuH_2 (0.10 mmol, 0.013 g, 1 eq.) was added to a 25 mL round bottom flask with methanol (3.0 mL) and triethylamine (0.50 mL) or ammonium hydroxide (10 drops), leading to the 2-thiouracilato (tuH) compound. To this solution the (triphenylphosphine)gold(I) supernatant was added, and the mixture was refluxed for 18 h. After concentration by evaporation of the solvents, the 2-thiouracilato(triphenylphosphine)gold(I) complex precipitated as a pale-yellow solid. The solid was washed with cold methanol and diethyl ether and dried under low pressure. Elemental analysis: Calcd. for $[Au(C_{18}H_{15}P)(C_4H_3N_2OS)]$ (%): C, 45.1 ; H, 3.09 ; N, 4.78. Found (%): C, 44.7 ; H, 2.74 ; N, 4.41. Crystals were obtained from slow evaporation of the mother liquor. The complex is soluble in chloroform, acetone and methanol. This complex will be further referred to as Ph_3P-Au-tuH.

Equipments

Chemical analyses: Elemental analyses for carbon, hydrogen and nitrogen were performed using a Perkin Elmer 2400 CHNS/O Analyzer. Atomic emission spectrometry measurements were performed in a flame photometer model Analyser C-910M (São Paulo, Brazil), kindly done by Professor Fabiana C. A. Corbi from FATEC/Campinas (Brazil). Inductively coupled plasma atomic emission spectroscopy (ICP-OES) measurements were performed in a Perkin Elmer-Optima 8300 equipment.

Thermogravimetric analyses: Thermogravimetric analyses were performed in a TA Instruments 2050 TGA equipment in the following conditions: synthetic air, flow rate of 100 mL min^{-1}, and heating rate of 5°C min^{-1}, from 25°C to 1000°C.

Mass spectrometric measurements: Electrospray ionization quadrupole time-of-flight mass spectrometric (ESI-QTOF-MS) measurements were carried out in a Waters Synapt HDMS instrument (Manchester, UK) in the positive mode for Ag-5fu, Pt-5fu and Ph_3P-Au-tuH, while for Pd-5fu it was performed in the negative mode. Samples of the complexes were dissolved/suspended in the respective solvents (Ag-5fu in DMSO; Pd-5fu in methanol; Pt-5fu in water; Ph_3P-Au-tuH in methanol) before being further diluted in methanol with 0.1% (v/v) formic acid. Such mixtures were then further diluted 100-fold in methanol and directly infused into the instruments ESI source.

Nuclear magnetic resonance measurements: The ^{13}C and ^{15}N nuclear magnetic resonance (NMR) spectra of Ag-5fu, Pd-5fu, Pt-5fu and [Ag_2(dtu)] were recorded in the solid state on a Bruker 300 MHz spectrometer, using the combination of cross-polarization and magic angle spinning (CP/MAS) at 10 kHz for both ^{13}C and ^{15}N. For Ph_3P-Au-tuH, NMR spectra were recorded in solution. Solution-state ^{1}H and ^{13}C NMR of tuH_2 and Ph_3P-Au-Cl were recorded on a Bruker Avance III 400 MHz. The ^{1}H and ^{13}C NMR of Ph_3P-Au-tuH were recorded on a Bruker Avance III 500 MHz. ^{31}P NMR of both Au(I) complexes were recorded on the Bruker Avance III 500 MHz. Samples of the Au(I) complexes were analyzed in $CDCl_3$, while tuH_2 was recorded in DMSO-d6, and the chemical shifts were given relative to tetramethylsilane (TMS) for ^{1}H and ^{13}C and relative to phosphoric acid for ^{31}P.

Infrared spectroscopy: For 5fu, Ag-5fu, Pd-5fu and Pt-5fu the infrared (IR) spectra were measured in KBr pellets using a Bomem MB-Series Model B100 FT-IR spectrophotometer in the range 4000-400 cm^{-1} with resolution of 4 cm^{-1} and 16 scans. For tuH_2, $dtuH_2$, Ph_3P-Au-tuH and [Ag_2(dtu)] IR spectra were measured on an Agilent Cary 630 FTIR spectrometer, using the Attenuated Total Reflectance (ATR) method with a diamond cell. All spectra were recorded from 4000 to 400 cm^{-1}, with 64 scans and resolution of 4 cm^{-1}.

Single crystal X-ray diffraction: The crystal structure of the Ph_3P-Au-tuH complex was confirmed by single crystal X-ray diffraction on a Bruker APEX II DUO area detector diffractometer, equipped with a low-temperature device (Oxford Cryosystems CRYOSTREAM 700). Data were collected at 150 K crystal temperature, using Cu Kα radiation (λ = 1.54184 Å; Incoatec microfocus X-ray source), based on a strategy combining omega and phi scans, width of 0.5° and acquisition time of 10 s per frame. Cell refinement and data reduction were performed using SAINT [121] and multi-scan absorption correction was performed with SADABS-2014/5 [121]. The structure was solved by direct methods using SHELXTL XT-2014/4 [122] and refined by least-squares methods against F2, using SHELXle [123], with all non-hydrogen atoms refined anisotropically and all hydrogen atoms added geometrically.

Antiproliferative assays in vitro

The antiproliferative activities of Ag-5fu, Pd-5fu and Pt-5fu were investigated on nine human tumor cell lines: U251 (glioma), MCF-7 (breast), NCI/ADR-RES (ovarian expressing phenotype of multiple drugs resistance), 786-O (kidney), NCI-H460 (lung, non-small cells), PC-3 (prostate), OVCAR-03 (ovarian), HT-29 (colon adenocarcinoma) and K-562 (chronic myeloid leukemia)], kindly provided by Frederick Cancer Research & Development Center, National Cancer Institute, Frederick, MA, USA. The non-tumor cell line HaCat (human keratinocyte) used for cell viability was provided by

Dr. Ricardo Della Coletta (University of Campinas-UNICAMP, Brazil). The antiproliferative activities of [Ag_2(dtu)] and Ph_3P-Au-tuH were investigated on eight tumor cell lines and also on HaCat. The same cells were used as in the assays for Ag-5fu, Pd-5fu and Pt-5fu, despite the prostate (PC-3) cell line. For cell culture maintenance and experiments stock cultures were grown in 5 mL of RPMI-1640 supplemented with 5% fetal bovine serum (RPMI/FBS 5%) at 37 ºC in 5% CO_2 with a 1% penicillin:streptomycin mixture (1000 U mL^{-1}) (complete medium).

The Ag-5fu, Pd-5fu, Pt-5fu, [Ag_2(dtu)] and Ph_3P-Au-tuH compounds were prepared directly in complete medium (5 mg mL^{-1}) and then diluted in the same medium, affording the final concentrations of 0.025, 0.25, 2.5 and 25 µg mL^{-1} for Pd-5fu and Pt-5fu, and 0.25, 2.5, 25 and 250 µg mL^{-1} for Ag-5fu, [Ag_2(dtu)] and Ph_3P-Au-tuH. Free ligands 5fu, tuH_2 and $dtuH_2$, the starting metals $K_2[PdCl_4]$, $K_2[PtCl_4]$, $AgNO_3$ and Ph_3P-Au-Cl (final concentrations of 0.025, 0.25, 2.5 and 25 µg mL^{-1} for 5fu, Pd(II) and Pt(II) salts, and 0.25, 2.5, 25 and 250 µg mL^{-1} for tuH_2, $dtuH_2$, Ag(I) and Au(I), all in complete medium), and the chemotherapeutic drugs cisplatin and doxorubicin (final concentrations of 0.025, 0.25, 2.5 and 25 µg mL^{-1} in complete medium) were used as controls.

Cells in 96-well plates (100 µL cells/well, inoculation density: 3.5 to 6.0 x 10^4 cell mL^{-1}) were exposed to different concentrations of sample and controls (100 µL/well) in triplicate, for 48 h at 37 °C and 5% of CO_2. Before (T0 plate, after 24 h from seeding) and after the sample addition (T1 plates, after 72 h from seeding), cells were fixed with 50% trichloroacetic acid, washed with water, and cell proliferation was determined by the spectrophotometric quantification (540 nm) of cellular protein content using the sulforhodamine B assay [124–126]. The GI_{50} values (concentration that inhibits 50% cell growth or cytostatic effect) and TGI values (*total growth inhibition*, concentration that inhibits 100% cell growth or cytotoxic effect) were determined through non-linear regression, type sigmoidal, analyzed using Origin 8.0 software [127].

Gel electrophoresis assay

For the gel electrophoresis assay, 1.0 mg of a given compound (in this case $AgNO_3$, 5fu or Ag-5fu) was primarily dissolved in 100 µL of H_2O (for $AgNO_3$) or suspended in 100 µL of DMSO (for 5fu and Ag-5fu). Then, 10 µL of the solution or suspension containing the respective compounds were mixed with 5 µL of pIRES DNA plasmid solution and incubated at 37°C for 1 h. The samples were electrophoresed for 10 minutes at 50 V and 1 hour at 100 V using a 0.8% agarose gel matrix in Tris-Borate-EDTA 0.5x buffer at pH 8.3. After electrophoresis, the gel was stained with 1x SYBR green for 1 hour and photodocumented using a GelDoc-It Imager [49]. As control pure pIRES DNA plasmid was used. A DNA Ladder was used as a weight marker. The pIRES DNA plasmid was kindly provided by Professor Marcelo Lancellotti from the Faculty of Pharmaceutical Sciences/UNICAMP, Brazil.

Colony formation assay

NCI/ADR-RES and NCI-H460 cells were seeded in RPMI-1640 supplemented with 5% FBS and 1% penicillin:streptomycin (complete medium) T25 flasks ($5x10^4$ cells mL^{-1} and $4x10^4$ cells mL^{-1}, respectively, 5 mL/flask) and incubated at 37 ºC in 5% CO_2 to reach ~ 80% confluence. For NCI/ADR-RES, seven T25 flasks were prepared, being one for each treatment (two concentrations of each sample) plus one for untreated cells. Then, cells were treated in the flasks with 5fu (0.75 and 1.5 µg mL^{-1}), $AgNO_3$ (0.75 and 1.5 µg mL^{-1}) or Ag-5fu (1.5 and 3.0 µg mL^{-1}) for 24 h. For NCI-H460, five T25 flasks were prepared, being one for each treatment (two concentrations of each sample) plus one for untreated cells. NCI-H460 cells were treated in the flasks with Ph_3P-Au-Cl (5.05 and 10.1 µg mL^{-1}) and Ph_3P-Au-tuH (6.0 and 12.0 µg mL^{-1}) for 24 h. All compounds were prepared in complete medium.

After trypsinization, each resulting cell suspension was adjusted to 50 or 100 cells mL^{-1} (NCI-H460 and NCI/ADR-RES, respectively) and seeded in complete medium in triplicate in 6-well microplates (2 mL/well). For NCI/ADR-RES, cells were allowed to grow during 12 days, with complete medium being substituted once after the first 5 days. For NCI-H460, cells were allowed to grow during 6 days, with complete medium being substituted once. At last, for both cell lines, cells were rinsed with DPBS (Dulbecco's phosphate-buffered saline), fixed with methanol/DPBS 1:1 for 2 minutes, and afterwards with methanol for 10 minutes. Cells were stained with 0.1% crystal violet for 30 minutes and washed with water. Using a light microscope, the number of colonies was counted, considered as one grouping with at least 50 cells. Using these results, plating efficiency (PE) and surviving fraction (SF) were calculated according to formulas [128]:

$$PE = 100\ x\ \frac{number\ of\ formed\ colonies}{number\ of\ seeded\ cells}$$

$$SF = \frac{number\ of\ colonies\ formed\ after\ treatment}{number\ of\ cells\ seeded\ x\ PE}$$

Flow cytometry: cell culture and treatments

The human tumor cell lines NCI/ADR-RES (ovarian expressing phenotype of multiple drug resistance), NCI-H460 (lung, non-small cells) and OVCAR-8 (ovarian) were used. Stock cultures were grown in RPMI-1640 supplemented with 5% FBS and 1% penicillin:streptomycin (complete medium) at 37 ºC in 5% CO_2. These conditions were used both for cell lines maintenance and for experiments. The compounds Ag-5fu, 5fu, $AgNO_3$, Ph_3P-Au-tuH and Ph_3P-Au-Cl were prepared directly in complete medium (1.0 mg mL^{-1}) and then diluted in the same medium, affording the final concentrations for each experiment. Only for the measurement of intracellular oxidants the compounds were prepared in DPBS

and further diluted in this buffer. In all experiments, cells without treatment were used as control. Flow cytometry experiments and analysis were performed using Guava EasyCyte Mini Flow Cytometry System (Millipore). A total of 5,000 events per replicate were acquired for flow cytometry assays.

Cell cycle arrest

NCI/ADR-RES ($5x10^4$ cells mL^{-1}) and NCI-H460 cells ($4x10^4$ cells mL^{-1}) were seeded on 6-well microplates (2 mL/well) and incubated. After 24 h, cell medium was changed to RPMI-1640 supplemented with 1% penicillin:streptomycin without FBS and cells were incubated for more 24 h. Then, NCI/ADR-RES cells were treated with 5fu (0.37 and 0.75 µg mL^{-1}), $AgNO_3$ (0.37 and 0.75µg mL^{-1}) or Ag-5fu (0.75 and 1.5 µg mL^{-1}) for 36 h, while NCI-H460 cells were treated with Ph_3P-Au-tuH (6.0 and 12.0 µg mL^{-1}) and Ph_3P-Au-Cl (5.05 and 10.1 µg mL^{-1}) for 18 h. After trypsinization, cells were washed with PBS and fixed with ethanol 70% for at least 12 h. After washing with PBS, each treated or untreated cellular pellet was suspended in 200 µL Guava Cell Cycle Reagent, kept in the dark during 20 min at room temperature and analyzed in the flow cytometer.

Mitochondrial membrane depolarization – Rhodamine-123 assay

NCI/ADR-RES ($6x10^4$ cells mL^{-1}), NCI-H460 ($4x10^4$ cells mL^{-1}) and OVCAR-8 cells ($6x10^4$ cells mL^{-1}) were seeded on 12-well microplates (1 mL/well) and incubated for 24 h. Then, NCI/ADR-RES cells were treated with 5fu (1.5 µg mL^{-1}), $AgNO_3$ (1.5 µg mL^{-1}) or Ag-5fu (3.0 µg mL^{-1}); NCI-H460 cells were treated with Ph_3P-Au-tuH (24.0 µg mL^{-1}) and Ph_3P-Au-Cl (20.2 µg mL^{-1}); and OVCAR-8 cells were treated only with Ag-5fu (3.0 µg mL^{-1}). Cells were incubated (37 °C, 5% CO_2) for 1, 2 and 3 h. Afterwards, cells were trypsinized and Rhodamine-123 (Rh123) solution (1 µg mL^{-1} solution in PBS, 200 µL per cell suspension) was added to cells. After 15 min-incubation (37 °C, 5% CO_2, in the dark), each cell suspension was centrifuged, washed with PBS to eliminate unincorporated probe and suspended in fresh PBS (300 µL per suspension) before injection in the flow cytometer.

Phosphatidylserine externalization – Nexin assay

NCI/ADR-RES ($5x10^4$ cells mL^{-1}) and NCI-H460 ($4x10^4$ cells mL^{-1}) cells were seeded on 12-well microplates (1 mL/well) and incubated for 24 h. Then, NCI/ADR-RES cells were treated with 5fu (0.75 and 1.5 µg mL^{-1}), $AgNO_3$ (0.75 and 1.5 µg mL^{-1}) or Ag-5fu (1.5 and 3.0 µg mL^{-1}) for 8 and 24 h, while NCI-H460 cells were treated with Ph_3P-Au-tuH (12.0 and 24.0 µg mL^{-1}) and Ph_3P-Au-Cl (10.1 and 20.2 µg mL^{-1}) for 24 h. In a second experiment, NCI/ADR-RES cells were treated with 5fu (1.5 µg mL^{-1}), $AgNO_3$ (1.5 µg mL^{-1}) or Ag-5fu (3.0 µg mL^{-1}) for 14 and 18 h, and NCI-H460 cells were treated with Ph_3P-Au-tuH (24.0 µg mL^{-1}) and Ph_3P-Au-Cl (20.2 µg mL^{-1}) for 18 h. After each exposition time

cells were harvested with trypsin-EDTA 0.25%, washed with PBS and re-suspended in 100 µL Guava Nexin Reagent (Annexin-V PE/7-AAD) for 20 min at room temperature and in the dark before injection in the flow cytometer.

Detection of activated caspases

NCI/ADR-RES ($5x10^4$ cells mL^{-1}) and NCI-H460 ($4x10^4$ cells mL^{-1}) cells were seeded on 12-well microplates (1 mL/well) and incubated for 24 h. NCI/ADR-RES cells were then treated with 5fu (1.5 µg mL^{-1}), $AgNO_3$ (1.5 µg mL^{-1}) or Ag-5fu (3.0 µg mL^{-1}) and incubated for 17 h, while NCI-H460 cells were treated with Ph_3P-Au-tuH (24.0 µg mL^{-1}) and Ph_3P-Au-Cl (20.2 µg mL^{-1}) and incubated for 18 h. Afterwards, cells were trypsinized, washed with PBS and re-suspended in 10 µL of Guava Caspase Reagent Working Solution. After 1h-incubation in the dark at 37 °C and 5% CO_2, cells were washed with 100 µL 1x Apoptosis Wash Buffer and re-suspended in 200 µL Caspase/7-AAD Reagent Working Solution. After 10 min at room temperature in the dark, each cell suspension was analyzed by the flow cytometer.

Measurement of intracellular oxidants – DCFH-DA assay

NCI/ADR-RES cells ($6x10^4$ cells mL^{-1}) were seeded on 12-well microplates (1 mL/well) and incubated for 24 h. Afterwards, cells were trypsinized and 2′,7′-dichlorofluorescein diacetate (DCFH-DA) solution (10 µmol L^{-1} solution in DPBS with 1% DMSO, 100 µL per cell suspension) was added to cells followed by 30 min-incubation (37 °C, 5% CO_2) in the dark. Then, cells were treated in suspension with 5fu (1.5 µg mL^{-1}), $AgNO_3$ (1.5 µg mL^{-1}), Ag-5fu (3.0 µg mL^{-1}) or hydrogen peroxide (H_2O_2, 200 µmol L^{-1}, positive control) and incubated (37 °C, 5% CO_2) for 1, 2 or 3 h, before injection in the flow cytometer.

Statistical analysis

Data were expressed as mean ± standard deviation (SD) of at least two independent experiments with duplicate or triplicate samples. Statistical analyses were performed using 2-way ANOVA followed by Bonferroni test comparing treated cells to untreated ones, and p-values less than 0.05 were regarded as significant. For these analyses, the GraphPad Prism 5 software was used.

Characterization and antiproliferative assays of Ag(I), Pd(II) and Pt(II) metal complexes with 5-fluorouracil

Results and Discussion

Synthesis

Metal complexes of Ag(I), Pd(II) and Pt(II) with 5-fluorouracil were first described in the literature by Gel'fman and Kustova in the 1970's [108–110]. Some of the coordination compounds described by these authors were re-prepared and it was possible to compare the results that will be presented in this Thesis with the first data previously published by the authors.

It is important to emphasize that all synthesis here described were performed in alkaline medium, by using KOH for deprotonation of the ligand, since 5-fluorouracil contains two heterocyclic nitrogen atoms, which may act as Lewis bases to coordinate to metal ions. Gel'fman and Kustova described different methodologies to obtain Pd(II), Ag(I) and Pt(II) complexes, in which they obtained different compositions for each metal ion, with many of them containing potassium as a counter ion. In addition, the authors suggested different charges for the 5-fluorouracil ligand, with one or two nitrogen atoms deprotonated (here described as fuH and fu, respectively). Therefore, flame atomic emission spectrometric measurements were performed to determine the presence or absence of potassium in the compounds here described.

Ag-5fu complex: for the Ag(I) complex, no potassium content was found. Considering this information and the results of elemental analysis of carbon, hydrogen and nitrogen, the molar composition 3:2 metal/ligand was suggested. To maintain electroneutrality, one 5-fluorouracil ligand is supposed to have one nitrogen deprotonated (fuH), while the other has both nitrogen atoms deprotonated (fu). Therefore, the minimal formula of the complex can be suggested as $[Ag_3(fu)(fuH)]$, which is dissimilar from those early described by Gel'fman and Kustova [108].

Pd-5fu complex: for the Pd(II) complex 6.6% of potassium was found. Considering elemental analysis of carbon, hydrogen and nitrogen, and ICP-OES results (palladium content), the molar composition 1:2 metal/ligand was suggested, with one coordinated chlorido ion and one potassium as a counter ion, and one hydration water molecule. To maintain electroneutrality, both ligands are supposed to be deprotonated (fuH). Therefore, the minimal formula of the complex can be suggested as $K[PdCl(fuH)_2]\cdot H_2O$, also being dissimilar from those early described by Gel'fman and Kustova [109].

Pt-5fu: for the Pt(II) complex 30.7% of potassium content was found. Considering the elemental analysis of carbon, hydrogen and nitrogen, and ICP-OES results (platinum content), the molar composition 1:2 metal/ligand was suggested, with two coordinated chlorido ligands and two potassium as counter ions. To maintain electroneutrality, both ligands are supposed to be deprotonated (fuH). Therefore, the minimal formula of the complex can be suggested as $K_2[PtCl_2(fuH)_2]$, being the only coordination compound here described that is similar from one previously reported by Gel'fman and Kustova [110].

Thermogravimetric analyses

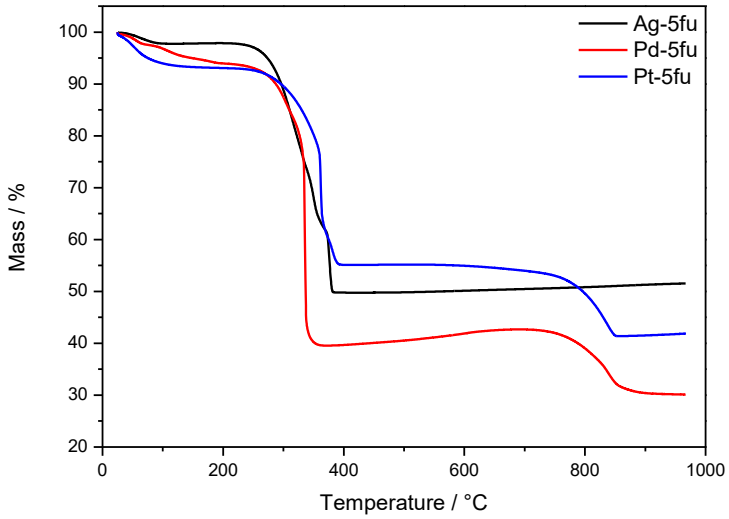

Figure 8. Thermogravimetric curves of Ag-5fu (black), Pd-5fu (red), and Pt-5fu (blue).

Figure 8 shows the thermogravimetric curves for Ag-5fu, Pd-5fu, and Pt-5fu. For Ag-5fu, the decomposition of the complex starts at 250 °C and continues until 380 °C, with weight loss of 48.0%. Such weight loss is attributed to two 5-fluorouracil ligands (anal. calcd. for the loss of fuH and fu, 44.2%). The final residue of 49.7% was assigned to metallic silver (calcd. 55.7%).

For Pd-5fu, the complex loses 6.0% of weight until 200 °C, which is consistent with one hydration water molecule as proposed by elemental analysis (calcd. 3.9%). Decomposition of the ligand starts at 250 °C until 360 °C, with 52.2% weight loss, which is attributed to two 5-fluorouracil ligands. In this case, while the ligand decomposes the formation of $PdCl_2$ and K_2O is suggested, with the oxygen being provided by the ligand (anal. calcd. for the loss of two fuH, 44.2%). At 350 °C there is a residue

of 40.1% (suggested formation of $PdCl_2$ and K_2O), and from 350 °C to 745 °C there is the decomposition of $PdCl_2$ and suggested formation of PdO [129].

For Pt-5fu, the decomposition of the complex starts at 270 °C and continues until 390 °C with weight loss of 36.8%. Such weight loss is attributed to two 5-fluorouracil ligands (anal. calcd. for the loss of two fuH, 42.9%). At 390 °C until 770 °C there is a residue of 55.2%, consistent with the suggested formation of $PtCl_2$ and K_2O (calcd. 59.8%).

Mass spectrometric studies

High-resolution mass spectrum of the Ag-5fu complex is shown in Figure 9-a. The most abundant peak was observed at *m/z* 580.7721, being consistent with the formation of the $[Ag_3(C_4HFN_2O_2)(C_4H_2FN_2O_2)+H]^+$ ion. The presence of this peak confirmed the 3:2 metal/ligand composition as earlier suggested by thermal and elemental analyses. Other peaks at *m/z* 474.8398, 688.6959 and 818.7207 were also observed, being attributed to the species $[Ag_2(C_4H_2FN_2O_2)_2+H]^+$, $[Ag_4(C_4HFN_2O_2)(C_4H_2FN_2O_2)]^+$ and $[Ag_4(C_4HFN_2O_2)(C_4H_2FN_2O_2)_2+H]^+$. The presence of species with four silver atoms led us to consider a polymeric arrangement for the silver(I) complex with 5-fluorouracil. The multiple species observed in the spectrum of the complex may be result of the polymer fragmentation. Such remark was reported previously in the literature for silver complexes [130].

A comparison between the theoretical and experimental isotopic pattern for the $[Ag_3(C_4HFN_2O_2)(C_4H_2FN_2O_2)+H]^+$ ion is presented in Figures 9-b and 9-c. The mass error for this ion was +63 ppm $[C_8H_4F_2N_4O_4Ag_3]^+$ (calcd. *m/z* 580.7350, exp. *m/z* 580.7721), considering the monoisotopic ion. Table 2 shows the different species of the isotopic pattern of Ag-5fu.

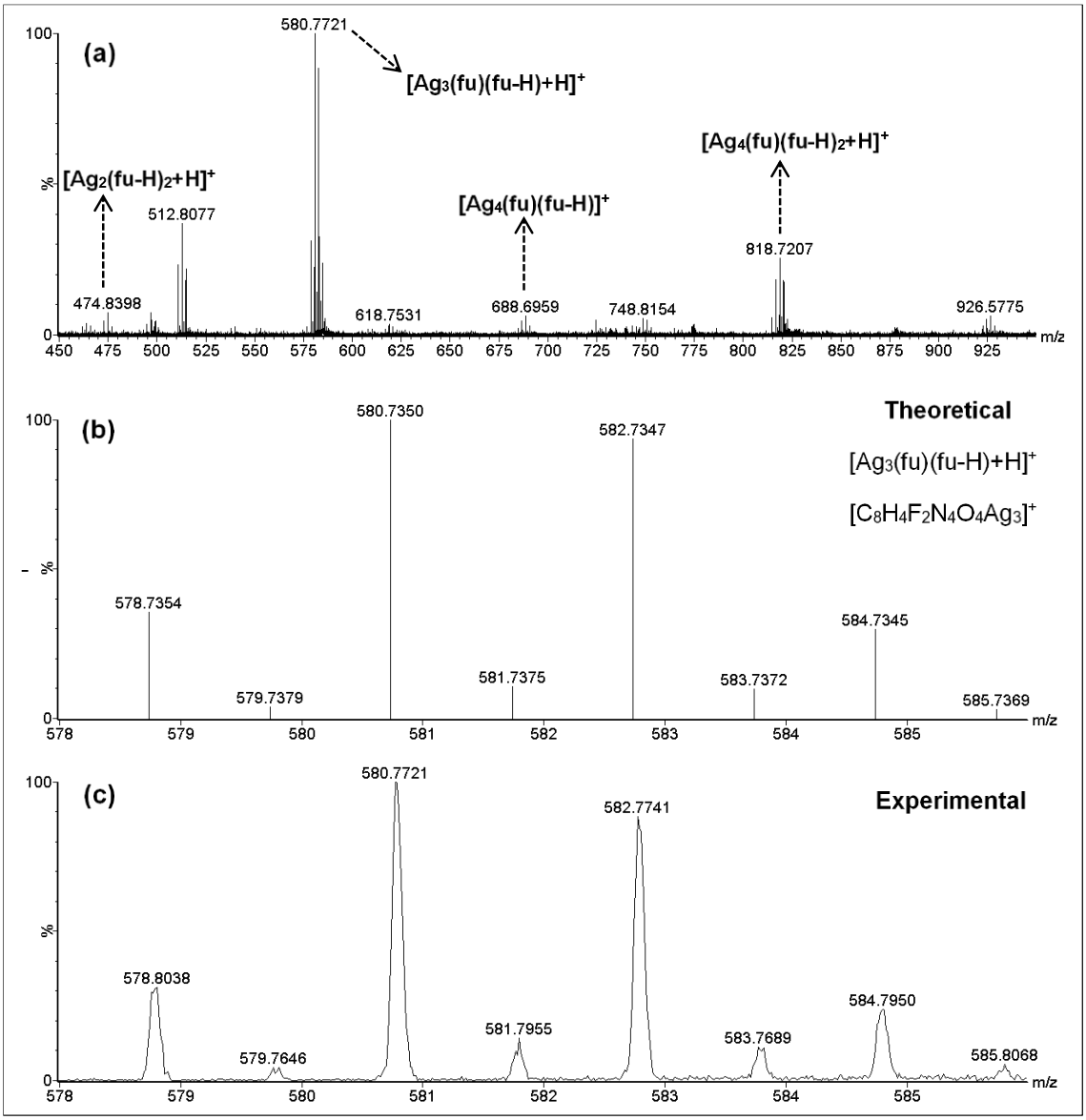

Figure 9. Mass spectra for the Ag-5fu complex. (a) ESI(+)QTOF mass spectrum from *m/z* 450 to 930, showing the $[Ag_3(fu)(fu\text{-}H)+H]^+$ ion as the most abundant species. (b) Calculated and (c) experimental isotope pattern comparison for the $[Ag_3(fu)(fu\text{-}H)+H]^+$ ion at *m/z* 580.7721 (mass error +63 ppm).

Table 2. Different species of the isotopic pattern of Ag-5fu.

m/z	**Species**
578.8	$[^{107}Ag_3(C_4HFN_2O_2)(C_4H_2FN_2O_2)+H]^+$
580.8	$[^{107}Ag_2{}^{109}Ag(C_4HFN_2O_2)(C_4H_2FN_2O_2)+H]^+$
582.8	$[^{107}Ag^{109}Ag_2\ (C_4HFN_2O_2)(C_4H_2FN_2O_2)+H]^+$
584.8	$[^{109}Ag_3(C_4HFN_2O_2)(C_4H_2FN_2O_2)+H]^+$

High-resolution mass spectrum of the Pd-5fu complex is shown in Figure 10-a. The most abundant peak was observed at *m/z* 400.8918, being consistent with the formation of the $[PdCl(C_4H_2FN_2O_2)_2]^-$ ion. The presence of this peak confirmed the 1:2 metal/ligand composition as earlier suggested by thermal and elemental analyses. A comparison between the theoretical and experimental isotopic pattern for the $[PdCl(C_4H_2FN_2O_2)_2]^-$ ion is presented in Figures 10-b and 10-c. The mass error for this ion was -0.75 ppm $[C_8H_4F_2ClN_4O_4Pd]^-$ (calcd. *m/z* 400.8921, exp. *m/z* 400.8918), considering the monoisotopic ion. Table 3 shows the different species of the isotopic pattern of Pd-5fu.

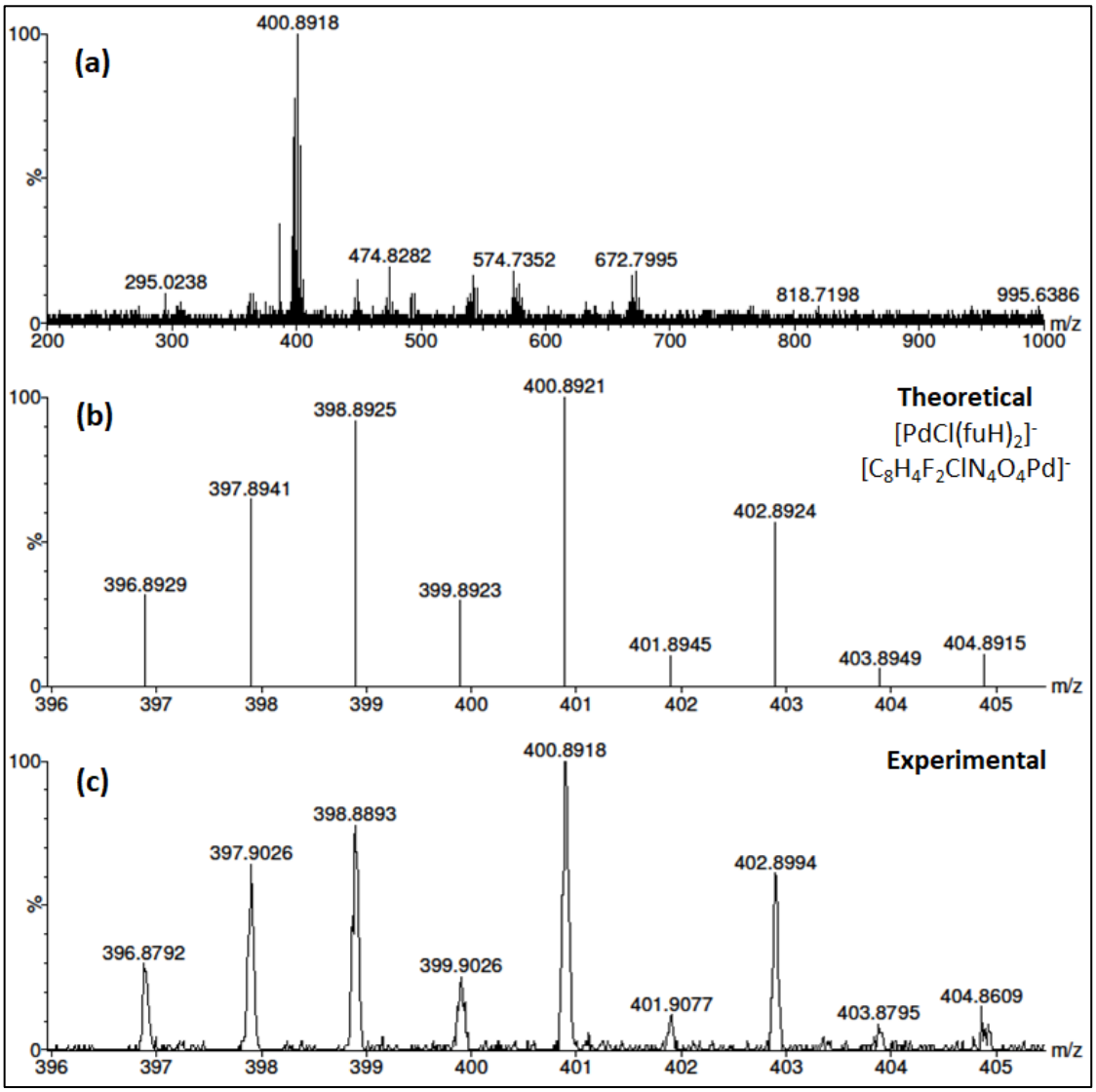

Figure 10. Mass spectra for the Pd-5fu complex. (a) ESI(-)QTOF mass spectrum from *m/z* 200 to 1000, showing the $[PdCl(C_4H_2FN_2O_2)_2]^-$ ion as the most abundant species. (b) Calculated and (c) experimental isotope pattern comparison for the $[PdCl(C_4H_2FN_2O_2)_2]^-$ ion (mass error -0.75 ppm).

Table 3. Different species of the isotopic pattern of Pd-5fu.

m/z	Species
396.8	$[^{102}Pd^{37}Cl(C_4H_2FN_2O_2)_2]^-$
	$[^{104}Pd^{35}Cl(C_4H_2FN_2O_2)_2]^-$
397.9	$[^{105}Pd^{35}Cl(C_4H_2FN_2O_2)_2]^-$
398.8	$[^{104}Pd^{37}Cl(C_4H_2FN_2O_2)_2]^-$
	$[^{106}Pd^{35}Cl(C_4H_2FN_2O_2)_2]^-$
399.9	$[^{105}Pd^{37}Cl(C_4H_2FN_2O_2)_2]^-$
400.8	$[^{106}Pd^{37}Cl(C_4H_2FN_2O_2)_2]^-$
	$[^{108}Pd^{35}Cl(C_4H_2FN_2O_2)_2]^-$
402.8	$[^{108}Pd^{37}Cl(C_4H_2FN_2O_2)_2]^-$
	$[^{110}Pd^{35}Cl(C_4H_2FN_2O_2)_2]^-$
404.8	$[^{110}Pd^{37}Cl(C_4H_2FN_2O_2)_2]^-$

High-resolution mass spectrum of the Pt-5fu complex is shown in Figure 11-a, presenting many ions with high abundance. This may be due to the decomposition of the complex in solution; however, the decomposition products could not be assigned. The $[K_2PtCl_2(fuH)_2+K]^+$ ion is present in the ESI+ mass spectra (Figure 11-c), however with low abundance. The presence of this peak confirmed the 1:2 metal/ligand composition as earlier suggested by thermal and elemental analyses. A comparison between the theoretical and experimental isotopic pattern for the $[K_2PtCl_2(C_4H_2FN_2O_2)_2+K]^+$ ion is presented in Figures 11-b and 11-c. The mass error for this ion was -4.68 ppm $[C_8H_4F_2K_3Cl_2N_4O_4Pt]^+$ (calcd. *m/z* 640.8115, exp. *m/z* 640.8085), considering the monoisotopic ion. Table 4 shows the different species of the isotopic pattern of Pt-5fu.

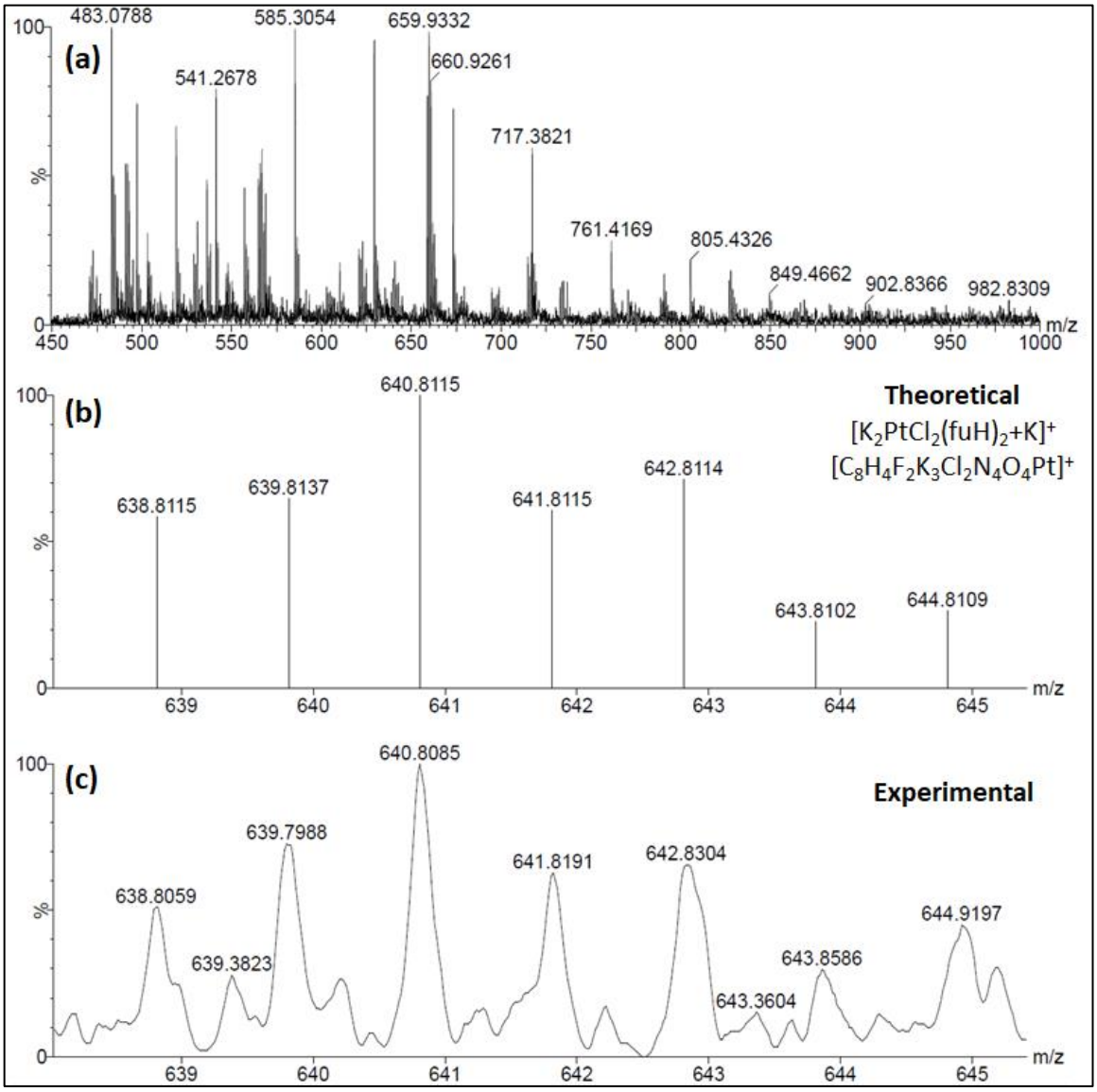

Figure 11. Mass spectra for the Pt-5fu complex. (a) ESI(+)QTOF mass spectrum from *m/z* 450 to 1000. (b) Calculated and (c) experimental isotope pattern comparison for the $[K_2PtCl_2(C_4H_2FN_2O_2)_2+K]^+$ ion (mass error -4.68 ppm).

Table 4. Different species in the isotopic pattern of Pt-5fu.

m/z	Species
638.8	$[K_2{}^{195}Pt^{35}Cl_2(C_8H_4N_4O_4F_2)_2+K]^+$
639.8	$[K_2{}^{194}Pt^{35}Cl_2(C_8H_4N_4O_4F_2)_2+K]^+$
640.8	$[K_2{}^{194}Pt^{35}Cl^{37}Cl(C_8H_4N_4O_4F_2)_2+K]^+$
	$[K_2{}^{196}Pt^{35}Cl_2(C_8H_4N_4O_4F_2)_2+K]^+$
641.8	$[K_2{}^{195}Pt^{35}Cl^{37}Cl(C_8H_4N_4O_4F_2)_2+K]^+$
	$[K_2{}^{196}Pt^{35}Cl^{37}Cl(C_8H_4N_4O_4F_2)_2+K]^+$
642.8	$[K_2{}^{194}Pt^{37}Cl_2(C_8H_4N_4O_4F_2)_2+K]^+$
	$[K_2{}^{198}Pt^{35}Cl_2(C_8H_4N_4O_4F_2)_2+K]^+$
643.9	$[K_2{}^{195}Pt^{37}Cl_2(C_8H_4N_4O_4F_2)_2+K]^+$
644.8	$[K_2{}^{196}Pt^{37}Cl_2(C_8H_4N_4O_4F_2)_2+K]^+$

Solid-state NMR spectroscopy

Nuclear magnetic resonance (NMR) studies of the metal complexes with 5fu were carried out in solid state due to the insolubility of the Ag-5fu complex in common solvents, and also because both Pd-5fu and Pt-5fu decompose in the solvents in which they are soluble. The ^{13}C and ^{15}N solid-state NMR spectra of free 5fu, Ag-5fu, Pd-5fu and Pt-5fu are shown in Figures 12 and 13, respectively, and assignments are in Table 5.

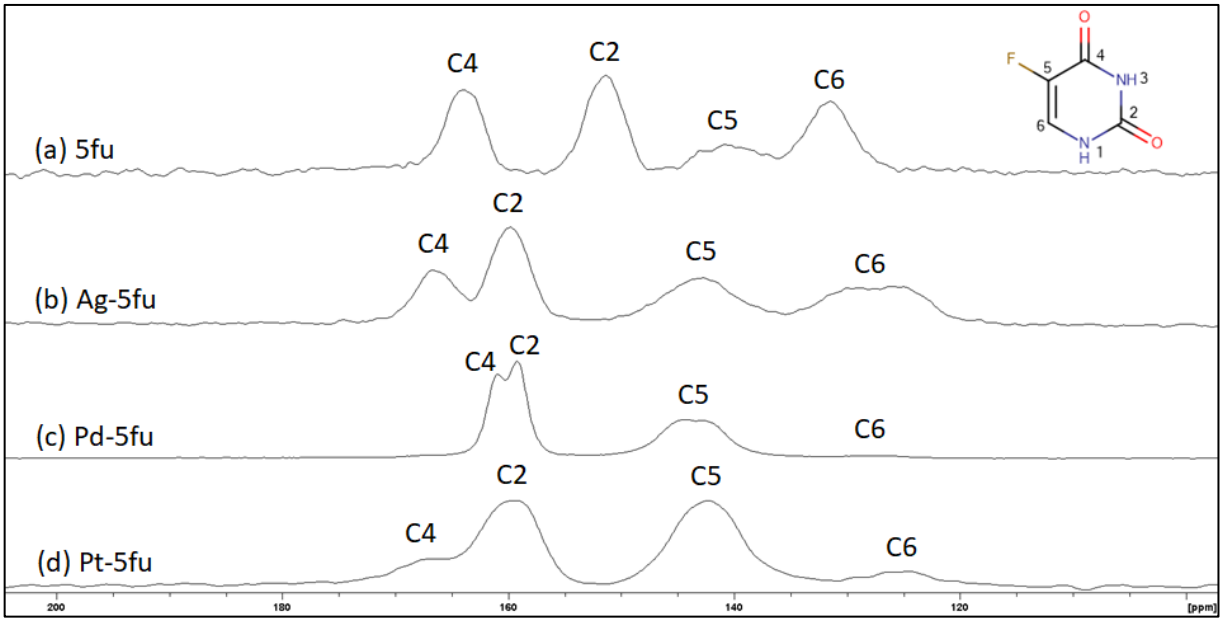

Figure 12. Solid-state ^{13}C NMR spectra of (a) 5fu, (b) Ag-5fu, (c) Pd-5fu, and (d) Pt-5fu.

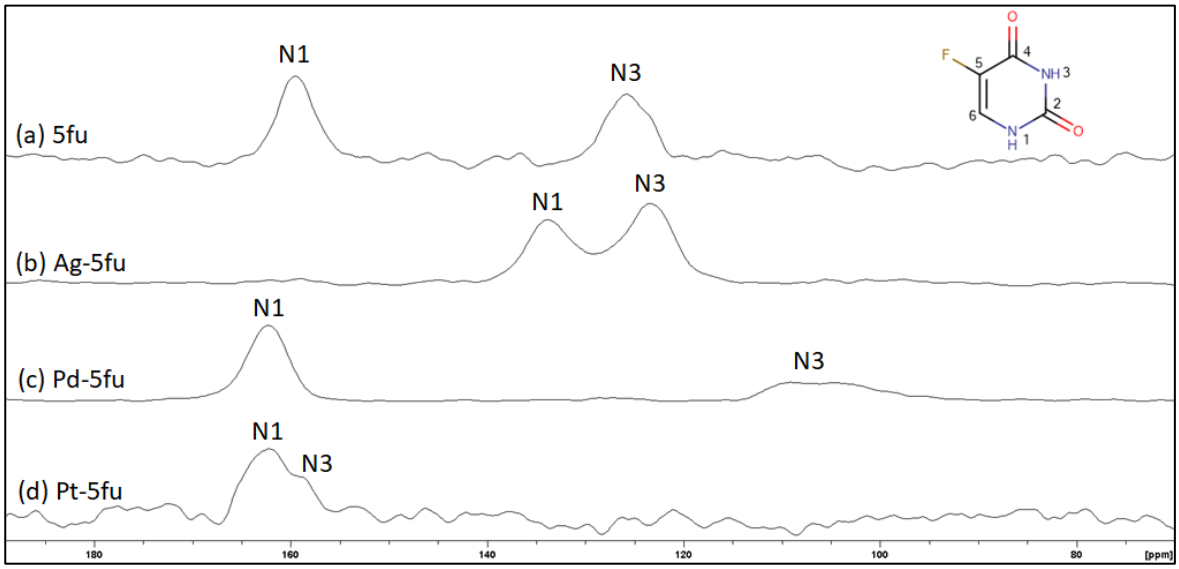

Figure 13. Solid-state ^{15}N NMR spectra of (a) 5fu, (b) Ag-5fu, (c) Pd-5fu, and (d) Pt-5fu.

Table 5. Solid-state ^{13}C and ^{15}N NMR assignments for 5fu, Ag-5fu, Pd-5fu and Pt-5fu.

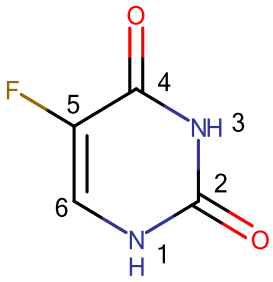

Atom	5fu (ppm)	Ag-5fu (ppm)	Pd-5fu (ppm)	Pt-5fu (ppm)
N1	160	134	162	162
C2	151	160	159	160
N3	126	123	107	159
C4	164	167	161	167
C5	141	143	144	143
C6	132	128	127	126

For ^{13}C-NMR spectrum of Ag-5fu, the highest shift is observed for carbon C2 (Δ = 9 ppm) when compared to free 5fu, while other carbons showed only minor differences. Considering that carbon C2 is bounded to an oxygen, it is suggested that this oxygen atom (O2) coordinates to silver(I). Considering now the ^{15}N-NMR spectrum an upfield shift is observed for the signals of the nitrogen atoms when the spectra of the Ag-5fu complex and the ligand are compared, and for N1 it is more pronounced (Δ = -26 ppm) when compared to N3 (Δ = -3 ppm). These results suggested that the coordination of the ligand to silver also occurs by the nitrogen atoms, being more pronounced for nitrogen atom N1.

Concerning the ^{15}N-NMR spectra of Pt-5fu and Pd-5fu, the highest shifts are observed for nitrogen atom N3, with Δ = -19 ppm for Pd-5fu and Δ = 33 ppm for Pt-5fu. Both complexes showed the same shift for nitrogen atom N1, with Δ = 2 ppm. These results show that 5fu may coordinate by nitrogen

N3 to Pd(II) and Pt(II). It is interesting that for the Pd(II) complex nitrogen N3 is shielded, while for the Pt(II) complex nitrogen N3 is unshielded.

Infrared spectroscopy

The infrared (IR) spectra of 5fu, Ag-5u, Pd-5fu and Pt-5fu are presented in Figure 14. Considering the structure of 5fu, the characteristic absorption bands of the ligand in the IR spectrum can be assigned to the following vibration modes: ν(N-H) at 3184 cm^{-1} and 3138 cm^{-1} [131], ν(=C-H) at 3069 cm^{-1}, ν(C=O) at 1725 cm^{-1} and 1675 cm^{-1} (carbons C2 and C4, respectively, numeration as in Table 4), δ(C-N-H) at 1635 cm^{-1} (shoulder), ν(C-N) at 1430 cm^{-1} and ν(C-F) at 1248 cm^{-1} [132]. In this way, we can conclude that 5fu is in the keto form in the solid state.

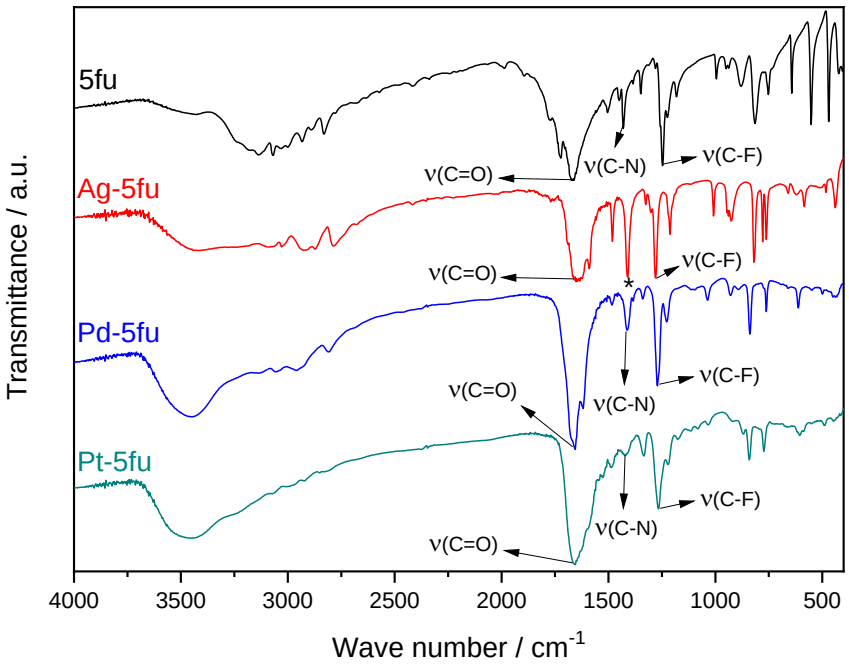

Figure 14. Infrared spectra of 5fu (black), Ag-5fu (red), Pd-5fu (blue), and Pt-5fu (green), from 4000-400 cm^{-1}.

For all complexes a broad band is observed in the region of the N-H group from 3200 to 3000 cm^{-1}. Due to the enlargement of the bands, no conclusions can be taken for the N-H stretching modes. The ν(C=O) modes are observed in the region 1664-1619 cm^{-1} for Ag-5fu, 1676-1655 cm^{-1} for Pd-5fu, and 1663-1623 cm^{-1} for Pt-5fu. These results lead to the conclusion that the 5fu ligand remains in the keto form after complexation. Since one nitrogen atom of the ligand remains protonated in the complexes

(fuH), a δ(C-N-H) band is observed at 1589 cm^{-1} for Ag-5fu, 1618 cm^{-1} for Pd-5fu, and 1596 cm^{-1} for Pt-5fu. The ν(C-N) is observed at 1410 cm^{-1} for Ag-5fu, 1412 cm^{-1} for Pd-5fu, and 1421 cm^{-1} for Pt-5fu. The ν(C-F) is observed at 1280 cm^{-1} for Ag-5fu, 1271 cm^{-1} for Pd-5fu, and 1267 cm^{-1} for Pt-5fu. We can infer that coordination causes modifications in the vibrational modes of the chemical groups of 5-fluorouracil, so the shifts in the IR spectrum of the complex, when compared to the ligand, reinforce the coordination of 5-fluorouracil to the metal ions.

Considering the experimental data set, a structural proposition for the silver(I) complex with 5-fluorouracil is presented in Figure 15. For the palladium(II) and platinum(II) complexes no structural propositions could be done.

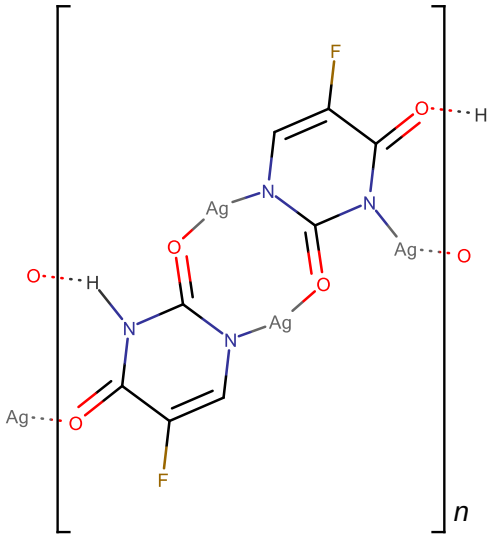

Figure 15. Coordination structure proposal for [Ag_3(fu)(fuH)] complex.

Antiproliferative assays

All three metal complexes were evaluated concerning their *in vitro* antiproliferative activities over nine human tumor cell lines and over one non-tumor cell, and they were compared to the controls (free 5fu, metal reagents and cisplatin). The Ag-5fu, Pd-5fu and Pt-5fu complexes were evaluated by the GI_{50} parameter (concentration that inhibits 50% cell growth), because of the antiproliferative profile of 5fu (for comparison). GI_{50} data are presented in Table 6, while graphics of the antiproliferative profiles are presented from Figures 16 to 18. GI_{50} data in µM can be found in Appendix, Table A1.

Table 6. GI_{50} values in μg mL^{-1} of the *in vitro* antiproliferative activity of free 5fu, Ag-5fu, Pd-5fu, Pt-5fu, $K_2[PdCl_4]$, $K_2[PtCl_4]$.

Compounds	Cell lines*									
	2	M	A	7	4	P	O	H	K	Cat
5fu	0.78	0.061	2.3	0.17	0.085	0.51	0.091	0.42	0.19	0.087
Ag-5fu	1.13	<0.25	0.36	0.29	0.46	2.28	0.39	0.34	0.25	<0.25
Pd-5fu	3.22	0.11	>25	0.73	0.44	2.05	1.15	2.57	>25	0.41
Pt-5fu	>25	8.14	>25	>25	5.69	>25	4.99	22.2	>25	10.0
$AgNO_3$	3.37	1.66	3.21	3.56	5.75	2.99	2.88	2.87	0.48	2.7
$K_2[PdCl_4]$	>25	>25	>25	>25	>25	>25	>25	>25	>25	>25
$K_2[PtCl_4]$	7.30	4.74	5.99	5.07	5.73	3.09	5.78	5.69	2.50	3.50
Cisplatin	1.28	2.17	2.49	1.12	0.18	2.61	3.21	5.11	2.42	1.14

*Human tumor cell lines: 2: U251 (glioma); M = MCF-7 (breast); A = NCI/ADR-RES (ovarian multidrug resistant); 7 = 786-0 (renal); 4 = NCI-H460 (lung, non-small cells); P = PC-3 (prostate); O = OVCAR-3 (ovarian); H = HT29 (colon); K = K562 (leukemia); Non-tumor human line: Cat = HaCat (immortal keratinocyte). GI_{50} values were determined by nonlinear regression analysis using ORIGIN 8.0.

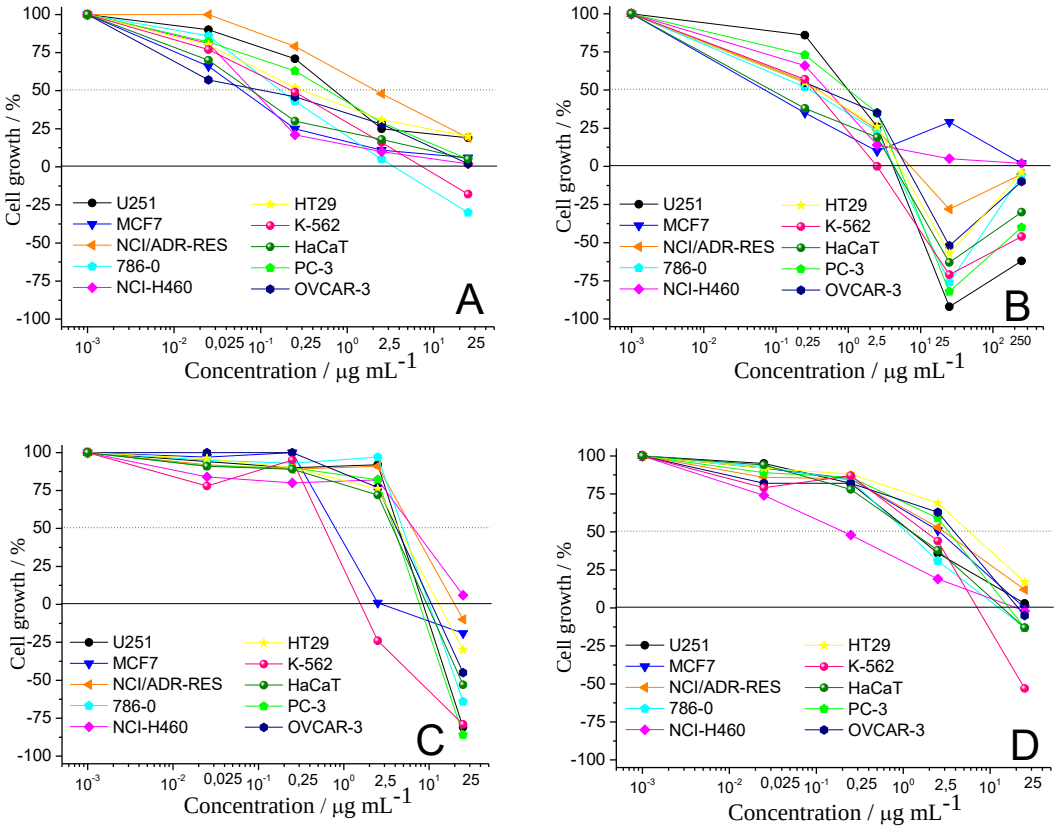

Figure 16. Cell growth profiles after 48h-exposition 5fu (A), Ag-5fu (B), $AgNO_3$ (C) and cisplatin (D). For Ag-5fu a measurement error was observed for MCF-7 cells at 25 μg mL^{-1} and for all cell lines at concentrations above 25 μg mL^{-1}, due to the colorimetric assay.

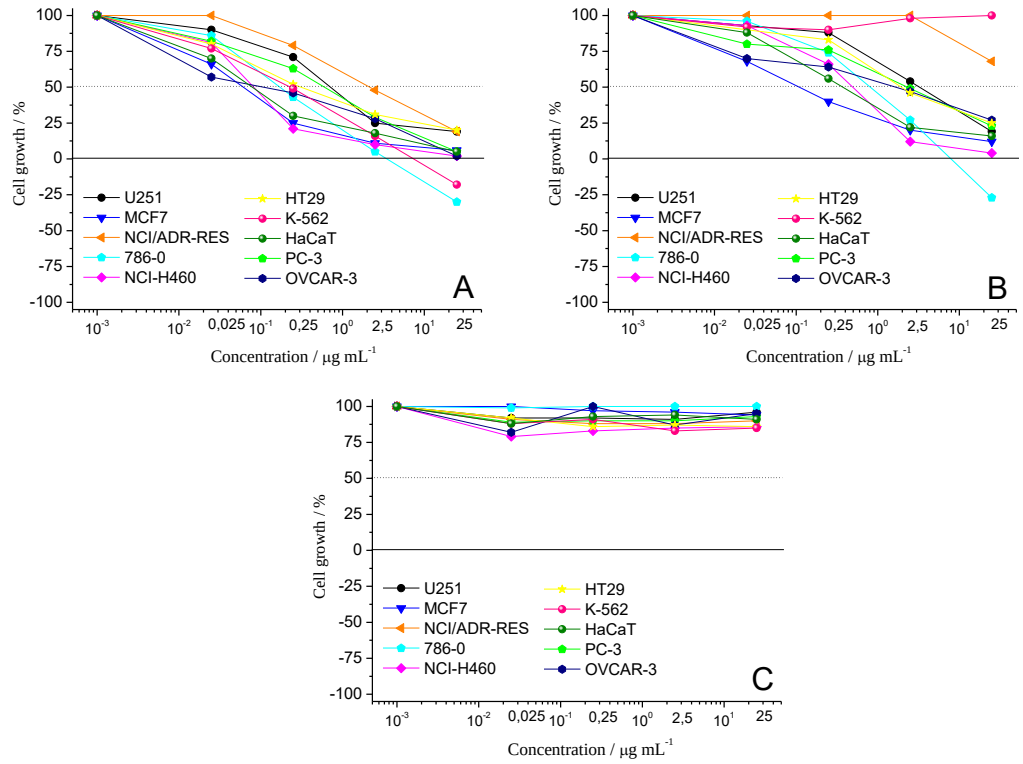

Figure 17. Cell growth profiles after 48h-exposition to 5fu (A), Pd-5fu (B), and K_2PdCl_4 (C).

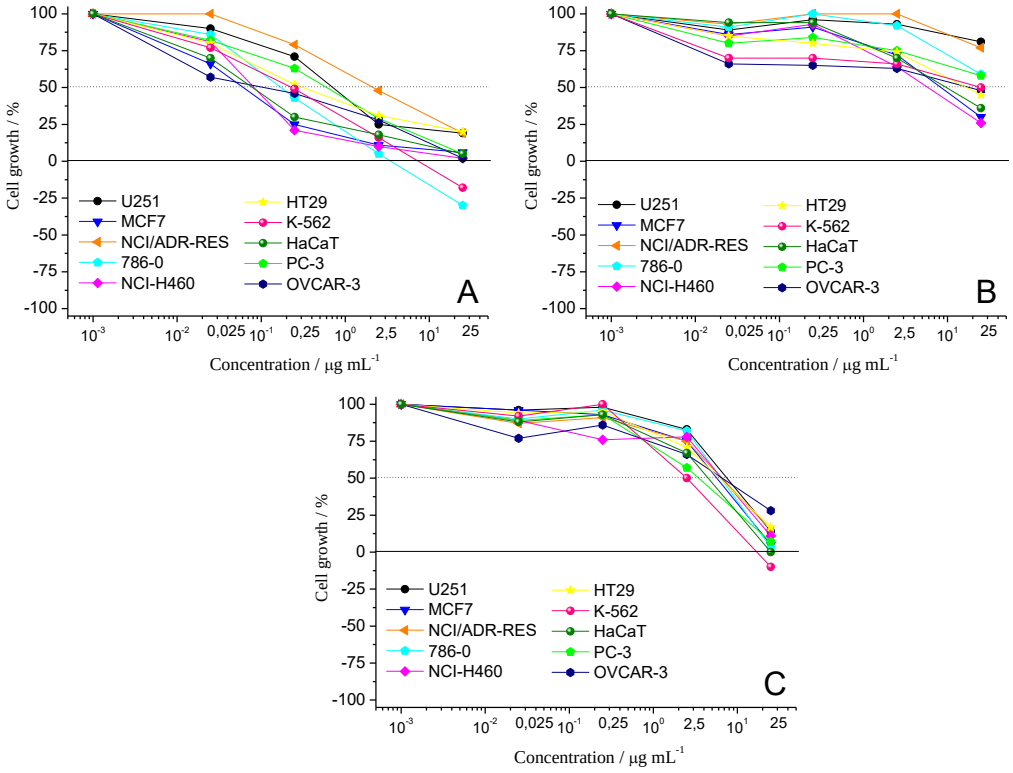

Figure 18. Cell growth profiles after 48h-exposition to 5fu (A), Pt-5fu (B), and K_2PtCl_4 (C).

Considering Figure 16, silver nitrate showed a cytocidal effect (negative values for cell growth) at the highest concentration (25 μg mL^{-1}), while 5fu was mainly a cytostatic agent. For all tested cell lines, Ag-5fu presented lower GI_{50} values than those observed for $AgNO_3$. Moreover, GI_{50} values for Ag-5fu were lower than those of 5fu for ovarian multidrug resistant (NCI/ADR-RES) tumor cells and similar to 5fu for K562 (leukemia), HT29 (colon) and 786-0 (renal) cells. Similarly to 5fu, the Ag-5fu complex also inhibited cell proliferation of the immortalized keratinocytes (HaCat).

Comparing 5fu with cisplatin, it is interesting to observe that the differences in cell growth profiles (Figures 16-A and 16-D, respectively) and in GI_{50} values (Table 5) reflect the differences in the mechanism of action between the two compounds. According to Zaharevitz *et al.* [133], similarities and differences in the antiproliferative profile in a tumor cell panel could be an important indicative of the mechanism of action by comparison with known chemotherapeutics. Cisplatin is a DNA-reactive drug inducing DNA damage by coordination of Pt(II) ions with nitrogen bases (mainly guanine), while 5fu is a DNA replication disruptor by inhibiting thymidylate synthase enzyme [103,106,134]. Moreover, in the Ag-5fu complex, the silver(I) ions can have multiple mechanisms, for example being able to bind proteins and DNA [92].

The combination of Ag(I) and 5-fluorouracil may thus be responsible for the increasing on the antiproliferative activity on ovarian multidrug resistant (NCI/ADR-RES) tumor cell line observed for Ag-5fu (GI_{50} = 0.36 μg mL^{-1}) when compared to the free ligand. 5-Fluorouracil is not commonly used in the treatment of ovarian tumors [106]. Therefore, the activity observed by the Ag-5fu complex may be related to a combination effect of the silver(I) ions and 5-fluorouracil, with the release of the individual compounds inside the cell. Since NCI/ADR-RES is resistant to cisplatin [135], this result is of high significance. Therefore, this complex was chosen to be further studied regarding the mechanism of cell death of Ag-5fu in NCI/ADR-RES cells.

Considering the metal complexes of Pd(II) and Pt(II) with 5fu, they did not show relevant antiproliferative activities, in a different way from Ag-5fu. Although Pd-5fu showed a better activity (lower GI_{50} values) when compared to $K_2[PdCl_4]$, it has a minor activity when compared to free 5fu. The best result for Pd-5fu was over the MCF-7 (breast cancer) tumor cell line (GI_{50} = 0.11 μg mL^{-1}). In the case of Pt-5fu, the complex decomposes in aqueous medium and this may be the reason for its lack of activity when compared to free 5fu and $K_2[PtCl_4]$. The antiproliferative profile in this case is a combination of all the decomposition sub products, which probably did not reach the concentration to inhibit proliferation. The best obtained results for Pt-5fu were over the OVCAR-3 (ovarian cancer) and NCI-H460 (lung cancer) tumor cells (GI_{50} = 4.99 and 5.69 μg mL^{-1}, respectively).

The selectivity index (SI) is a parameter which can be used to compare the toxicity of compounds towards non-tumor and tumor cells [136]. Here, it can be calculated by the ratio between the GI_{50} of a non-tumor line (HaCat) and the GI_{50} of tumor lines. The higher the SI values, the greater

the selectivity of a compound towards a tumor cell when compared to a normal one. According to the literature, considerable SI values would be higher than 2.0 or 3.0, which means that a compound would be twice or three times more toxic to a tumor cell when compared to a non-tumor one [136]. The SI values for 5fu, Ag-5fu, Pd-5fu, Pt-5fu and cisplatin are presented in Table 7. Pd-5fu was shown to be selective over the MCF-7 (breast) tumor cells (SI = 3.7), while Pt-5fu was selective over the OVCAR-3 (ovarian) tumor cells (SI = 2.0) and cisplatin was very selective over the NCI-H460 (lung) tumor cells (SI = 6.3).

Table 7. SI values for 5fu, Ag-5fu, Pd-5fu, Pt-5fu and cisplatin.

Compounds	**Cell lines***								
	2	M	A	7	4	P	O	H	K
5fu	0.11	1.4	0.037	0.51	1.0	0.17	0.96	0.21	0.46
Ag-5fu	<0.22	1.0	<0.69	<0.86	<0.54	<0.11	<0.64	<0.73	<1.0
Pd-5fu	0.13	3.7	<0.02	0.56	0.93	0.20	0.36	0.16	<0.02
Pt-5fu	<0.40	1.23	<0.40	<0.40	1.8	<0.40	2.0	0.45	<0.40
Cisplatin	0.89	0.52	0.46	1.0	6.3	0.44	0.35	0.22	0.47

*Human tumor cell lines: 2: U251 (glioma); M = MCF-7 (breast); A = NCI/ADR-RES (ovarian multidrug resistant); 7 = 786-0 (renal); 4 = NCI-H460 (lung, non-small cells); P = PC-3 (prostate); O = OVCAR-3 (ovarian); H = HT29 (colon); K = K562 (leukemia); Non-tumor human line: HaCat (immortal keratinocyte). SI = GI_{50}(HaCat)/GI_{50}(tumor line).

Partial conclusions

Three complexes with 5-fluorouracil were synthesized and characterized by chemical and spectroscopic techniques. The silver(I) complex, Ag-5fu, presented a 3:2 metal/ligand composition, with formula $[Ag_3(C_4HFN_2O_2)(C_4H_2FN_2O_2)]$. The palladium(II) complex, Pd-5fu, presented a 2:1 metal/ligand composition, with formula $K[PdCl(C_4H_2FN_2O_2)_2]$, while the platinum(II) complex, Pt-5fu, also presented a 2:1 metal/ligand composition, with formula $K_2[PtCl_2(C_4H_2FN_2O_2)_2]$. Antiproliferative activity assays were performed with free 5-fluorouracil, the metal complexes and their respective metal salts, and results were also compared to cisplatin. The Ag-5fu complex presented the best antiproliferative profile, and its activity seems to be a combination of the activities of 5fu and silver(I), probably due to the release of the individual compounds inside the cell. Also, Ag-5fu presented a better activity than free 5fu and cisplatin over the NCI/ADR-RES cell line. The Pd-5fu complex presented a better activity than its respective metal salt, $K_2[PdCl_4]$, although not presenting a better activity than free 5fu and cisplatin. Best antiproliferative results were found for the MCF-7 cell line for Pd-5fu. The Pt-5fu complex did not show considerable antiproliferative results, probably due to hydrolyzation of the complex in solution, and did not present a better activity than $K_2[PtCl_4]$. The best results for Pt-5fu were for the NCI-H460 cell line. Although not very cytotoxic when compared to Ag-5fu, Pd-5fu and Pt-5fu presented selectivity over MCF-7 and OVCAR-3 tumor cells, respectively. Data for the silver(I) complex with 5-fluorouracil presented in this section was published in Journal of Fluorine Chemistry 195 (2017) 93-101.

Characterization and antiproliferative assays of the Au(I) complex with 2-thiouracil and the Ag(I) complex with 2,4-dithiouracil

Results and Discussion

Synthesis of the [Ag_2(dtu)] complex

A silver(I) complex with 2,4-dithiouracil ($dtuH_2$) was described in 1972 by Dwivedi and Agarwala [137]. In this paper, the authors described different metal complexes with $dtuH_2$, and there was no indication of the used amounts of metal salt or ligand in synthesis, nor specification of which silver metal salt was used for preparing the silver(I) complex. Mostly, the authors described the results of elemental analysis (of nitrogen, sulfur and silver) and assignments of the major infrared bands. By elemental analysis they conclude that the complex has a 2:1 silver/dithiouracil composition. Consequently, this was the stoichiometry chosen for the synthesis of the silver(I) complex here presented. Elemental analyses (CHN and ICP-OES) corroborate with 2:1 metal/ligand composition, with electroneutrality achieved with complete deprotonation of the ligand (dtu, charge -2) and two silver(I) ions.

Thermogravimetric analysis of the [Ag_2(dtu)] complex

The thermogravimetric analysis for the [Ag_2(dtu)] complex is shown in Figure 19. The decomposition of the complex starts at 270 °C and continues until 660 °C with weight loss of 33.8%. Such weight loss is attributed to one dithiouracil ligand (calcd. for loss of dtu, 39.7%). The final residue of 64.7% was assigned to metallic silver (calcd. 60.3%). This analysis reinforces the 2:1 metal/ligand composition of the [Ag_2(dtu)] complex.

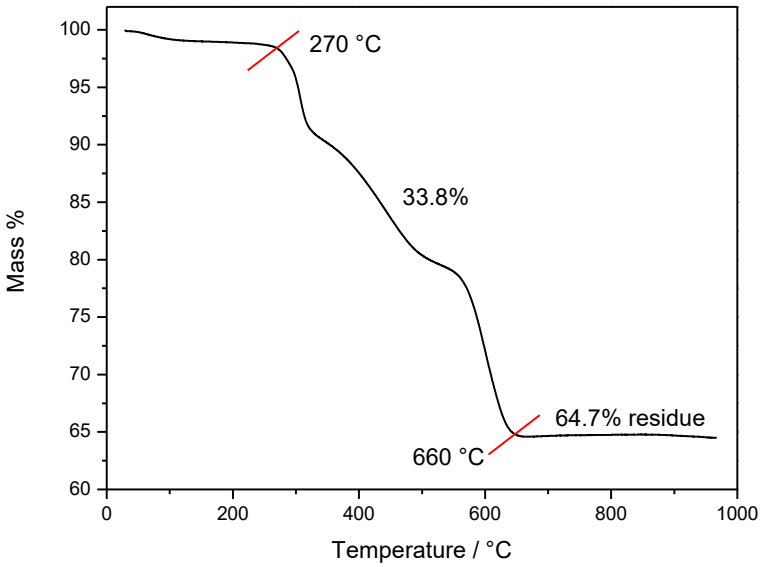

Figure 19. Thermogravimetric analysis of [Ag_2(dtu)].

Infrared spectroscopy of the [Ag_2(dtu)] complex

The infrared (IR) spectra of $dtuH_2$ and [Ag_2(dtu)] complex are presented in Figure 20. The IR spectrum of the complex was analyzed in comparison to the spectrum of the ligand. Considering the structure of $dtuH_2$, the characteristic absorption bands of the ligand in the IR spectrum can be assigned to the following vibration modes: ν(N-H) at 3077 cm^{-1}, and ν(C=S) at 1610 cm^{-1} and 1563 cm^{-1}.

In the spectrum of the complex no absorption bands are observed in the region of the N-H group from 3200 to 3000 cm^{-1}, confirming the total deprotonation of the ligand. Moreover, the ν(C=S) stretching mode is shifted to lower energies, to 1526 cm^{-1} and 1492 cm^{-1}. This shift may be due to coordination of the thiol groups to silver(I) since the new S–Ag bond weakens the C=S bond.

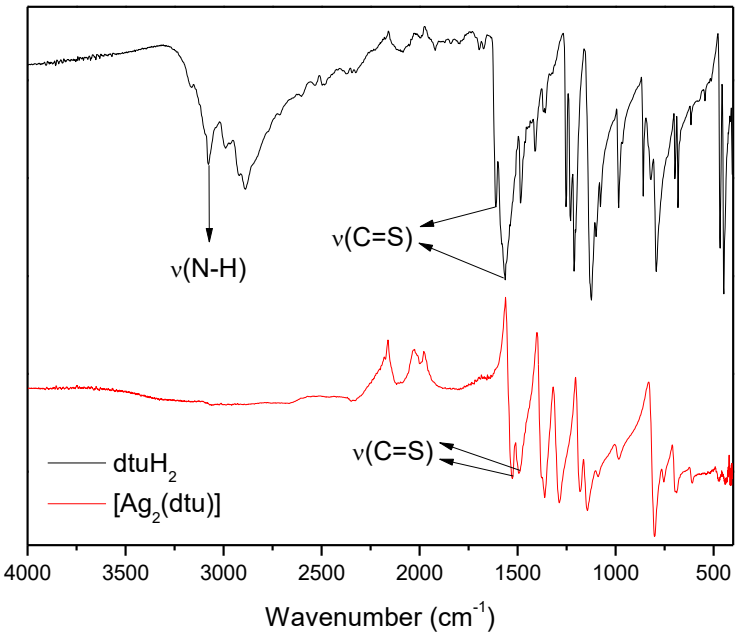

Figure 20. Infrared spectra of $dtuH_2$ (black) and $[Ag_2(dtu)]$ (red).

Solid-state NMR spectroscopy of the $[Ag_2(dtu)]$ complex

Nuclear magnetic resonance (NMR) studies of the $[Ag_2(dtu)]$ complex were carried out in solid state due to the insolubility of the complex in common solvents. Figure 21 shows the ^{13}C NMR spectrum of the complex in comparison to the one of the free ligand.

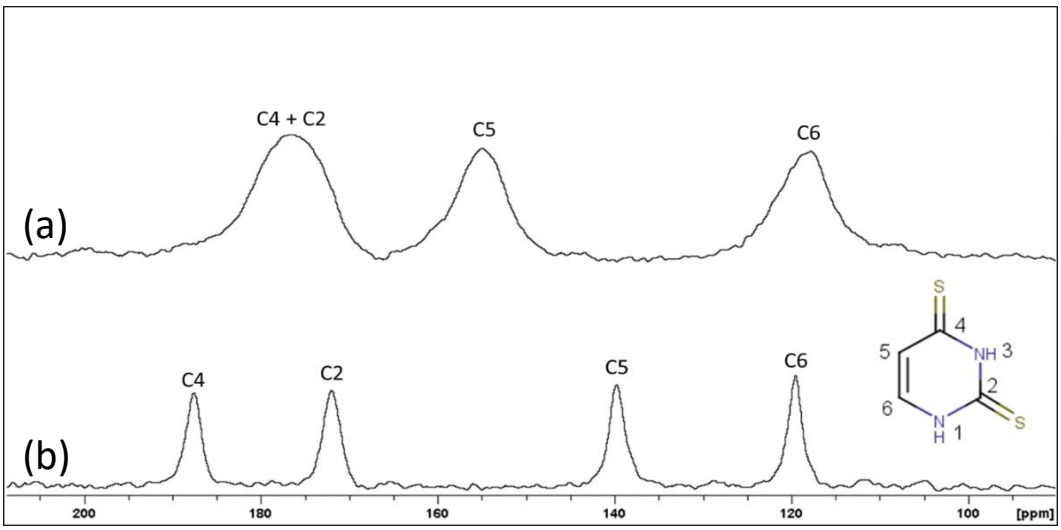

Figure 21. Solid-state ^{13}C NMR spectra of (a) $[Ag_2(dtu)]$ and (b) $dtuH_2$.

The ^{13}C NMR spectrum of tuH_2 shows the following chemical shifts (and assignments): 120 ppm (C6), 139 ppm (C5), 172 ppm (C2), 188 ppm (C4) 37. For the [Ag_2(dtu)] complex the chemical shifts are 118 ppm (C6), 155 ppm (C5) and 177 ppm (C2 + C4). Considering the lack of information from the ^{15}N NMR spectrum, and that carbon C6 in the ^{13}C NMR spectrum showed the minor chemical shift, coordination may not occur near this environment, so it probably does not occur by nitrogen N1. As thiol groups present high affinity for soft metal ions, as silver(I), it is probable that the ligand coordinated by these S-donor groups. In fact, carbons C2 and C4, which are bonded to the sulfur atoms, seemed to aggregate in one broad signal at 177 ppm. Also, the highest shift is observed for carbon C5 (Δ = 16 ppm), which is close to a sulfur atom (possible coordination site).

Synthesis of the Ph_3P-Au-tuH complex

This complex was already reported in the literature by Hoskins *et al.*, however only the crystal structure and IR spectroscopic studies of the crystal were presented by that time [138]. The synthesis previously described involves the mixture of 2-thiouracil and chlorido(triphenylphosphine)gold(I) in methanol and alkaline medium. The authors obtained a precipitate, which was recrystallized, and the obtained crystals are used for posterior analyses. Here, the synthesis described involves the use of silver nitrate to eliminate the chloride from chlorido(triphenylphosphine)gold(I) before reaction with 2-thiouracil, because some previous attempts of synthesis showed some chlorido(triphenylphosphine)gold(I) residue without the use of silver nitrate. Despite the crystal structure solved by single-crystal X-ray diffraction, all other analyses were done with the precipitate and not with the crystals. The synthesis of the complex was performed in alkaline medium, with deprotonation of 2-thiouracil (tuH_2) to the thiouracilato (tuH) anion, which corroborates elemental analysis (only one deprotonation). Thus, electroneutrality is achieved with one tuH (charge -1) and one gold(I).

Infrared spectroscopy of the Ph_3P-Au-tuH complex

Considering free tuH_2, this molecule can present keto/enol and thione/thiol tautomeric forms (Figure 22), which is of high importance for the determination of the coordination sites. Using infrared spectroscopy to determine the tautomeric form of free tuH_2 in the solid state (Figure 23), we were able to determine the prevalence of the keto/thione form of tuH_2 by the presence of the ν(N-H) band of tuH_2 at 3038 cm^{-1} and the absence of the ν(O-H) (~3300 cm^{-1}) and ν(S-H) (~2570 cm^{-1}) bands [41].

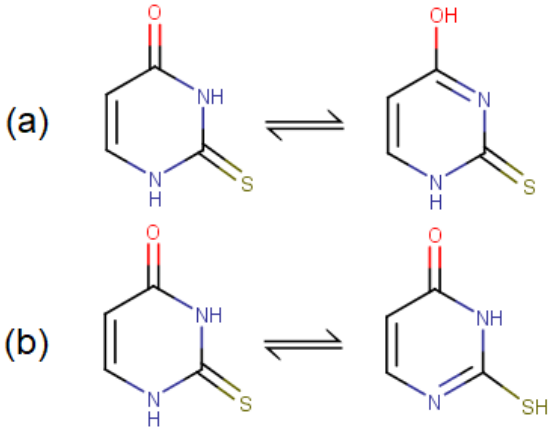

Figure 22. Tautomeric forms of 2-thiouracil, (a) keto/enol form, (b) thione/thiol form.

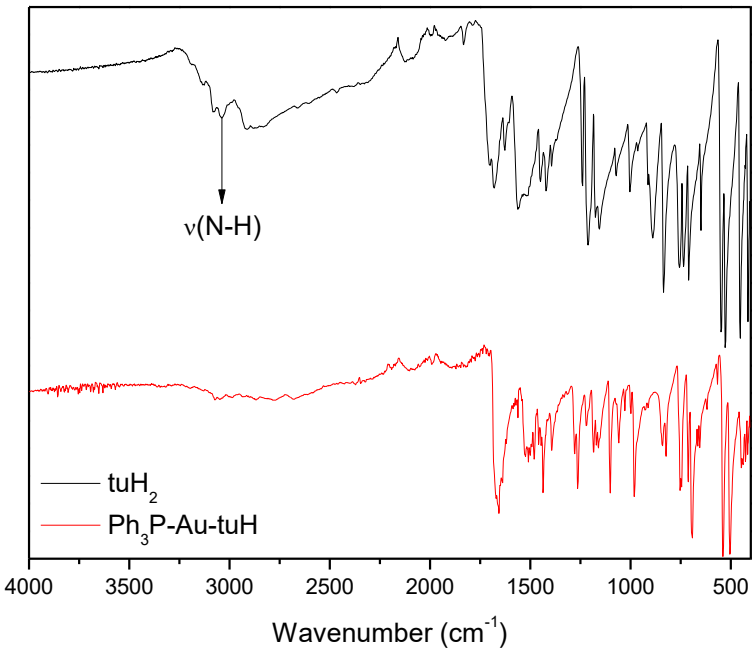

Figure 23. Infrared spectra of tuH_2 (black) and Ph_3P-Au-tuH (red).

Previous computational studies of 2-thiouracil showed that deprotonation of the nitrogen atom N1 is more favorable than for the nitrogen atom N3 (see Figure A1 in Appendix for atom numbering) [139]. In this way, deprotonation will enhance the basicity of the ligand, favoring a nucleophilic attack on gold(I). Considering deprotonation at nitrogen atom N1, three possible coordination sites are expected: *O*-, *N*- and *S*- (Figure 24). Previous computational studies have also shown that the negative charge is largely localized on the sulfur atom, which might be a more favorable coordination site [139]. Considering hard-hard and soft-soft interactions, gold(I) is a soft acid and it is readily coordinated to

triphenylphosphine, which enhances its softness. Consequently, it is most probable that tuH will coordinate by the S-donor atom, which is the softest base. An example from the literature shows that mercaptothiazoline, a molecule which also presents thione/thiol tautomeric forms, can coordinate to gold(I) through a N-donor group when gold(I) is coordinated to cyanide, but coordinates through the S-donor group when gold(I) is coordinated to triphenylphosphine [140,141]. Here, however, just observing the IR spectra of the complex it is not possible to address the coordination site of the tuH_2 ligand.

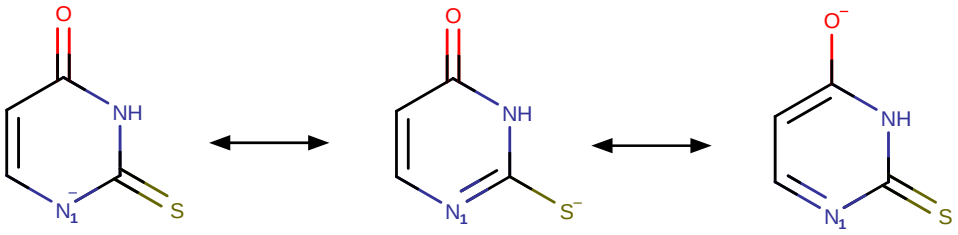

Figure 24. Resonance structures of tuH with deprotonation of nitrogen atom N1.

Crystal structure of the Ph_3P-Au-tuH complex

Crystals of the Ph_3P-Au-tuH complex suitable for single-crystal X-ray diffraction were obtained by slow evaporation of a methanol/chloroform mixture. The details about the analyzed crystal, data collection and structure refinement are shown in Table 8(a), (b) and (c).

Table 8. Crystallographic data, data collection and refinement for the Ph_3P-Au-tuH crystal.

(a) Crystal data

$C_{22}H_{18}AuN_2OPS$	D_x = 1.876 Mg m^{-3}
M_r = 586.38	Cu $K\alpha$ radiation, λ = 1.54178 Å
Monoclinic, $P2_1/n$	Cell parameters from 120 reflections
a = 17.4687 (8) Å	θ = 8.0–37.5°
b = 11.2334 (5) Å	μ = 15.10 mm^{-1}
c = 21.1684 (10) Å	T = 150 K
β = 91.401 (2)°	Plate, colorless
V = 4152.7 (3) Å^3	0.12 × 0.11 × 0.06 mm
Z = 8	
F(000) = 2256	

(b) Data collection

Absorption correction: multi-scan SADABS (Bruker, 2010)	R_{int} = 0.053
T_{min} = 0.524, T_{max} = 0.753	θ_{max} = 68.2°, θ_{min} = 4.7°
27145 measured reflections	h = −20 21
7386 independent reflections	k = −13 13
6686 reflections with $I > 2\sigma(I)$	l = −24 25

(c) Refinement

Refinment on F^2	H-atom parameters not refined
Least-squares matrix: full	$w = 1/[\sigma^2(F_o^2) + (0.1264P)^2]$ where $P = (F_o^2 + 2F_c^2)/3$
$R[F^2 > 2\sigma(F^2)] = 0.053$	$(\Delta/\sigma)_{max} = 0.001$
$wR(F^2) = 0.160$	$\Delta\rho_{max} = 3.82$ e Å^{-3}
$S = 1.07$	$\Delta\rho_{min} = -3.02$ e Å^{-3}
7386 reflections	
508 parameters	

The crystal structure here presented belongs to $P2_{1/n}$ space group, whose asymmetric unit contains two Ph_3P-Au-tuH complex units (Figure 25-a). The tuH ligand coordinates to gold(I) by the sulfur atom, showing that the thiol form is predominant upon coordination, as expected. Each Ph_3P-Au-tuH complex unit is composed by one triphenylphosphine, one gold(I), and one 2-thiouracilato ligand (tuH, charge -1) (Figure 25-b). For clarity, it is important to emphasize that atom numbering for the crystal is different from that of Figure A1 (Appendix).

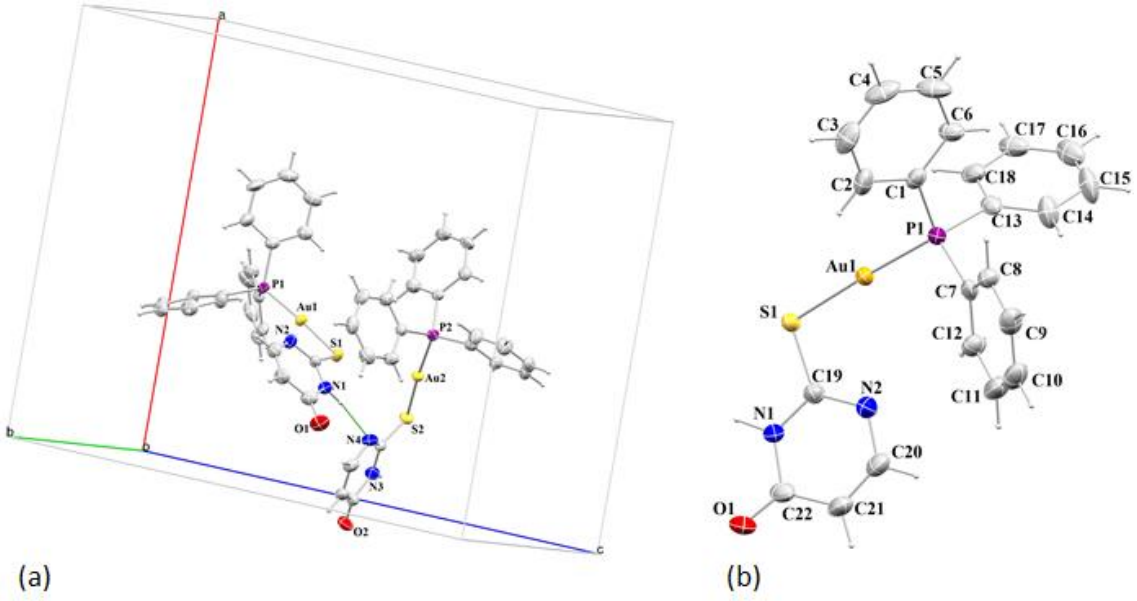

Figure 25. (a) The two Ph_3P-Au-tuH complex units in the asymmetric unit of the crystal, with selected atoms labels and 50% probability displacement ellipsoids. Ph_3P-Au-tuH complex unit 1 containing Au1 and Ph_3P-Au-tuH complex unit 2 containing Au2. H-bond (N1—H1A···N4) shown in green dashed line. (b) The structure of the Ph_3P-Au-tuH complex unit 1 with atom labels and 50% probability displacement ellipsoids.

Triphenylphosphine, gold(I) and tuH are in an almost linear geometry (P1—Au1—S1 angle of 176.31(6) ° for unit 1, and P2—Au2—S2 angle of 175.90(6) ° for unit 2). Au1—P1 and Au1—S1 bond lengths are similar to each other (2.253(2) Å and 2.307(2) Å, respectively), and the same is observed for Au2—P2 and Au2—S2 (2.254(2) Å and 2.306(2) Å, respectively). These bond lengths and angles are in agreement with the structure previously described by Hoskins and Zhenrong [138]. The differences in the P—Au—S angles of the two Ph_3P-Au-tuH units in the asymmetric unit of the crystal may be due to the different orientations of the phenyl groups and different intermolecular interactions from each Ph_3P-Au-tuH motif, as also observed in the structure previously reported [138].

In the crystal, nitrogen atom N4 is deprotonated, confirming the (-1) charge of the tuH ligand. The two Ph_3P-Au-tuH complex units interact via a classical intermolecular hydrogen bond (N1—H1*A*···N4), while neighbor asymmetric units are connected by other two classical intermolecular hydrogen bonds (N3—H3*A*···O2), building up a chain of unit 1 – unit 2 – unit 2 – unit 1 sequence (Figure 26). It is important to mention that the N3—H3*A*···O2 H-bond is also observed for the 2-thiouracilato(triethylphosphine)gold(I) complex previously reported [142]. Hydrogen bonds for the crystal here presented are described in Table 9.

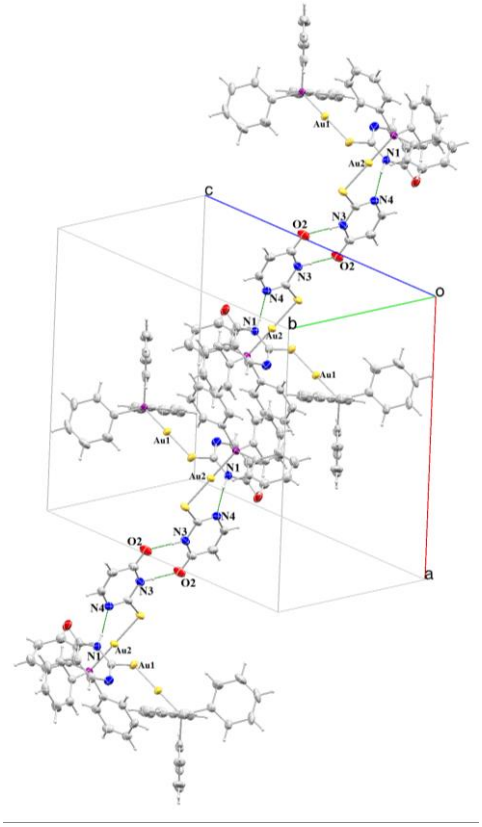

Figure 26. Crystal packing of Ph_3P-Au-tuH showing hydrogen bonds (N1—H1A···N4 and N3—H3A···O2 as green dashed lines) that form unit 1 – unit 2 – unit 2 – unit 1 sequences, with two sequences represented. Labels for selected atoms to allow identification of units 1 and 2 and 50% probability displacement ellipsoids.

Table 9. Hydrogen-bond geometry of Ph_3P-Au-tuH crystal.

D—H···*A*	*D*—H (Å)	H···*A* (Å)	*D*···*A* (Å)	*D*—*H*···*A* (°)
N1—H1a···N4	0.94(10)	2.02(10)	2.955(9)	171(8)
N3—H3a···O2	0.88	1.84	2.716(9)	178

Based on the bond distances from the X-ray data, the predominant tautomer form of the ligand upon coordination to gold(I) can be determined. The most relevant bond distances are presented in Table 10, together with data of the free ligand from the literature [143].

Table 10. Bond lengths in thiouracil moieties of units 1 and 2 of Ph_3P-Au-tuH complex in the crystal (atom labels as depicted in Figure 25-b) in comparison to the crystal structure of free tuH_2 [143].

Atoms *Complex unit 1 / Complex unit 2*	*Bond lengths* (Å)	*Bond lengths* (Å) *of* tuH_2 [143]
S1-C19 / S2-C41	1.754 (7) / 1.749 (8)	1.683(3)
N1-C19 / N3-C41	1.348 (9) / 1.355 (9)	1.357(3)
N1-C22 / N3-C42	1.408 (9) / 1.387 (10)	1.389(4)
N2-C19 / N4-C41	1.322 (9) / 1.319 (10)	1.338(4)
N2-C20 / N4-C44	1.371 (10) / 1.371 (11)	1.373(4)
O1-C22 / O2-C42	1.228 (10) / 1.237 (9)	1.227(4)
C20-C21 / C43-C44	1.337 (12) / 1.357 (11)	1.338(5)
C21-C22 / C42-C43	1.430 (12) / 1.432 (12)	1.432(5)

Considering the carbon-sulfur bond, C—S single bonds are of 1.82 Å, while C=S double bonds are of 1.61 Å [144]. In the crystal here presented the C19—S1 bond is of 1.75 Å, therefore being an intermediate between a single and a double bond. When compared to free tuH_2, an elongation of the C—S bond is observed upon coordination of the sulfur atom to gold(I), which can also be interpreted as the changing from a double bond to a single bond. Therefore, free tuH_2 is in the thione form, while upon complexation to gold(I) the thiol form is preferable. Now, considering the carbon-nitrogen bonds, C—N single bonds are of 1.46 Å and C=N double bonds are of 1.21 Å [144]. Here, the C19—N2 bond (1.32 Å) has a greater double bond character, so the predominant tautomer of the ligand upon coordination would be the thiol form (see Figure 24). For the free ligand this bond is longer, showing the shift from a single bond to a double one. The C20—N2 (1.37 Å) bond has a greater single bond character. Also, for the carbon-oxygen bond, C—O single bonds are of 1.42 Å and C=O double bonds are of 1.21 [144]. Here the C22—O1 (1.23 Å) is a double bond, proving that the ligand is in the keto/thiol form. When compared to the free ligand no major changes were observed for the C—O bond (free ligand is also in the keto form). For carbon-carbon bonds, C—C single bonds are of 1.53 Å and C=C double bonds are of 1.34 Å [144]. Here, the C—C bonds have a greater double bond character and did not change upon coordination. The different bond distances of the complex when compared to the free ligand show the modification of the electronic structure of the ligand upon coordination to gold(I).

Mass spectrometric studies of the Ph_3P-Au-tuH complex

High-resolution mass spectrum of the Ph_3P-Au-tuH complex is shown in Figure 27. The peak at *m/z* 587.0639, which is one of the most abundant species, is consistent with the formation of the $[Au(C_4H_3N_2OS)(C_{18}H_{15}P)+H]+$ ion. The presence of this peak confirmed the 1:1 metal/ligand composition as suggested before. Other peaks at *m/z* 459.0456 and 721.1308 were attributed to the $[Au(C_{18}H_{15}P)]+$ and $[Au(C_{18}H_{15}P)_2]+$ species, respectively, due to fragmentation and recombination of the gold(I) complex in solution.

A comparison between the theoretical and experimental isotopic pattern for the $[Au(C_4H_3N_2OS)(C_{18}H_{15}P)+H]+$ ion is also presented. The mass error for this ion was -3.1 ppm, (calcd. *m/z* 587.0621, exp. *m/z* 587.0639), considering the monoisotopic ion.

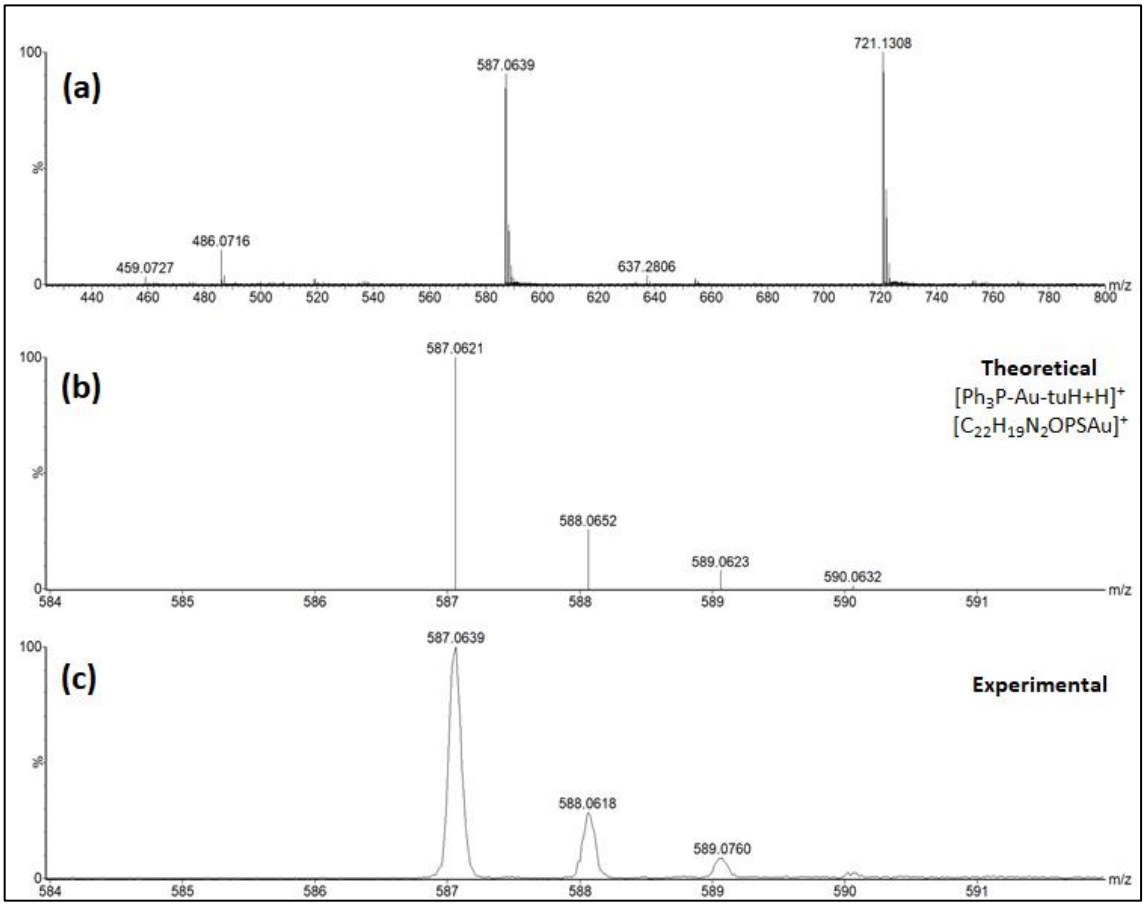

Figure 27. Mass spectra for the Ph_3P-Au-tuH complex. (a) ESI(+)QTOF mass spectrum from *m/z* 430 to 800, showing the $[(C_{18}H_{15}P)Au(C_4H_3N_2OS)+H]+$ ion as one of the most abundant species. (b) Calculated and (c) experimental isotope pattern comparison for the $[(C_{18}H_{15}P)Au(C_4H_3N_2OS)+H]+$ ion (mass error -3.1 ppm).

Solution NMR spectroscopy of the Ph_3P-Au-tuH complex

Solution state ^{1}H, ^{13}C and ^{31}P NMR spectra of Ph_3P-Au-Cl and Ph_3P-Au-tuH were acquired to confirm the coordination of 2-thiouracil to (triphenylphosphine)gold(I). ^{1}H and ^{13}C NMR spectra of free tuH_2 were recorded in DMSO-d6, because of the high solubility of the ligand in this solvent. ^{1}H NMR spectra are presented in Figure 28 and assignments are in Table 11.

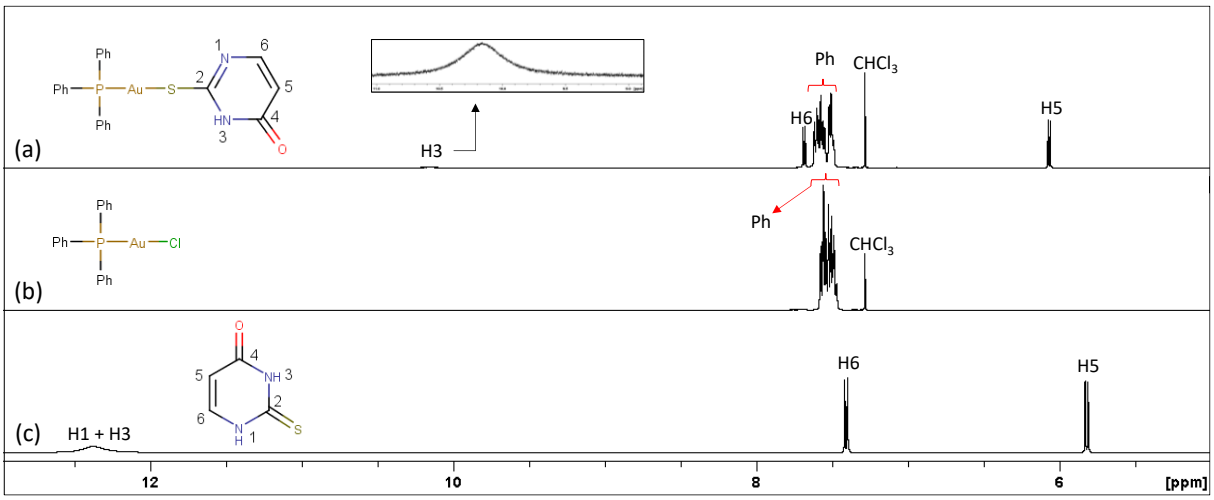

Figure 28. ^{1}H NMR spectra of (a) Ph_3P-Au-tuH complex in $CDCl_3$, with an inset of the 9.0-11.0 ppm region; (b) Ph_3P-Au-Cl complex in $CDCl_3$; (c) tuH_2 free ligand in DMSO-d6. In (a) and (b) the signal at 7.28 ppm is referred to $CHCl_3$.

Table 11. ^{1}H NMR assignments for free tuH_2, Ph_3P-Au-Cl complex and Ph_3P-Au-tuH complex.

Assignment	**tuH_2 (ppm)**	**Ph_3P-Au-Cl (ppm)**	**Ph_3P-Au-tuH (ppm)**	**Multiplicity**
1	12.38	-	-	s
3	12.38	-	10.17	s
5	5.82	-	6.07	d
6	7.41	-	7.69	d
Ph	-	7.52	7.55	m

It is possible to notice the disappearance of the hydrogen H1 in the Ph_3P-Au-tuH complex spectrum, confirming the ligand deprotonation. Also, the presence of the hydrogen atoms H3, H5, H6

of the ligand and also the hydrogen atoms of triphenylphosphine (Ph) confirmed the formation of Ph_3P-Au-tuH complex. The ^{13}C NMR spectra and assignments are presented in Figure 29 and Table 12, respectively.

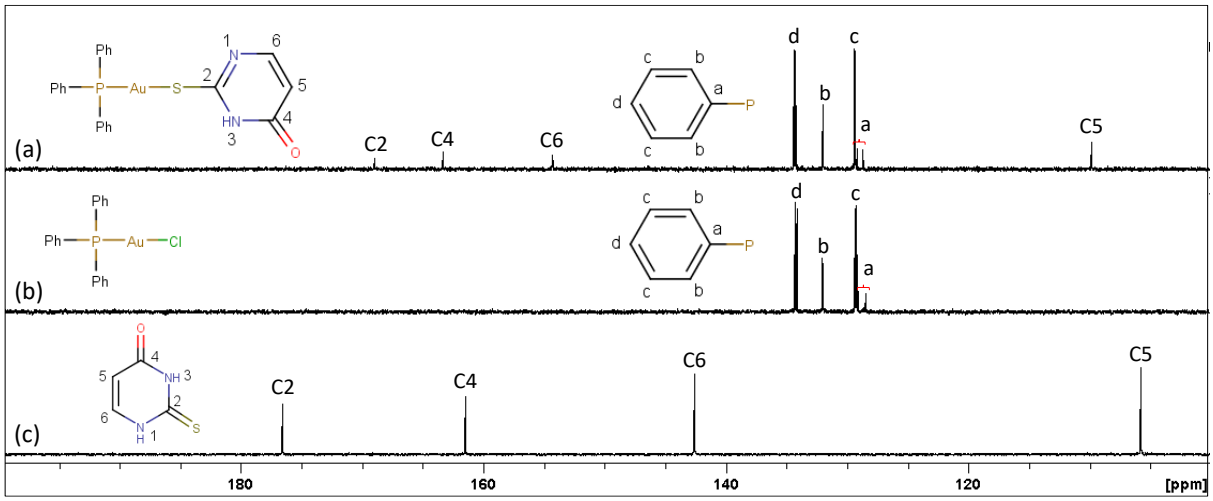

Figure 29. ^{13}C NMR spectra of (a) Ph_3P-Au-tuH complex in $CDCl_3$; (b) Ph_3P-Au-Cl complex in $CDCl_3$; (c) tuH_2 free ligand in DMSO-d6.

Table 12. ^{13}C NMR assignments for free tuH_2, Ph_3P-Au-Cl complex and Ph_3P-Au-tuH complex.

Assignment	tuH_2 (ppm)	Ph_3P-Au-Cl (ppm)	Ph_3P-Au-tuH (ppm)	Multiplicity
2	176.6	-	169.0	s
4	161.5	-	163.3	s
5	105.8	-	109.8	s
6	142.6	-	154.3	s
a	-	128.7	129.0	d
b	-	132.0	132.0	d
c	-	129.3	129.4	d
d	-	134.2	134.3	d

Comparing the ^{13}C NMR spectra of the Ph_3P-Au-Cl and Ph_3P-Au-tuH complexes, carbons from the phenyl rings of the phosphine did not show considerable chemical shifts. Considering the tuH ligand,

only carbon C2 from the Ph_3P-Au-tuH complex was shifted to an upper field when compared to the free ligand (tuH). Carbon C2 is the one directly bonded to the sulfur atom which coordinates to gold(I). Other carbons (C4, C5, C6) follow the trend of being unshielded upon coordination of the thiol group to gold(I). At last, Figure 30 presents the ^{31}P spectra of Ph_3P-Au-Cl and Ph_3P-Au-tuH, in which the phosphorous atom is shifted to a lower field upon coordination of the 2-thiouracilato ligand to gold(I). As the chlorido ion is a α,π-donor ligand, the electronic density of gold(I) and consequently of the phosphorous atom is higher in the Ph_3P-Au-Cl complex when compared to Ph_3P-Au-tuH.

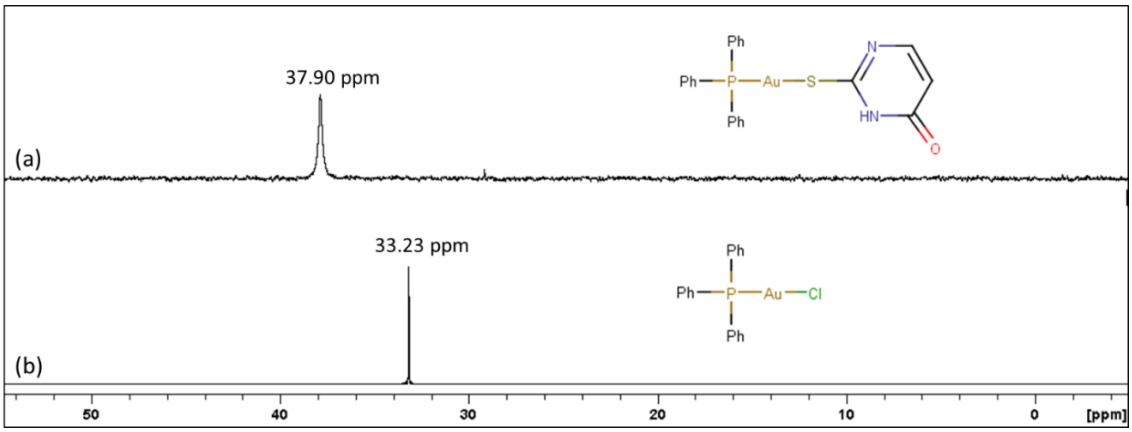

Figure 30. ^{31}P NMR spectra in $CDCl_3$ of (a) Ph_3P-Au-tuH complex; b) Ph_3P-Au-Cl complex. The phosphorous atom is shifted to a lower field upon coordination of the 2-thiouracilato ligand to gold(I).

Antiproliferative assays

The antiproliferative activities of $[Ag_2(dtu)]$ and Ph_3P-Au-tuH were compared to controls ($dtuH_2$ and $AgNO_3$ for $[Ag_2(dtu)]$, and tuH_2, Ph_3P-Au-Cl and doxorubicin for Ph_3P-Au-tuH) through the TGI parameter (concentration that inhibits 100% cell growth), provided by *in vitro* evaluation assay. Here the TGI was chosen due to the antiproliferative profile of the gold(I) complexes and lack of activity of the ligands and silver(I) complex. The obtained data are provided in Table 13 and Figures 31 and 32. TGI data in µM can be found in Appendix, Table A2.

Table 13. TGI values in μg mL^{-1} of the *in vitro* antiproliferative activity of $dtuH_2$, $[Ag_2(dtu)]$, $AgNO_3$, tuH_2, Ph_3P-Au-tuH, Ph_3P-Au-Cl, and doxorubicin.

Compounds	**Cell lines***								
	2	M	A	7	4	O	H	K	Cat
$dtuH_2$	141.4	>250	>250	>250	>250	>250	>250	>250	>250
$[Ag_2(dtu)]$	>250	>250	>250	>250	>250	>250	>250	>250	>250
$AgNO_3$	7.2	3.0	33.7	22.8	23.8	6.1	13.6	1.1	38.4
tuH_2	>250	>250	>250	>250	>250	>250	>250	>250	>250
Ph_3P-Au-tuH	1.5	5.1	11.0	2.3	26.7	10.4	28.5	<0.25	6.1
Ph_3P-Au-Cl	2.3	4.7	10.5	4.0	>250	5.9	>250	3.3	14.5
Doxorubicin	0.81	0.57	>25	1.1	>25	1.8	>25	1.2	0.58

*Human tumor cell lines: 2: U251 (glioma); M = MCF-7 (breast); A = NCI-ADR/RES (multidrug resistant ovarian); 7 = 786-0 (renal); 4 = NCI-H460 (lung, non-small cells); O = OVCAR-3 (ovarian); H = HT29 (colon); K = K562 (leukemia); Non-tumor human line: Cat = HaCat (immortal keratinocyte). TGI values were determined by nonlinear regression analysis using ORIGIN 8.0.

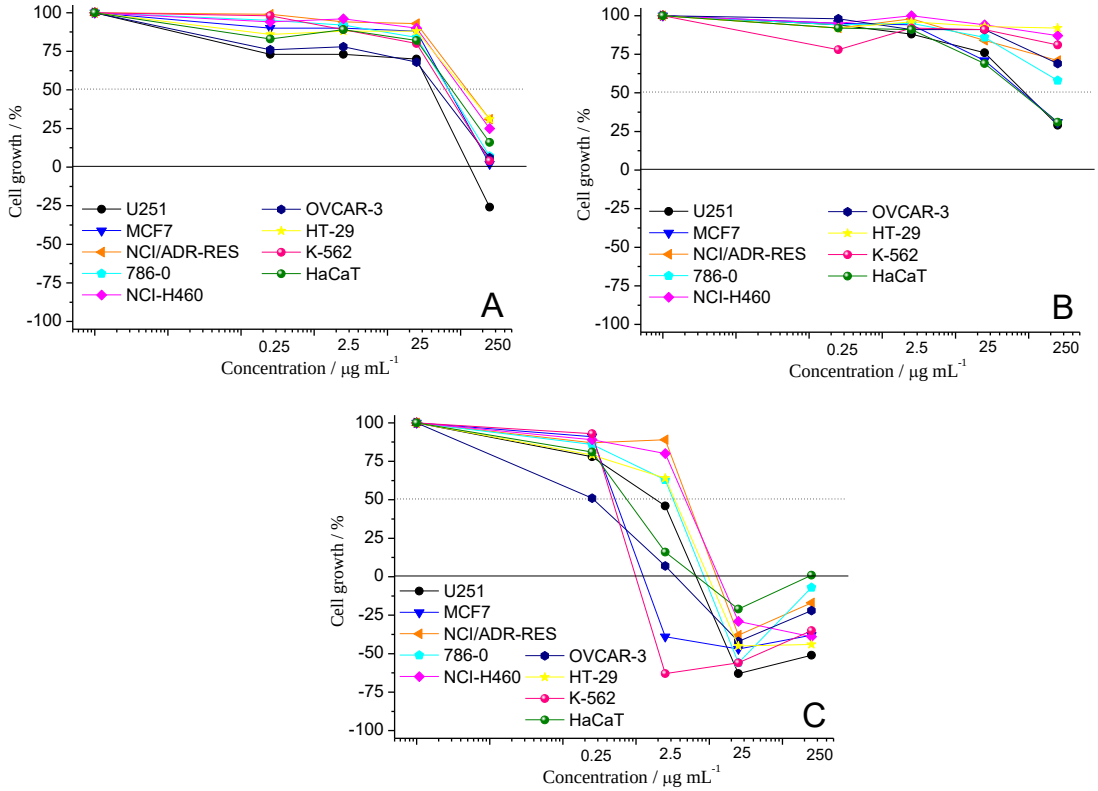

Figure 31. Cell growth profiles after 48h-exposition to $dtuH_2$ (A), $[Ag_2(dtu)]$ (B), and $AgNO_3$ (C). For $AgNO_3$ measurement errors were observed for MCF-7 and K-562 cells at 2.5 µg mL^{-1} and for all cell lines at concentrations above 25 µg mL^{-1}, due to the colorimetric assay.

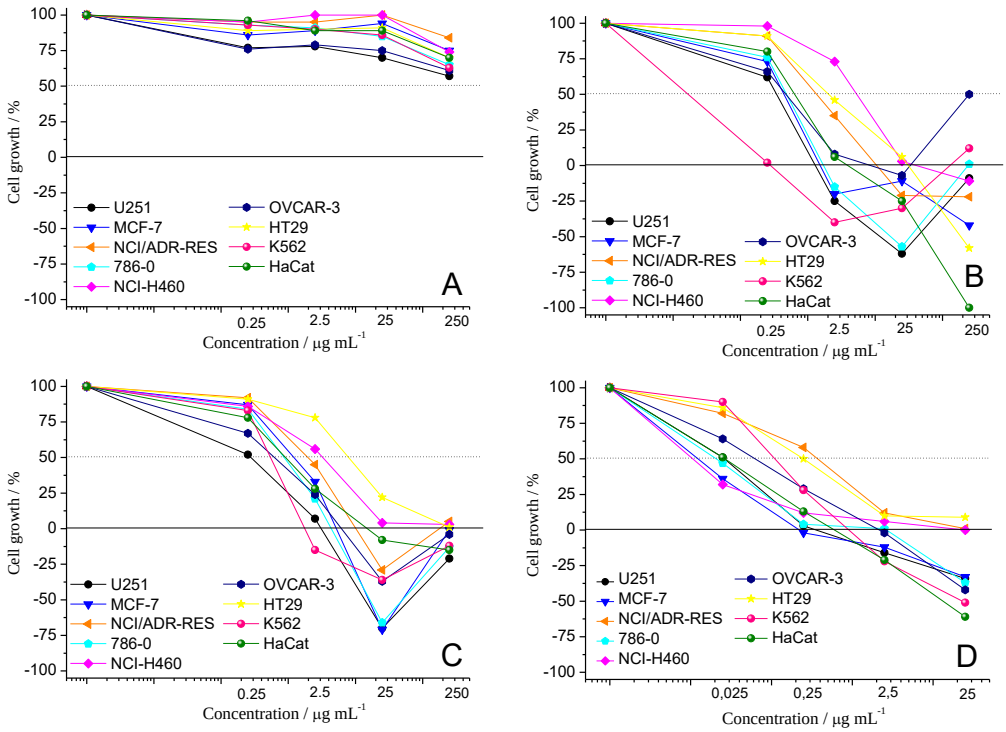

Figure 32. Cell growth profiles after 48h-exposition to tuH_2 (A), Ph_3P-Au-tuH (B), Ph_3P-Au-Cl (C) and doxorubicin (D). For Ph_3P-Au-tuH measurement errors were observed for MCF-7 and K-562 cells at 2.5 µg mL^{-1} and for OVCAR-3, K-562, 786-0 and U251 cells at concentrations above 25 µg mL^{-1}. For Ph_3P-Au-Cl measurement errors were observed for most cell lines at concentrations above 25 µg mL^{-1}. Errors were observed due to the colorimetric assay.

Considering $dtuH_2$ and the $[Ag_2(dtu)]$ complex (Figure 31), none of them presented considerable antiproliferative effects. The $dtuH_2$ ligand presented some activity only at the highest tested concentration, while the $[Ag_2(dtu)]$ complex was not active, despite $AgNO_3$ has shown to be quite cytotoxic. The poor solubility of the $[Ag_2(dtu)]$ complex may be responsible for its lack of activity.

Considering tuH_2, Ph_3P-Au-tuH and Ph_3P-Au-Cl, free tuH_2 did not present antiproliferative activity, even at the highest tested concentration (Figure 32-A). On the other hand, Ph_3P-Au-tuH and Ph_3P-Au-Cl complexes showed cytocidal effects (negative values for cell growth) for almost all cell lines, with Ph_3P-Au-tuH being cytotoxic at lower concentrations (2.5 µg mL^{-1}, Figure 32-B) when compared to Ph_3P-Au-Cl (25 µg mL^{-1}, Figure 32-C). Both compounds were also cytotoxic for the non-tumor line (HaCat).

In general, the Ph_3P-Au-tuH and Ph_3P-Au-Cl complexes presented TGI values of the same order of magnitude. Therefore, both complexes presented the same activity for glioma (U251), breast (MCF-7), ovarian multidrug resistant (NCI/ADR-RES), renal (786-0) and ovarian (OVCAR-3) tumor cells.

The Ph_3P-Au-tuH complex was more active against leukemia (K-562, TGI <0.25 µg mL^{-1}), lung (NCI-H460; TGI = 26.7 µg mL^{-1}) and colon (HT-29; TGI = 28.5 µg mL^{-1}) tumor cells than the Ph_3P-Au-Cl complex. Also, the Ph_3P-Au-tuH complex was more active against leukemia than doxorubicin (Figure 32-D), which is an antitumor drug used in clinics.

As discussed before, the selectivity index (SI) is a parameter which can be used to compare the toxicity of compounds towards non-tumor and tumor cells [136]. In this case, it can be calculated by the ratio between the TGI of a non-tumor line (HaCat) and the TGI of tumor lines. Again, the higher the SI values, the greater the selectivity of a compound towards a tumor cell when compared to a normal one (considerable SI values would be higher than 2.0 or 3.0). The SI values for Ph_3P-Au-tuH, Ph_3P-Au-Cl and doxorubicin can be found in Table 14. The best SI values for Ph_3P-Au-tuH complex were found for the glioma (U251, SI = 4.07), renal (786-0, SI = 2.65) and leukemia lines (K-562, SI = 24.4).

Table 14. SI values for Ph_3P-Au-tuH, Ph_3P-Au-Cl and doxorubicin.

Compounds	**Cell lines***							
	2	M	A	7	4	O	H	K
Ph_3P-Au-tuH	4.07	1.20	0.55	2.65	0.23	0.59	0.21	24.40
Ph_3P-Au-Cl	6.30	3.09	1.38	3.63	0.06	2.46	0.06	4.39
Doxorubicin	0.72	1.02	0.02	0.53	0.02	0.32	0.02	0.48

*Tumor human cell lines: 2: U251 (glioma); M = MCF-7 (breast); A = NCI/ADR-RES (multidrug resistant ovarian); 7 = 786-0 (kidney); 4 = NCI-H460 (lung, non-small cells); O = OVCAR-3 (ovarian); H = HT29 (colon); K = K562 (leukemia); Non-tumor human line: HaCat (immortal keratinocyte). SI = TGI(HaCat)/TGI(tumor line)

According to the literature, the chlorido(triphenylphosphine)gold(I) (Ph_3P-Au-Cl) compound is able to induce apoptosis in breast tumor cells (MCF-7) with low level of ct-DNA interaction, and Ph_3P-Au-Cl interacts with sulphydryl groups present in serum albumin (BSA) [145]. These activities could partially explain the antiproliferative effect observed for Ph_3P-Au-Cl. It is possible that some of the effects caused by Ph_3P-Au-Cl can also be promoted by the Ph_3P-Au-tuH complex. Therefore, these complexes were chosen to be further studied regarding the mechanism of cell death in NCI-H460 cells.

Partial conclusions

Two complexes with thiouracils were synthesized and characterized by elemental and spectroscopic techniques. The silver(I) complex with 2,4-dithiouracil, [Ag_2(dtu)], presented a 2:1 metal ligand composition, with formula [$Ag_2(C_4H_2N_2S_2)$]. The triphenylphosphinegold(I) complex with 2-thiouracil, Ph_3P-Au-tuH, presented a 1:1 metal/ligand composition, with formula [$Au(C_4H_2N_2OS)(C_{18}H_{15})$]. For the latter complex the crystal structure shows the coordination of the 2-thiouracilato ligand to gold(I) by its thiol group. Antiproliferative activity assays were performed with the metal complexes and also with the free ligands, 2-thiouracil and 2,4-dithiouracil, silver nitrate (metal salt) and chloridotriphenylphosphinegold(I) precursor complex (Ph_3P-Au-Cl). The results were also compared to doxorubicin. The [Ag_2(dtu)] complex presented no antiproliferative activity, probably due to its lack of solubility. The Ph_3P-Au-tuH complex and its precursor complex, Ph_3P-Au-Cl, showed noticeable antiproliferative profiles. The Ph_3P-Au-tuH complex showed a better activity than doxorubicin over the K562 cell line. Data obtained for the gold(I) complex with 2-thiouracil presented in this section was published in Journal of Molecular Structure 1178 (2019) 169-178.

Studies of the cell death mechanism caused by Ag-5fu and Ph_3P-Au-tuH complexes in ovarian and lung tumor cells

A short introduction to flow cytometry

Flow cytometry is a technique in which it is possible to measure multiple physical characteristics of a single cell simultaneously as the cell flows in suspension. Its working depends on the light scattering features of the cells under investigation, which may be derived, for example, from dyes targeting either extracellular molecules located on the surface or intracellular molecules inside the cell. In this way, flow cytometry can measure the fluorescence characteristics of a single cell in a fluid stream when they pass through a light source [146].

The principle of flow cytometry is related to light scattering and fluorescence emission, which occurs as light from a laser strikes the moving cells. The fluorescence emission that derives from a fluorescence probe will be proportional to the amount of fluorescent probe bound to the cell or cellular component. Therefore, it is possible to determine the influence of a compound in a cell or on cell components by choosing the appropriate dyes for each of them and using flow cytometry to study the extent of this influence.

Results and Discussion

The noteworthy antiproliferative activities observed for Ag-5fu and Ph_3P-Au-tuH complexes led to further *in vitro* studies of these compounds. In this way, different cell lines were chosen to be studied for each compound. For the Ag-5fu complex the NCI/ADR-RES cells (multidrug resistant ovarian tumor cells) were chosen, because the Ag-5fu complex was shown to be more active than cisplatin over this cell line, showing that Ag-5fu may overcome the resistance mechanism. Also, 5fu and $AgNO_3$ were used as controls, in order to understand the role of each one of them in the activity of the complex. Now, for the Ph_3P-Au-tuH complex the NCI-H460 cells (lung tumor cells, non-small) were chosen and compared to Ph_3P-Au-Cl, because the Ph_3P-Au-tuH complex was shown to be more active than Ph_3P-Au-Cl over this cell line, and also because the results could be further compared to *in vivo* lung tumor models, as a possible further investigation. Free 2-thiouracil was not tested, because it did not present antiproliferative activity in the highest tested concentration.

The compounds were evaluated by the colony formation capacity and flow cytometry assays to analyze cell cycle and cell death induction [phosphatidylserine residues (PS) exposition, multicaspases activation, production of reactive oxygen species (ROS) and mitochondrial membrane depolarization].

For Ag-5fu preliminary studies of interaction with plasmid DNA by gel electrophoresis were done and are also presented.

Gel electrophoresis assay

In order to investigate the mechanism of action of the Ag-5fu complex, preliminary studies about the interaction of this compound with biomolecules such as DNA are of interest. Considering the differences in cell growth profiles observed in the antiproliferative assays, the mechanism of action of the Ag-5fu complex may differ from that of cisplatin. As already mentioned, the main target of cisplatin is DNA, where Pt(II) ions form covalent bonds with nitrogen bases [46]. Therefore, a preliminary gel electrophoresis assay was performed to evaluate a possible interaction of Ag-5fu with DNA [48,49].

$K_2[PdCl_4]$, $K_2[PtCl_4]$, $AgNO_3$, 5fu and Ag-5fu were mixed and incubated with pIRES DNA plasmid (pIRES: internal ribosome entry site plasmid). Pure pIRES DNA plasmid was used as control and $K_2[PdCl_4]$ and $K_2[PtCl_4]$ were controls of compounds that interact with DNA. DNA Ladder was used as a weight marker, based on the number of nucleotide base pairs (bp). The compounds were electrophoresed in agarose gel and the results are presented in Figure 33.

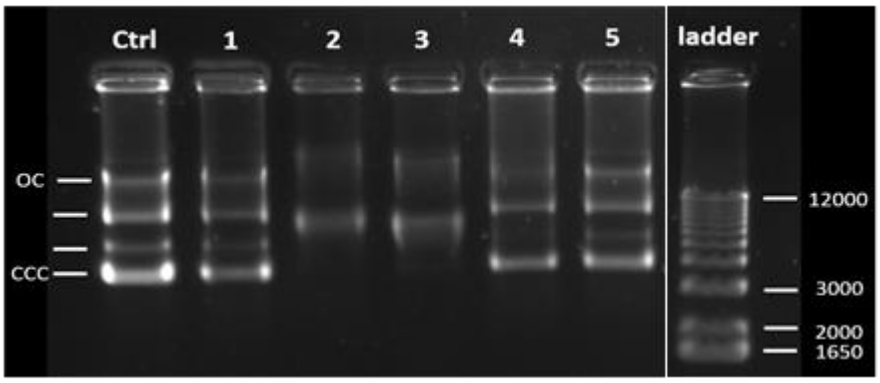

Figure 33. Electrophoresis agarose gel. Control (Ctrl) is pure pIRES DNA plasmid, (1) $AgNO_3$, (2) $K_2[PdCl_4]$, (3) $K_2[PtCl_4]$, (4) 5fu, (5) Ag-5fu. OC is the open circular form of the plasmid DNA (slower migration) and CCC is the supercoil form (faster migration). Ladder shows bands of 12000 bp to 1650 bp. Separate parts of the figure are from the same gel.

The pIRES DNA plasmid presents four different forms (control, Figure 33) in the electrophoresis agarose gel. The form which presents the slower migration is the open circular form (OC) and the form which presents the faster migration is the supercoil form (CCC). We can observe that 5fu has a minor interaction with the DNA in the open circular form (absence of the band, Figure 33), when compared to $K_2[PdCl_4]$ and $K_2[PtCl_4]$, while $AgNO_3$ and Ag-5fu do not seem to interact with DNA, due to the presence of all four bands (same pattern as the control). The observed results suggest

that the mechanism of antiproliferative action of the complex is dissimilar from that of cisplatin and does not involve interaction with DNA.

Cell cycle arrest

We investigated the influence of Ag-5fu and its precursors (5fu and $AgNO_3$) on NCI-ADR/RES cell cycle, and the influence of Ph_3P-Au-tuH and Ph_3P-Au-Cl on NCI-H460 cell cycle. Divided in two steps (interphase and mitosis), the cell cycle comprises the molecular events that occur since the formation of a cell until its division into new cells. While in the interphase cell grows and prepares itself for a new division (divided into G1, S and G2 phases), mitosis is the proper cell division process, characterized by the formation of new cells (division of both nuclei and cytoplasm) [147]. According to literature, the doubling time (i.e. the period required to complete one cell cycle) varies depending on the cell line, and for NCI/ADR-RES it is reported as 34 h, while for NCI-H460 it is of 17.8 h [148]. The most used method to cell cycle evaluation is flow cytometry analysis of the DNA content. By using a fluorescent DNA dye, for example propidium iodide (PI), it is possible to observe three different cell subpopulations named G1 (DNA = 2n), S (2n < DNA < 4n) and G2/M (DNA = 4n) phases according to the DNA quantity [149]. Figure 34 shows the results on NCI/ADR-RES cell cycle after treatment with Ag-5fu, 5fu and $AgNO_3$ (histograms are in Figures A2 to A4, Appendix), while Figure 35 shows the results on NCI-H460 cell cycle after treatment with Ph_3P-Au-tuH and Ph_3P-Au-Cl (histograms are in Figures A5 to A6, Appendix).

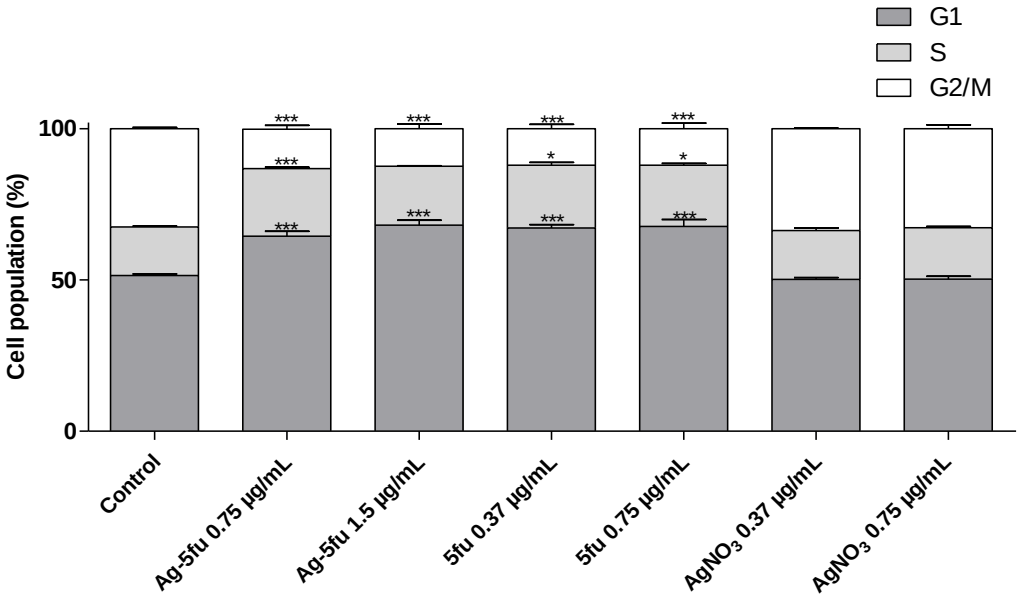

Figure 34. Influence of Ag-5fu, 5fu and $AgNO_3$ on NCI/ADR-RES cell cycle. NCI/ADR-RES cells were treated for 36 h with Ag-5fu (0.75 and 1.5 µg mL^{-1}), 5fu (0.37 and 0.75 µg mL^{-1}) or $AgNO_3$ (0.37 and 0.75 µg mL^{-1}). Cell subpopulation (%) after propidium iodide staining: G1 (DNA = 2n), S (2n < DNA < 4n) and G2/M (DNA = 4n) phases. Statistical analysis: 2way-ANOVA followed by Bonferroni test (*$p < 0.05$, **$p < 0.01$ and ***$p < 0.001$, relative to untreated cells).

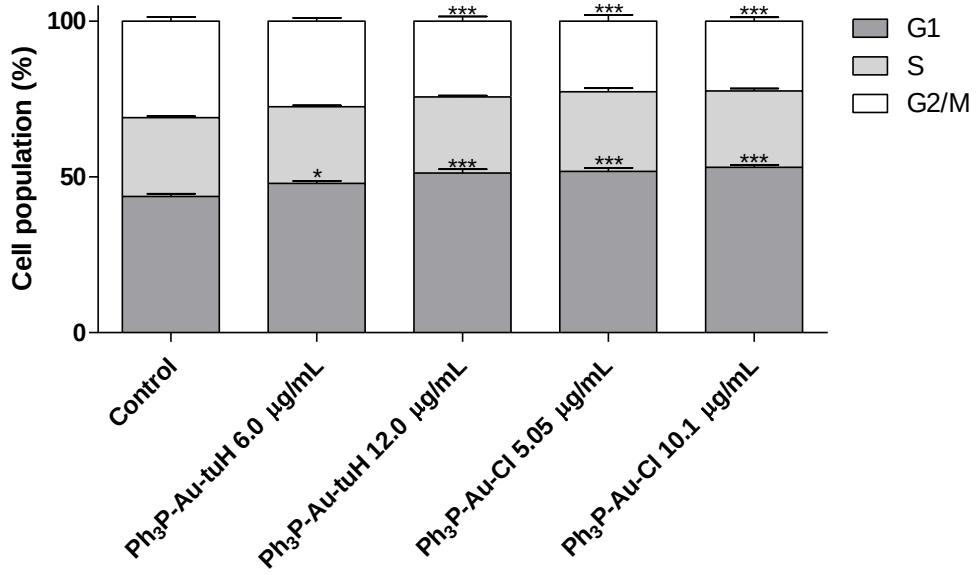

Figure 35. Influence of Ph_3P-Au-tuH and Ph_3P-Au-Cl on NCI-H460 cell cycle. NCI-H460 cells were treated for 18 h with Ph_3P-Au-tuH (6.0 and 12.0 µg mL^{-1}), or Ph_3P-Au-Cl (5.05 and 10.1 µg mL^{-1}). Cell subpopulation (%) after propidium iodide staining: G1 (DNA = 2n), S (2n < DNA < 4n) and G2/M (DNA = 4n) phases. Statistical analysis: 2way-ANOVA followed by Bonferroni test (*$p < 0.05$, and ***$p < 0.001$, relative to untreated cells).

Regarding NCI/ADR-RES cells, (Figure 34) when compared to the untreated ones (control), both Ag-5fu and 5fu promoted cell cycle arrest at G1 phase (G1 = 51% for untreated cells, 66% for Ag-5fu and 67% for 5fu-treated cells, respectively), independent on the concentration. No significant changes induced by $AgNO_3$ were observed, independent on the concentration (G1 = 50%). According to the literature, DNA damage caused by 5fu can activate the p53 protein [106,150], which influences proliferation by acting predominantly in the G1 phase of cell cycle progression [151], as already observed on smooth muscle cells treated with 5fu [152]. The results on cell cycle (Figure 34) may suggest that the effect of Ag-5fu on NCI/ADR-RES cells could be due to 5fu, since both compounds present the same pattern of cell cycle arresting, without participation of silver(I) ions.

Now, for NCI-H460 cells, both Ph_3P-Au-tuH and Ph_3P-Au-Cl caused arrest at G1 phase (G1 = 44% for untreated cells, 48% for Ph_3P-Au-tuH and 52% for Ph_3P-Au-Cl), and for Ph_3P-Au-tuH the effect was greater at the highest concentration. It seems here that the phosphinegold(I) moiety is causing the effect on NCI-H460 cell cycle.

Colony formation assay

To expand the knowledge about how the compounds are acting on cells, we evaluated their influence on the colony forming ability. The colony formation assay determines the ability of one cell to proliferate, retaining its reproductive ability to form a colony after ceasing the sample exposition. By counting the aggregates of at least 50 cells (named one colony), this assay allowed to infer whether the sample promotes reversible or irreversible effects on cell proliferation [128,153,154]. Figure 36 shows the survival fraction of NCI/ADR-RES cells for cells treated with Ag-5fu, 5fu, and $AgNO_3$ (number of counted colonies is in Table A3, Appendix; Figures A7 to A9 show pictures of the stained plates).

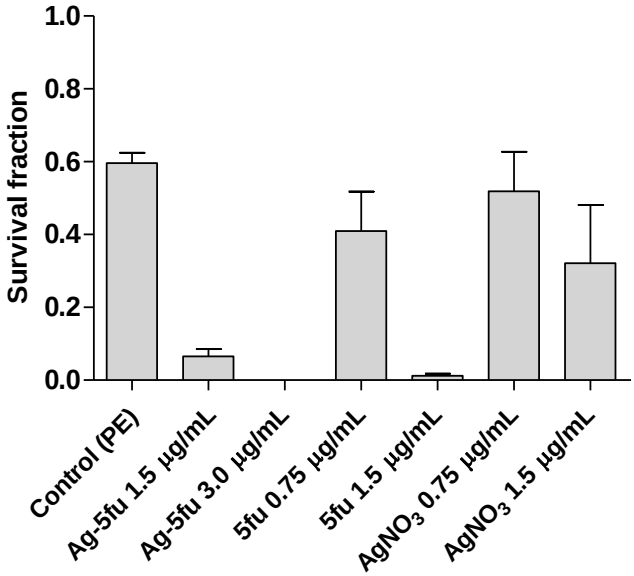

Figure 36. Survival fraction of NCI/ADR-RES cells for cells treated with Ag-5fu, 5fu, and $AgNO_3$ in the concentration range of 0.75 – 3.0 µg mL^{-1}. Control shows the plating efficiency (PE).

Considering the NCI/ADR-RES doubling time (34 h), even after about 8 cell cycles, Ag-5fu was able to totally inhibit colony formation [Survival Fraction (SF) = 6.5 and 0% at 1.5 and 3.0 µg mL^{-1}, respectively] after one single exposition, being the effect dependent on complex concentration. Besides, 5fu almost totally inhibited colony formation only at the higher concentration (SF = 41 and 1.2% at concentrations 0.75 and 1.5 µg mL^{-1}, respectively) (Figure 35), while $AgNO_3$ partially inhibited NCI/ADR-RES colony formation (SF = 52 and 32% at 0.75 and 1.5 µg mL^{-1}, respectively).

Figure 37 shows the survival fraction of NCI-H460 cells for cells treated with Ph_3P-Au-tuH and Ph_3P-Au-Cl (number of counted colonies is in Table A4, Appendix; Figures A10 and A11 show pictures of the stained plates).

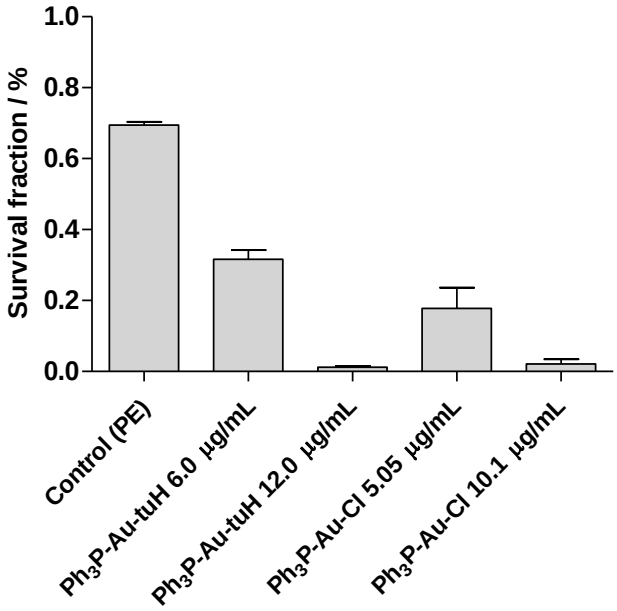

Figure 37. Survival fraction of NCI-H460 cells for cells treated with Ph_3P-Au-tuH and Ph_3P-Au-Cl in the concentration range of 6.0 – 12.0 µg mL^{-1}. Control shows the plating efficiency (PE).

Considering the NCI-H460 doubling time (17.8 h), even after about 8 cell cycles, Ph_3P-Au-tuH was able to almost totally inhibit colony formation after one single exposition only at the highest concentration (SF = 32% and 1% at 6.0 and 12.0 µg mL^{-1}, respectively). Ph_3P-Au-Cl presented the same pattern of effect (SF = 18% and 2% at concentrations 5.05 and 10.1 µg mL^{-1}, respectively), however being more potent than Ph_3P-Au-tuH at the lowest concentration.

The results indicate that the antiproliferative effect of Ag-5fu, Ph_3P-Au-tuH and Ph_3P-Au-Cl cannot be reverted by cells after complex removal. Moreover, for Ag-5fu, considering the effect of both precursors (5fu and $AgNO_3$), the inhibition of colony formation promoted by Ag-5fu could be partially explained by a combination effect of silver(I) ions and 5fu. Considering the results of cell cycle arrest and of colony formation, it is possible to infer that the increasing survival of the NCI/ADR-RES cells observed at G1 phase after Ag-5fu or 5fu treatments, and of the NCI-H460 cells at G1 phase after treatment with Ph_3P-Au-tuH or Ph_3P-Au-Cl, may actually be cells entering G0 phase, since cell replication was not observed in the colony formation assay. Therefore, we started to evaluate whether these compounds promoted other alterations triggering the cell death.

Mitochondrial membrane depolarization – Rhodamine-123 assay

The depolarization of the mitochondrial membrane is an indicative of early stages of cell death [155]. One strategy to evaluate this event by flow cytometry is using the fluorescent probe Rhodamine 123 (Rh123). When mitochondrial membranes show the normal polarization, Rh123 accumulates within mitochondria, while the depolarization process results in loss of Rh123 with consequent decrease of intracellular fluorescence [156,157]. For the interpretation of the obtained results, cells were divided into three subpopulations according to the respective fluorescence intensities as M1 (10^0-10^1, total depolarization), M2 (10^1-10^3, partial/transient depolarization) and M3 (10^3-10^4, normal polarization).

Figure 38 shows cell population of NCI/ADR-RES cells stained with Rh123 after 1 h, 2 h and 3 h of treatment with Ag-5fu, 5fu and $AgNO_3$. After 1h-exposition, only $AgNO_3$ promoted a significant increase in M2 population (91%) when compared to untreated cells (83%). As the exposure time increased up to 3 h, Ag-5fu promoted M1 population increasing (M1 = 25 and 28% for Ag-5fu-treated cells after 2 h and 3 h, respectively) followed by M2 subpopulation decreasing (M2 = 78 and 53% for Ag-5fu-treated cells after 2 h and 3 h, respectively) in comparison to untreated cells (M1 = 13 and 10%, M2 = 91 and 82% for untreated cells after 2 h and 3 h, respectively). In addition, 5fu did not promote any change in subpopulation distribution.

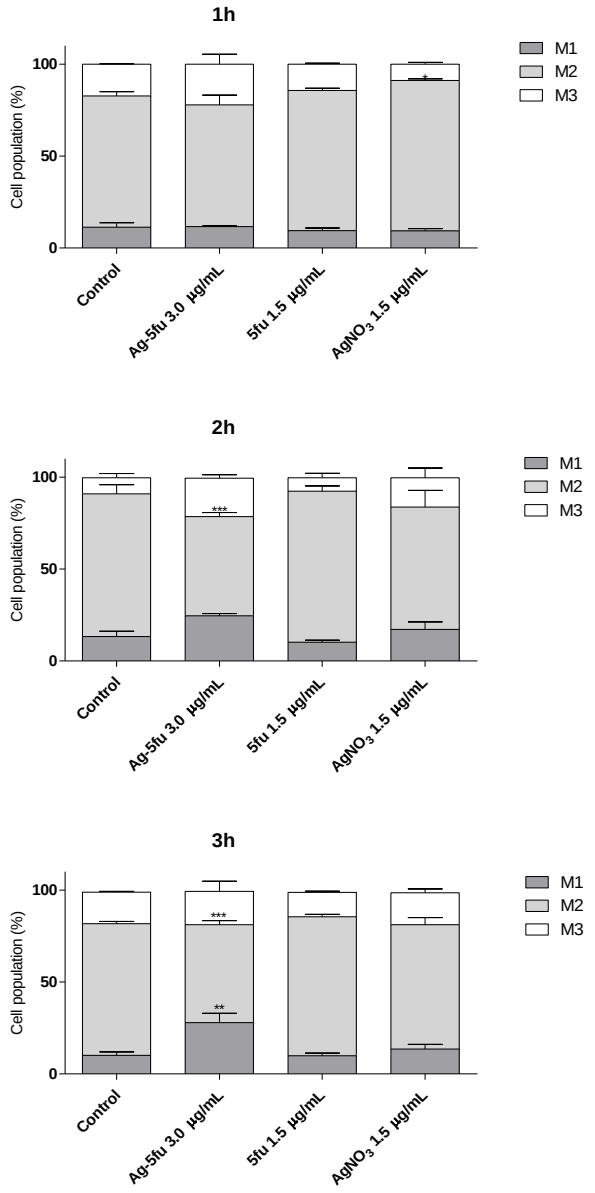

Figure 38. Cell population of NCI/ADR-RES stained with Rh123. NCI/ADR-RES cells were treated for 1 h, 2 h and 3 h with Ag-5fu (3.0 µg mL^{-1}), 5fu (1.5 µg mL^{-1}) and $AgNO_3$ (1.5 µg mL^{-1}). Cell subpopulation (%) in M1, M2 and M3 after Rh123 staining. M1 is the fluorescence intensity between 10^0-10^1 (total depolarization), while M2 is the fluorescence intensity between 10^1-10^3 (partial/transient depolarization), and M3 is the fluorescence intensity between 10^3-10^4 (normal polarization). Statistical analysis: 2way-ANOVA followed by Bonferroni test (*$p < 0.05$, **$p < 0.01$, ***$p < 0.001$, relative to untreated cells).

The obtained results (Figure 38) were suggestive to the disruption of the mitochondrial membrane potential of NCI/ADR-RES cells by Ag-5fu. However, one limitation of this protocol regards on the presence of P-glycoprotein (P-gp) in the chosen cell line. The P-glycoprotein promotes drug efflux from the intracellular environment and Rh123 can be used to evaluate this characteristic (a decrease in the intracellular fluorescence is proportional to P-gp activation) [158]. Considering that NCI/ADR-RES cells express multiple drug resistance because of the super expression of P-gp [159,160], a reduction in the fluorescent intensity after Rh123 staining may indicate the Ag-5fu-induced mitochondrial membrane depolarization or just the P-gp activity promoting Rh123 and drug efflux. To clarify this question and considering that NCI/ADR-RES cells derive from OVCAR-8 cells, which do not super express P-gp [159], the Rh123 assay was performed on OVCAR-8 cells after treatment with Ag-5fu (Figure 39).

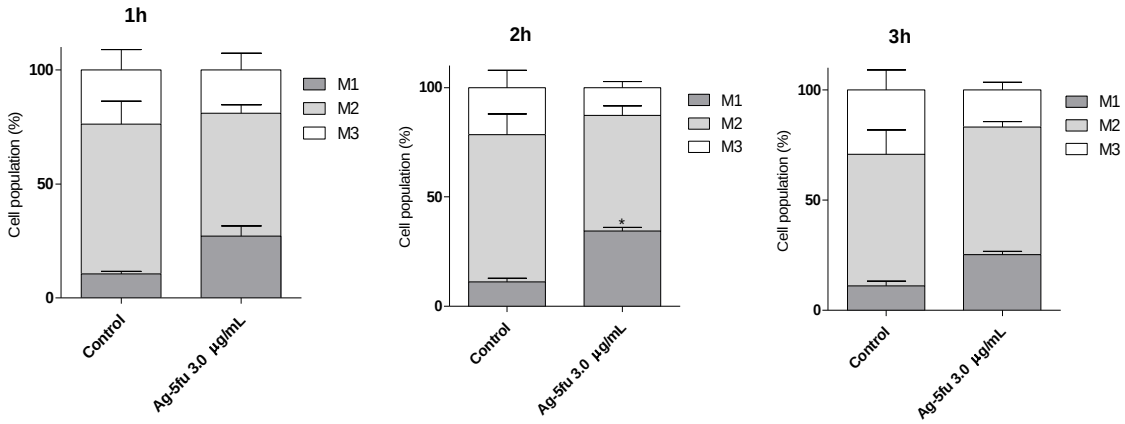

Figure 39. Cell population of OVCAR-8 stained with Rh123. OVCAR-8 cells were treated for 1 h, 2 h and 3 h with Ag-5fu (3.0 µg mL^{-1}). Cell subpopulation (%) in M1, M2 and M3 after Rh123 staining. M1 is the fluorescence intensity between 10^0-10^1 (total depolarization), while M2 is the fluorescence intensity between 10^1-10^3 (partial/transient depolarization), and M3 is the fluorescence intensity between 10^3-10^4 (normal polarization). Statistical analysis: 2way-ANOVA followed by Bonferroni test (*$p < 0.05$, **$p < 0.01$, ***$p < 0.001$, relative to untreated cells).

Ag-5fu was able to promote depolarization of the mitochondrial membrane in OVCAR-8 cells, as observed by M1 subpopulation increasing after 2h-treatment (34% of cells treated with Ag-5fu compared to 11% of untreated cells). This result corroborates the hypothesis of Ag-5fu-induced mitochondrial membrane depolarization in NCI/ADR-RES cells rather than just P-gp-induced Rh123 efflux. Depolarization of the mitochondrial membrane was reported before for silver(I) complexes [161,162]. However, in a different way from the other assays here reported, only the Ag-5fu complex promoted the depolarization, which was not observed for the free ligand or the free metal ion. It seems that the combination of ligand (5fu) and silver(I) plays an important role for mitochondrial membrane depolarization of NCI/ADR-RES cells.

For NCI-H460 cells and Ph_3P-Au-tuH and Ph_3P-Au-Cl compounds, the Rh123 assay was also performed and, in this case, it will show loss of Rh123 from the mitochondria if depolarization occurs, with a decrease of intracellular fluorescence. P-gp is not super expressed in this cell line, therefore not evaluated here. Figure 40 shows cell population of NCI-H460 cells stained with Rh123 after 1 h, 2 h and 3 h of treatment with Ph_3P-Au-tuH and Ph_3P-Au-Cl.

It is interesting that only Ph_3P-Au-tuH caused depolarization of the mitochondrial membrane within 1 h (37% of cells treated with Ph_3P-Au-tuH compared to 24% of untreated cells) and 2h (33% of cells treated with Ph_3P-Au-tuH compared to 23% of untreated cells) of treatment, while Ph_3P-Au-Cl did not present a statistical relevant effect. Here, it may be that 2-thiouracil plays a role in mitochondrial membrane depolarization.

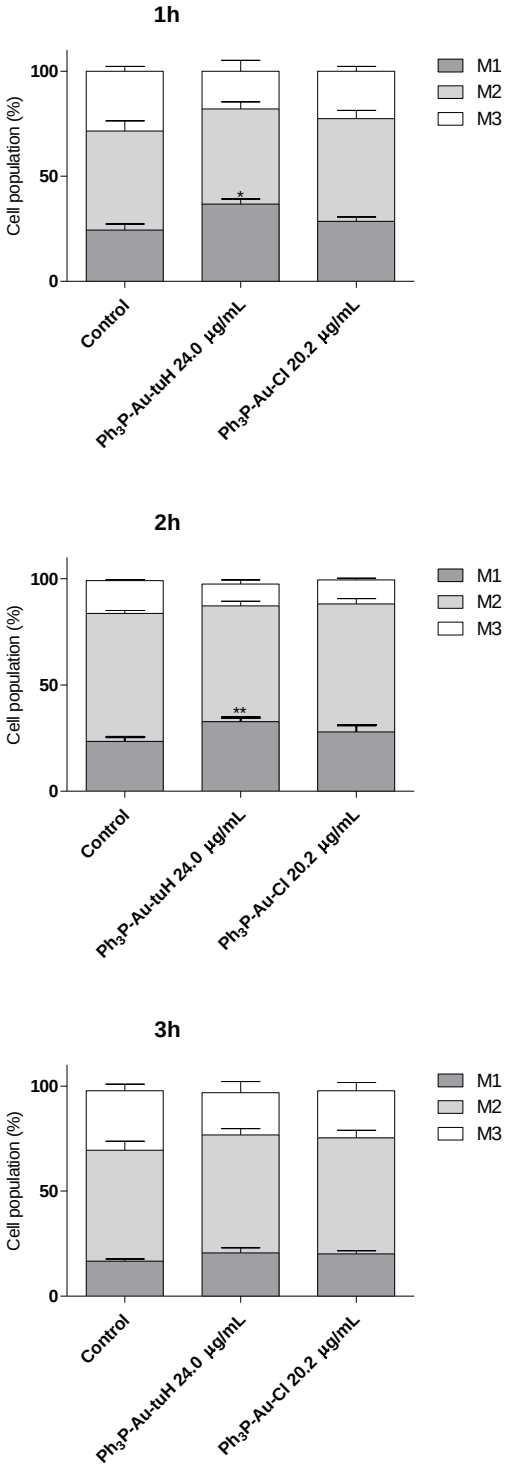

Figure 40. Cell population of NCI-H460 stained with Rh123. NCI-H460 cells were treated for 1 h, 2 h and 3 h with Ph_3P-Au-tuH (24.0 µg mL^{-1}) and Ph_3P-Au-Cl (20.2 µg mL^{-1}). Cell subpopulation (%) in M1, M2 and M3 after Rh123 staining. M1 is the fluorescence intensity between 10^0-10^1 (total depolarization), while M2 is the fluorescence intensity between 10^1-10^3 (partial/transient depolarization), and M3 is the fluorescence intensity between 10^3-10^4 (normal polarization). Statistical analysis: 2way-ANOVA followed by Bonferroni test (*$p < 0.05$, **$p < 0.01$, relative to untreated cells).

Phosphatidylserine externalization – Nexin assay

There are many different mechanisms of cell death [163]. Apoptosis is the cell death mechanism that occurs naturally when cells get old and start developing problems. It is an active and regulated process of cellular dismantling that avoids eliciting inflammation [164]. It is important to notice that cancer cells do not trigger cell death, so they proliferate indefinitely. Considering this, one desired feature of an anticancer compound is to induce cell death through modulating an endogenous "suicide" mechanism, such as apoptosis or autophagy [165]. Phosphatidylserine (PS) is a phospholipid contained in the inner side of the cell membrane, and the exposure or externalization of PS to the outer side is a cellular event involved in some cell death mechanisms, such as apoptosis [156,166]. This characteristic allowed the development of assays to evaluate mechanisms of regulated cell death by assessing PS externalization. One strategy is based on the high affinity of Annexin-V for PS residues. As Annexin-V is not fluorescent by itself, it is chemically coupled to a fluorescent probe. Moreover, to differentiate whether PS residues were in the inner or in the outer side of the cell membrane, a second dye, such as 7-aminoactinomycin D (7-AAD), with low permeability through unimpaired plasmatic membrane and high DNA affinity, is used to evaluate the membrane integrity [167].

As a dynamic process, we evaluated the PS externalization in NCI/ADR-RES cells induced by Ag-5fu, 5fu and $AgNO_3$ after different exposition times (8 h, 14 h, 18 h and 24 h), and in NCI-H460 cells induced by Ph_3P-Au-tuH and Ph_3P-Au-Cl (18 h and 24 h). Figure 41 shows phosphatidylserine externalization of NCI/ADR-RES after 18 h of treatment with Ag-5fu, 5fu and $AgNO_3$. For 8 h, 14 h and 24 h, see Figures A12 to A14 in Appendix. Dot-plot graphs for 18 h of treatment is in Figure A15, Appendix.

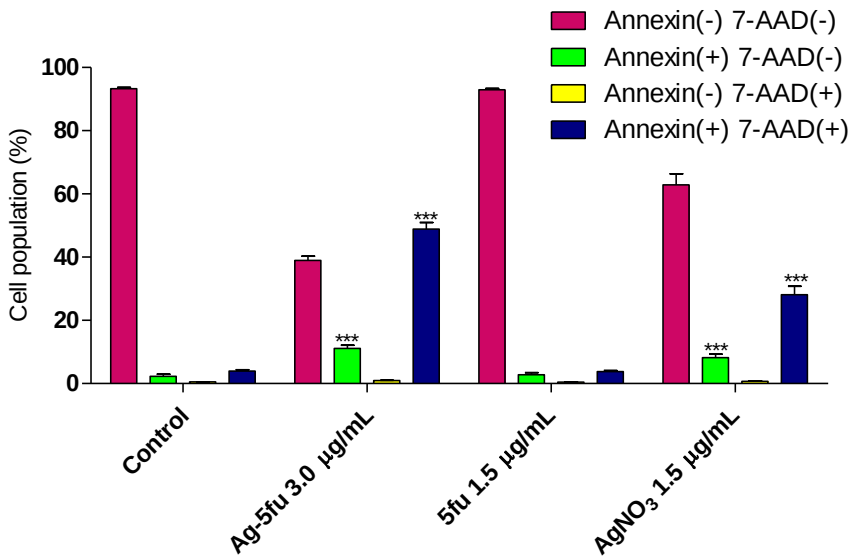

Figure 41. Influence of Ag-5fu, 5fu, and $AgNO_3$ on phosphatidylserine externalization. NCI/ADR-RES cells were treated for 18h with Ag-5fu (3.0 µg mL^{-1}), 5fu (1.5 µg mL^{-1}) or $AgNO_3$ (1.5 µg mL^{-1}). Cell subpopulation (%) after Annexin-V and 7-AAD staining. Statistical analysis: 2way-ANOVA followed by Bonferroni test (***$p < 0.001$, relative to untreated cells).

The obtained results show that silver(I) ions and Ag-5fu induced PS externalization on NCI/ADR-RES cells [Annexin-V(+)/7-AAD(-) = 2% in untreated cells, 8 and 11% in cells treated with $AgNO_3$ and Ag-5fu, respectively]. Also, the PS externalization effect was greater ($p < 0.001$) for Ag-5fu (49%) when compared to $AgNO_3$ (28%) after 18 h for cells with both PS externalization and loss of membrane integrity [Annexin-V(+)/7-AAD(+)]. Moreover, 5fu did not alter the PS externalization profile observed for untreated NCI/ADR-RES cells after 18h-treatment.

After 18h-exposition, both Ag-5fu and $AgNO_3$ induced significant increasing on the subpopulations showing PS externalization, with or without loss of membrane integrity, in comparison to untreated cells (Figure 41). The obtained results suggest that the silver(I) ions present in the metal complex contributed to Ag-5fu-induced PS externalization on NCI/ADR-RES cells. According to the literature, 24h-exposition to $AgNO_3$ (10 µM) induced programed cell death in *Vitis vinifera* cells [168]. Depending on the cell line and the exposition period, 5fu may (as in colon carcinoma cells after 1 – 3 days of treatment) or may not (as in smooth muscle cells after 24h-exposition) cause PS externalization apoptosis [152].

Figure 42 shows phosphatidylserine externalization of NCI-H460 cells after 18 h of treatment with Ph_3P-Au-tuH and Ph_3P-Au-Cl. For 24 h exposition time, see Figure A16 in Appendix, and for dot-plot graphs of 18 h of treatment see Figure A17.

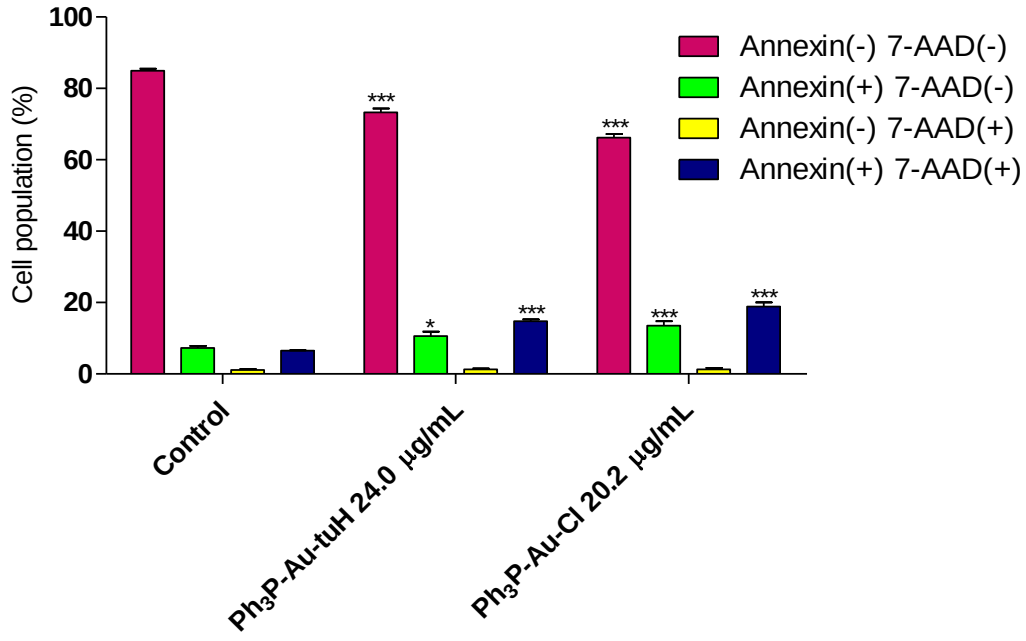

Figure 42. Influence of Ph_3P-Au-tuH and Ph_3P-Au-Cl on phosphatidylserine externalization. NCI-H460 cells were treated for 18 h with Ph_3P-Au-tuH (24.0 µg mL^{-1}) or Ph_3P-Au-Cl (20.2 µg mL^{-1}). Cell subpopulation (%) after Annexin-V and 7-AAD staining. Statistical analysis: 2way-ANOVA followed by Bonferroni test (*$p < 0.05$ and ***$p < 0.001$, relative to untreated cells).

Both Ph_3P-Au-tuH and Ph_3P-Au-Cl compounds induced PS externalization in NCI-H460 cells after 18 h of treatment [Annexin-V(+)/7-AAD(-) = 7% in untreated cells, 11 and 14% in cells treated with Ph_3P-Au-tuH and Ph_3P-Au-Cl, respectively]. The effect was greater ($P < 0.05$) for cells treated with Ph_3P-Au-Cl with both PS externalization and loss of membrane integrity [Annexin-V(+)/7-AAD(+) = 6% in untreated cells, 15 and 19% in cells treated with Ph_3P-Au-tuH and Ph_3P-Au-Cl, respectively].

Detection of activated caspases

As suggested by PS externalization, it seems that the compounds are inducing cell death in the NCI cells by apoptosis. This mechanism of regulated cell death begins with cellular signalization in the cytosol mediated by a group of proteases called caspases, which are triggered in response to pro-apoptotic signals. Once activated, caspases cleave protein substrates leading to the eventual dismantling of the cell, as cytosol condensation and nuclear membrane disintegration. Caspases can be divided into "initiators", which regulate apoptosis upstream (caspases 8, 9, and 10) and "effectors", which are responsible for proteolytic cleavages that lead to cell disassembly (caspases 3, 6, and 7) [169]. To evaluate the multicaspases activation (initiators and effectors) we choose the method based on the

unspecific caspase inhibitor SR-VAD-FMK dye (SR: sulforhodamine B; VAD: trimer Val-Ala-Asp; FMK: fluoromethylketone) [170] that binds covalently to active caspases. Once again, 7-AAD was used as an indicator of membrane integrity [156].

Figure 43 shows the caspases activation of NCI/ADR-RES after 17 h of treatment with Ag-5fu, 5fu and $AgNO_3$. Dot-plot graphs are in Figure A18, Appendix.

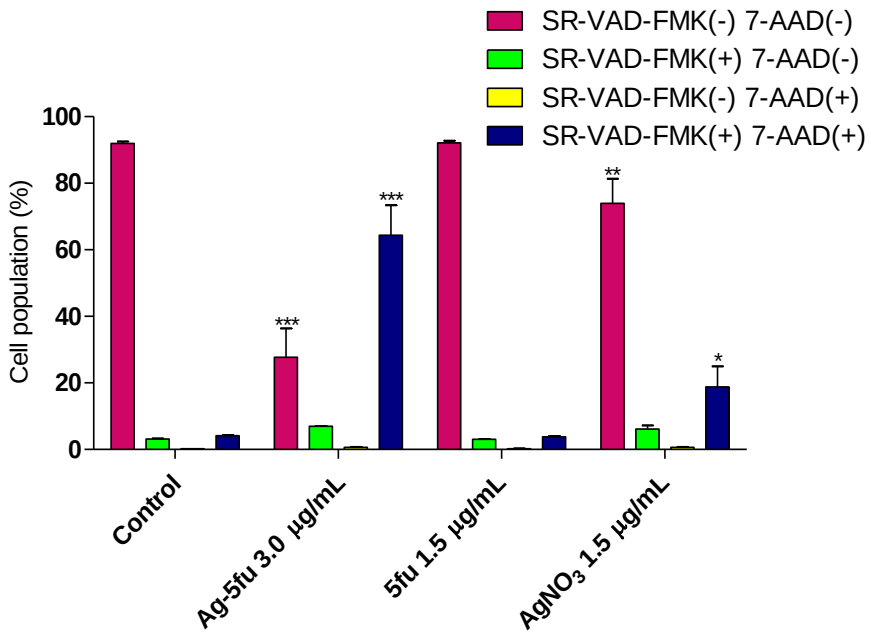

Figure 43. Influence of Ag-5fu, 5fu, and $AgNO_3$ on caspases activation. NCI/ADR-RES cells were treated for 17h with Ag-5fu (3.0 µg mL^{-1}), 5fu (1.5 µg mL^{-1}) and $AgNO_3$ (1.5 µg mL^{-1}). Cell subpopulation (%) after SR-VAD-FMK and 7-AAD staining. Statistical analysis: 2way-ANOVA followed by Bonferroni test (*$p < 0.05$, **$p < 0.01$, ***$p < 0.001$, relative to untreated cells).

Ag-5fu and $AgNO_3$ promoted significant reduction on NCI/ADR-RES cells subpopulation without caspase activation and loss of membrane integrity [SR-VAD-FMK (-)/7-AAD (-) = 92, 74 and 28%, for untreated cells, $AgNO_3$ and Ag-5fu treatments, respectively). Besides, both Ag-5fu and $AgNO_3$ increased NCI/ADR-RES cell subpopulation with both caspase activation and loss of membrane integrity after 17h-exposition [SR-VAD-FMK (+)/7-AAD (+) = 4, 19 and 64% for untreated cells, $AgNO_3$ and Ag-5fu treatments, respectively]. As expected, 5fu did not promote caspases activation on NCI/ADR-RES cells after 17 h of treatment. In agreement with the PS externalization results, Ag-5fu and $AgNO_3$ promoted significant reduction on NCI/ADR-RES cells subpopulation without caspase activation and loss of membrane integrity [SR-VAD-FMK (-)/7-AAD (-)]. Besides, both Ag-5fu and $AgNO_3$ increased NCI/ADR-RES cell subpopulation with both caspase activation and loss of membrane integrity after 17 h-exposition [SR-VAD-FMK (+)/7-AAD (+)]. As observed in colony formation and

PS externalization assays, the caspase activation by Ag-5fu was much more intense than that promoted by $AgNO_3$ (Figure 43). Furthermore, the loss of membrane integrity occurred almost simultaneously with PS externalization and caspases activation. These characteristics reinforce the suggestion that Ag-5fu might be inducing apoptosis on NCI/ADR-RES cells.

Figure 44 shows the caspases activation of NCI-H460 cells after 18 h of treatment with Ph_3P-Au-tuH and Ph_3P-Au-Cl. Dot-plot graphs are in Figure A19, Appendix.

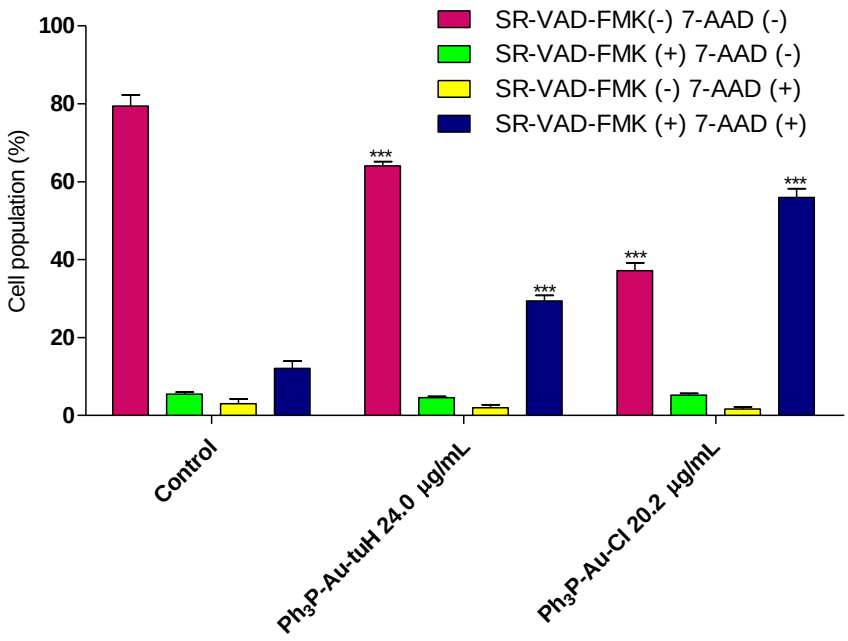

Figure 44. Influence of Ph_3P-Au-tuH and Ph_3P-Au-Cl on caspases activation. NCI-H460 cells were treated for 18 h with Ph_3P-Au-tuH (24.0 µg mL^{-1}) and Ph_3P-Au-Cl (20.2 µg mL^{-1}). Cell subpopulation (%) after SR-VAD-FMK and 7-AAD staining. Statistical analysis: 2way-ANOVA followed by Bonferroni test (***$p < 0.001$, relative to untreated cells).

Both compounds promoted reduction on NCI-H460 cells subpopulation without caspase activation and loss of membrane integrity [SR-VAD-FMK (-)/7-AAD (-) = 79, 64 and 37%, for untreated cells, Ph_3P-Au-tuH and Ph_3P-Au-Cl, respectively). Also, both increased NCI-H460 cell subpopulation with both caspase activation and loss of membrane integrity after 18h-exposition [SR-VAD-FMK (+)/7-AAD (+) = 12, 29 and 56% for untreated cells, Ph_3P-Au-tuH and Ph_3P-Au-Cl treatments, respectively]. Again, effect was greater ($P < 0.001$) for cells treated with Ph_3P-Au-Cl with both caspases activation and loss of membrane integrity. These results, together with PS externalization, reinforce the suggestion that Ph_3P-Au-tuH and Ph_3P-Au-Cl may be inducing the regulated cell death of NCI-H460 by apoptosis.

Measurement of intracellular oxidants – DCFH-DA assay

Considering the previous experiments (mitochondrial membrane depolarization, PS externalization, caspases activation), it was observed that the metal compounds here evaluated induced cell death in the tested cells by apoptosis. This regulated cell death mechanism can be initialized by two different ways. The extrinsic apoptosis is initiated by extracellular microenvironment perturbations and propagated by caspase activation, while the intrinsic apoptosis can be initiated both by extra or intracellular microenvironment perturbations, and limited by caspase activation [155].

In this context, we evaluated whether Ag-5fu and its precursors 5fu and $AgNO_3$ induce the production of intracellular reactive oxygen species (ROS) as an initiation event of regulated cell death in NCI/ADR-RES cells. The NCI-H460 cells treated with Ph_3P-Au-tuH and Ph_3P-Au-Cl were not evaluated so far. One protocol used to evaluate intracellular ROS generation is based on the probe 2′,7′-dichlorofluorescein diacetate (DCFH-DA) [171]. This probe can readily diffuse into the cells and get deacetylated by intracellular enzymes (esterases) to the non-fluorescent 2,7-dichlorodihydrofluorescein (DCFH). In a proportional way, DCFH is oxidized by intracellular hydrogen peroxide into the highly fluorescent 2,7-dichlorofluorescein (DCF) [156,172]. In addition, cells treated with hydrogen peroxide were used as a positive control. Based on DCF fluorescence, cells can be divided into two subpopulations of increasing fluorescence, named as M1 (fluorescence intensity between 10^0 and 10^1, non-marked cells), and M2 (fluorescence intensity between 10^1 and 10^4, marked with DCF because of high concentration of intracellular ROS).

Figure 45 shows the intracellular ROS formation in NCI/ADR-RES after 1 h, 2 h and 3 h of treatment with Ag-5fu, 5fu and $AgNO_3$.

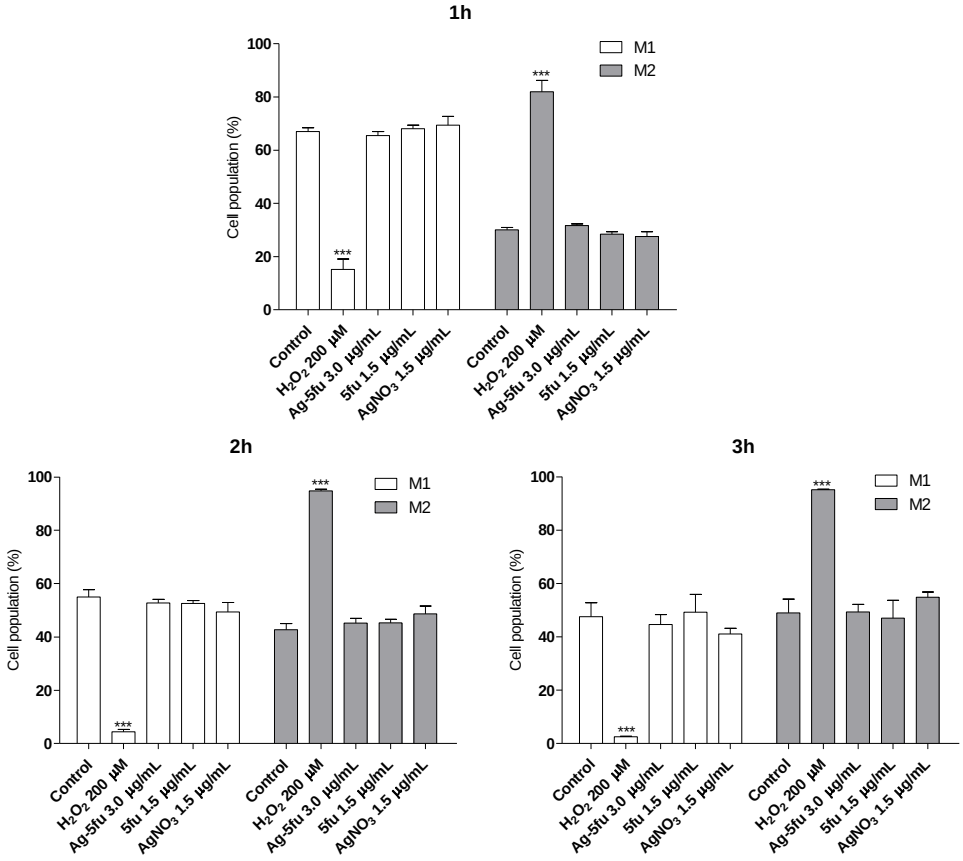

Figure 45. Influence of Ag-5fu, 5fu, and $AgNO_3$ on intracellular ROS formation in NCI/ADR-RES. NCI/ADR-RES cells were treated for 1 h, 2 and 3 h with Ag-5fu (3.0 µg mL^{-1}), 5fu (1.5 µg mL^{-1}), $AgNO_3$ (1.5 µg mL^{-1}) and H_2O_2 (200 µM). Cell subpopulation (%) in M1 and M2 after DCFH-DA staining. M1 is the fluorescence intensity between 10^0 and 10^1 (non-marked cells), while M2 is the fluorescence intensity between 10^1 and 10^4 (marked with DCF). Statistical analysis: 2way-ANOVA followed by Bonferroni test (***$p < 0.001$, relative to untreated cells).

As expected, hydrogen peroxide promoted a significant increase on intracellular ROS concentration as observed by increased M2 subpopulations in comparison to the untreated NCI/ADR-RES cells (M2 = 30 and 82% for untreated cells and H_2O_2-treated cells after 1 h, respectively). In addition, Ag-5fu, 5fu or $AgNO_3$ did not promote any alteration on intracellular ROS concentration (Figure 42). In this way, the observed results suggest that up to 3h-treatment the Ag-5fu complex did not induce intracellular microenvironment perturbations that could initiate the apoptotic mechanism in NCI/ADR-RES cells.

Partial conclusions

The antiproliferative activity of Ag-5fu over multi-resistant ovarian tumor cells (NCI/ADR-RES) was shown to be a combination of the activities of free 5fu and silver(I) ions. The Ag-5fu complex may induce regulated cell death in NCI-ADR/RES cells considering mitochondrial membrane depolarization, PS externalization and multicaspases activation. Moreover, the Ag-5fu complex promoted cell cycle arrest at G1 and inhibited colony formation, indicating that the cancer cells, which do not go through a regulated cell death pathway, lost their proliferation ability. However, the mechanism of cell death could not be completely elucidated. The production of ROS by the complex was not observed, what means that the reason for cell death triggering is still unknown. Moreover, the differentiation between intrinsic and extrinsic apoptosis could not be done.

Furthermore, the Ph_3P-Au-tuH complex showed a higher antiproliferative activity when compared to Ph_3P-Au-Cl over NCI-H460 cells. Both compounds induced regulated cell death in NCI-H460 cells, considering PS externalization and multicaspases activation. Both compounds promoted cell cycle arrest at G1 and inhibited colony formation. For the gold(I) complexes only Ph_3P-Au-tuH showed mitochondrial membrane depolarization. Again, the mechanism of cell death could not be completely elucidated for the same reasons observed for Ag-5fu.

Data for the silver(I) complex with 5-fluorouracil presented in this section was published in Journal of Fluorine Chemistry 195 (2017) 93-101, and Toxicology In Vitro 60 (2019) 359-368.

PART 2: Thiosemicarbazones and their metal complexes

This part of the Thesis was done in a 9-month internship in the Institute of Inorganic Chemistry of the University of Vienna (Vienna, Austria), under the supervision of Ass. Prof. Dr. Christian Kowol (Keppler Group). The biological investigations were done in the Institute for Cancer Research of the Medical University of Vienna, under the supervision of Assoc. Prof. Dr. Petra Heffeter. The internship was funded by OeAD (Austrian service center for European and international mobility and cooperation programmes in the fields of education, science and research).

Introduction

α-(N)-Heterocyclic thiosemicarbazones (TSCs) are an important class of metal chelating agents. They are formed by condensation of carbonyl compounds and thiosemicarbazides, resulting in N,N,S-donor ligands [173]. TSCs, as well as their metal complexes, are widely investigated as antibacterial, antiviral, and anticancer agents [174]. More specifically, concerning the anticancer activities of TSCs, the investigations started in 1956, when Brockman *et al.* observed the antileukemic activity of pyridine-2-carboxaldehyde thiosemicarbazone [175]. At that time, no evidences were found concerning the mode of action of this compound. In 1958, French and Freedlander observed the activity of glyoxal bis-(thiosemicarbazones) against Sarcoma 180 and proposed a possible mechanism of action involving inactivation or translocation of metal ions in the tumor due to chelation by α-(N)-heterocyclic thiosemicarbazones [176].

As a result of the first investigations, many TSCs were studied for their anticancer activities. For example, 2-keto-3-ethoxybutyraldehyde bis(thiosemicarbazone) (KTS) was shown to be active against several tumors in rats [177] and studies showed the dependence of KTS's activity with the presence of metal ions such as copper(II) and zinc(II) in the animals' diet [178]. Further research indicated the antitumor activity of the Cu(II)KTS metal complex, confirming the dependence of the interaction of the TSC with copper as being part of the mechanism of action [179]. Also, the Zn(II)KTS complex presented antitumor activity [180], although being less active than the Cu(II)KTS complex and considered to potentiate the activity of Cu(II)KTS [179]. In addition, Booth and Sartorelli [181] observed a greater assimilation of copper by neoplasic cells treated with Cu(II)KTS than with $CuCl_2$, due to the greater lipid solubility of the metal complex. Besides, they detected at least three distinct copper-induced biochemical lesions by Cu(II)KTS. Moreover, studies by Petering *et al.* with bis(thiosemicarbazonato) copper(II) complexes described a correlation between the cytotoxicity and the reactivity toward thiol groups, with the antitumor activity being related to the reduction of Cu(II) to Cu(I) [182,183].

Regarding the mechanism of action of TSCs, Moore *et al.* showed the interference of 1-formylisoquinoline thiosemicarbazone (IQ-1) with the biosynthesis of DNA [184]. This was found to be due to the inhibition of the ribonucleotide diphosphate reductase (RR) enzyme. The inhibition was thought to be related to the binding of IQ-1 to an iron-containing form of RR or by formation of an iron-complex with IQ-1, which binds to the RR. Further studies by Thelander and Graslund indicated the target of IQ-1 to be the tyrosine free radical of a subunit of RR. It was suggested that the active form of the drug is the iron(II) complex [Fe(II)IQ-1], which reacts with molecular oxygen, leading to reversible destruction of the tyrosine free radical [185]. Regarding the redox properties of iron complexes, the pathway most likely involves the oxidation of Fe(II) to Fe(III), with the release of one electron and inactivation of the tyrosine free radical, followed by the reduction of the Fe(III) complex by cellular thiols [186,187]. Therefore, the redox activity of the metal complexes seems to be correlated with their cytotoxicity [187–189].

The first member of the α-(N)-heterocyclic thiosemicarbazone series to be clinically evaluated was 5-hydroxy-2-formylpyridine thiosemicarbazone (5-HP, Figure 46-a) in 1972 [190]. However, the promising antineoplasic activity found in animals could not be found in humans. 5-HP presented low affinity to the human ribonucleotide reductase (RR) enzyme, with rapid excretion, due to the formation of the *O*-glucuronide conjugate. Therefore, structure-activity relationships investigations were performed in order to develop second generation α-(N)-heterocyclic thiosemicarbazones with greater affinity for the target [187].

Triapine (3-aminopyridine-2-carboxaldehyde thiosemicarbazone; Figure 46-b) was the most investigated TSC, and it was evaluated in several phase I and II clinical trials against a number of different cancers [191]. Despite these numerous clinical trials, Triapine showed only promising activity against advanced leukemia but failed against a variety of solid tumors [192]. The reasons are currently widely unknown and might be due to the inappropriate drug delivery and/or fast excretion/metabolism. Since 2004 Richardson *et al.* developed a series of di-2-pyridylketone thiosemicarbazones [193,194], the DpT series, which are ligands similar to Triapine, but with much higher cytotoxic activity in the nanomolar range due to a terminal dimethylation. Terminal nitrogen dimethylation of α-N-heterocyclic thiosemicarbazones was found to enhance the toxicity of the compounds, and also of their metal complexes [195–197]. Recently, the Richardson group developed a new analog, di-2-pyridilketone 4-cyclohexyl-4-methyl-3-thiosemicarbazone, known as DpC (Figure 46-c) [183,198] which due to its promising antitumor activity and pharmacological characteristics entered phase I clinical trials in 2016 [199].

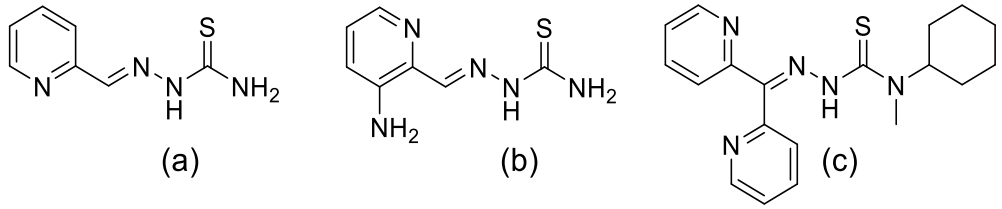

Figure 46. Molecular structures of (a) 5-HP, (b) Triapine and (c) DpC.

More recently, *Cotinga Pharmaceuticals* (formerly *Critical Outcome Technologies Inc.*, Boston, MA, United States) developed a third generation TSC known as COTI-2 (4-(pyridine-2-yl)-N-{[(8E)-5,6,7,8-tetrahydroquinolin-8-ylidene]amino}piperazine-1-carbothiamide; Figure 47) which entered phase I clinical trials for the treatment of gynecologic malignancies in 2017 [200]. It is a small molecule and an anticancer drug candidate, designed using a computational platform, which can be obtained in a three-step synthesis procedure [201,202]. Biological investigations revealed that COTI-2 possesses high efficacy against multiple cancers both *in vitro* and *in vivo*. Additionally, COTI-2 demonstrated a low toxicity profile in mice and better efficacy when compared to standard chemotherapeutic agents, as cetuximab and erlotinib, for example. Regarding the mechanism of action, it was found that COTI-2 activates the caspase signaling cascade, inducing apoptosis in cancer cells [202]. In addition, it was found that COTI-2 is more active in mutant p53 tumors, and it increases intracellular zinc concentrations [203]. This fact shows that COTI-2 may also act as a chelating agent, but different to other thiosemicarbazones.

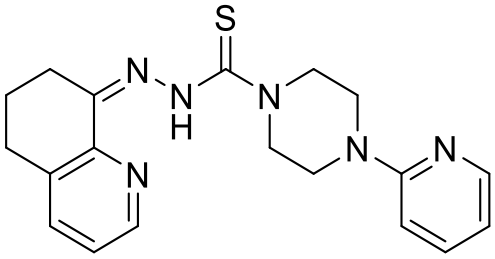

Figure 47. Molecular structure of COTI-2.

Nevertheless, studies about structure-activity relationships of COTI-2 or metal complexes with this molecule have not been reported so far. Therefore, considering the background of α-N-heterocyclic thiosemicarbazones and their importance in metal metabolism, the synthesis of the first metal complexes with COTI-2 are presented, with the biologically relevant ions Fe(III), Cu(II) and Zn(II), which could help elucidate the biological properties of this compound. Also, new COTI-derivatives (COTI-NH_2,

COTI-NMe_2, COTI-Nchexyl, Figure 48) were prepared, and the cytotoxic activities of these compounds were evaluated, in order to try to address structure-activity relationships.

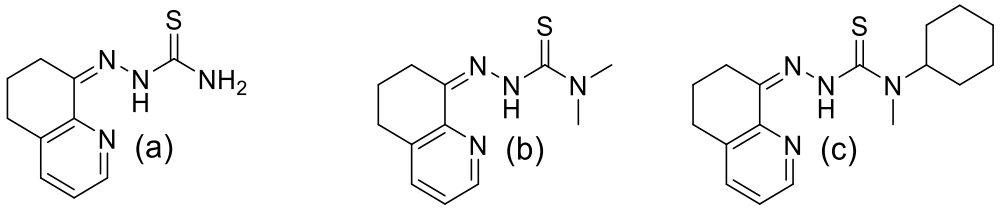

Figure 48. The COTI-derivatives: (a) COTI-NH_2 [2-(6,7-dihydroquinolin-8(5H)-ylidene)hydrazine-1-carbothioamide], (b) COTI-NMe_2 [2-(6,7-dihydroquinolin-8(5H)-ylidene)-N,N-dimethylhydrazine-1-carbothioamide], and (c) COTI-Nchexyl [N-cyclohexyl-2-(6,7-dihydroquinolin-8(5H)-ylidene)-N-methylhydrazine-1-carbothioamide].

Objectives

The objective of the second part of this Thesis was the synthesis, characterization and evaluation of the cytotoxic activities of COTI-2 and new COTI-derivatives, and of Fe(III), Cu(II), and Zn(II) metal complexes with COTI-2.

Materials and Methods

Starting Materials

N-(2-pyridyl)piperazine was purchased from Alfa Aesar; 1,1'-thiocarbonyldiimidazole, hydrazine hydrate, N-methylcyclohexylamine, carbon disulfide, sodium chloroacetate and zinc(II) chloride were purchased from Sigma-Aldrich; 5,6,7,8-tetrahydroquinolin-8-one was purchased from abcr; hydrazinecarbothioamide was purchased from Fluka; 4,4-dimethyl-3-thiosemicarbazide was purchased from TCI; copper(II) chloride dehydrate was purchased from Merck; iron(III) nitrate nonahydrate was purchased from Acros Organics. All reagents were used without further purification.

Equipments

Chemical analyses: Elemental analyses were performed on a Perkin Elmer 2400 CHNS Elemental Analyzer at the Microanalytical Laboratory of the University of Vienna.

Mass spectrometric measurements: Electrospray ionization (ESI) mass spectra were recorded on a Bruker anaZon SL ion trap mass spectrometer in positive mode by direct infusion (COTI-2, COTI-NMe_2, Cu-COTI-2, Zn-COTI-2). High resolution mass spectra were measured on a Bruker maXis UHR ESI time of flight mass spectrometer (COTI-NH_2, COTI-Nchexyl, Fe-COTI-2) [M = metal; HL = protonated ligand; L = deprotonated ligand]. Spectra are shown in Figures A20 to A26 in Appendix.

Nuclear magnetic resonance measurements: One- and two-dimensional ^{1}H-NMR and ^{13}C-NMR spectra were recorded on a Bruker Avance III 600 MHz spectrometer at 298 K. For ^{1}H-NMR spectra the solvent residual peak was taken as internal reference [s = singlet; d = doublet; t = triplet; quint = quintet; dd = doublet of doublets; ddd = doublet of doublet of doublets; br = broad signal; m = multiplet; py = pyridine; compound numbering for NMR can be found in Appendix, Figures A27 to A30]. Spectra for the final products (COTI-2, COTI-derivatives and Zn-COTI-2) are shown in Figures A31 to A47, in Appendix.

Single crystal X-ray diffraction: The X-ray intensity data were measured on a Bruker D8 Venture diffractometer equipped with multilayer monochromator, MoKα for COTI-2 and CuKα for Cu-COTI-2, INCOATEC micro focus sealed tube and Oxford cooling system. The structures were solved by direct methods and refined by full-matrix least-squares techniques. Non-hydrogen atoms were refined with anisotropic displacement parameters. Hydrogen atoms were inserted at calculated positions and refined

with riding model. The following software was used: Bruker SAINT software package [204] using a narrow-frame algorithm for frame integration, SADABS [205] for absorption correction, OLEX2 [206] for structure solution, refinement, molecular diagrams and graphical user-interface, Shelxle [207] for refinement and graphical user-interface SHELXS-2015 [208] for structure solution, SHELXL-2015 [209] for refinement, Platon [210] for symmetry check. Experimental parameters for COTI-2 and Cu-COTI-2 are in Appendix, Table A5.

*Synthesis of N'-(6,7-dihydroquinolin-8(5H)-ylidene-4-(pyridine-2-yl)piperazine-1-carbothiohydrazide (**COTI-2**)*

The compound was prepared in three steps according to the patent US8034815B2 [201].

Synthesis of 1H-imidazol-1-yl-(4-(pyridin-2-yl)piperazin-1-yl)methanethione (1a):

Thiocarbonyldiimidazole (0.89 g, 5.0 mmol, 1eq.) was dissolved in dichloromethane (30 mL) and N-(2-pyridyl)piperazine (762 µL, 5.0 mmol, 1eq.) was added. The solution was stirred for 20 hours and further washed three times with water. The organic phase was dried over magnesium sulphate, which was filtered off, and the solvent was evaporated. The resulting yellow oil of **1a** was dried under vacuum and used in the next step without further purification. Yield: 1.36 g (99%). ^{1}H-NMR (DMSO-d_6): δ = 2.77 (m, 2H, piperazine), 3.38 (m, 2H, piperazine), 6.70 (ddd, 1H, py), 6.84 (d, 1H, py), 7.06 (dd, 1H, imidazole), 7.56 (t, 1H, imidazole), 7.59 (ddd, 1H, py), 8.08 (t, 1H, imidazole), 8.15 (ddd, 1H, py).

Synthesis of 4-(pyridin-2-yl)-piperazine-1-carbothiohydrazide (1b):

The compound **1a** (1.36 g, 5.0 mmol, 1 eq.) was dissolved in ethanol (20 mL) and hydrazine hydrate was added (267 µL, 5.5 mmol, 1.1 eq.). The mixture was stirred under reflux for 2 h, and a white solid of **1b** was formed which was collected by filtration, washed with cold ethanol, dried under vacuum and used in the next step without further purification. Yield: 0.77 g (65%). ^{1}H-NMR (DMSO-d_6): δ = 3.53 (m, 2H, piperazine), 3.85 (m, 2H, piperazine), 4.84 (br, 1H, NH), 6.66 (ddd, 1H, py), 6.83 (d, 1H, py), 7.55 (ddd, 1H, py), 8.12 (ddd, 1H, py), 9.35 (s, 1H, NH_2), 10.23 (s, 1H, NH_2).

Synthesis of N'-(6,7-dihydroquinolin-8(5H)-ylidene-4-(pyridine-2-yl)piperazine-1-carbothiohydrazide (COTI-2):

The compound **1b** (0.77 g, 3.26 mmol, 1 eq.) was suspended in ethanol (25 mL) and 5,6,7,8-tetrahydroquinolin-8-one was added (0.48 g, 3.26 mmol, 1 eq.). The mixture was stirred under reflux for 20 h, resulting in a yellow solid, which was collected by filtration, washed with cold ethanol and

diethyl ether, and dried under vacuum. Yield: 1.01 g (85%). Elemental analysis: Calcd. For $C_{19}H_{22}N_6S$ (%): C, 62.27 ; H, 6.05 ; N, 22.9 ; S, 8.75. Found (%): C, 61.87 ; H, 5.93 ; N, 22.58 ; S, 8.61. MS in ACN/MeOH + 1% H_2O (positive): *m/z* 367.60, $[HL + H]^+$; 389.6, $[HL + Na]^+$. ^{1}H-NMR (DMSO-d_6): Major isomer (91%) δ = 1.98 (quint, 2H, CH_2, H6), 2.90 (t, 2H, CH_2, H7), 3.09 (t, 2H, CH_2, H5), 3.56 (t, 2H, CH_2, H12,13), 4.10 (s, 2H, CH_2, H11,14), 6.66 (dd, 1H, CH, H16), 6.85 (d, 1H, CH, H18), 7.45 (dd, 1H, CH py, H2), 7.56 (ddd, 1H, CH, H17), 7.78 (dd, 1H, CH py, H3), 8.13 (dd, 1H, CH, H19), 8.59 (dd, 1H, CH py, H1), 14.57 (s, 1H, NH, N3). ^{13}C NMR (125.75 MHz, DMSO-d_6): δ = 20.2 (CH_2, C6), 26.3 (CH_2, C5), 27.2 (CH_2, C7), 44.4 (CH_2, C12,13), 47.9 (CH_2, C11,14), 107.1 (C_{py}, C18), 113.1 (C_{py}, C16), 125.4 (C_{py}, C2), 136.4 (C_q, C4), 137.6 (C_{py}, C17), 137.8 (C_{py}, C3), 148.3 (C_q, C9), 148.2 (C_{py}, C1), 143.3 (C=N, C8), 147.6 (C_{py}, C19), 158.8 (C_q, C15), 184.0 (C=S, C10). ^{1}H-NMR (DMSO-d_6): Minor isomer (9%) δ = 15.52 (s, 1H, NH, **N3**). Crystals were obtained from slow evaporation of the mother liquor.

*Synthesis of 2-(6,7-dihydroquinolin-8(5H)-ylidene)hydrazine-1-carbothioamide (**COTI-NH$_2$**)*

This compound was synthesized by a procedure from reference [211] with slight modifications to avoid column chromatography.

Hydrazinecarbothioamide (0.37 g, 4.0 mmol, 1 eq.) was suspended in isopropanol (10 mL), and the mixture was stirred at 80 ºC. Then, 5,6,7,8-tetrahydroquinolin-8-one (0.59 g, 4.0 mmol, 1 eq.) was added, and the mixture was stirred under reflux for 5 h. A pale-yellow solid was formed, which was collected by filtration, washed with cold isopropanol and dried under vacuum. Yield: 0.65 g (74%). Elemental analysis: Calcd. For $C_{10}H_{12}N_4S$ (%): C, 54.52 ; H, 5.49 ; N, 25.43 ; S, 14.55. Found (%): C, 54.53 ; H, 5.48 ; N, 25.35 ; S, 14.59. MS in ACN/MeOH + 1% H_2O (positive): *m/z* 243.0675, $[HL + Na]^+$. ^{1}H NMR (DMSO-d_6): δ = 1.93 (quint, 2H, CH_2, H6), 2.69 (m, 2H, CH_2, H7), 2.91 (t, 2H, CH_2, H5), 7.47 (dd, 1H, CH py, H2), 7.85 (dd, 1H, CH py, H3), 7.96 (s, 1H, NH_2, N4), 8.37 (s, 1H, NH_2, N4), 8.61 (dd, 1H, CH py, H1), 14.28 (s, 1H, NH, N3). ^{13}C NMR (DMSO-d_6): δ = 22.2 (CH_2, C6), 28.9 (CH_2, C5), 33.4 (CH_2, C7), 124.4 (C_{py}, C2), 137.7 (C_q, C4), 138.6 (C_{py}, C3), 139.2 (C=N, C8), 145.9 (C_{py}, C1), 148.7 (C_q, C9), 178.2 (C=S, C10). No isomerization was observed for this compound.

*Synthesis of 2-(6,7-dihydroquinolin-8(5H)-ylidene)-N,N-dimethylhydrazine-1-carbothioamide (**COTI-NMe$_2$**)*

5,6,7,8-Tetrahydroquinolin-8-one (0.37 g, 2.5 mmol, 1 eq.) was dissolved in isopropanol (10 mL) and concentrated HCl (1 drop) was added. Then, 4,4-dimethyl-3-thiosemicarbazide (0.30 g, 2.5 mmol, 1 eq.) was added, and the mixture was stirred under reflux for 5 h. A yellow solid was formed,

which was collected by filtration, washed with cold isopropanol and diethyl ether, and dried under vacuum. Yield: 0.45 g (71%). Elemental analysis: Calcd. For $C_{12}H_{16}N_4S \cdot 0.25H_2O$ (%): C, 57.00 ; H, 6.58 ; N, 22.16 ; S, 12.68. Found (%): C, 57.25 ; H, 6.42 ; N, 25.53 ; S, 12.44. ESI-MS in ACN/MeOH + 1% H_2O (positive): *m/z* 271.20, $[HL + Na]^+$. Major isomer (67%) ^{1}H-NMR (DMSO-d_6): δ = 1.93 (quint, 2H, CH_2, H6), 2.72 (t, 2H, CH_2, H7), 2.91 (t, 2H, CH_2, H5), 3.34 (s, 6H, $N(CH_3)_2$, H11,12), 7.47 (dd, 1H, CH py, H2), 7.88 (dd, 1H, CH py, H3), 8.62 (dd, 1H, CH py, H1), 14.48 (s, 1H, NH, N3). ^{13}C NMR (DMSO-d_6): δ = 22.1 (CH_2, C6), 28.8 (CH_2, C5), 33.4 (CH_2, C7), 40.7 (CH_3, C11,12), 124.1 (C_{py}, C2), 136.0 (C_q, C4), 138.7 (C_{py}, C3), 141.1 (C=N, C8), 145.4 (C_{py} C1), 148.4 (C_q, C9), 179.9 (C=S, C10). Minor isomer (33%) ^{1}H-NMR (DMSO-d_6): δ = 1.96 (quint, 2H, CH_2, H6), 2.88 (t, 2H, CH_2, H7), 3.05 (t, 2H, CH_2, H5), 3.34 (s, 6H, $N(CH_3)_2$, H11,12), 7.42 (dd, 1H, CH py, H2), 7.76 (dd, 1H, CH py, H3), 8.57 (dd, 1H, CH py, H1), 15.51 (s, 1H, NH, N3). ^{13}C NMR (DMSO-d_6): δ = 20.0 (CH_2, C6), 26.3 (CH_2, C5), 27.4 (CH_2, C7), 40.7 (CH_3, C11,12), 125.1 (C_{py}, C2), 137.1 (C_q, C4), 137.7 (C_{py}, C3), 141.6 (C=N, C8), 148.2 (C_{py}, C1), 144.1 (C_q, C9), 184.4 (C=S, C10).

*Synthesis of N-cyclohexyl-2-(6,7-dihydroquinolin-8(5H)-ylidene)-N-methylhydrazine-1-carbothioamide (**COTI-Nchexyl**)*

The first two steps were prepared according to a modified procedure from reference [212].

Synthesis of 2-((cyclohexyl(methyl)carbomothioyl)thio)acetic acid (2a):

N-Methylcyclohexylamine (1.3 mL, 10.0 mmol, 1 eq.) was added to 1M NaOH (12 mL), resulting in a white suspension. This suspension was stirred while 0.6 mL of carbon disulfide (10.0 mmol, 1 eq.) was added dropwise. A yellow precipitate was formed, and the mixture was stirred for 20 min. Then, sodium chloroacetate (1.16 g, 10.0 mmol, 1 eq.) in water (8 mL) was added. The mixture was stirred for 18 h at room temperature. After that, concentrated HCl (30 drops) was added to the yellow solution and the resulting white precipitate (**2a**, see Figure 50) was separated by filtration, washed with water, dried under vacuum and used in the next step without further purification. Yield: 1.89 g (76%). ^{1}H-NMR (DMSO-d_6): δ = 1.16-1.83 (m, 10H, CH_2 cyclohexyl), 3.20 (s, 3H, NCH_3), 4.09 (s, 2H, CH_2), 4.34-5.27 (m, 1H, CH cyclohexyl), 12.78 (br, 1H, OH).

Synthesis of *N*-cyclohexyl-*N*-methylhydrazinecarbothioamide (2b):

Compound **2a** (1.04 g, 4.23 mmol, 1 eq.) was dissolved in hydrazine hydrate (5 mL, 0.10 mol, excess) and 2 mL of water was added. The mixture was stirred at 50-60 ºC for 2 h. A white precipitate (**2b**, see Figure 50) was formed, which was filtered, washed with water, dried under vacuum and used in the next step without further purification. Yield: 1.05 g (75%). ^{1}H-NMR (DMSO-d_6): δ = 1.04-1.76

(m, 10H, CH_2 cyclohexyl), 2.85 (s, 1H, CH cyclohexyl), 3.34 (s, 3H, NCH_3), 4.70 (s, 1H, NH), 4.85 (s, 1H, NH_2), 8.70 (s, 1H, NH_2).

Synthesis of N-cyclohexyl-2-(6,7-dihydroquinolin-8(5H)-ylidene)-N-methylhydrazine-1-carbothioamide (COTI-Nchexyl):

Compound **2b** (0.58 g, 3.12 mmol, 1 eq.) was suspended in isopropanol (8 mL), and the mixture was stirred at 80 ºC. Then, 5,6,7,8-tetrahydroquinolin-8-one (0.46 g, 3.12 mmol, 1 eq.) was added, and the mixture was stirred under reflux for 3 h. A yellow solid was formed, which was separated by filtration, washed with cold isopropanol and dried under vacuum. Yield: 0.59 g (60%). Elemental analysis: Calcd. For $C_{17}H_{24}N_4S$ (%): C, 64.52 ; H, 7.64 ; N, 17.70 ; S, 10.13. Found (%): C, 64.24 ; H, 7.64 ; N, 17.65 ; S, 9.94. ESI-MS in ACN/MeOH + 1% H_2O (positive): *m/z* 339.1607, $[HL + Na]^+$. ^{1}H-NMR (DMSO-d_6): Major isomer (97%) δ = 1.12 (m, 2H, CH_2, H14), 1.50 (m, 2H, CH_2, H12,16), 1.64 (m, 2H, CH_2, H13,15), 1.96 (quint, 2H, CH_2, H6), 2.88 (t, 2H, CH_2, H7), 3.04 (t, 2H, CH_2, H5), 3.23 (s, 3H, NCH_3, H17), 5.09 (s, 1H, CH, H11), 7.41 (dd, 1H, CH py, H2), 7.76 (dd, 1H, CH py, H3), 8.58 (dd, 1H, CH py, H1), 14.65 (s, 1H, NH, N3). ^{13}C NMR (DMSO-d_6): δ = 20.0 (CH_2, C6), 25.1 (CH_2, C13,15), 25.4 (CH_2, C14), 26.2 (CH_2, C5), 27.2 (CH_2, C7), 29.5 (CH_2, C12,16), 30.1 (CH_3, C17), 58.4 (CH, C11), 125.0 (C_{py}, C2), 135.9 (C_q, C4), 137.7 (C_{py}, C3), 144.2 (C_q, C9), 148.2 (C_{py}, C1), 148.4 (C=N, C8), 183.8 (C=S, C10). ^{1}H-NMR (DMSO-d_6): Minor isomer (3%) δ = 15.38 (s, 1H, NH, N3).

*Synthesis of the iron(III) complex with COTI-2 (**Fe-COTI-2**)*

COTI-2 (0.20 g, 0.54 mmol, 2 eq.) was suspended in methanol (10 mL) and stirred at 50 ºC. Next, a solution of iron(III) nitrate nonahydrate (0.13 g, 0.30 mmol, 1.1 eq.) in methanol (2 mL) was added dropwise. A dark green solution was formed, which was stirred under reflux for 2 h. The solvent volume was reduced by evaporation under reduced pressure and the solution was cooled in the freezer overnight. On the next day a dark brown-greenish solid was formed, which was filtered, washed with cold methanol, and dried under vacuum. Yield: 21%. Elemental analysis: Calcd. For $[Fe(C_{19}H_{22}N_6S)_2](NO_3)_3 \cdot 3H_2O$ (%): C, 44.36 ; H, 4.90 ; N, 20.42 ; S, 6.23. Found (%): C, 44.61 ; H, 4.48 ; N, 20.08 ; S, 6.17. ESI-MS in ACN/MeOH + 1% H_2O (positive): *m/z* 393.60, $[ML(HL)]^{2+}$; 786.24, $[ML_2]^+$. The complex is soluble in methanol, ethanol and DMSO.

*Synthesis of the copper(II) complex with COTI-2 (**Cu-COTI-2**)*

Copper(II) chloride dihydrate (0.17 g, 1.0 mmol, 1,1 eq.) was dissolved in methanol (10 mL) at 40 ºC, and concentrated HCl (134 µL) was added. Next, a suspension of COTI-2 (0.30 g, 0.8 mmol, 1 eq.) was added dropwise to the copper(II) solution. A dark green solid was formed. The mixture was stirred for 2 h, and the solid was filtered and washed with cold methanol and diethyl ether and dried under vacuum. Yield: 0.28 g (72%). Elemental analysis: Calcd. For [$CuCl_2(C_{19}H_{22}N_6S)$] (%): C, 45.56; H, 4.43; N, 16.78; S, 6.40. Found (%): C, 45.25; H, 4.41; N, 16.47; S, 6.14. ESI-MS in ACN/MeOH + 1% H_2O (positive): *m/z* 214.5, $[M(HL)]^{2+}$; 428.09, $[ML]^+$. The synthesis was repeated without HCl, yielding the same complex (Calcd. For [$CuCl_2(C_{19}H_{22}N_6S)\cdot 0.25H_2O$] (%): C, 45.15; H, 4.49; N, 16.63; S, 6.34. Found (%): C, 44.85; H, 4.39; N, 16.47; S, 6.36). Green crystals were obtained by slow evaporation of the mother-liquor from the synthesis without HCl. The complex is partially soluble in DMSO.

*Synthesis of the zinc(II) complex with COTI-2 (**Zn-COTI-2**)*

COTI-2 (0.10 g, 0.28 mmol, 1 eq.) was suspended in methanol (5 mL) at 50 ºC under stirring. Next, a solution of zinc(II) chloride (0.06 g, 0.31 mmol, 1.1 eq.) in methanol (5 mL) was added dropwise at 50 ºC. A pale-yellow solid was formed, which was stirred at 50 ºC for 20 min. The solid was separated by filtration, washed with cold methanol and diethyl ether, and dried under vacuum. Yield: 0.10 g (71%). Elemental analysis: Calcd. For [$ZnCl_2(C_{19}H_{22}N_6S)]\cdot 0.5H_2O$ (%): C, 44.59 ; H, 4.53 ; N, 16.42 ; S, 6.26. Found (%): C, 44.72 ; H, 4.24 ; N, 16.20 ; S, 6.23. ESI-MS in ACN/MeOH + 1% H_2O (positive): *m/z* 429.38, $[ML]^+$. ^{1}H-NMR (D_2O): δ = 1.96 (quint, 2H, CH_2, H6), 2.92 (t, 2H, CH_2, H7), 2.97 (t, 2H, CH_2, H5), 3.79 (m, 2H, CH_2, H12,13), 4.18 (m, 2H, CH_2, H11,14), 6.92 (t, 1H, CH, H16), 7.21 (m, 1H, CH, H18), 7.48 (dd, 1H, CH py, H2), 7.70 (d, 1H, CH py, H3), 7.84 (dd, 1H, CH, H19), 7.95 (t, 1H, CH, H17), 8.34 (d, 1H, CH py, H1). The complex is slighlty soluble in DMSO and partially soluble in water.

Cell culture

The following human cell line and chemoresistant sublines were used: the colon carcinoma cell line SW480 (from American Type Culture Collection, Manassas, VA), and the drug resistant lines SW480/COTI and SW480/tria (generated by continuous exposure of SW480 cells to increasing concentrations of COTI-2 and Triapine, respectively). Cells were grown in minimal essential medium with 10% fetal bovine serum (FBS). To maintain the resistance of the chemoresistant lines, compounds (COTI-2 and Triapine) were administered to the cells once a week at the day after passage, when cells had attached to the cell culture flasks.

Cytotoxicity assays

Cells were seeded ($2x10^4$ cells/well for SW480 and SW480/COTI; $3x10^4$ cells/well for SW480/tria) in 100 µL/well in 96-well plates and allowed to attach for 24 h at 37 ºC and 5% CO_2. Compounds were diluted in DMSO and then further diluted in growth medium (DMSO concentration < 1%), being added in 100 µL/well, affording the final concentrations of 0, 0.005, 0.01, 0.05, 0.1, 1, 5, 10 and 20 µM, depending on the compound and the cell line (see Table A6, Appendix). Afterwards, cells were exposed for 72 h, being incubated at 37 ºC and 5% CO_2. The proportion of viable cells was determined by 3-(4,5-dimethylthiazole-2-yl)-2,5-diphenyltetrazolium assay (MTT) following the manufacturer's recommendations (EZ4U, Biomedica, Vienna, Austria). Cytotoxicity was expressed as IC_{50} values (drug concentrations inducing 50% reduction of cell survival in comparison to the control cultured in parallel, untreated cells) calculated from full concentration-response curves using GraphPad Prism software.

Results and Discussion

Syntheses and characterizations

COTI-2 and three derivatives with N^4-modifications were synthesized by different methods. COTI-2 was obtained in a three-step procedure, starting with the piperazine insertion to thiocarbonyldiimidazole (**1a**, Figure 49). Next, the COTI-2 thiosemicarbazide (**1b**, Figure 49) was prepared by reaction of **1a** with hydrazine hydrate, and at last, **1b** was condensed with the appropriate ketone, leading to **COTI-2**.

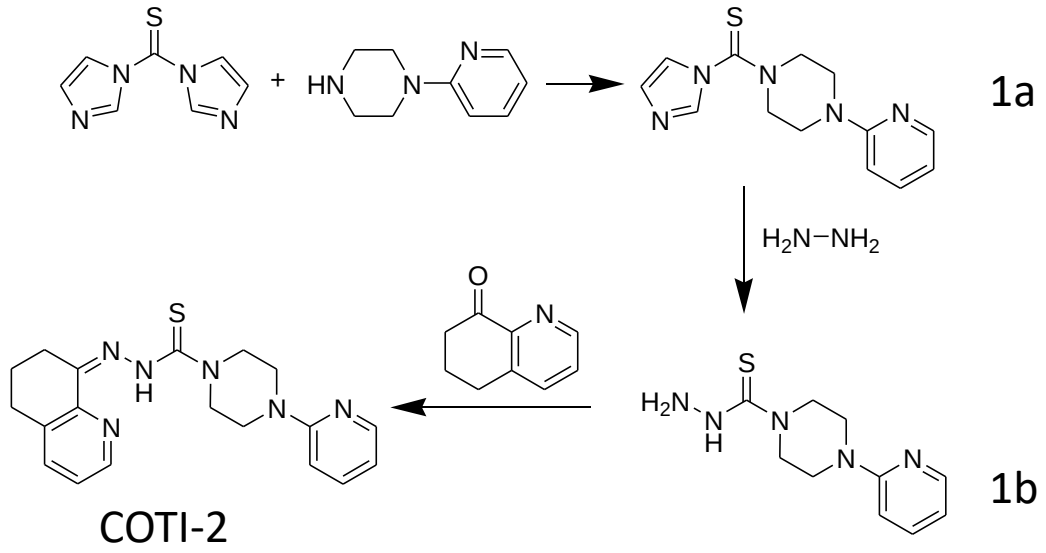

Figure 49. Synthetic route for COTI-2

For the COTI-Nchexyl derivative a different route was used, starting with the obtainment of the differentiated N^4-moiety by reacting carbon disulfide with N-methyl-cyclohexylamine and sodium chloroacetate (**2a**, Figure 50). The thiosemicarbazide (**2b**, Figure 50) was obtained by reacting **2a** with hydrazine hydrate, and the **COTI-Nchexyl** was obtained by the condensation of **2b** with the ketone. **COTI-NH_2** and **COTI-NMe_2** were obtained by the simple condensation of the ketone with the appropriate N^4-NH_2 and N^4-NMe_2 thiosemicarbazides.

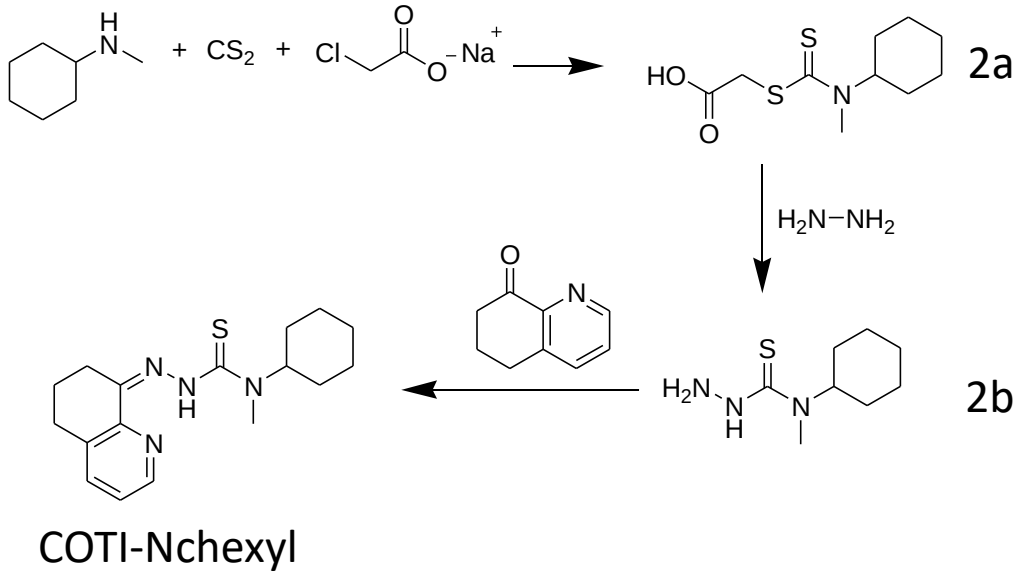

Figure 50. Synthetic route for COTI-Nchexyl.

The ^{1}H NMR spectra of the different COTI-derivatives in dimethylsulfoxide-d6 (DMSO-d6) show interesting trends. Despite COTI-NH_2, which only shows one isomer in solution, COTI-2 and the other two N^4-substituted compounds show two isomers. Due to the high chemical shifts observed for the N-H proton (in the range of 14.5 - 15.5 ppm), it can be affirmed that the Z-isomer and E'-isomer are observed, which present intramolecular hydrogen bonding [213]. For the E-isomer (no intramolecular hydrogen bonding) it is reported that the N-H signal appears around 9.0 ppm [213], and it was not observed for COTI-2 or the COTI-derivatives here presented (the different isomers for COTI-2 are represented in Figure 51).

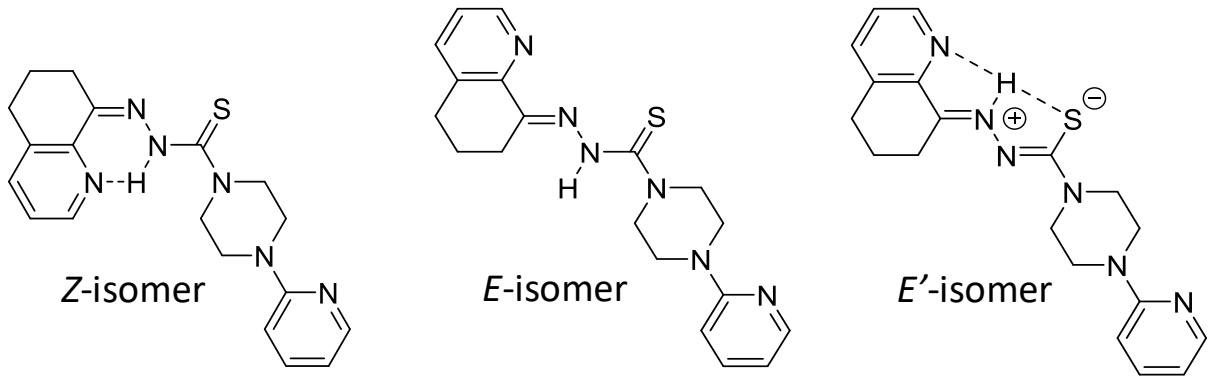

Figure 51. Different possible isomers of COTI-2.

The metal compounds were obtained by reaction of COTI-2 with appropriate metal salts. For the iron(III) complex (Fe-COTI-2), the reaction of COTI-2 with $Fe(NO_3)_3 \cdot 9H_2O$ resulted in a complex

with 1:2 metal ligand ratio, with two protonated ligands and a (+3) charge, with three nitrates as counter-ions. This composition is different from what was observed for the iron(III) complex with Triapine, in which both ligands are deprotonated and the complex presents a (+1) charge and one nitrate as counter-ion [195]. For the copper(II) and zinc(II) complexes (Cu-COTI-2 and Zn-COTI-2, respectively) COTI-2 was reacted with the $CuCl_2 \cdot 2H_2O$ and $ZnCl_2$ metal salts, yielding complexes with 1:1 metal ligand ratios, where two chloride ions are coordinated to the metal center, in addition to one protonated ligand. This composition was observed for other Cu(II) and Zn(II) thiosemicarbazone complexes [214,215].

Regarding the mass spectra, the isotopic patterns of the signals fit well with the theoretical isotopic distributions of the complexes. In this way, considering the compositions based on elemental analysis and mass spectrometry, Figure 52 shows the proposed structures for the complexes.

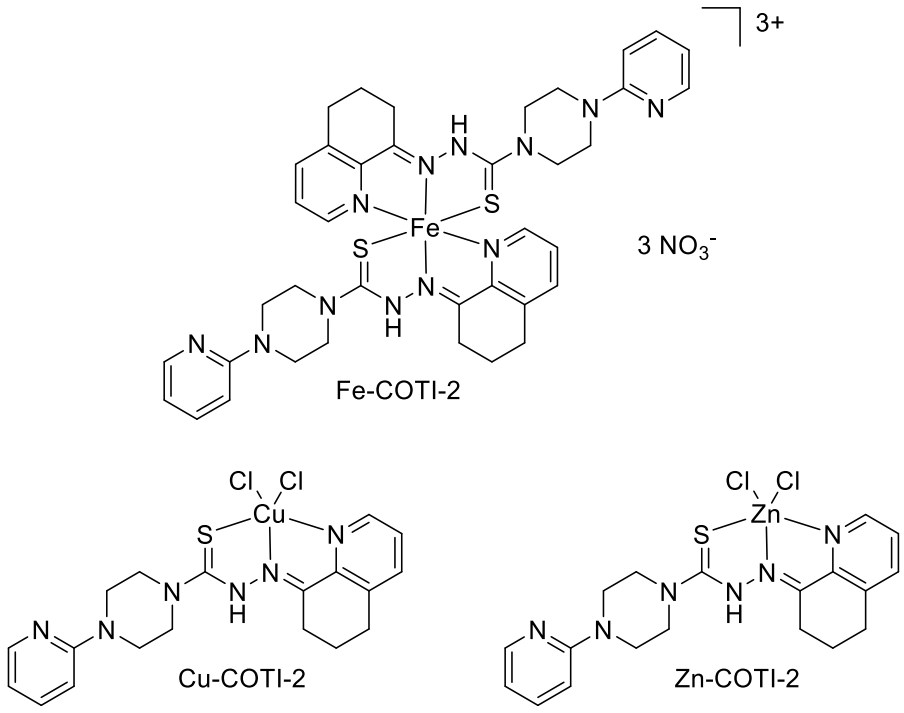

Figure 52. Proposed structures for Fe(III), Cu(II), and Zn(II) complexes with COTI-2.

Single crystal X-ray diffraction

Crystals were obtained for COTI-2 and Cu-COTI-2, which were suitable for analysis by single crystal X-ray diffraction technique. The solved structure for COTI-2 crystal is presented in Figure 53, and Tables 15 and 16 show the crystal data, data collection and structure refinement details for COTI-2.

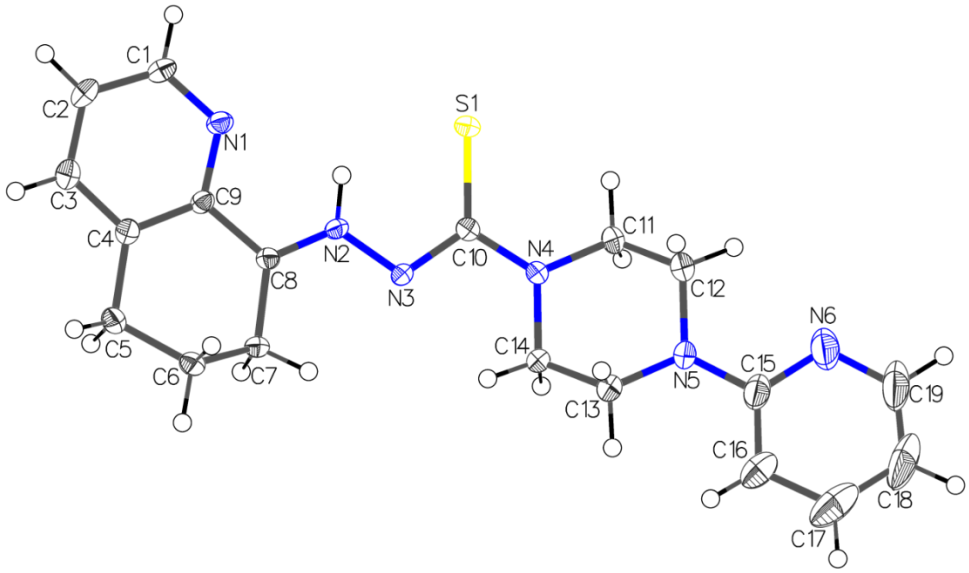

Figure 53. ORTEP plot of COTI-2 with atom numbering. Ellipsoids are drawn at 50% probability level. Selected bond lengths (Å) and bond angles (º): C8–N2 1.300(9), N2–N3 1.354(3), N3–C10 1.351(8), C10–S 1.717(1), C10–N4 1.361(4); N1–C9–C8 116.3, N2–N3–C10 112.0.

Table 15. Crystal data for COTI-2.

Chemical formula	$C_{19}H_{22}N_6S$	**Crystal system**	triclinic	
Formula weight [g/mol]	366.48	**Space group**	*P-1*	
Temperature [K]	100	**Z**	2	
Measurement method	\f and \w scans	**Volume [Å^3]**	891.36(3)	
Radiation (Wavelength [Å])	MoKα (λ=0.71073)	**Unit cell dimensions [Å] and [°]**	6.98620(10)	80.7487(7)
Crystal size / [mm^3]	0.1 × 0.08 × 0.04		7.7749(2)	89.3429(7)
Crystal habit	clear brown block		16.8747(3)	80.2082(8)
Density (calculated) / [g/cm^3]	1.365	**Absorption coefficient / [mm^{-1}]**	0.198	
Abs. correction Tmin	0.6911	**Abs. correction Tmax**	0.746	
Abs. correction type	multiscan	**F(000) [e$^-$]**	388	

Table 16. Data collection and structure refinement for COTI-2.

Index ranges	$-9 \leq h \leq 9$, $-10 \leq k \leq 10$, $-23 \leq l \leq 22$	**Theta range for data collection [°]**	4.892 to 60.168	
Reflections number	30290	**Data / restraints / parameters**	5204/0/239	
Refinement method	Least squares	**Final R indices**	all data	R1 = 0.0711, wR2 = 0.1308
Function minimized	$\Sigma\, w(F_o^2 - F_c^2)^2$		$I>2\sigma(I)$	R1 = 0.0565, wR2 = 0.1205
Goodness-of-fit on F^2	1.073	**Weighting scheme**	$w=1/[\sigma^2(F_o^2)+(0.0382P)^2 +1.0496P]$	
Largest diff. peak and hole [e $Å^{-3}$]	0.65/-0.61		where $P=(F_o^2+2F_c^2)/3$	

COTI-2 crystalized in the triclinic $P\bar{1}$ space group. Selected bond distances and angles are quoted in the legend of Figure 53. COTI-2 crystal adopted the E'-isomeric form [213] (also observed in NMR spectrum, see Figure 51), in which an intramolecular hydrogen bonding is observed between N1, S1, and the hydrogen H–N2. The parameters for this hydrogen bonding (bond lengths and angles) are as follows: N1···H 2.28 Å, N1···N2 2.67 Å, N2–H···N1 106.8 °, S1···H 2.35 Å, N2···S1 2.85 Å, N2–H···S1 116.4 °, N2–H 0.880(0) Å. Also, the piperazine moiety is in a chair configuration, while the cyclohexyl from the tetrahydroquinolin moiety is in a half-chair configuration.

The structure for Cu-COTI-2 crystal is presented in Figure 54, and Tables 17 and 18 show the crystal data, data collection and structure refinement details for Cu-COTI-2. It is important to note here that the crystal structure obtained for Cu-COTI-2 differs from the one proposed for the powder sample (see Figure 52), since crystals were obtained from slow evaporation of the mother-liquor and recombination in solution might have occurred.

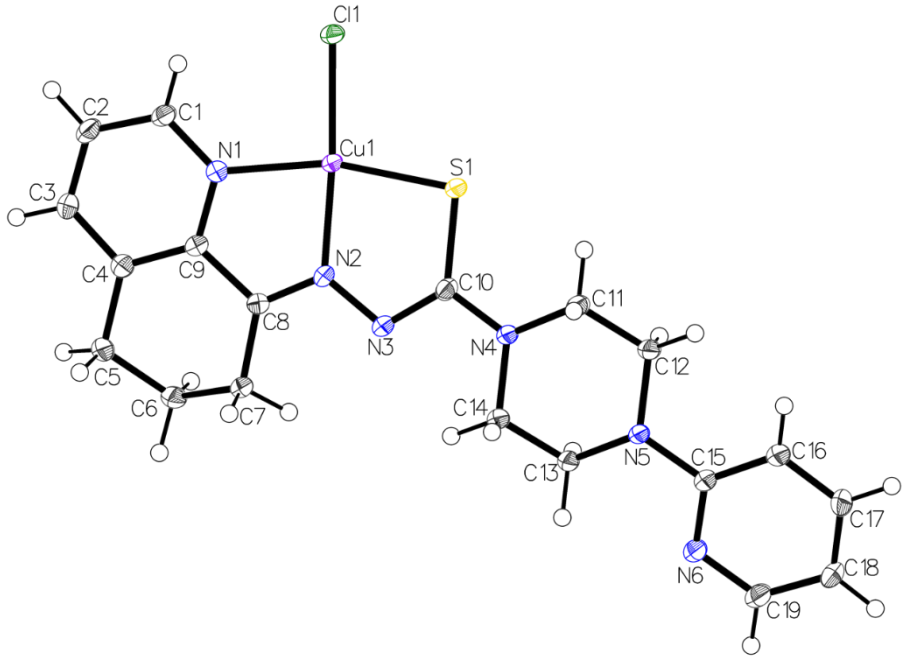

Figure 54. ORTEP plot of the asymmetric unit of Cu-COTI-2 crystals with atom numbering. Ellipsoids are drawn at 50% probability level. Selected bond lengths (Å) and bond angles (º): Cu–Cl 2.255(8), N1–Cu 2.029(9) Å, N2–Cu 1.961(3), S1–Cu 2.268(2) Å, Cl–Cu–S 97.8, N1–Cu–N2 80.9, N2–Cu–S 84.2, N1–Cu1–Cl 96.3.

Table 17. Crystal data for Cu-COTI-2.

Chemical formula	$C_{19}H_{21}ClCuN_6S$	**Crystal system**	triclinic	
Formula weight [g/mol]	464.47	**Space group**	*P-1*	
Temperature [K]	100	**Z**	2	
Measurement method	\f and \w scans	**Volume [Å^3]**	961.59(4)	
Radiation (Wavelength [Å])	CuKα (λ = 1.54178)	**Unit cell dimensions [Å] and [°]**	7.7583(2)	84.8825(8)
Crystal size / [mm^3]	0.2 × 0.15 × 0.05		10.6920(3)	83.7478(8)
Crystal habit	clear green block		11.7233(3)	86.5583(8)
Density (calculated) / [g/cm^3]	1.604	**Absorption coefficient / [mm^{-1}]**	4.043	
Abs. correction Tmin	0.5536	**Abs. correction Tmax**	0.7535	
Abs. correction type	multiscan	**F(000) [e$^-$]**	478	

Table 18. Data collection and structure refinement for Cu-COTI-2.

Index ranges	$-9 \leq h \leq 9, -13 \leq k \leq 13, -14 \leq l \leq 14$	**Theta range for data collection [°]**	8.314 to 144.116	
Reflections number	13178	**Data / restraints / parameters**	3733/0/253	
Refinement method	Least squares	**Final R indices**	all data	R1 = 0.0319, wR2 = 0.0811
Function minimized	$\Sigma\, w(F_o^2 - F_c^2)^2$		I>2σ(I)	R1 = 0.0300, wR2 = 0.0792
Goodness-of-fit on F^2	1.045	**Weighting scheme**	$w=1/[\sigma^2(F_o^2)+(0.0406P)^2 +0.7951P]$	
Largest diff. peak and hole [e $Å^{-3}$]	0.53/-0.41		where $P=(F_o^2+2F_c^2)/3$	

Cu-COTI-2 also crystalized in the triclinic $P\bar{1}$ space group. While Figure 54 shows the asymmetric unit of the complex, Figure 55 shows two bridging chlorido anions which are observed in between the copper(II) centers, what has already been reported for copper(II) complexes [216–219]. Selected bond distances and angles are quoted in the legend of Figure 54, and are in agreement with distances and angles of the copper(II) complex with Triapine previously reported [214]. The copper-copper distance is Cu···Cu 3.52 Å and the angle in between the copper ion and the chloride ligands is of Cl–Cu–Cl' 191.2 °. The copper(II) ion here presents the coordination number of five, being in a square-pyramidal geometry, where N1, N2, S1 and Cl1 are the base of the pyramid (forming the asymmetric unit of the complex), and the Cl' from another unit is in the axial position (2.749 Å). The C10–S1 bond length is of 1.754 Å, showing the elongation of the C–S bond due to coordination to Cu(II) (for COTI-2 crystal structure C10–S1 = 1.717 Å).

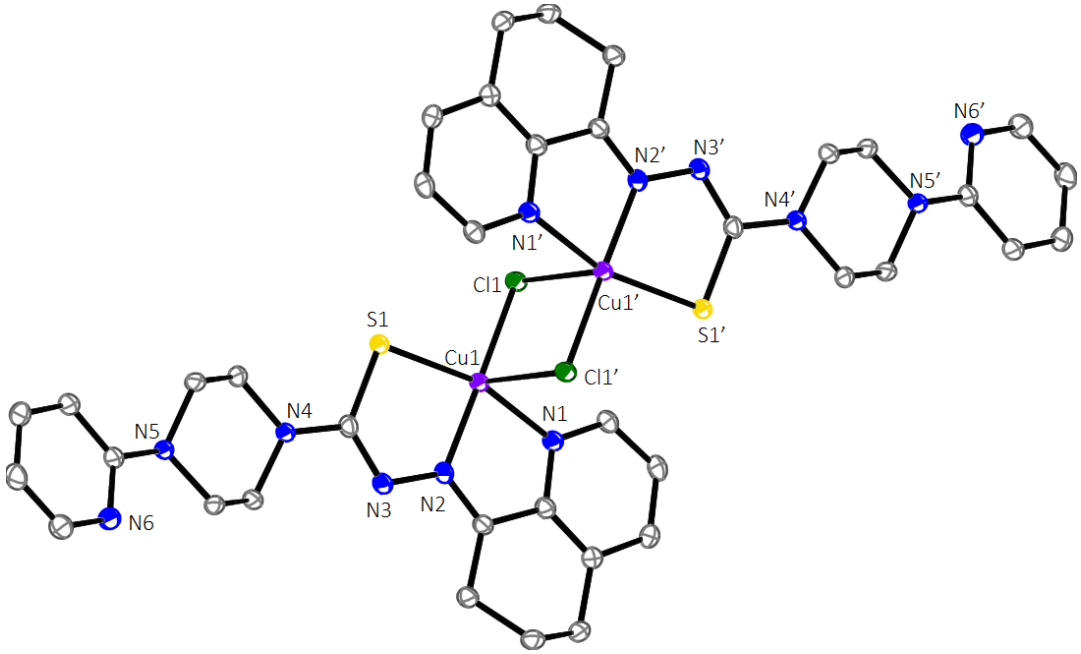

Figure 55. Structure of the Cu-COTI-2 complex, showing the bridging chlorido ions (in green) between the copper(II) centers (in purple). Hydrogen atoms were omitted for clarity and only non-carbon atoms are discriminated.

Cytotoxicity in SW480 cells

Cytotoxicity of COTI-2, COTI-derivatives and metal complexes was determined by concentration-response curves (0.005 – 20 µM, depending on the compound – concentration range for each compound can be found in Table A6 in Appendix) based on the MTT assay. Results are summarized in Table 19.

Table 19. Cytotoxic activity of COTI-2, COTI-derivatives and metal complexes with COTI-2 over chemoresistant SW480 sublines compared to their SW480 parental line.

Compound	SW480 (IC_{50}, μM)[a]	SW480/COTI (IC_{50}, μM)[a]	Relative resistance[b] (parental x COTI)	SW480/tria (IC_{50}, μM)[a]	Relative resistance[b] (parental x tria)
COTI-2	0.56 ± 0.16	6.87 ± 0.29	12.2	0.41 ± 0.16	0.7
COTI-NH_2	7.78 ± 1.03	4.39 ± 0.56	0.6	>20	>2.6
COTI-NMe_2	0.07 ± 0.01	0.08 ± 0.01	1.1	0.07 ± 0.01	1.0
COTI-Nchexyl	0.64 ± 0.10	3.98 ± 0.40	6.2	0.71 ± 0.17	1.1
Fe-COTI-2	7.10 ± 1.32	7.46 ± 0.78	1.1	3.23 ± 0.10	0.5
Cu-COTI-2	0.06 ± 0.01	0.46 ± 0.05	8.0	0.07 ± 0.01	1.1
Zn-COTI-2	0.12 ± 0.06	4.00 ± 0.28	33.0	0.13 ± 0.07	1.0
Triapine	0.77 ± 0.18	0.81 ± 0.08	1.1	>20	>26

a) IC_{50} values were calculated from concentration-response curves. Values are given as mean ± SD of three independent experiments, in triplicates.

b) Differences in sensitivity calculated by dividing the IC_{50} values of the chemoresistant subline by those of the parental line.

The SW480/COTI resistant cell line was generated by continuous exposure of SW480 cells to increasing concentrations of COTI-2 over a period of approximately one year. COTI-2 was administered to the cells once a week at the day after passage, when cells had attached to the cell culture flasks, which was the same protocol adopted to generate the SW480/tria cells [220].

As observed in Table 18, the SW480/COTI presented a 12-fold resistance to COTI-2 when compared to the parental line. Interestingly, the SW480/COTI line also presented resistance to COTI-Nchexyl (6-fold), Cu-COTI-2 (8-fold), and Zn-COTI-2 (33-fold). However, it was not resistant to COTI-NMe_2, which was the only compound active over the SW480/COTI line in the nanomolar range (IC_{50} = 0.08 μM). This shows that the terminal dimethylation not only enhanced the activity of the thiosemicarbazone [195], as it could overcome the resistance mechanism [196].

The SW480/COTI line was also not resistant to Fe-COTI-2, however it presented high IC_{50} values when compared to the other compounds (12-7 fold when compared to COTI-2 against the SW480

line, and 1.1-fold when compared to COTI-2 against the SW480/COTI line). The same was observed for COTI-NH_2, but in this case it presented a collateral sensitivity, being more active in the SW480/COTI than in the parental line (0.6-fold), what was unexpected. Also, this compound was the only COTI-derivative to which the SW480/tria cells were resistant (2.6-fold). This is probably due to the terminal-NH_2 of COTI-NH_2 and Triapine, showing that this structural feature may be related to the acquired resistance to Triapine.

Despite COTI-NH_2, COTI-2 and the other compounds did not present cross-resistance to Triapine. These results can be better observed in the dose-response curves, which are comprised in Figures 56 and 57, and Figure A48 in Appendix (where different compounds can be observed in a same graph).

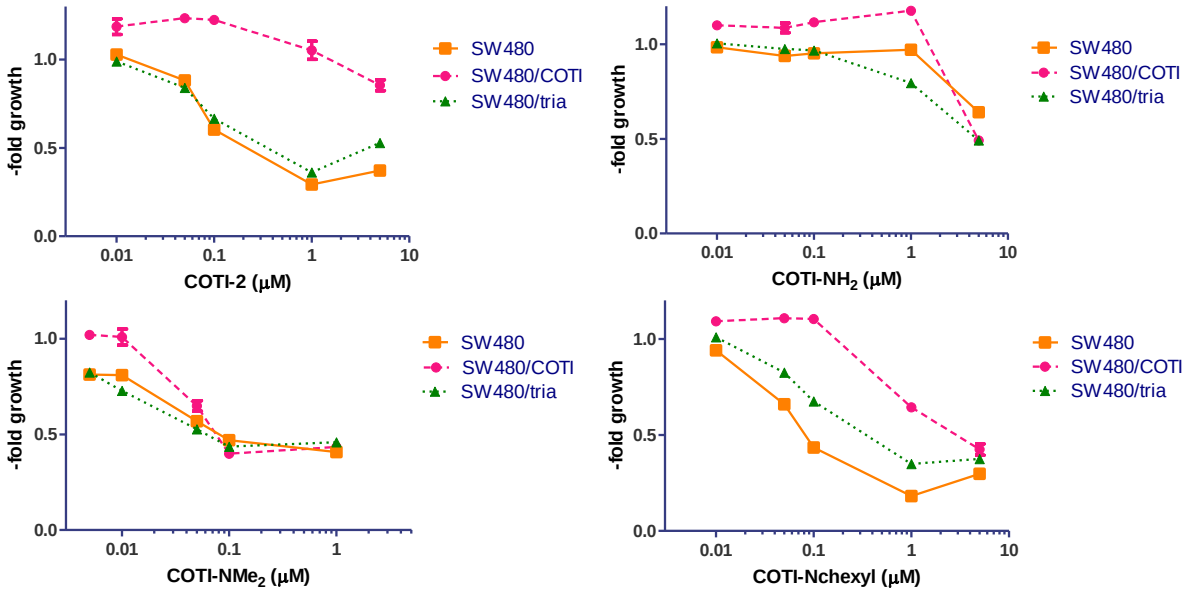

Figure 56. Concentration-response curves for COTI-2, COTI-NH_2, COTI-NMe_2 and COTI-Nchexyl over the SW480 line and the chemoresistant lines SW480/COTI and SW480/tria.

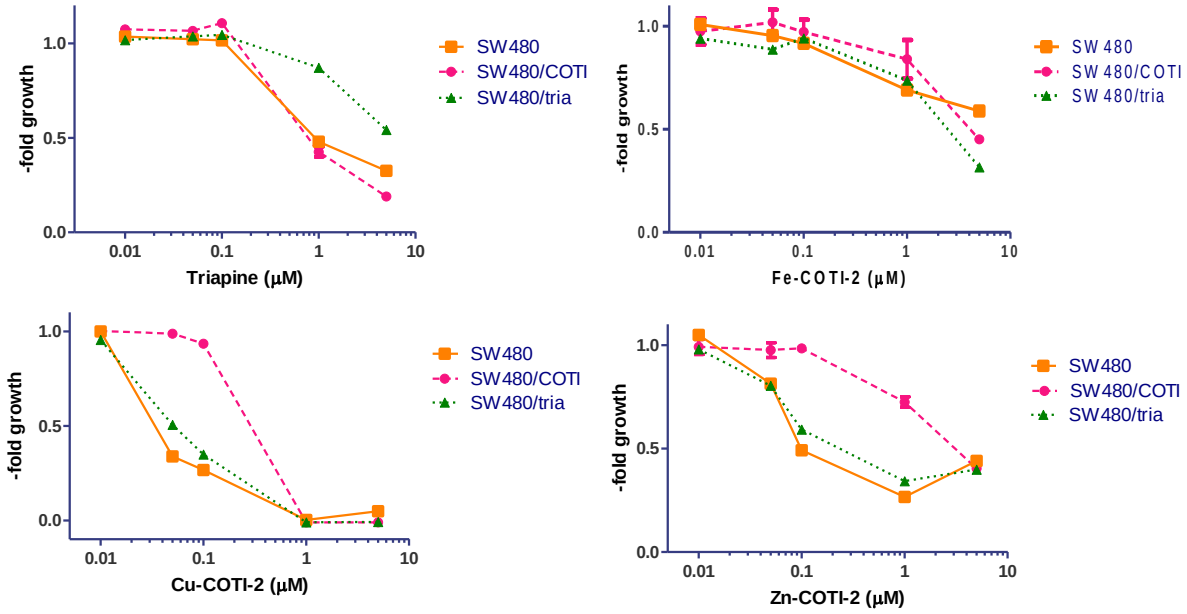

Figure 57. Concentration-response curves for Triapine, Fe-COTI-2, Cu-COTI-2 and Zn-COTI-2 over the SW480 line and the chemoresistant lines SW480/COTI and SW480/tria.

It was previously shown that the SW480/tria line overexpresses P-gp, this being an acquired resistance mechanism of SW480 to Triapine [220]. It can be supposed that ABC-transporter overexpression may be related to the acquired resistance of SW480/COTI, since this was previously observed for thiosemicarbazones [196,221]. Due to the absence of cross-resistance between Triapine and COTI-2, the resistance mechanism of SW480/COTI may not be overexpression of P-gp, but of another ABC-transporter. This hypothesis must still be evaluated.

Partial conclusions

COTI-2, as well as three COTI-derivatives with N^4-terminal modifications, COTI-NH_2, COTI-NMe_2 and COTI-Nchexyl, were synthesized and characterized, as well as three metal complexes of Fe(III), Cu(II) and Zn(II) with COTI-2. All compounds had their cytotoxic activities evaluated in SW480 cells by the MTT assay. For the parental cell line COTI-NMe_2 (IC_{50} = 0.07 µM), Cu-COTI-2 (IC_{50} = 0.06 µM), Zn-COTI-2 (IC_{50} = 0.12 µM) presented a better activity when compared to COTI-2 (IC_{50} = 0.56 µM). The COTI-NH_2 compound presented cross-resistance to Triapine, showing that the terminal-NH_2 may play a role in Triapine resistance. The SW480/COTI line presented a 12.2-fold resistance to COTI-2 when compared to the parental line, and the COTI-NMe_2 could overcome the resistance of SW480/COTI (IC_{50} = 0.08 µM), showing that the terminal dimethylation not only enhanced the activity of COTI-2, as it could overcome the resistance mechanism.

Conclusions

In the first part of the Thesis five complexes with 5-fluorouracil, 2-thiouracil and 2,4-dithiouracil were described. The Ag-5fu, complex presented a 3:2 metal/ligand composition, with formula $[Ag_3(C_4HFN_2O_2)(C_4H_2FN_2O_2)]$. The Pd-5fu presented a 2:1 metal/ligand composition, with formula $K[PdCl(C_4H_2FN_2O_2)_2]$, and the Pt-5fu complex also presented a 2:1 metal/ligand composition, with formula $K_2[PtCl_2(C_4H_2FN_2O_2)_2]$. The $[Ag_2(dtu)]$ complex presented a 2:1 metal ligand composition, with formula $[Ag_2(C_4H_2N_2S_2)]$, and the triphenylphosphinegold(I) complex with 2-thiouracil, Ph_3P-Au-tuH, presented a 1:1 metal/ligand composition, with formula $[Au(C_4H_2N_2OS)(C_{18}H_{15})]$. For this last complex the crystal structure shows the coordination of the 2-thiouracilato ligand to gold(I) by its thiol group. The Ag-5fu complex presented the best antiproliferative profile among the complexes with 5fu, and its activity seems to be a combination of the activities of 5fu and silver(I). Also, Ag-5fu presented a better activity than free 5fu and cisplatin over the NCI/ADR-RES cell line. Considering the complexes with thiouracils, the $[Ag_2(dtu)]$ complex presented no antiproliferative activity, probably due to its lack of solubility. The Ph_3P-Au-tuH complex and its precursor complex, Ph_3P-Au-Cl, showed interesting antiproliferative profiles, while the Ph_3P-Au-tuH complex showed a better activity than doxorubicin over the K562 cell line and a better activity when compared to Ph_3P-Au-Cl over the NCI-H460 line.

The Ag-5fu and Ph_3P-Au-tuH complexes were chosen to have their mechanisms of cell death studied in NCI/ADR-RES and NCI-H460 cells, respectively. Both compounds were evaluated by colony formation capacity and flow cytometry assays to analyze cell cycle and cell death induction [phosphatidylserine residues exposition, multicaspases activation, and mitochondrial membrane depolarization]. It was shown that the Ag-5fu complex may induce regulated cell death in NCI-ADR/RES cells considering mitochondrial membrane depolarization, PS externalization and multicaspases activation. Moreover, the Ag-5fu complex promoted cell cycle arrest at G1 and inhibited colony formation, indicating that the cancer cells, which do not go through a regulated cell death pathway, lost their proliferation ability.

Considering Ph_3P-Au-tuH and Ph_3P-Au-Cl, both compounds induced regulated cell death in NCI-H460 cells, considering PS externalization and multicaspases activation. Also, both compounds promoted cell cycle arrest at G1 and inhibited colony formation. For the gold(I) complexes only Ph_3P-Au-tuH showed mitochondrial membrane depolarization.

The second part of the Thesis was based on the thiosemicarbazone COTI-2. COTI-2 and COTI-derivatives, as well as the first metal complexes of Fe(III), Cu(II), and Zn(II) with COTI-2, were synthesized and characterized. All compounds had their cytotoxic activities evaluated *in vitro* by the MTT assay over the SW480 tumor cell line, and SW480 chemoresistant lines. COTI-2 presented a 12.2-

fold resistance when comparing the SW480 parental line to the SW480/COTI resistant one. Despite COTI-NH_2, all other COTI-derivatives and the metal complexes did not present cross-resistance to Triapine. The COTI-NMe_2 not only presented an enhanced activity when compared to COTI-2, as it could overcome the resistance mechanism of the SW480/COTI line. The Cu-COTI-2 complex presented the best results among the metal complexes, being more active than COTI-2 itself.

References

[1] INCA, O que é câncer, (2019). https://www.inca.gov.br/o-que-e-cancer (accessed August 5, 2019).

[2] National Cancer Institute, What is cancer?, (2015). https://www.cancer.gov/about-cancer/understanding/what-is-cancer (accessed August 5, 2019).

[3] American Cancer Society, Oncogenes and tumor suppressor genes, (2014). https://www.cancer.org/cancer/cancer-causes/genetics/genes-and-cancer/oncogenes-tumor-suppressor-genes.html (accessed October 1, 2019).

[4] The Cancer Atlas, Major cancer risk factors include tobacco, infections, diet and body composition, and UV radiation, (2019). http://canceratlas.cancer.org/risk-factors/cancer-risk-factors/ (accessed August 5, 2019).

[5] INCA, O que causa câncer, (2018). https://www.inca.gov.br/causas-e-prevencao/o-que-causa-cancer (accessed August 5, 2019).

[6] The Cancer Atlas, Smoking causes more than 16 types of cancer and accounts for a fifth of all global cancer deaths, (2019). http://canceratlas.cancer.org/risk-factors/tobacco/ (accessed August 5, 2019).

[7] The Cancer Atlas, UV radiation causes cancers of the skin—the most common cancers, (2019). http://canceratlas.cancer.org/risk-factors/ultraviolet-radiation/ (accessed August 5, 2019).

[8] National Cancer Institute, Infectious agents, (2019). https://www.cancer.gov/about-cancer/causes-prevention/risk/infectious-agents (accessed August 5, 2019).

[9] The Cancer Atlas, Many of the most common cancers are attributable to infection, (2019). http://canceratlas.cancer.org/risk-factors/infection/ (accessed August 5, 2019).

[10] National Cancer Institute, Risk factors for cancer, (2015). https://www.cancer.gov/about-cancer/causes-prevention/risk (accessed December 4, 2018).

[11] World Health Organization, All cancers fact sheet, (2018). http://gco.iarc.fr/today/data/factsheets/cancers/39-All-cancers-fact-sheet.pdf (accessed August 5, 2019).

[12] World Health Organization, Brazil fact sheets on cancer, (2018). http://gco.iarc.fr/today/data/factsheets/populations/76-brazil-fact-sheets.pdf (accessed August 5, 2019).

[13] INCA, Estatísticas do câncer, (2019). https://www.inca.gov.br/numeros-de-cancer (accessed August 5, 2019).

[14] American Cancer Society, Early History of Cancer, (2018). https://www.cancer.org/cancer/cancer-basics/history-of-cancer/what-is-cancer.html (accessed August 5, 2019).

[15] Akulapalli Sudhakar, History of Cancer, Ancient and Modern Treatment Methods, J Cancer Sci Ther. 1 (2009) 1–4. doi:10.4172/1948-5956.100000e2.History.

[16] American Cancer Society, Cancer in the Sixteenth to Eighteenth Centuries, (2014). https://www.cancer.org/cancer/cancer-basics/history-of-cancer/sixteenth-to-eighteenth-centuries.html (accessed August 5, 2019).

[17] American Cancer Society, Cancer in the Nineteenth Century, (2014). https://www.cancer.org/cancer/cancer-basics/history-of-cancer/nineteenth-century.html (accessed August 5, 2019).

[18] D. Hanahan, R.A. Weinberg, The Hallmarks of Cancer, Cell. 100 (2000) 57–70. doi:10.1007/s00262-010-0968-0.

[19] D. Hanahan, R.A. Weinberg, Hallmarks of cancer: The next generation, Cell. 144 (2011) 646–674. doi:10.1016/j.cell.2011.02.013.

[20] National Cancer Institute, Types of Cancer Treatment, (2019). https://www.cancer.gov/about-cancer/treatment/types (accessed August 5, 2019).

[21] V.T. DeVita, E. Chu, A history of cancer chemotherapy, Cancer Res. 68 (2008) 8643–8653. doi:10.1158/0008-5472.CAN-07-6611.

[22] Cancer Treatment Centers of America, Chemotherapy, (2019). https://www.cancercenter.com/treatments/chemotherapy/ (accessed August 5, 2019).

[23] S.Y. Qin, Y.J. Cheng, Q. Lei, A.Q. Zhang, X.Z. Zhang, Combinational strategy for high-performance cancer chemotherapy, Biomaterials. 171 (2018) 178–197. doi:10.1016/j.biomaterials.2018.04.027.

[24] M.W. English, Principles of chemotherapy, Paediatr. Child Health (Oxford). 20 (2010) 123–128. doi:10.1016/j.paed.2009.10.003.

[25] E. Dickens, S. Ahmed, Principles of cancer treatment by chemotherapy, Surg. (United Kingdom). 36 (2018) 134–138. doi:10.1016/j.mpsur.2017.12.002.

[26] H.S. Walter, S. Ahmed, Targeted therapies in cancer, Surg. (United Kingdom). 36 (2018) 134–138. doi:10.1016/j.mpsur.2017.12.010.

[27] L. Chiang, M. R. Jones, C. L. Ferreira, T. Storr, Multifunctional Ligands in Medicinal Inorganic Chemistry- Current Trends and Future Directions, Curr. Top. Med. Chem. 12 (2012) 122–144. doi:10.2174/156802612799078973.

[28] I. Ott, R. Gust, Non platinum metal complexes as anti-cancer drugs, Arch. Pharm. (Weinheim). 340 (2007) 117–126. doi:10.1002/ardp.200600151.

[29] U. Ndagi, N. Mhlongo, M. Soliman, Metal complexes in cancer therapy – an update from drug design perspective, Drug Des. Devel. Ther. 11 (2017) 599–616. doi:10.2147/DDDT.S119488.

[30] R.H. Demling, L. DeSanti, Effects of silver in wound treatment, Wounds. 13 (2001) 1–15.

[31] Q.P.D. D. Chen, V. Milacic, M. Frezza, Metal Complexes, their Cellular Targets and Potential for Cancer Therapy, Curr. Pharm. Des. (2009) 777–791. doi:10.2174/138161209787582183.

[32] H.J. Klasen, Historical review of the use of silver in the treatment of burns. I. Early uses, Burns. 26 (2000) 117–130. doi:https://doi.org/10.1016/S0305-4179(99)00108-4.

[33] T.C. Johnstone, K. Suntharalingam, S.J. Lippard, Third row transition metals for the treatment of cancer, Philos. Trans. A. 373 (2014) 1–12. doi:10.1098/rsta.2014.0185.

[34] C.S. Allardyce, P.J. Dyson, Metal-based drugs that break the rules, Dalt. Trans. 45 (2016) 3201–3209. doi:10.1039/c5dt03919c.

[35] B. Rosenberg, L. VanCamp, J.E. Trosko, V.H. Mansou, Platinum compounds: a new class of potent antitumor agents, Nature. 222 (1969) 385–386.

[36] S. Dasari, P.B. Tchounwou, Cisplatin in cancer therapy: Molecular mechanisms of action, Eur. J. Pharmacol. 740 (2014) 364–378. doi:10.1016/j.ejphar.2014.07.025.

[37] B. Rosenberg, L. Van Camp, T. Krigas, Inhibition of Cell Division in Escherichia coli by Electrolysis Products from a Platinum Electrode, Nature. 205 (1965) 698–699. doi:10.1038/205698a0.

[38] B. Rosenberg, L. VanCamp, The Successful Regression of Large Solid Sarcoma 180 Tumors by Platinum Compounds, Cancer Res. 30 (1970) 1799–1802.

[39] Food and Drug Administration, FDA Approved Drug - Cisplatin, (1978). https://www.accessdata.fda.gov/scripts/cder/daf/index.cfm?event=overview.process&varApplNo=018057 (accessed December 19, 2018).

[40] F. Trudu, F. Amato, P. Vaňhara, T. Pivetta, E.M. Peña-Méndez, J. Havel, Coordination compounds in cancer: Past, present and perspectives, J. Appl. Biomed. 13 (2015) 79–103. doi:10.1016/j.jab.2015.03.003.

[41] J.A. Mello, S. Acharya, R. Fishe, J.M. Essigmann, The mismatch-repair protein hMSH2 binds selectively to DNA adducts of the anticancer drug cisplatin, Chem. Biol. 3 (1996) 579–589.

[42] S.J. Lippard, U.-M. Ohndorf, M.A. Rould, Q. He, C.O. Pabo, Basis for recognition of cisplatin-modified DNA by high-mobility-group proteins, Nature. 399 (1999) 708–712. doi:10.1038/21460.

[43] E.R. Jamieson, S.J. Lippard, Structure, Recognition, and Processing of Cisplatin − DNA Adducts, (1999).

[44] L. Kelland, The resurgence of platinum-based cancer chemotherapy., Nat. Rev. Cancer. 7 (2007) 573–584. doi:10.1038/nrc2167.

[45] R.J. Knox, F. Friedlos, D.A. Lydall, J.J. Roberts, Mechanism of Cytotoxicity of Anticancer Platinum Drugs: Evidence and cis-Diammine Differ Only in the Kinetics of Their Interaction with DNA, Cancer Res. 46 (1986) 1972–1979.

[46] D.J. Stewart, Mechanisms of resistance to cisplatin and carboplatin, Crit. Rev. Oncol. Hematol. 63 (2007) 12–31. doi:10.1016/j.critrevonc.2007.02.001.

[47] R.E. Meyn, S.F. Jenkins, L.H. Thompson, Defective Removal of DNA Cross-Links in a Repair-Deficient Mutant of Chinese Hamster Cells, Cancer Res. 42 (1982) 3106–3110.

[48] D. Fink, S. Nebel, S. Aebi, H. Zheng, B. Cenm, A. Nehmã, D. Christen, S.B. Howell, The Role of DNA Mismatch Repair in Platinum Drug Resistance, Cancer Res. 56 (1996) 4881–4886.

[49] Z.Z. Zdraveski, J.A. Mello, C.K. Farinelli, J.M. Essigmann, M.G. Marinus, MutS preferentially recognizes cisplatin-over oxaliplatin-modified DNA, J. Biol. Chem. 277 (2002) 1255–1260. doi:10.1074/jbc.M105382200.

[50] N. Farrell, L. Kelland, J. Roberts, M. Van Beusichem, Trans geometry in platinum antitumor complexes: a survey of the cytotoxicity of trans complexes containing planar ligands in murine L1210 and human tumor panels, Cancer Res. 52 (1992) 5065–5072. http://cancerres.aacrjournals.org/content/52/18/5065.short.

[51] M. Van Beusichem, N. Farrell, Activation of the Trans Geometry in Platinum Antitumor Complexes. Synthesis, Characterization, and Biological Activity of Complexes with the Planar Ligands Pyridine, N-Methylimidazole, Thiazole, and Quinoline. Crystal and Molecular Structure of Trans-Dich, Inorg. Chem. 31 (1992) 634–639. doi:10.1021/ic00030a021.

[52] V. Brabec, K. Neplechova, J. Kasparkova, N. Farrell, Steric control of DNA interstrand cross-link sites of trans platinum complexes: Specificity can be dictated by planar nonleaving groups, J. Biol. Inorg. Chem. 5 (2000) 364–368. doi:10.1007/PL00010665.

[53] J.B. Mangrum, N.P. Farrell, Excursions in polynuclear platinum DNA binding, Chem. Commun. 46 (2010) 6640–6650. doi:10.1039/c0cc01254h.

[54] S. Komeda, Y. Qu, J.B. Mangrum, A. Hegmans, L.D. Williams, N.P. Farrell, The phosphate clamp as recognition motif in platinum-DNA interactions, Inorganica Chim. Acta. 452 (2016) 25–33. doi:10.1016/j.ica.2016.04.052.

[55] N.P. Farrell, Multi-platinum anti-cancer agents. Substitution-inert compounds for tumor selectivity and new targets, Chem. Soc. Rev. 44 (2015) 8773–8785. doi:10.1039/C5CS00201J.

[56] M.D. Hall, H.R. Mellor, R. Callaghan, T.W. Hambley, Basis for Design and Development of Platinum(IV) Anticancer Complexes, J. Med. Chem. 50 (2007) 3403–3411. doi:10.1021/JM070280U.

[57] A. Eastman, Glutathione-mediated activation of anticancer platinum(IV) complexes, Biochem. Pharmacol. 36 (1987) 4177–4178. doi:10.1016/0006-2952(87)90581-8.

[58] M.D. Hall, W. Hambley, Platinum(IV) antitumour compounds: Their bioinorganic chemistry, Coord. Chem. Rev. 232 (2002) 49–67. doi:10.1016/S0010-8545(02)00026-7.

[59] T.C. Johnstone, K. Suntharalingam, S.J. Lippard, The Next Generation of Platinum Drugs: Targeted Pt(II) Agents, Nanoparticle Delivery, and Pt(IV) Prodrugs, Chem. Rev. 116 (2016) 3436–3486. doi:10.1021/acs.chemrev.5b00597.

[60] K.R. Barnes, A. Kutikov, S.J. Lippard, Synthesis, characterization, and cytotoxicity of a series of estrogen-tethered platinum(IV) complexes, Chem. Biol. 11 (2004) 557–564. doi:10.1016/j.

[61] S.H. van Rijt, P.J. Sadler, Current applications and future potential for bioinorganic chemistry in the development of anticancer drugs, Drug Discov. Today. 14 (2009) 1089–1097. doi:10.1016/j.drudis.2009.09.003.

[62] Z.-F. Chen, C. Orvig, H. Liang, Multi-Target Metal-Based Anticancer Agents, Curr. Top. Med. Chem. 17 (2017) 3131–3145. doi:10.2174/1568026617666171004155437.

[63] T. Lazarević, A. Rilak, Ž.D. Bugarčić, Platinum, palladium, gold and ruthenium complexes as anticancer agents: Current clinical uses, cytotoxicity studies and future perspectives, Eur. J. Med. Chem. 142 (2017) 8–31. doi:10.1016/j.ejmech.2017.04.007.

[64] Z.D. Bugarcic, J. Bogojeski, R. van Eldik, Kinetics, mechanism and equilibrium studies on the substitution reactions of Pd(II) in reference to Pt(II) complexes with bio-molecules, Coord. Chem. Rev. 292 (2015) 91–106. doi:10.1016/j.ccr.2015.02.016.

[65] E.Z. Jahromi, A. Divsalar, A.A. Saboury, S. Khaleghizadeh, H. Mansouri-Torshizi, I. Kostova, Palladium complexes: new candidates for anti-cancer drugs, J. Iran. Chem. Soc. 13 (2016) 967–989. doi:10.1007/s13738-015-0804-8.

[66] M.N. Alam, F. Huq, Comprehensive review on tumour active palladium compounds and structure-activity relationships, Coord. Chem. Rev. 316 (2016) 36–67. doi:10.1016/j.ccr.2016.02.001.

[67] A.R. Azzouzi, S. Vincendeau, E. Barret, A. Cicco, F. Kleinclauss, H.G. van der Poel, C.G. Stief, J. Rassweiler, G. Salomon, E. Solsona, A. Alcaraz, T.T. Tammela, D.J. Rosario, F. Gomez-Veiga, G. Ahlgren, F. Benzaghou, B. Gaillac, B. Amzal, F.M.J. Debruyne, G. Fromont, C. Gratzke, M. Emberton, Padeliporfin vascular-targeted photodynamic therapy versus active surveillance in men with low-risk prostate cancer (CLIN1001 PCM301): an open-label, phase 3, randomised controlled trial, Lancet Oncol. 18 (2017) P181-191. doi:10.1016/S1470-2045(16)30661-1.

[68] National Cancer Institute, Padeliporfin, (2019). https://www.cancer.gov/publications/dictionaries/cancer-drug/def/padeliporfin (accessed August 5, 2019).

[69] B.F.P. Dwyer, E.C.G.Y. Arfas, W.P. Rogers, J.H. Koch, Biological activity of complex ions, Nature. 170 (1952) 190–191.

[70] U. Jungwirth, C.R. Kowol, B.K. Keppler, C.G. Hartinger, W. Berger, P. Heffeter, Anticancer Activity of Metal Complexes: Involvement of Redox Processes, Antioxid. Redox Signal. 15 (2011) 1085–1127. doi:10.1089/ars.2010.3663.

[71] N. Graf, S.J. Lippard, Redox activation of metal-based prodrugs as a strategy for drug delivery, Adv. Drug Deliv. Rev. 64 (2012) 993–1004. doi:10.1016/j.addr.2012.01.007.

[72] K.D. Mjos, C. Orvig, Metallodrugs in medicinal inorganic chemistry, Chem. Rev. 114 (2014) 4540–4563. doi:10.1021/cr400460s.

[73] R. Trondl, P. Heffeter, C.R. Kowol, M.A. Jakupec, W. Berger, B.K. Keppler, NKP-1339, the first ruthenium-based anticancer drug on the edge to clinical application, Chem. Sci. 5 (2014) 2925–2932. doi:10.1039/c3sc53243g.

[74] E. Reisner, V.B. Arion, B.K. Keppler, A.J.L. Pombeiro, Electron-transfer activated metal-based anticancer drugs, Inorganica Chim. Acta. 361 (2008) 1569–1583. doi:10.1016/j.ica.2006.12.005.

[75] C. Orvig, M.J. Abrams, Medicinal Inorganic Chemistry: Introduction, Chem. Rev. 99 (1999) 2201–2203. doi:10.1021/cr980419w.

[76] R.E.F. de Paiva, P.P. Corbi, Bioinorganic applications of gold and platinum coordination compounds: a brief historical overview and recent advances in 2017, Int. J. Adv. Med. Biotechnol. 1 (2018) 1–6.

[77] J.H. Bormio Nunes, D.A. Simoni, L.E.O. Braga, A.L.T.G. Ruiz, J. Ernesto de Carvalho, P.P. Corbi, Synthesis, characterization, crystal structure and in vitro antiproliferative assays of the 2-thiouracilato(triphenylphosphine)gold(I) complex, J. Mol. Struct. 1178 (2019) 169–178. doi:10.1016/j.molstruc.2018.10.026.

[78] C. Shaw, Gold-based therapeutic agents, Chem. Rev. 99 (1999) 2589–2600. doi:10.1021/cr980431o.

[79] C. Roder, M.J. Thomson, Auranofin: Repurposing an Old Drug for a Golden New Age, Drugs R D. 15 (2015) 13–20. doi:10.1007/s40268-015-0083-y.

[80] C. Marzano, V. Gandin, A. Folda, G. Scutari, A. Bindoli, M.P. Rigobello, Inhibition of thioredoxin reductase by auranofin induces apoptosis in cisplatin-resistant human ovarian cancer cells, Free Radic. Biol. Med. 42 (2007) 872–881. doi:10.1016/j.freeradbiomed.2006.12.021.

[81] J.S. Darc Chaves, F. Neumann, T. Martins Francisco, C. Cimini Corrêa, M. Teresa Paz Lopes, H. Silva, A.S. Paula Fontes, M. V de Almeida, Synthesis and cytotoxic activity of gold(I) complexes containing phosphines and 3-benzyl-1,3-thiazolidine-2-thione or 5-phenyl-1,3,4-oxadiazole-2-thione as ligands, Inorganica Chim. Acta. 414 (2014) 85–90. doi:10.1016/j.ica.2014.01.042.

[82] J.S. Darc Chaves, L. Guimar, A. Tunes, C.J. Hebert de Franco, T. Martins Francisco, C. Cimini Corr, S.M. Murta, R. Lima Monte-Neto, H. Silva, A.S. Paula Fontes, M. V de Almeida, Novel gold(I) complexes with 5-phenyl-1,3,4-oxadiazole-2-thione and phosphine as potential anticancer and antileishmanial agents, Eur. J. Med. Chem. 127 (2017) 727–739. doi:10.1016/j.ejmech.2016.10.052.

[83] V. Gandin, A.P. Fernandes, M.P. Rigobello, B. Dani, F. Sorrentino, F. Tisato, M. Björnstedt, A. Bindoli, A. Sturaro, R. Rella, C. Marzano, Cancer cell death induced by phosphine gold(I) compounds targeting thioredoxin reductase, Biochem. Pharmacol. 79 (2010) 90–101. doi:10.1016/j.bcp.2009.07.023.

[84] M.P. Chrysouli, C.N. Banti, N. Kourkoumelis, N. Panayiotou, G.S. Markopoulos, A.J. Tasiopoulos, S.K. Hadjikakou, Chloro(triphenylphosphine)gold(I) a forefront reagent in gold chemistry as apoptotic agent for cancer cells, J. Inorg. Biochem. 179 (2018) 107–120. doi:10.1016/j.jinorgbio.2017.11.004.

[85] H. Scheffler, Y. You, I. Ott, Comparative studies on the cytotoxicity, cellular and nuclear uptake of a series of chloro gold(I) phosphine complexes, Polyhedron. 29 (2010) 66–69. doi:10.1016/j.poly.2009.06.007.

[86] C.J. Lima, L. Rodríguez, Phosphine-Gold (I) Compounds as Anticancer Agents: General Description and Mechanisms of Action, Anticancer. Agents Med. Chem. 11 (2011) 921–928. doi:10.2174/187152011797927670.

[87] M.J. McKeage, L. Maharaj, S.J. Berners-Price, Mechanisms of cytotoxicity and antitumor activity of gold(I) phosphine complexes: The possible role of mitochondria, Coord. Chem. Rev. 232 (2002) 127–135. doi:10.1016/S0010-8545(02)00048-6.

[88] F. Caruso, R. Villa, M. Rossi, C. Pettinari, F. Paduano, M. Pennati, M.G. Daidone, N. Zaffaroni, Mitochondria are primary targets in apoptosis induced by the mixed phosphine gold species chlorotriphenylphosphine-1, 3-bis(diphenylphosphino)propanegold(I) in melanoma cell lines, Biochem. Pharmacol. 73 (2007) 773–781. doi:10.1016/j.bcp.2006.11.018.

[89] L. Messori, F. Abbate, G. Marcon, P. Orioli, M. Fontani, E. Mini, T. Mazzei, S. Carotti, T. O'Connell, P. Zanello, Gold(III) complexes as potential antitumor agents: Solution chemistry and cytotoxic properties of some selected gold(III) compounds, J. Med. Chem. 43 (2000) 3541–3548. doi:10.1021/jm990492u.

[90] C.L. Fox, Silver Sulfadiazine - A New Topical Therapy for Pseudomonas in Burns, Arch. Surg. 96 (1968) 184–188. doi:10.1001/archsurg.1968.01330200022004.

[91] C.L. Fox, S.M. Modak, Mechanism of silver sulfadiazine action on burn wound infections., Antimicrob. Agents Chemother. 5 (1974) 582–588. doi:10.1128/AAC.5.6.582.

[92] S.M. Modak, C.L. Fox, Binding of silver sulfadiazine to the cellular components of Pseudomonas aeruginosa, Biochem. Pharmacol. 22 (1973) 2391–2404. doi:10.1016/0006-2952(73)90341-9.

[93] D.E. Marx, D.J. Barillo, Silver in medicine: The basic science, Burns. 40 (2014) S9–S18. doi:10.1016/j.burns.2014.09.010.

[94] S.J. Tan, Y.K. Yan, P.P.F. Lee, K.H. Lim, Copper, gold and silver compounds as potential new anti-tumor metallodrugs, Future Med. Chem. 2 (2010) 1591–1608. doi:10.4155/fmc.10.234.

[95] C.N. Banti, S.K. Hadjikakou, Anti-proliferative and anti-tumor activity of silver(I) compounds, Metallomics. 5 (2013) 569–596. doi:10.1039/c3mt00046j.

[96] S. Medici, M. Peana, G. Crisponi, V.M. Nurchi, J.I. Lachowicz, M. Remelli, M.A. Zoroddu, Silver coordination compounds: A new horizon in medicine, Coord. Chem. Rev. 327–328 (2016) 349–359. doi:10.1016/j.ccr.2016.05.015.

[97] M. He, C. He, Z. Yin, Y. Zou, L. Yin, X. Song, Z. Yuan, W. Zhang, C. Lv, X. Liang, S. Luan, L. Li, Recent advances in the medical use of silver complex, Eur. J. Med. Chem. 157 (2018) 62–80. doi:10.1016/j.ejmech.2018.07.057.

[98] S. Medici, M. Peana, V.M. Nurchi, M.A. Zoroddu, Medical Uses of Silver: History, Myths, and Scientific Evidence, J. Med. Chem. (2019). doi:10.1021/acs.jmedchem.8b01439.

[99] R.B.K. Wakshlak, R. Pedahzur, D. Avnir, Antibacterial activity of silver-killed bacteria: The "zombies" effect, Sci. Rep. 5 (2015) 1–5. doi:10.1038/srep09555.

[100] M. Pellei, V. Gandin, M. Marinelli, C. Marzano, M. Yousufuddin, H.V.R. Dias, C. Santini, Synthesis and biological activity of ester- and amide-functionalized imidazolium salts and related water-soluble coinage metal N-heterocyclic carbene complexes, Inorg. Chem. 51 (2012) 9873–9882. doi:10.1021/ic3013188.

[101] M. He, C. He, Z. Yin, Y. Zou, L. Yin, X. Song, Z. Yuan, W. Zhang, C. Lv, X. Liang, S. Luan, L. Li, Recent advances in the medical use of silver complex, Eur. J. Med. Chem. 157 (2018) 62–80. doi:10.1016/j.ejmech.2018.07.057.

[102] T. Storr, K.H. Thompson, C. Orvig, Design of targeting ligands in medicinal inorganic chemistry, Chem. Soc. Rev. 35 (2006) 534–544. doi:10.1039/b514859f.

[103] C. Isanbor, D. O 'hagan, Fluorine in medicinal chemistry: A review of anti-cancer agents, J. Fluor. Chem. 127 (2006) 303–319. doi:10.1016/j.jfluchem.2006.01.011.

[104] A. Pałasz, D. Cież, In search of uracil derivatives as bioactive agents. Uracils and fused uracils: Synthesis, biological activity and applications, Eur. J. Med. Chem. 97 (2015) 582–611. doi:10.1016/j.ejmech.2014.10.008.

[105] H.J. Lenz, S. Stintzing, F. Loupakis, TAS-102, a novel antitumor agent: A review of the mechanism of action, Cancer Treat. Rev. 41 (2015) 777–783. doi:10.1016/j.ctrv.2015.06.001.

[106] D.B. Longley, D.P. Harkin, P.G. Johnston, 5-Fluorouracil: Mechanisms of Action and Clinical Strategies., Nat. Rev. Cancer. 3 (2003) 330–338. doi:10.1038/nrc1074.

[107] J.P. Bégué, D. Bonnet-Delpon, Recent advances (1995-2005) in fluorinated pharmaceuticals based on natural products, J. Fluor. Chem. 127 (2006) 992–1012. doi:10.1016/j.jfluchem.2006.05.006.

[108] M.I. Gel'fman, N.A. Kustova, Complexes of Silver(I) with 5-Fluorouracil, Russ. J. Inorg. Chem. 15 (1970) 47–49.

[109] M.I. Gel'fman, N.A. Kustova, Complexes of Palladium(II) with 5-Fluoro-uracil, Russ. J. Inorg. Chem. 14 (1969) 985–988.

[110] M.I. Gel'fman, N.A. Kustova, Complexes of Platinum(II) with 5-Fluorouracil, Russ. J. Inorg. Chem. 15 (1970) 1602–1604.

[111] J.H.B. Nunes, P.P. de Paiva, A.L.T.G. Ruiz, J.E. de Carvalho, P.P. Corbi, A platinum(II) complex with the antitumor drug 5-fluorouracil: synthesis, spectroscopic characterization and biological assays, in: J. Biol. Inorg. Chem. - 18th Int. Conf. Biol. Inorg. Chem., 2017: p. S93. doi:10.1007/s00775-017-1475-y.

[112] J.H. Bormio Nunes, F.R.G. Bergamini, W.R. Lustri, P.P. Paiva, A.L.T.G. Ruiz, J.E. Carvalho, P.P. Corbi, Synthesis, characterization and in vitro biological assays of a silver(I) complex with 5-fluorouracil: a strategy to overcome multidrug resistant tumor cells, J. Fluor. Chem. 195 (2017) 93–101. doi:10.1016/j.jfluchem.2017.01.016.

[113] G.W. Anderson, I.F. Halverstadt, W.H. Miller, R.O. Roblin, Studies in Chemotherapy. X. Antithyroid Compounds. Synthesis of 5- and 6- Substituted 2-Thiouracils from ß-Oxoesters and Thiourea, J. Am. Chem. Soc. 67 (1945) 2197–2200.

[114] M.S. Masoud, O.H.A. El-Hamid, Z.M. Zaki, 2-thiouracil-based cobalt(II), nickel(II) and copper(II) complexes, Transit. Met. Chem. 19 (1994) 21–24.

[115] Y. Wei-Da, H. Yin-Ping, Copper Complexes of 2-Thiouracil, Polyhedron. 9 (1990) 2747–2750.

[116] L.G. Golubyatnikova, R.A. Khisamutdinov, S.A. Grabovskii, N.N. Kabal'nova, Y.I. Murinov, Complexes of Palladium(II) and Platinum(II) with 6-tert-butyl-2-thiouracil, Russ. J. Gen. Chem. 87 (2017) 117–121.

[117] D.M.L. Goodgame, G.A. Leach, Complexes of 2-Thiouracil with Some Divalent Metal ions, Inorganica Chim. Acta. 37 (1979) L505–L506.

[118] J.R. Lusty, J. Peeling, M.A. Abdel-aal, Complexes of 6-Methyl-2-thiouracil with Rhodium, Iridium, Platinum and Palladium, Inorganica Chim. Acta. 56 (1981) 21–26.

[119] C. Vetter, G.N. Kaluderovic, R. Paschke, R. Kluge, J. Schmidt, D. Steinborn, Synthesis, characterization and in vitro cytotoxicity studies of platinum(IV) complexes with thiouracil ligands, Inorganica Chim. Acta. 363 (2010) 2452–2460. doi:10.1016/j.ica.2010.03.079.

[120] M.N. Shaikh, B.A. Al-Maythalony, M.I.M. Wazeer, A.A. Isab, Complexations of 2-thiouracil and 2,4-dithiouracil with Cd(SeCN)2 and Hg(SeCN)2: NMR and anti-bacterial activity studies, Spectroscopy. 25 (2011) 187–195. doi:10.3233/SPE-2011-0503.

[121] Bruker, APEX2, SAINT and SADABS, Bruker AXS Inc., Madison, Wisconsin, USA, 2010.

[122] G.M. Sheldrick, A short history of SHELX, Acta Crystallogr. A. A64 (2008) 112–122. doi:10.1107/S0108767307043930.

[123] G.M. Sheldrick, SHELXT - Integrated space-group and crystal-structure determination, Acta Crystallogr. A. A71 (2015) 3–8. doi:10.1107/S2053273314026370.

[124] V. Vichai, K. Kirtikara, Sulforhodamine B colorimetric assay for cytotoxicity screening, Nat. Protoc. 1 (2006) 1112–1116. doi:10.1038/nprot.2006.179.

[125] E.A. Orellana, A.L. Kasinski, Sulforhodamine B (SRB) Assay in Cell Culture to Investigate Cell Proliferation, Bio-Protocol. 6 (2016). doi:10.21769/BioProtoc.1984.

[126] R.H. Shoemaker, The NCI60 human tumour cell line anticancer drug screen, Nat. Rev. Cancer. 6 (2006) 813–823. doi:10.1038/nrc1951.

[127] A. Monks, D. Scudiero, P. Skehan, R. Shoemaker, K. Paull, D. Vistica, C. Hose, J. Langley, P. Cronise, A. Vaigro-Wolff, M. Gray-Goodrich, H. Campbell, J. Mayo, M. Boyd, Feasibility of a High-Flux Anticancer Drug Screen Using a Diverse Panel of Cultured Human Tumor Cell Lines, J. Natl. Cancer Inst. 83 (1991) 757–766. doi:10.1093/jnci/83.11.757.

[128] N.A.P. Franken, H.M. Rodermond, J. Stap, J. Haveman, C. van Bree, Clonogenic assay of cells in vitro, Nat. Protoc. 1 (2006) 2315–2319. doi:10.1038/nprot.2006.339.

[129] A.D. Katnani, K.I. Papathomas, D.P. Drolet, A.J. Lees, THERMAL DECOMPOSITION OF PALLADIUM-IMIDAZOLE COMPLEXES, J. Therm. Anal. 35 (1989) 147–152.

[130] K. Nomiya, S. Takahashi, R. Noguchi, S. Nemoto, T. Takayama, M. Oda, Synthesis and characterization of water-soluble silver(I) complexes with L-histidine (H2his) and (S)-(-)-2-pyrrolidone-5-carboxylic acid (H2pyrrld) showing a wide spectrum of effective antibacterial and antifungal activities. Crystal structures of chiral , Inorg. Chem. 39 (2000) 3301–3311. doi:10.1021/ic990526o.

[131] G. Socrates, Infrared and Raman Characteristic Group Frequencies, 3rd ed., John Wiley & Sons, Inc., 2001.

[132] D.L. Pavia, G.M. Lampman, G.S. Kriz, Introduction to Spectroscopy, Thomson Learning, 2001.

[133] D.W. Zaharevitz, S.L. Holbeck, C. Bowerman, P.A. Svetlik, COMPARE: A web accessible tool for investigating mechanisms of cell growth inhibition, J. Mol. Graph. Model. 20 (2002) 297–303. doi:10.1016/S1093-3263(01)00126-7.

[134] T. Priestman, The Theoretical Basis of Cancer Chemotherapy, in: Cancer Chemother. Clin. Pract., Springer London, London, 2008: pp. 1–34. doi:10.1007/978-1-84628-991-0_1.

[135] A.J. Wilson, A.Y. Liu, J. Roland, O.B. Adebayo, S.A. Fletcher, J.C. Slaughter, J. Saskowski, M.A. Crispens, H.W. Jones, S. James, O. Fadare, D. Khabele, TR3 modulates platinum resistance in ovarian cancer, Cancer Res. 73 (2013) 4758–4769. doi:10.1158/0008-5472.CAN-12-4560.

[136] P.F. De Oliveira, J.M. Alves, J.L. Damasceno, R. Aparecida, M. Oliveira, H.J. Dias, A.E.M. Crotti, D.C. Tavares, Cytotoxicity screening of essential oils in cancer cell lines, Brazilian J. Pharmacogn. 25 (2015) 183–188. doi:10.1016/j.bjp.2015.02.009.

[137] J.S. Dwivedi, U. Agarwala, 2,4-Dithiouracil as Complexing Agent: Part I - Complexes of Co(II), Ni(II), Cu(II), Cd(II), Ag(I), Tl(I) & Pb(II), Indian J. Chem. 10 (1972) 652–656.

[138] B.F. Hoskins, L. Zhenrong, E.R.T. Tiekink, The characterization of 2-thiouracilato(triphenylphosphine)gold(I), Inorganica Chim. Acta. 158 (1989) 7–8. doi:10.1016/S0020-1693(00)84007-4.

[139] G.M. Stewart, E.R.T. Tiekink, M.A. Buntine, Structural Aspects of the Coordination of Triethylphosphinegold(I) to 2-Thiouracil: A Comparison between Theory and Experiment, J. Phys. Chem. A. 101 (1997) 5368–5373.

[140] C. Abbehausen, J.F. Castro, M.B.M. Spera, T.A. Heinrich, C.M. Costa-Neto, W.R. Lustri, A.L.B. Formiga, P.P. Corbi, Synthesis, spectroscopic characterization, DFT studies and biological assays of a novel gold(I) complex with 2-mercaptothiazoline, Polyhedron. 30 (2011) 2354–2359. doi:10.1016/j.poly.2011.06.021.

[141] C. Abbehausen, C.M. Manzano, P.P. Corbi, N.P. Farrell, Effects of coordination mode of 2-mercaptothiazoline on reactivity of Au(I) compounds with thiols and sulfur-containing proteins, J. Inorg. Biochem. 165 (2016) 136–145. doi:10.1016/j.jinorgbio.2016.05.011.

[142] C.S.W. Harker, E.R.T. Tielink, M.W. Whitehouse, Studies on the interaction of gold(I) phosphines with 2-thiouracil. Related studies with silver(I) phosphines, Inorganica Chim. Acta. 181 (1991) 23–30. doi:10.1016/S0020-1693(00)85255-X.

[143] E.R.T. Tiekink, Crystal structure of 2-thiouracil, Zeitschrift Für Krist. 187 (1989) 79–84.

[144] D.R. Lide, CRC Handbook of Chemistry and Physics, Internet Version 2005, 85th ed, CRC Press, Boca Raton, FL, 2005.

[145] A. Sułkowska, W.W. Sułkowski, K. Nowak, D. Pentak, M. Maciazek-Jurczyk, J. Równicka-Zubik, Determination of the binding site of chloro(triethylphosphine)gold(I) in serum albumin, J. Mol. Struct. 970 (2010) 106–110. doi:10.1016/j.molstruc.2010.02.053.

[146] A. Adan, G. Alizada, Y. Kiraz, Y. Baran, A. Nalbant, Flow cytometry: basic principles and applications, Crit. Rev. Biotechnol. 37 (2017) 163–176. doi:10.3109/07388551.2015.1128876.

[147] L.C.U. Junqueira, J. Carneiro, Biologia Celular e Molecular, 9th ed., Guanabara Koogan, 2012.

[148] National Cancer Institute, Cell Lines in the In Vitro Screen, (2015). https://dtp.cancer.gov/discovery_development/nci-60/cell_list.htm (accessed August 5, 2019).

[149] Merk Millipore, Guava Cell Cycle, (2017). http://www.merckmillipore.com/BR/pt/product/Guava-Cell-Cycle-Reagent-for-Flow-Cytometry,MM_NF-4500-0220?ReferrerURL=https%3A%2F%2Fwww.google.com.br%2F&bd=1#anchor_UG.

[150] J.C. Chuang, G.T. Sheu, P.C. Wang, F.T. Liao, W.S. Liu, C.F. Huang, M.H. Tseng, M.F. Wu, Docetaxel and 5-fluorouracil induce human p53 tumor suppressor gene transcription via a short sequence at core promoter element, Toxicol. Vitr. 26 (2012) 678–685. doi:10.1016/j.tiv.2012.03.004.

[151] K. Vermeulen, Z.N. Berneman, D.R. Van Bockstaele, Cell cycle and apoptosis, Cell Prolif. 36 (2003) 165–175. doi:10.1046/j.1365-2184.2003.00267.x.

[152] M. de C. Filgueiras, A. Morrot, P.M.G. Soares, M.L. Costa, C. Mermelstein, Effects of 5-Fluorouracil in Nuclear and Cellular Morphology, Proliferation, Cell Cycle, Apoptosis, Cytoskeletal and Caveolar Distribution in Primary Cultures of Smooth Muscle Cells, PLoS One. 8 (2013). doi:10.1371/journal.pone.0063177.

[153] H. Rafehi, C. Orlowski, G.T. Georgiadis, K. Ververis, A. El-Osta, T.C. Karagiannis, Clonogenic Assay: Adherent Cells, J. Vis. Exp. (2011) 15–17. doi:10.3791/2573.

[154] A. Munshi, M. Hobbs, R.E. Meyn, Clonogenic Cell Survival Assay, in: R.D. Blumenthal (Ed.), Chemosensitivity. Methods Mol. Med., vol 110, Humana Press, 2005. doi:10.1385/1-59259-869-2:021.

[155] L. Galluzzi, I. Vitale, S.A. Aaronson, J.M. Abrams, D. Adam, P. Agostinis, E.S. Alnemri, L. Altucci, I. Amelio, D.W. Andrews, M. Annicchiarico-Petruzzelli, A. V Antonov, E. Arama, E.H. Baehrecke, N.A. Barlev, N.G. Bazan, F. Bernassola, M.J.M. Bertrand, K. Bianchi, M. V Blagosklonny, K. Blomgren, C. Borner, P. Boya, C. Brenner, M. Campanella, E. Candi, D. Carmona-Gutierrez, F. Cecconi, F.K.-M. Chan, N.S. Chandel, E.H. Cheng, J.E. Chipuk, J.A. Cidlowski, A. Ciechanover, G.M. Cohen, M. Conrad, J.R. Cubillos-Ruiz, P.E. Czabotar, V. D'Angiolella, T.M. Dawson, V.L. Dawson, V. De Laurenzi, R. De Maria, K.-M. Debatin, R.J. DeBerardinis, M. Deshmukh, N. Di Daniele, F. Di Virgilio, V.M. Dixit, S.J. Dixon, C.S. Duckett, B.D. Dynlacht, W.S. El-Deiry, J.W. Elrod, G.M. Fimia, S. Fulda, A.J. García-Sáez, A.D. Garg, C. Garrido, E. Gavathiotis, P. Golstein, E. Gottlieb, D.R. Green, L.A. Greene, H. Gronemeyer, A. Gross, G. Hajnoczky, J.M. Hardwick, I.S. Harris, M.O. Hengartner, C. Hetz, H. Ichijo, M. Jäättelä, B. Joseph, P.J. Jost, P.P. Juin, W.J. Kaiser, M. Karin, T. Kaufmann, O. Kepp, A. Kimchi, R.N. Kitsis, D.J. Klionsky, R.A. Knight, S. Kumar, S.W. Lee, J.J. Lemasters, B. Levine, A. Linkermann, S.A. Lipton, R.A. Lockshin, C. López-Otín, S.W. Lowe, T. Luedde, E. Lugli, M. MacFarlane, F. Madeo, M. Malewicz, W. Malorni, G. Manic, J.-C. Marine, S.J. Martin, J.-C. Martinou, J.P. Medema, P. Mehlen, P. Meier, S. Melino, E.A. Miao, J.D. Molkentin, U.M. Moll, C. Muñoz-Pinedo, S. Nagata, G. Nuñez, A. Oberst, M. Oren, M. Overholtzer, M. Pagano, T. Panaretakis, M. Pasparakis, J.M. Penninger, D.M. Pereira, S. Pervaiz, M.E. Peter, M. Piacentini, P. Pinton, J.H.M. Prehn, H. Puthalakath, G.A. Rabinovich, M. Rehm, R. Rizzuto, C.M.P. Rodrigues, D.C. Rubinsztein, T. Rudel, K.M. Ryan, E. Sayan, L. Scorrano, F. Shao, Y. Shi, J. Silke, H.-U. Simon, A. Sistigu, B.R. Stockwell, A. Strasser, G. Szabadkai, S.W.G. Tait, D. Tang, N. Tavernarakis, A. Thorburn, Y. Tsujimoto, B. Turk, T. Vanden Berghe, P. Vandenabeele, M.G. Vander Heiden, A. Villunger, H.W. Virgin, K.H. Vousden, D. Vucic, E.F. Wagner, H. Walczak, D. Wallach, Y. Wang, J.A. Wells, W. Wood, J. Yuan, Z. Zakeri, B. Zhivotovsky, L. Zitvogel, G. Melino, G. Kroemer, Molecular mechanisms of cell death: recommendations of the Nomenclature Committee on Cell Death 2018., Cell Death Differ. 25 (2018) 486–541. doi:10.1038/s41418-017-0012-4.

[156] G.B. Longato, G.F. Fiorito, D.B. Vendramini-Costa, I.M. de O. Sousa, S.V. Tinti, A.L.T.G. Ruiz, S.M.V. de Almeida, R.J.R. Padilha, M.A. Foglio, J.E. de Carvalho, Different cell death responses induced by eupomatenoid-5 in MCF-7 and 786-0 tumor cell lines, Toxicol. Vitr. 29 (2015) 1026–1033. doi:10.1016/j.tiv.2015.04.002.

[157] P. Ludovico, F. Sansonetty, M. Corte-Real, Assessment of mitochondrial membrane potential in yeast cell populations by flow cytometry, Microbiology. 147 (2001) 3335–3343. doi:10.1099/00221287-147-12-3335.

[158] K. Mohana, R. Srivalli, P.K. Lakshmi, Overview of P-glycoprotein inhibitors: a rational outlook, Brazilian J. Pharm. Sci. 48 (2012) 353–367. doi:10.1590/S1984-82502012000300002.

[159] Y. Ji, S. Wei, J. Hou, C. Zhang, P. Xue, J. Wang, X. Chen, X. Guo, F. Yang, Integrated proteomic and N-glycoproteomic analyses of doxorubicin sensitive and resistant ovarian cancer cells reveal glycoprotein alteration in protein abundance and glycosylation, Oncotarget. 8 (2017) 13413–13427. doi:10.18632/oncotarget.14542.

[160] Y. Bin Im, I. Ha, K.W. Kang, M.-Y. Lee, H.-K. Han, Macelignan: A New Modulator of P-Glycoprotein in Multidrug-Resistant Cancer Cells, Nutr. Cancer. 61 (2009) 538–543. doi:10.1080/01635580802666273.

[161] L. Eloy, A.S. Jarrousse, M.L. Teyssot, A. Gautier, L. Morel, C. Jolivalt, T. Cresteil, S. Roland, Anticancer Activity of Silver-N-Heterocyclic Carbene Complexes: Caspase-Independent Induction of Apoptosis via Mitochondrial Apoptosis-Inducing Factor (AIF), ChemMedChem. 7 (2012) 805–814. doi:10.1002/cmdc.201200055.

[162] Z. Engelbrecht, R. Meijboom, M.J. Cronjé, The ability of silver(I) thiocyanate 4-methoxyphenyl phosphine to induce apoptotic cell death in esophageal cancer cells is correlated to mitochondrial perturbations, BioMetals. 31 (2018) 189–202. doi:10.1007/s10534-017-0051-9.

[163] J.M. Brown, L.D. Attardi, The role of apoptosis in cancer development and treatment response, Nat. Rev. Cancer. 5 (2005) 231–237. doi:10.2174/138161210789941883.

[164] S.L. Fink, B.T. Cookson, Apoptosis, Pyroptosis, and Necrosis: Mechanistic Description of Dead and Dying Eukaryotic Cells, Infect. Immun. 73 (2005) 1907–1916. doi:10.1128/IAI.73.4.1907–1916.2005.

[165] F. Manning, K. Zuzel, Comparison of types of cell death: apoptosis and necrosis, J. Biol. Educ. 373 (2003) 141–145. doi:10.1080/00219266.2003.9655870.

[166] Merk Millipore, Guava Nexin Reagent, (2017). http://www.merckmillipore.com/BR/pt/product/Guava-Nexin-Reagent-for-Flow-Cytometry---100-tests,MM_NF-4500-0450.

[167] R.C. Barcelos, J.C. Pastre, D.B. Vendramini-Costa, V. Caixeta, G.B. Longato, P.A. Monteiro, J.E. De Carvalho, R.A. Pilli, Design and synthesis of N-acylated aza-goniothalamin derivatives and evaluation of their in vitro and in vivo antitumor activity, ChemMedChem. 9 (2014) 2725–2743. doi:10.1002/cmdc.201402292.

[168] A. Filippi, M. Zancani, E. Petrussa, E. Braidot, Caspase-3-like activity and proteasome degradation in grapevine suspension cell cultures undergoing silver-induced programmed cell death, J. Plant Physiol. 233 (2019) 42–51. doi:10.1016/j.jplph.2018.12.003.

[169] E.A. Slee, C. Adrain, S.J. Martin, Serial killers: Ordering caspase activation events in apoptosis, Cell Death Differ. 6 (1999) 1067–1074. doi:10.1038/sj.cdd.4400601.

[170] N. Akpan, C.M. Troy, Caspase Inhibitors, Neurosci. 19 (2013) 129–136. doi:10.1177/1073858412447875.

[171] A. Gomes, E. Fernandes, J.L.F.C. Lima, Fluorescence probes used for detection of reactive oxygen species, J. Biochem. Biophys. Methods. 65 (2005) 45–80. doi:10.1016/j.jbbm.2005.10.003.

[172] C.P. LeBel, H. Ischiropoulos, S.C. Bondy, Evaluation of the probe 2',7'-dichlorofluorescin as an indicator of reactive oxygen species formation and oxidative stress, Chem. Res. Toxicol. 5 (1992) 227–231. doi:10.1021/tx00026a012.

[173] T.S. Lobana, R. Sharma, G. Bawa, S. Khanna, Bonding and structure trends of thiosemicarbazone derivatives of metals-An overview, Coord. Chem. Rev. 253 (2009) 977–1055. doi:10.1016/j.ccr.2008.07.004.

[174] J. Shim, N.R. Jyothi, N.A.M. Farook, Biological applications of thiosemicarbazones and their metal complexes, Asian J. Chem. 25 (2013) 5838–5840. doi:10.14233/ajchem.2013.OH105.

[175] R.W. Brockman, J.R. Thomson, M.J. Bell, H.E. Skipper, Observations on the antileukemic activity of pyridine-2-carboxaldehyde thiosemicarbazone and thiocarbohydrazone, Cancer Res. 16 (1956) 167–170.

[176] F.A. French, B.L. Freedlander, Carcinostatic Action of Polycarbonyl Compounds and Their Derivatives: IV. Glyoxal Bis (thiosemicarbazone) and Derivatives, Cancer Res. 18 (1958) 1290–1300.

[177] H.G. Petering, H.H. Buskirk, G.E. Underwood, The Anti-Tumor Activity of 2-Keto-3-Ethoxybutyraldehyde Bis(Thiosemicarbazone) and Related Compounds., Cancer Res. 24 (1964) 367–372.

[178] H.G. Petering, H.H. Buskirk, J.A. Crim, G.J. Van Giessen, The Effect of Essential Metal Ions on the Antitumor Activity of Kethoxal Bis(thiosemicarbazone) (KTS), Pharmacologist. 5 (1963) 271.

[179] J.A. Crim, H.G. Petering, The Antitumor Activity of Cu(II) KTS, the Copper(II) Chelate of 3-Ethoxy-2-oxobutyraldehyde Bis(thisemicarbazone), Cancer Res. 27 (1967) 1278–1285.

[180] E. Mihich, A.I. Mulhern, In vivo Effects of the Zinc Chelate of Kethoxal Bis(thiosemicarbazone) (KTS-Zn), Pharmacologist. 7 (1965) 179.

[181] B.A. Booth, A.C. Sartorelli, Metabolic Activity Effects of Copper in Intact Cells: Comparative Activity of Cupric Chrolide and the Cupric Chelate of Kethoxal Bis (thiosemicarbazone), Mol. Pharmacol. 3 (1967) 290–302.

[182] D.T. Minkel, L.A. Saryan, D.H. Petering, Structure-Function Correlations in the Reaction of Bis(thiosemicarbazonato) Copper(II) Complexes with Ehrlich Ascites Tumor Cells, Cancer Res. 38 (1978) 124–129.

[183] D.S. Kalinowski, C. Stefani, S. Toyokuni, T. Ganz, G.J. Anderson, N. V. Subramaniam, D. Trinder, J.K. Olynyk, A. Chua, P.J. Jansson, S. Sahni, D.J.R. Lane, A.M. Merlot, Z. Kovacevic, M.L.H. Huang, C.S. Lee, D.R. Richardson, Redox cycling metals: Pedaling their roles in metabolism and their use in the development of novel therapeutics, Biochim. Biophys. Acta. 1863 (2016) 727–748. doi:10.1016/j.bbamcr.2016.01.026.

[184] E.C. Moore, M.S. Zedeck, K.C. Agrawal, A.C. Sartorelli, Inhibition of Ribonucleoside Diphosphate Reductase by 1-Formylisoquinolone Thiosemicarbazone and Related Compounds, Biochemistry. 9 (1970) 4492–4498.

[185] L. Thelander, A. Graslung, Mechanism of Inhibition of Mammalian Ribonucleotide Reductase by the Iron Chelate of 1-Formylisoquinoline Thiosemicarbazone, J. Biol. Chem. 258 (1983) 1063–1066.

[186] R.H.U. Borges, E. Paniago, H. Beraldo, Equilibrium and kinetic studies of iron(II) and iron(III) complexes of some a-(N)-heterocyclic thiosemicarbazones. Reduction of the iron(III) complexes of 2-formylpyridine thiosemicarbazone and 2-acetylpyridine thiosemicarbazone by cellular thiol-like red, J. Inorg. Biochem. 65 (1997) 267–275. doi:10.1016/S0162-0134(96)00142-0.

[187] B.S.P. H. Beraldo, B.S.P. D. Gambinob, The Wide Pharmacological Versatility of Semicarbazones, Thiosemicarbazones and Their Metal Complexes, Mini-Reviews Med. Chem. 4 (2004) 31–39. doi:10.2174/1389557043487484.

[188] J. García-Tojal, A. García-Orad, J.L. Serra, J.L. Pizarro, L. Lezama, M.I. Arriortua, T. Rojo, Synthesis and spectroscopic properties of copper(II) complexes derived from thiophene-2-carbaldehyde thiosemicarbazone. Structure and biological activity of [Cu(C6H6N3S2)2], J. Inorg. Biochem. 75 (1999) 45–54. doi:10.1016/S0162-0134(99)00031-8.

[189] J. García-Tojal, A. García-Orad, a a Díaz, J.L. Serra, M.K. Urtiaga, M.I. Arriortua, T. Rojo, Biological activity of complexes derived from pyridine-2-carbaldehyde thiosemicarbazone. Structure of., J. Inorg. Biochem. 84 (2001) 271–278. doi:10.1016/S0162-0134(01)00184-2.

[190] R.C. DeConti, B.R. Toftness, K.C. Agrawal, R. Tomchick, J.A.R. Mead, J.R. Bertino, A.C. Sartorelli, W.A. Creasey, Clinical and Pharmacological Studies with 5-Hydroxy-2-formylpyridine Thiosemicarbazone, Cancer Res. 32 (1972) 1455–1462.

[191] Y. Yu, D.S. Kalinowski, Z. Kovacevic, A.R. Siafakas, P.J. Jansson, C. Stefani, D.B. Lovejoy, P.C. Sharpe, P. V. Bernhardt, D.R. Richardson, Thiosemicarbazones from the old to new: Iron chelators that are more than just ribonucleotide reductase inhibitors, J. Med. Chem. 52 (2009) 5271–5294. doi:10.1021/jm900552r.

[192] K. Pelivan, W. Miklos, S. Van Schoonhoven, G. Koellensperger, L. Gille, W. Berger, P. Heffeter, C.R. Kowol, B.K. Keppler, Differences in protein binding and excretion of Triapine and its Fe(III) complex, J. Inorg. Biochem. 160 (2016) 61–69. doi:10.1016/j.jinorgbio.2015.10.006.

[193] J. Yuan, D.B. Lovejoy, D.R. Richardson, Novel di-2-pyridyl–derived iron chelators with marked and selective antitumor activity: in vitro and in vivo assessment, Blood. 104 (2004) 1450–1458. doi:10.1182/blood-2004-03-0868.

[194] M. Whitnall, J. Howard, P. Ponka, D.R. Richardson, A class of iron chelators with a wide spectrum of potent antitumor activity that overcomes resistance to chemotherapeutics, Proc. Natl. Acad. Sci. U. S. A. 103 (2006) 12901–14906. http://www.pnas.org/content/103/40/14901.full.pdf.

[195] C.R. Kowol, R. Trondl, P. Heffeter, V.B. Arion, M.A. Jakupec, A. Roller, M. Galanski, W. Berger, B.K. Keppler, Impact of Metal Coordination on Cytotoxicity of 3-Aminopyridine-2-carboxaldehyde Thiosemicarbazone (Triapine) and Novel Insights into Terminal Dimethylation, J. Med. Chem. 52 (2009) 5032–5043. doi:10.1021/jm900528d.

[196] P. Heffeter, C. Pirker, C.R. Kowol, G. Herrman, R. Dornetshuber, W. Miklos, U. Jungwirth, G. Koellensperger, B.K. Keppler, W. Berger, Impact of terminal dimethylation on the resistance profile of α-N-heterocyclic thiosemicarbazones, Biochem. Pharmacol. 83 (2012) 1623–1633. doi:10.1016/j.bcp.2012.03.004.

[197] C.R. Kowol, W. Miklos, S. Pfaff, S. Hager, S. Kallus, K. Pelivan, M. Kubanik, É.A. Enyedy, W. Berger, P. Heffeter, B.K. Keppler, Impact of Stepwise NH2-Methylation of Triapine on the Physicochemical Properties, Anticancer Activity, and Resistance Circumvention, J. Med. Chem. 59 (2016) 6739–6752. doi:10.1021/acs.jmedchem.6b00342.

[198] Z. Kovacevic, S. Chikhani, D.B. Lovejoy, D.R. Richardson, Novel Thiosemicarbazone Iron Chelators Induce Up-Regulation and Phosphorylation of the Metastasis Suppressor N-myc Down-Stream Regulated Gene 1: A New Strategy for the Treatment of Pancreatic Cancer, Mol. Pharmacol. 80 (2011) 598–609. doi:10.1124/mol.111.073627.

[199] Dose-finding and Pharmacokinetic Study of DpC, Administered Orally to Patients With Advanced Solid Tumors, (2016). https://clinicaltrials.gov/ct2/show/NCT02688101?term=DpC&rank=1.

[200] A Study of COTI-2 for the Treatment of Advanced or Recurrent Gynecologic Malignancies (COTI2-101), (2015). https://clinicaltrials.gov/ct2/show/NCT02433626?term=COTI-2&rank=1.

[201] W.R. Danter, M. Brown, F. Lepifre, Compounds and method for treatment of cancer. Patent US8034815B2, US8034815B2, 2011.

[202] K.Y. Salim, S. Maleki Vareki, W.R. Danter, J. Koropatnick, COTI-2, a novel small molecule that is active against multiple human cancer cell lines in vitro and in vivo., Oncotarget. 7 (2016) 41363–41379. doi:10.18632/oncotarget.9133.

[203] Critical Outcome Technologies Inc., COTI-2 Reactivating Mutant p53, (2014). https://pt.slideshare.net/CriticalOutcome/coti-2-p53-sweden-final.

[204] Bruker SAINT v8.38B, Bruker AXS, (2005) Copyright 2005-2019.

[205] G.M. Sheldrick, SADABS, (1996) University of Göttingen, Germany.

[206] O. V. Dolomanov, L.J. Bourhis, R.J. Gildea, J.A.K. Howard, H. Puschmann, OLEX2: a complete structure solution, refinement and analysis program, J. Appl. Crystallogr. 42 (2009) 339–341. doi:10.1107/S0021889808042726.

[207] C.B. Hübschle, G.M. Sheldrick, B. Dittrich, ShelXle: A Qt graphical user interface for SHELXL, J. Appl. Crystallogr. 44 (2011) 1281–1284. doi:10.1107/S0021889811043202.

[208] G.M. Sheldrick, SHELXS v 2016/4, (2015) University of Göttingen, Germany.

[209] G.M. Sheldrick, SHELXL v 2016/4, (2015) University of Göttingen, Germany.

[210] A.L. Spek, Structure validation in chemical crystallography, Acta Crystallogr. Sect. D Biol. Crystallogr. 65 (2009) 148–155. doi:10.1107/S090744490804362X.

[211] T.L. Lemke, T.W. Shek, L.A.L.K.S. Cates, L.A. Cosby, A.C. Sartorelli, Synthesis of thiosemicarbazones as potential antitumor agents, J. Med. Chem. 20 (1977) 1351–1354.

[212] M. Serda, D.S. Kalinowski, N. Rasko, E. Potůčková, A. Mrozek-Wilczkiewicz, R. Musiol, J.G. Małecki, M. Sajewicz, A. Ratuszna, A. Muchowicz, J. Gołąb, T. Šimůnek, D.R. Richardson, J. Polanski, Exploring the Anti-Cancer Activity of Novel Thiosemicarbazones Generated through the Combination of Retro-Fragments: Dissection of Critical Structure-Activity Relationships, PLoS One. 9 (2014) e110291. doi:10.1371/journal.pone.0110291.

[213] C.R. Kowol, R. Eichinger, M.A. Jakupec, M. Galanski, V.B. Arion, B.K. Keppler, Effect of metal ion complexation and chalcogen donor identity on the antiproliferative activity of 2-acetylpyridine N,N-dimethyl(chalcogen)semicarbazones, J. Inorg. Biochem. 101 (2007) 1946–1957. doi:10.1016/j.jinorgbio.2007.07.026.

[214] C.R. Kowol, P. Heffeter, W. Miklos, L. Gille, R. Trondl, L. Cappellacci, W. Berger, B.K. Keppler, Mechanisms underlying reductant-induced reactive oxygen species formation by anticancer copper(II) compounds, J. Biol. Inorg. Chem. 17 (2012) 409–423. doi:10.1007/s00775-011-0864-x.

[215] C.R. Kowol, R. Trondl, V.B. Arion, M.A. Jakupec, B.K. Keppler, Fluorescence properties and cellular distribution of the investigational anticancer drug Triapine (3-aminopyridine-2-carboxaldehyde thiosemicarbazone) and its zinc(II) complex, Dalt. Trans. 39 (2010) 704–706. doi:10.1039/b919119b.

[216] M. Joseph, M. Kuriakose, M.R.P. Kurup, E. Suresh, A. Kishore, S.G. Bhat, Structural, antimicrobial and spectral studies of copper(II) complexes of 2-benzoylpyridine N(4)-phenyl thiosemicarbazone, Polyhedron. 25 (2006) 61–70. doi:10.1016/j.poly.2005.07.006.

[217] S. Saswati, A. Chakraborty, S.P. Dash, A.K. Panda, R. Acharyya, A. Biswas, S. Mukhopadhyay, S.K. Bhutia, A. Crochet, Y.P. Patil, M. Nethaji, R. Dinda, Synthesis, X-ray structure and in vitro cytotoxicity studies of Cu(I/II) complexes of thiosemicarbazone: special emphasis on their interactions with DNA, Dalt. Trans. 44 (2015) 6140–6157. doi:10.1039/C4DT03764B.

[218] A.B. Beshir, S.K. Guchhait, J.A. Gascón, G. Fenteany, Synthesis and structure-activity relationships of metal-ligand complexes that potently inhibit cell migration, Bioorganic Med. Chem. Lett. 18 (2008) 498–504. doi:10.1016/j.bmcl.2007.11.099.

[219] Y.H. Liu, A. Li, J. Shao, C.Z. Xie, X.Q. Song, W.G. Bao, J.Y. Xu, Four Cu(II) complexes based on antitumor chelators: Synthesis, structure, DNA binding/damage, HSA interaction and enhanced cytotoxicity, Dalt. Trans. 45 (2016) 8036–8049. doi:10.1039/c6dt00451b.

[220] S. van Schoonhoven, C.R. Kowol, B.K. Keppler, M. Spitzwieser, C. Pirker, R. Dornetshuber-Fleiss, P. Heffeter, B. Englinger, M. Cichna-Markl, W. Berger, K. Pelivan, G. Koellensperger, W. Miklos, Triapine-mediated ABCB1 induction via PKC induces widespread therapy unresponsiveness but is not underlying acquired triapine resistance, Cancer Lett. 361 (2015) 112–120. doi:10.1016/j.canlet.2015.02.049.

[221] P. Heffeter, V.F.S. Pape, E.A. Enyedy, B.K. Keppler, G. Szakacs, C.R. Kowol, Anticancer thiosemicarbazones: chemical properties, interaction with iron metabolism, and resistance development, Antioxid. Redox Signal. 30 (2019) 1062–1082. doi:10.1089/ars.2017.7487.

Appendix

FIGURES

PART 1: Metal complexes with uracil derivatives

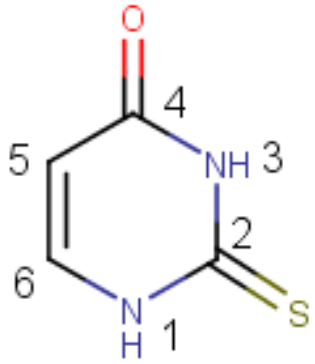

Figure A1. Molecular structure of tuH_2 ($C_4H_4N_2OS$) with atom numbering.

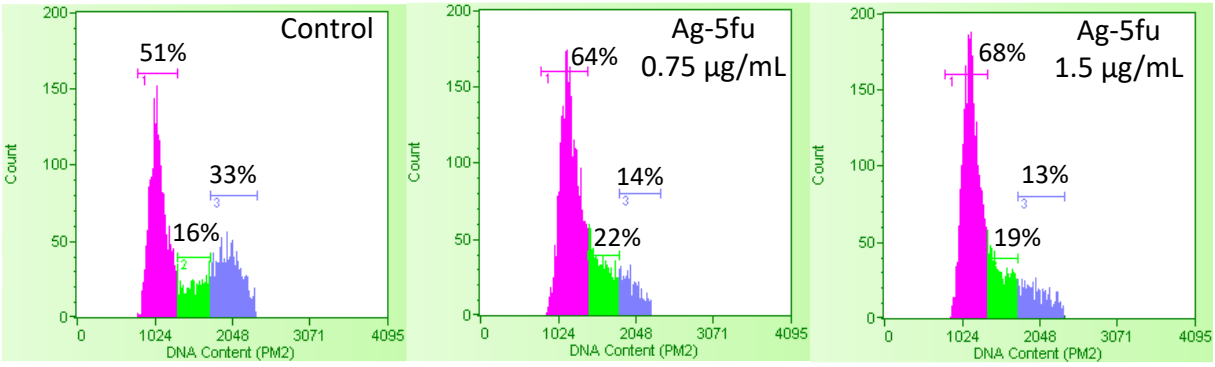

Figure A2. Histograms of cell cycle analysis of Ag-5fu over NCI/ADR-RES cells (36 h) in comparison to control.

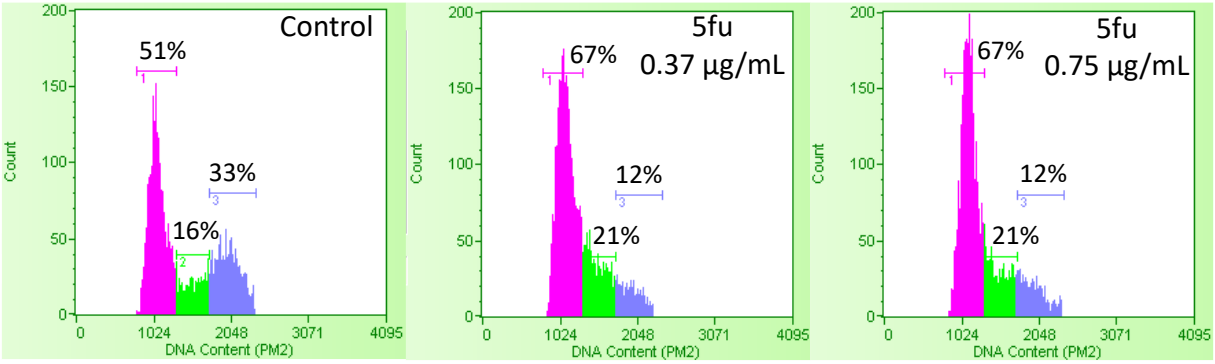

Figure A3. Histograms of cell cycle analysis of 5fu over NCI/ADR-RES cells (36 h) in comparison to control.

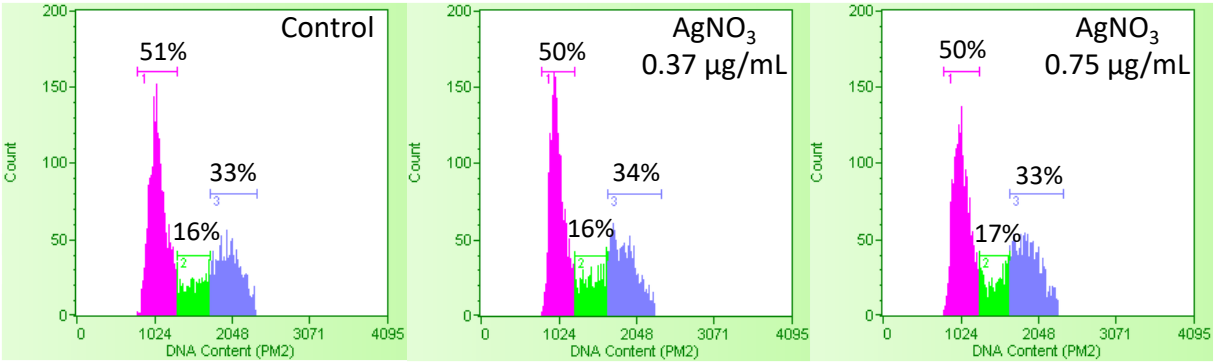

Figure A4. Histograms of cell cycle analysis of $AgNO_3$ over NCI/ADR-RES cells (36 h) in comparison to control.

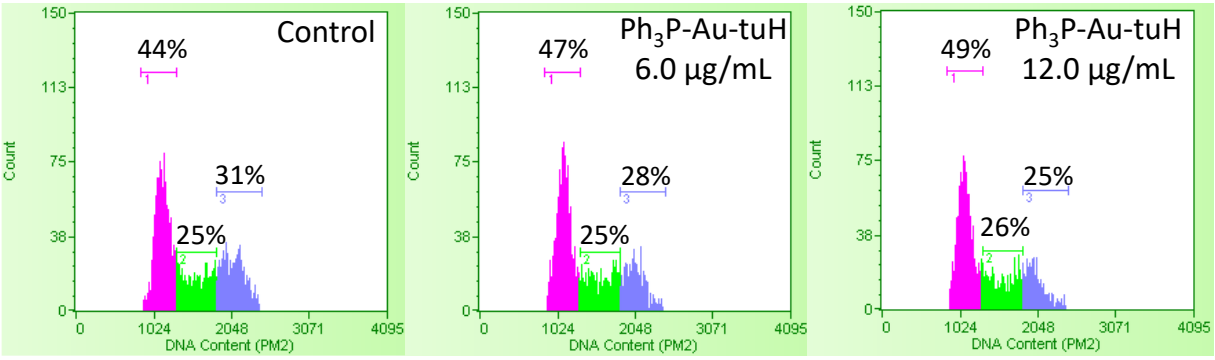

Figure A5. Histograms of cell cycle analysis of Ph_3P-Au-tuH over NCI-H460 cells (18 h) in comparison to control.

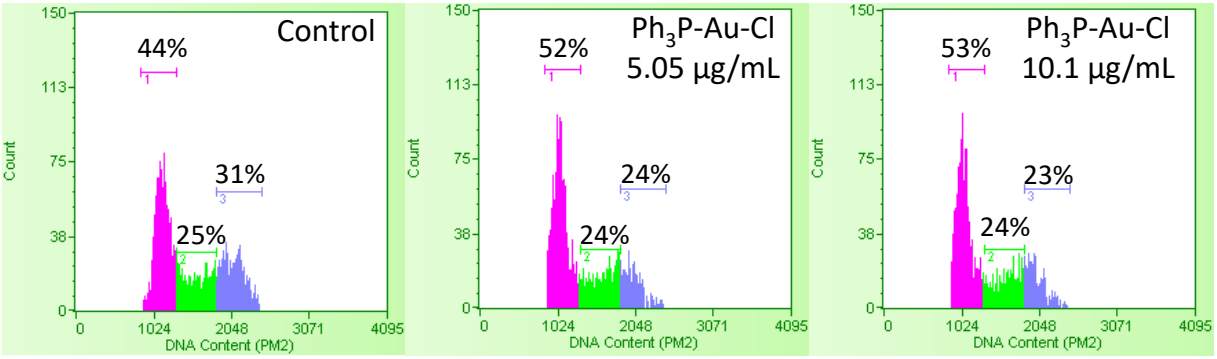

Figure A6. Histograms of cell cycle analysis of Ph_3P-Au-Cl over NCI-H460 cells (18 h) in comparison to control.

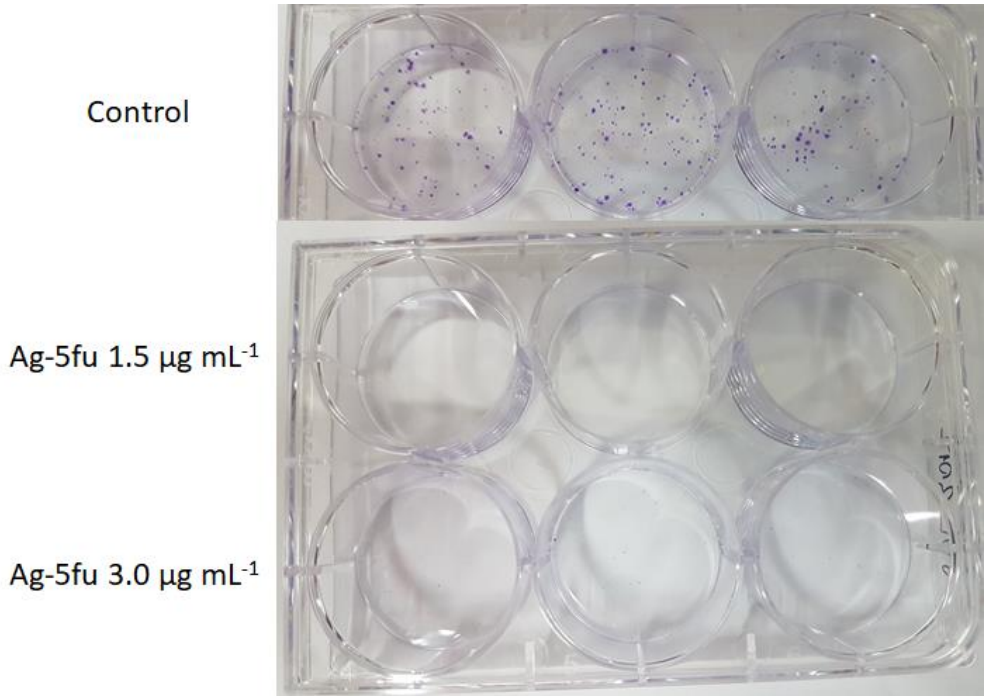

Figure A7. Plates with fixed NCI/ADR-RES cells after 12 days of growth from 200 cells previously treated with 1.5 and 3.0 µg mL^{-1} of Ag-5fu. Untreated cells are expressed as control.

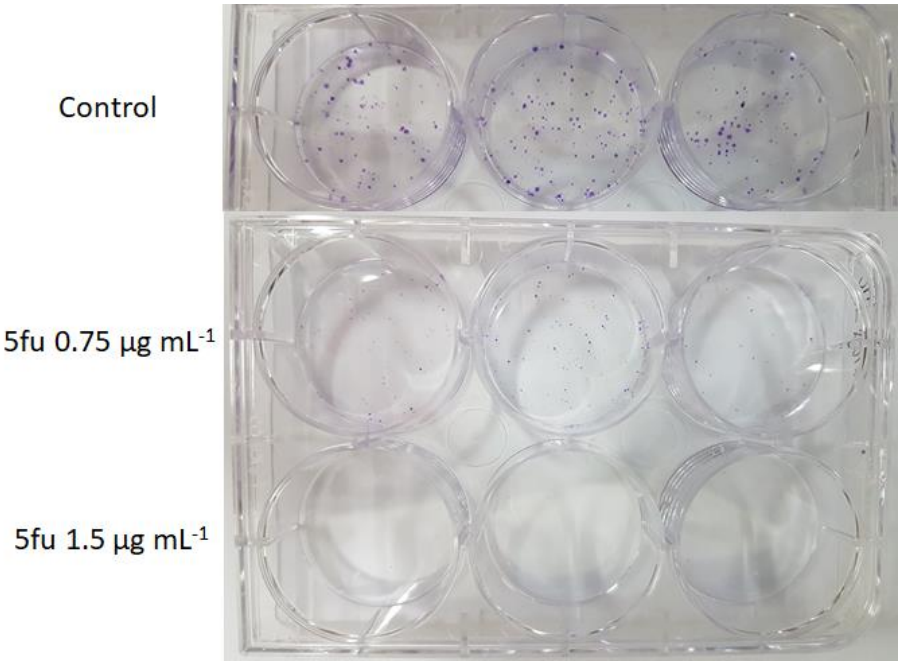

Figure A8. Plates with fixed NCI/ADR-RES cells after 12 days of growth from 200 cells previously treated with 0.75 and 1.5 µg mL^{-1} of 5fu. Untreated cells are expressed as control.

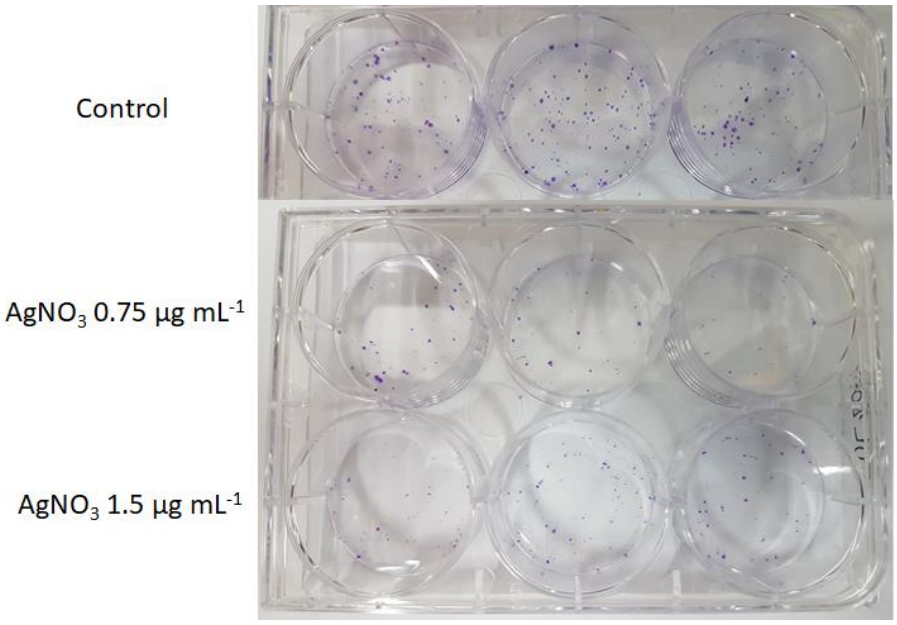

Figure A9. Plates with fixed NCI/ADR-RES cells after 12 days of growth from 200 cells previously treated with 0.75 and 1.5 µg mL^{-1} of $AgNO_3$. Untreated cells are expressed as control.

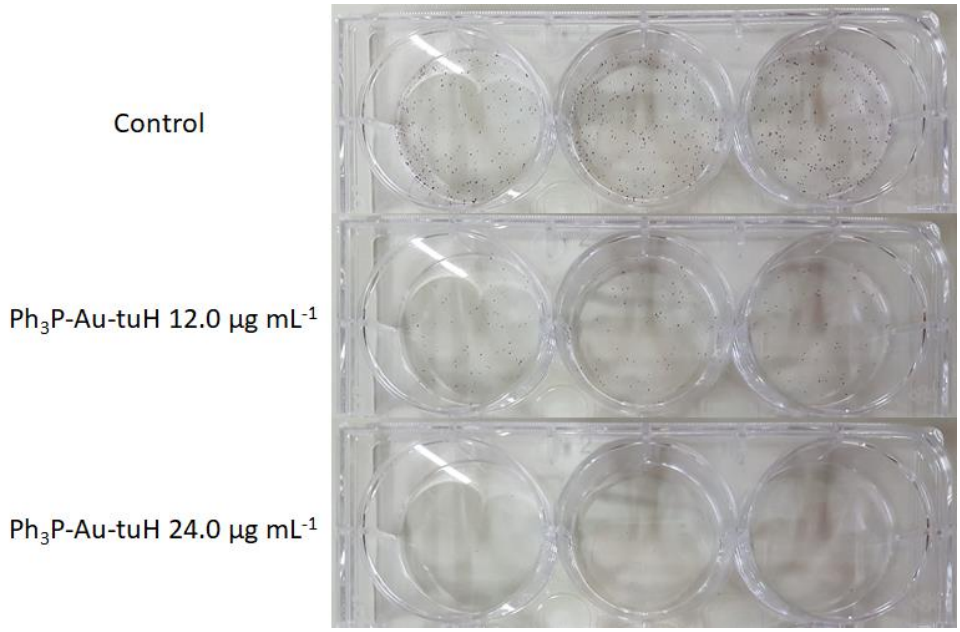

Figure A10. Plates with fixed NCI-H460 cells after 6 days of growth from 100 cells previously treated with 12.0 and 24.0 µg mL^{-1} of Ph_3P-Au-tuH. Untreated cells are expressed as control.

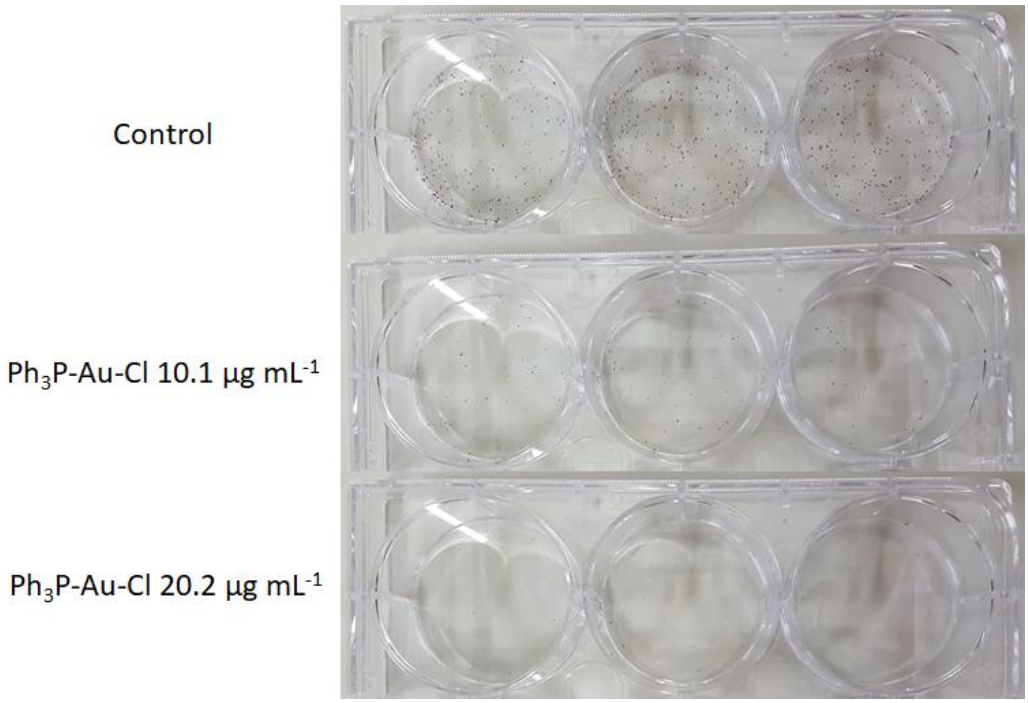

Figure A11. Plates with fixed NCI-H460 cells after 6 days of growth from 100 cells previously treated with 10.1 and 20.2 µg mL^{-1} of Ph_3P-Au-Cl. Untreated cells are expressed as control.

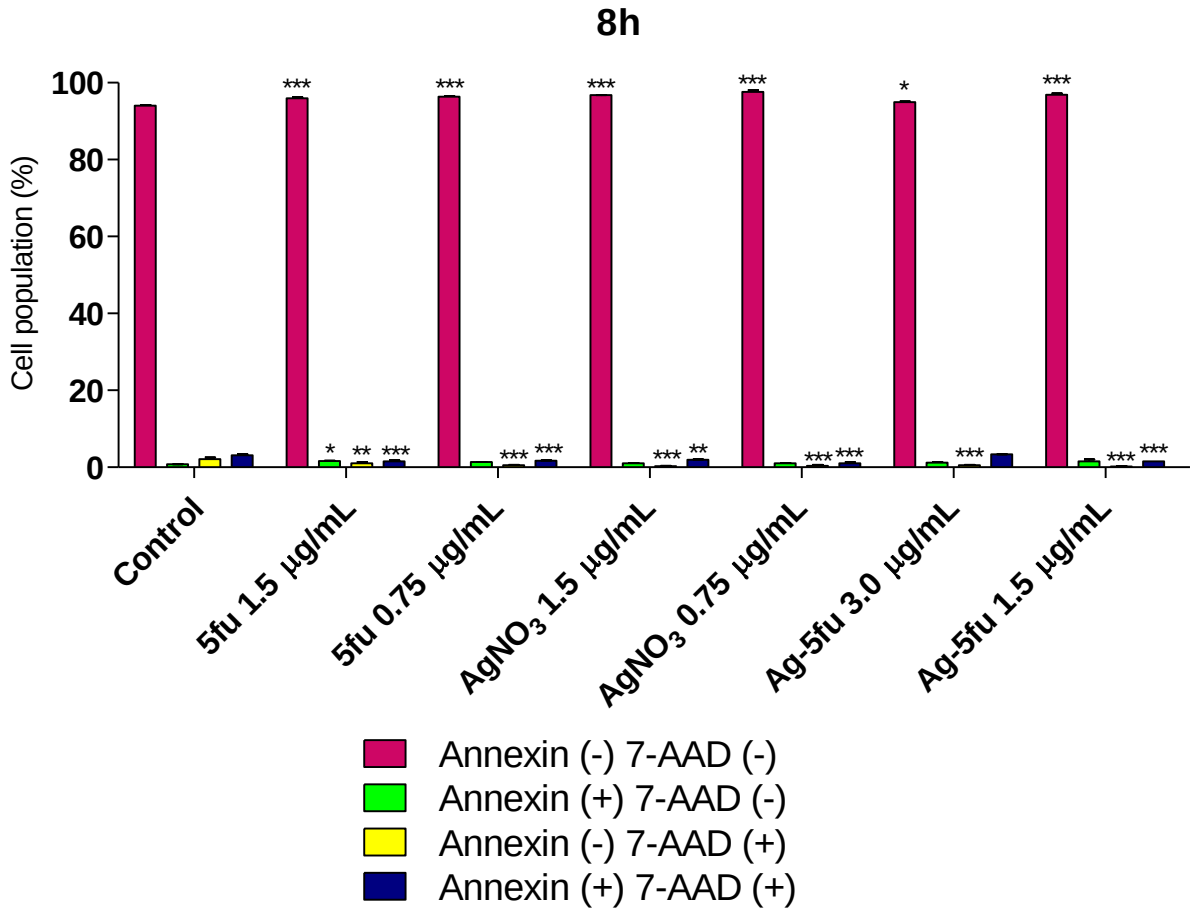

Figure A12. Influence of Ag-5fu, 5fu, and $AgNO_3$ on phosphatidylserine externalization of NCI/ADR-RES after 8 h of treatment. NCI/ADR-RES cells were treated for 8 h with Ag-5fu (1.5 and 3.0 µg/mL), 5fu (0.75 and 1.5 µg/mL) or $AgNO_3$ (0.75 and 1.5 µg/mL). Cell subpopulation (%) after Annexin-V and 7-AAD staining. Statistical analysis: 2way-ANOVA followed by Bonferroni test (*$p < 0.05$, **$p < 0.01$ and ***$p < 0.001$, relative to untreated cells).

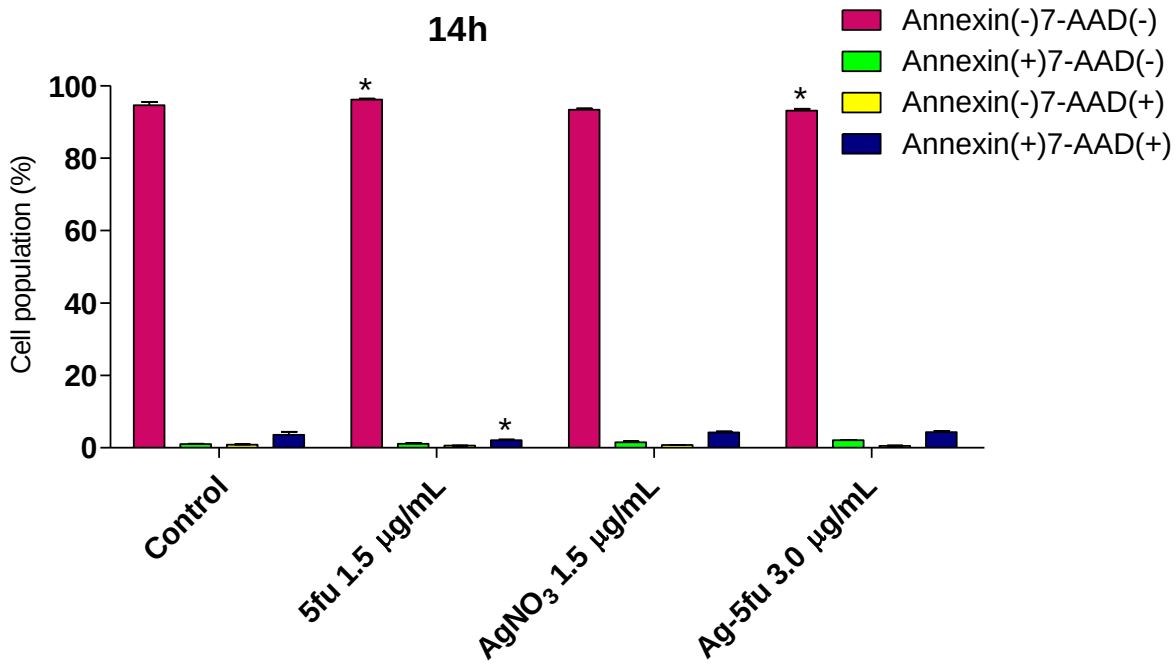

Figure A13. Influence of Ag-5fu, 5fu, and $AgNO_3$ on phosphatidylserine externalization of NCI/ADR-RES after 14 h of treatment. NCI/ADR-RES cells were treated for 14 h with Ag-5fu (3.0 µg/mL), 5fu (1.5 µg/mL) or $AgNO_3$ (1.5 µg/mL). Cell subpopulation (%) after Annexin-V and 7-AAD staining. Statistical analysis: 2way-ANOVA followed by Bonferroni test (*$p < 0.05$, relative to untreated cells).

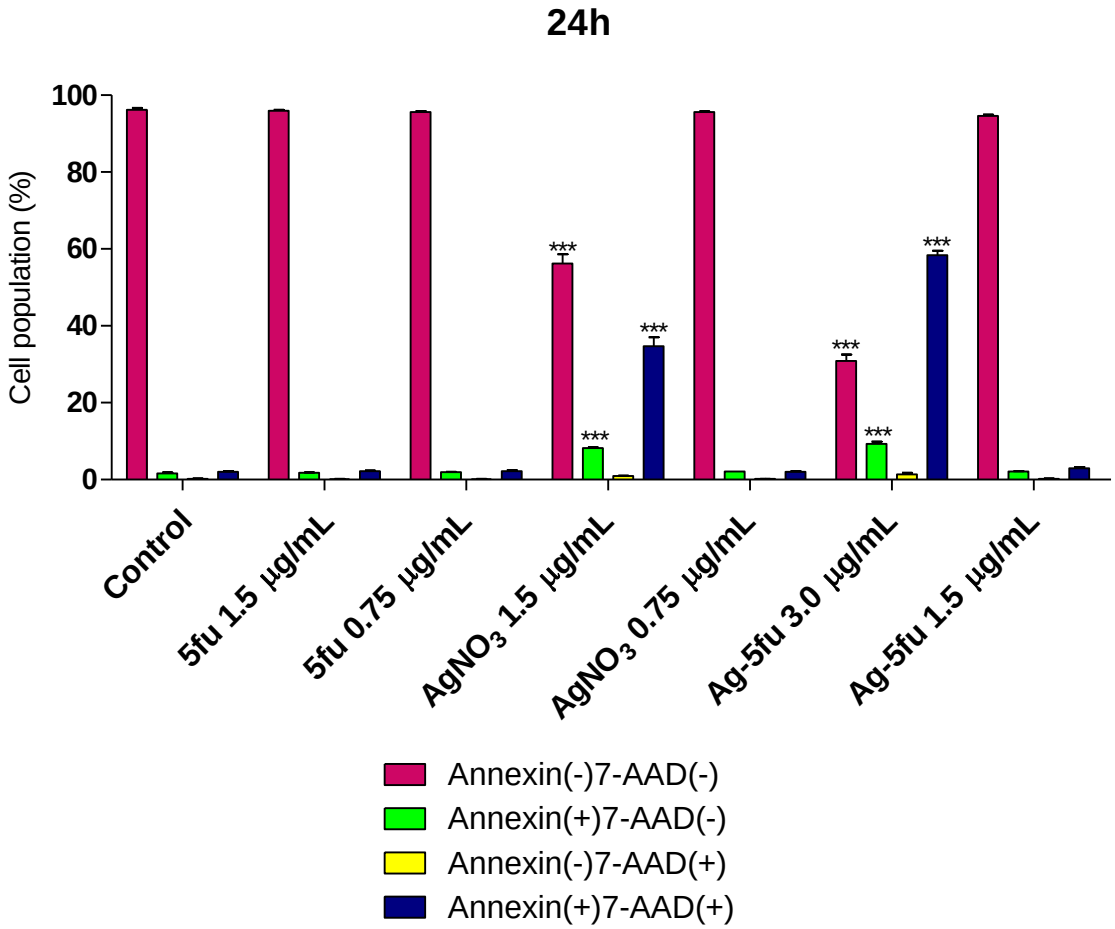

Figure A14. Influence of Ag-5fu, 5fu, and $AgNO_3$ on phosphatidylserine externalization of NCI/ADR-RES after 24 h of treatment. NCI/ADR-RES cells were treated for 24 h with Ag-5fu (1.5 and 3.0 µg/mL), 5fu (0.75 and 1.5 µg/mL) or $AgNO_3$ (0.75 and 1.5 µg/mL). Cell subpopulation (%) after Annexin-V and 7-AAD staining. Statistical analysis: 2way-ANOVA followed by Bonferroni test (***$p < 0.001$, relative to untreated cells).

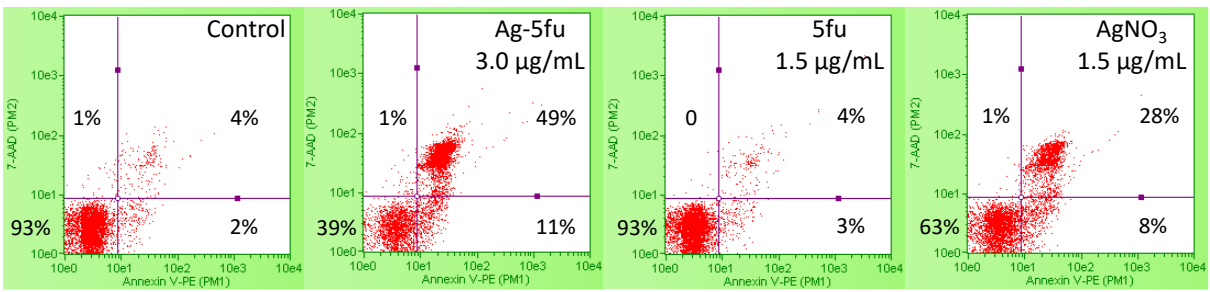

Figure A15. Dot-plot graphs of Nexin assay of Ag-5fu, 5fu and $AgNO_3$ over NCI/ADR-RES cells (18 h) in comparison to control.

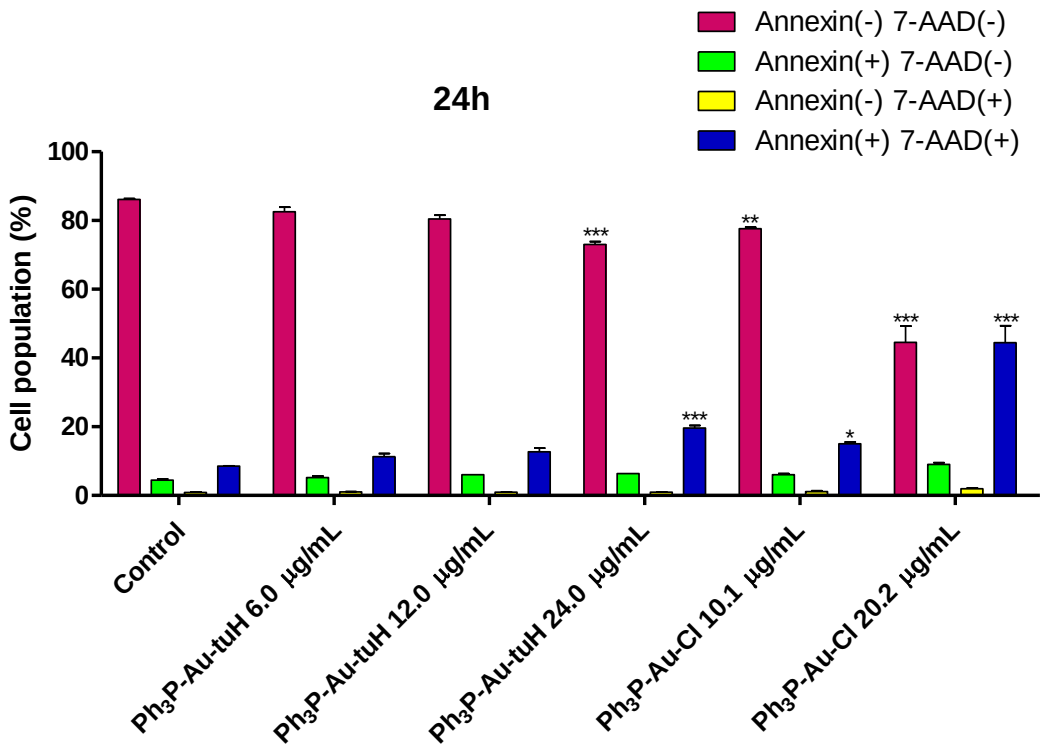

Figure A16. Influence of Ph_3P-Au-tuH and Ph_3P-Au-Cl on phosphatidylserine externalization of NCI-H460 after 24 h of treatment. NCI-H460 cells were treated for 24 h with Ph_3P-Au-tuH (6.0, 12.0 and 24.0 µg/mL), or Ph_3P-Au-Cl (10.1 and 20.2 µg/mL). Cell subpopulation (%) after Annexin-V and 7-AAD staining. Statistical analysis: 2way-ANOVA followed by Bonferroni test (*$p < 0.05$, **$p < 0.01$ and ***$p < 0.001$, relative to untreated cells).

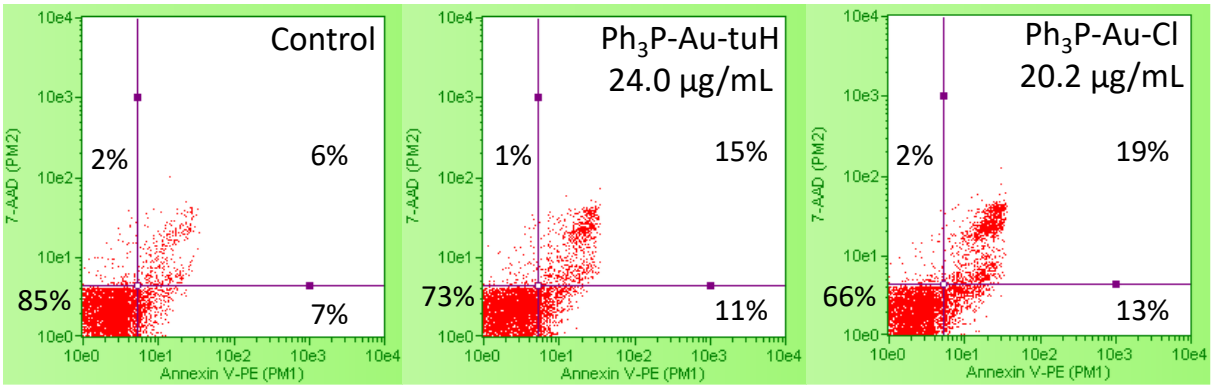

Figure A17. Dot-plot graphs of Nexin assay of Ph_3P-Au-tuH and Ph_3P-Au-Cl over NCI-H460 cells (18 h) in comparison to control.

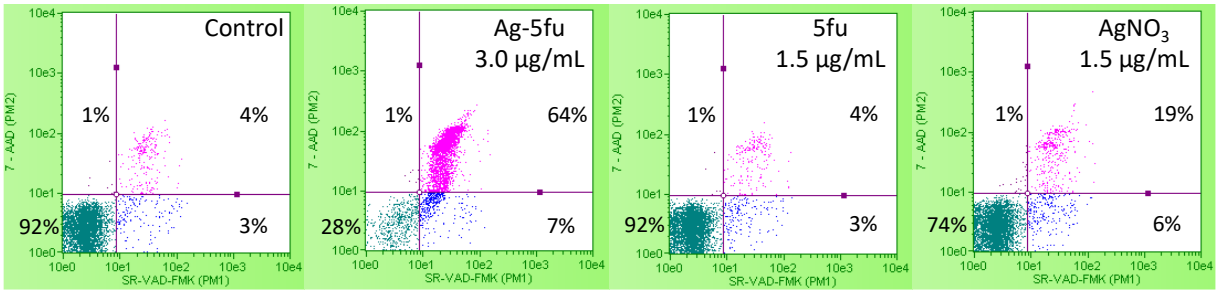

Figure A18. Dot-plot graphs of Caspases assay of Ag-5fu, 5fu and $AgNO_3$ over NCI/ADR-RES cells (17 h) in comparison to control.

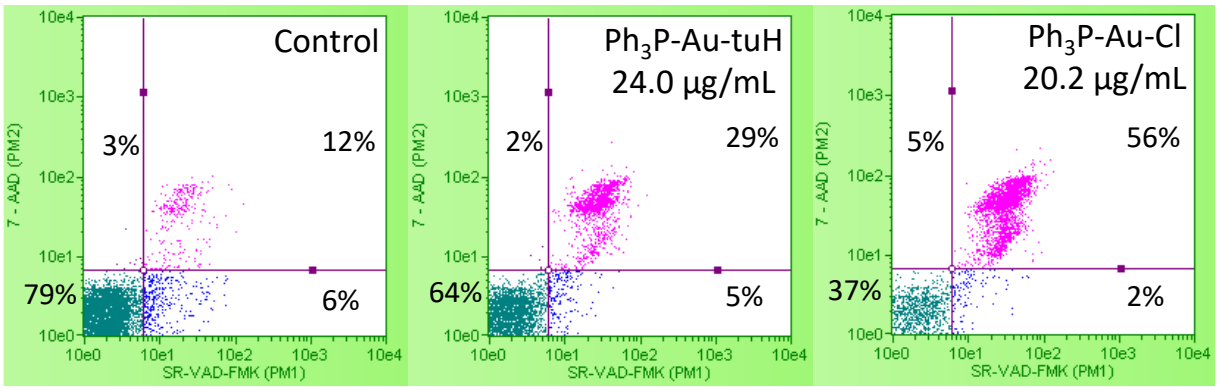

Figure A19. Dot-plot graphs of Caspases assay of Ph_3P-Au-tuH and Ph_3P-Au-Cl over NCI-H460 cells (18 h) in comparison to control.

PART 2: Thiosemicarbazones and their metal complexes

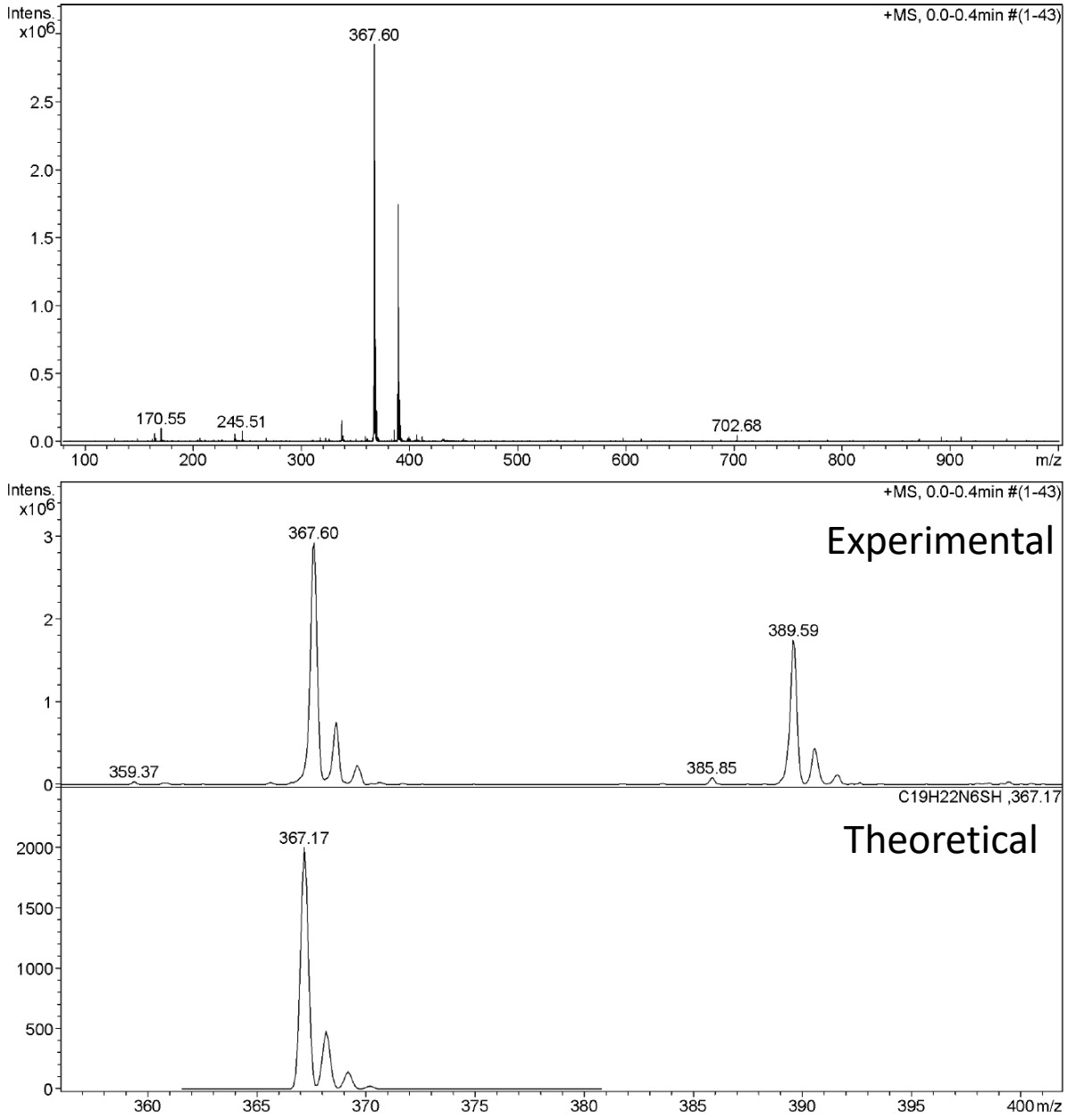

Figure A20. Mass spectrum of COTI-2.

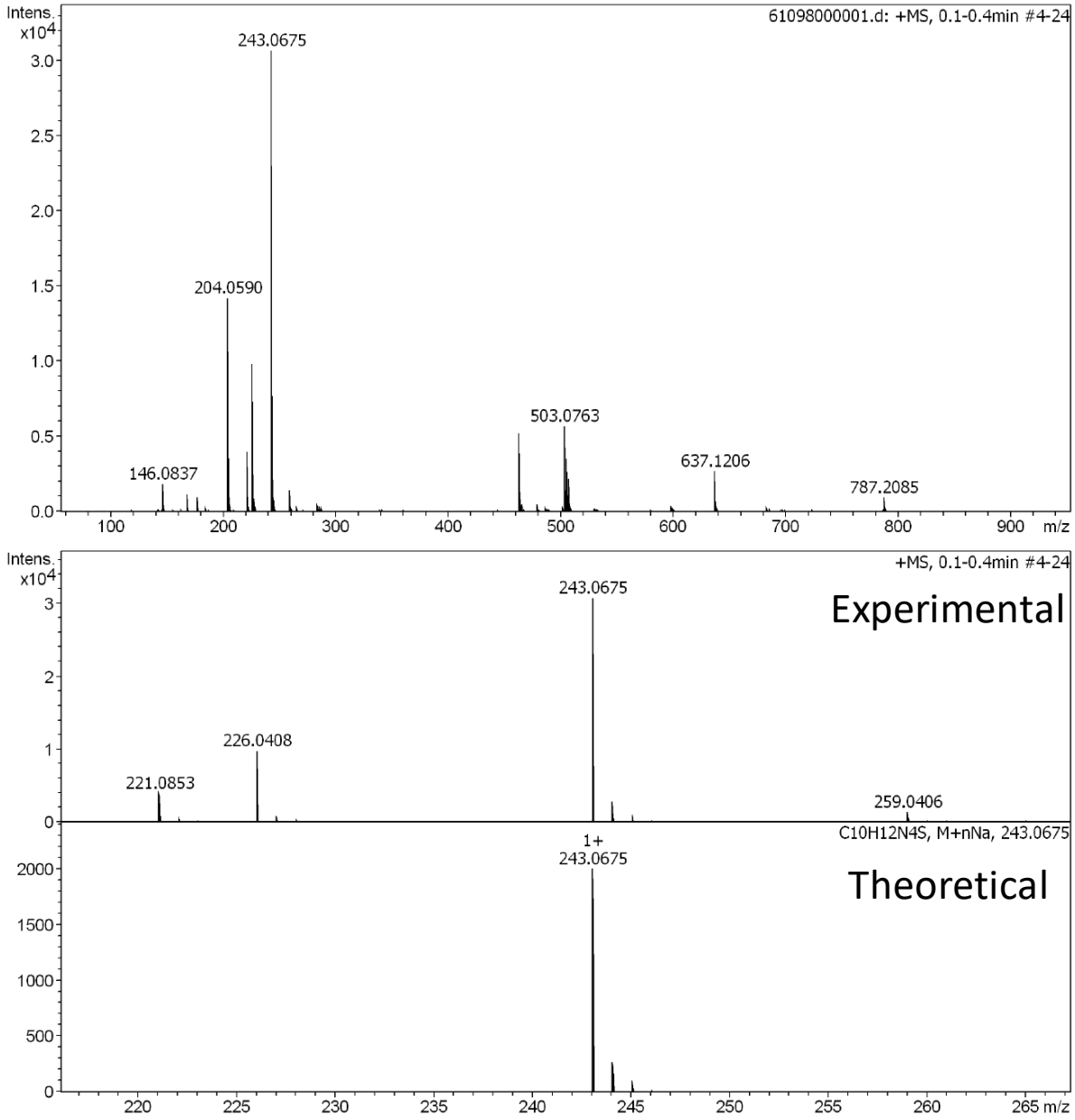

Figure A21. Mass spectrum of COTI-NH_2.

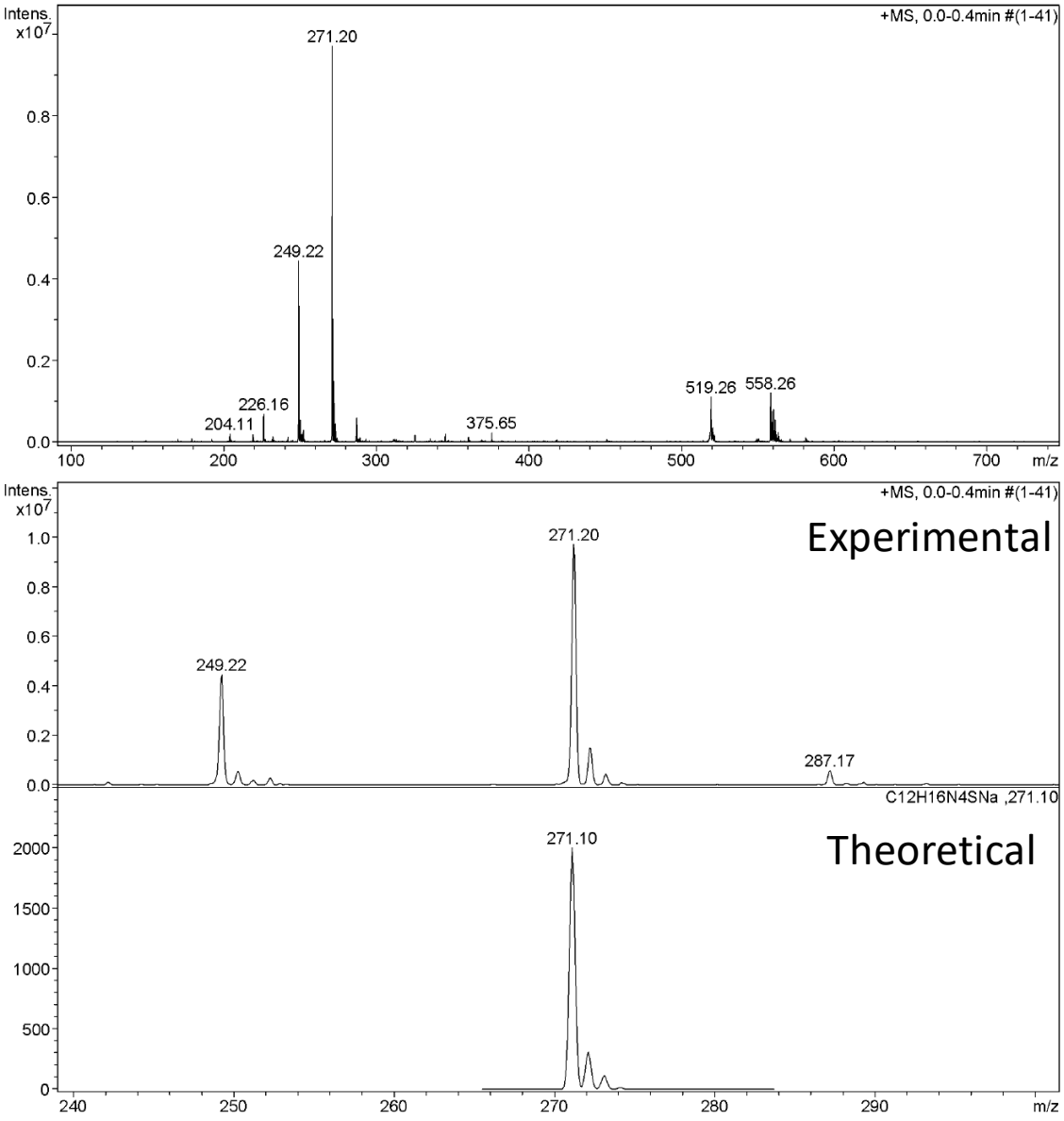

Figure A22. Mass spectrum of COTI-NMe_2.

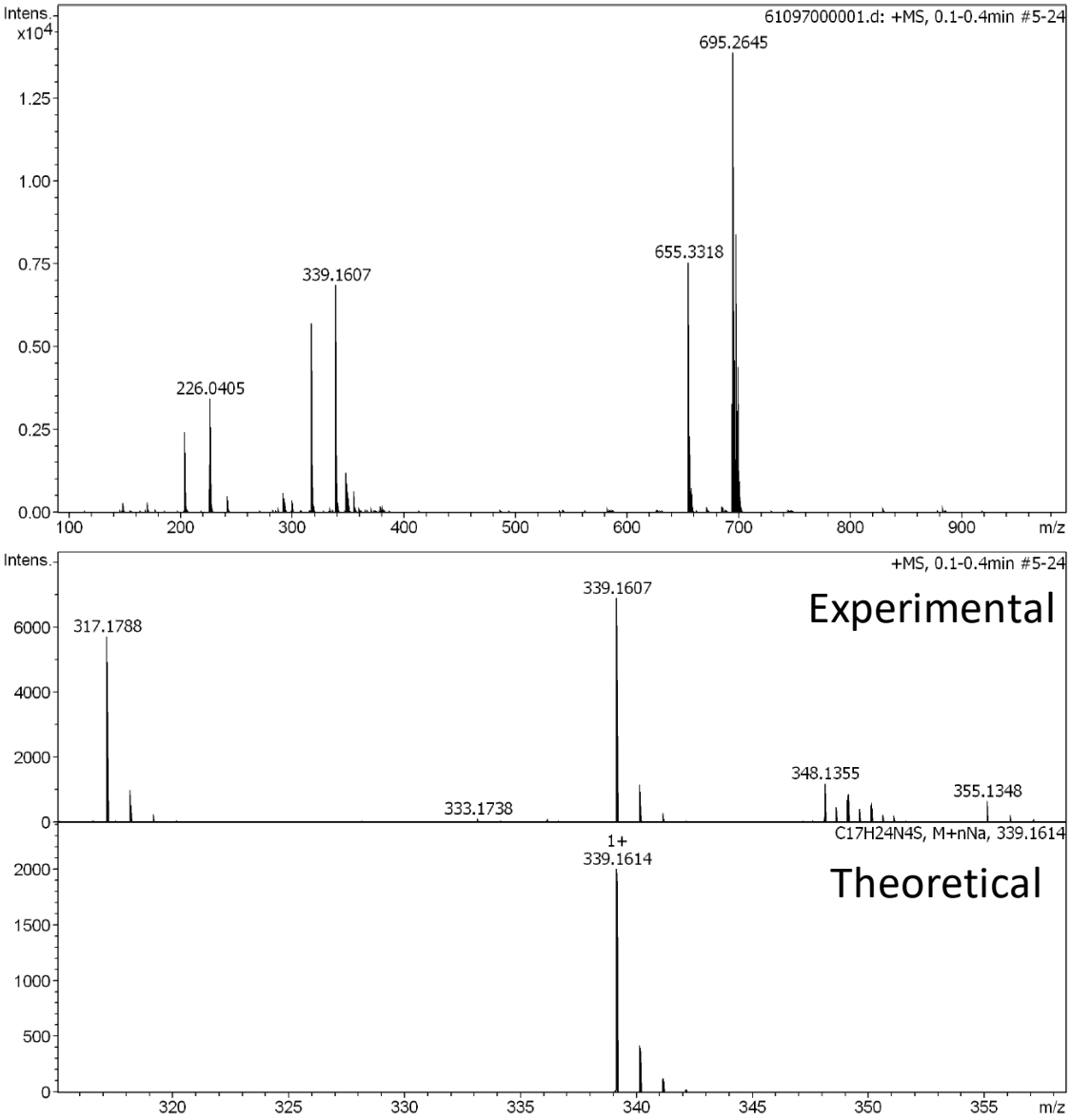

Figure A23. Mass spectrum of COTI-Nchexyl.

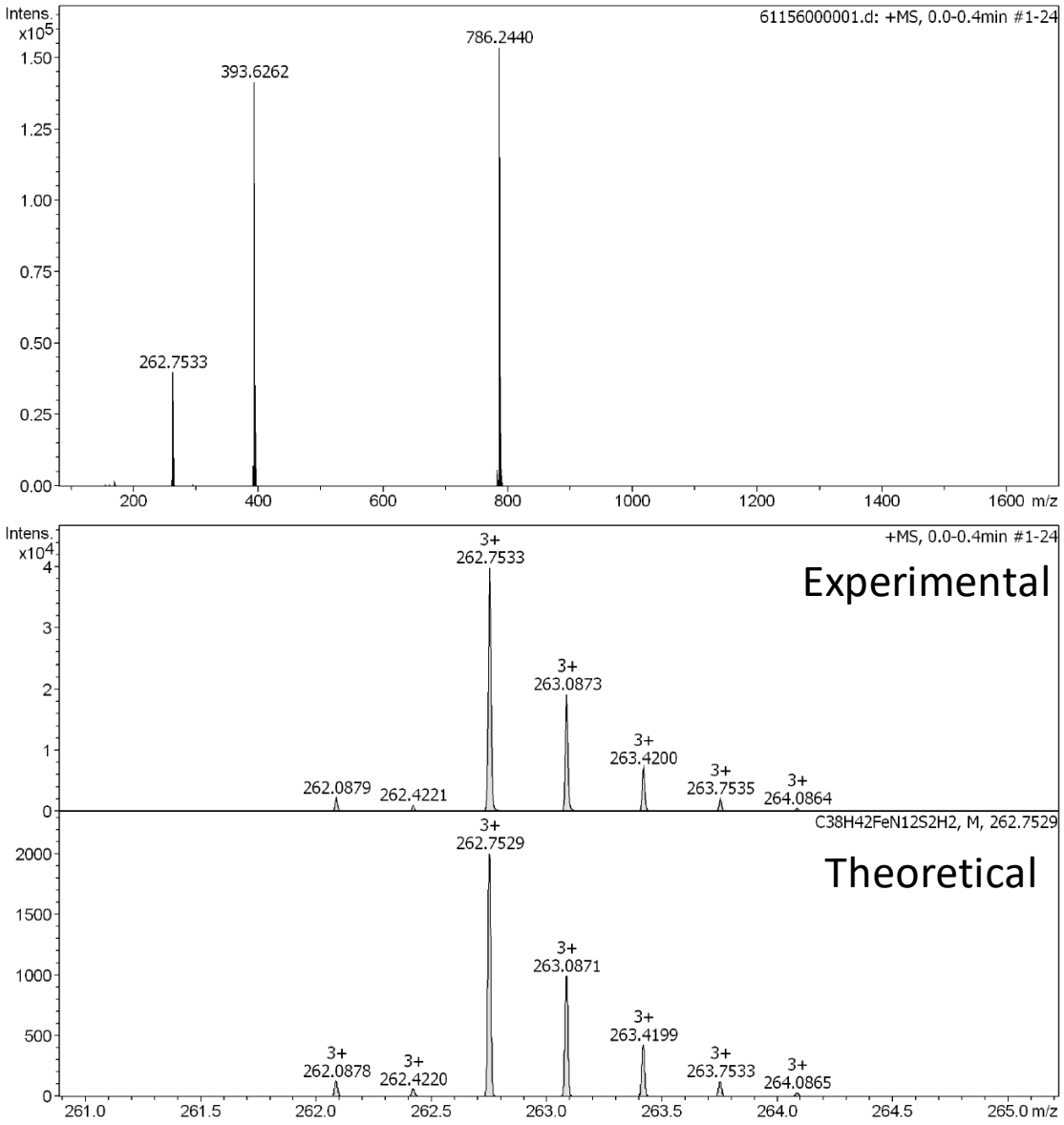

Figure A24. Mass spectrum of Fe-COTI-2.

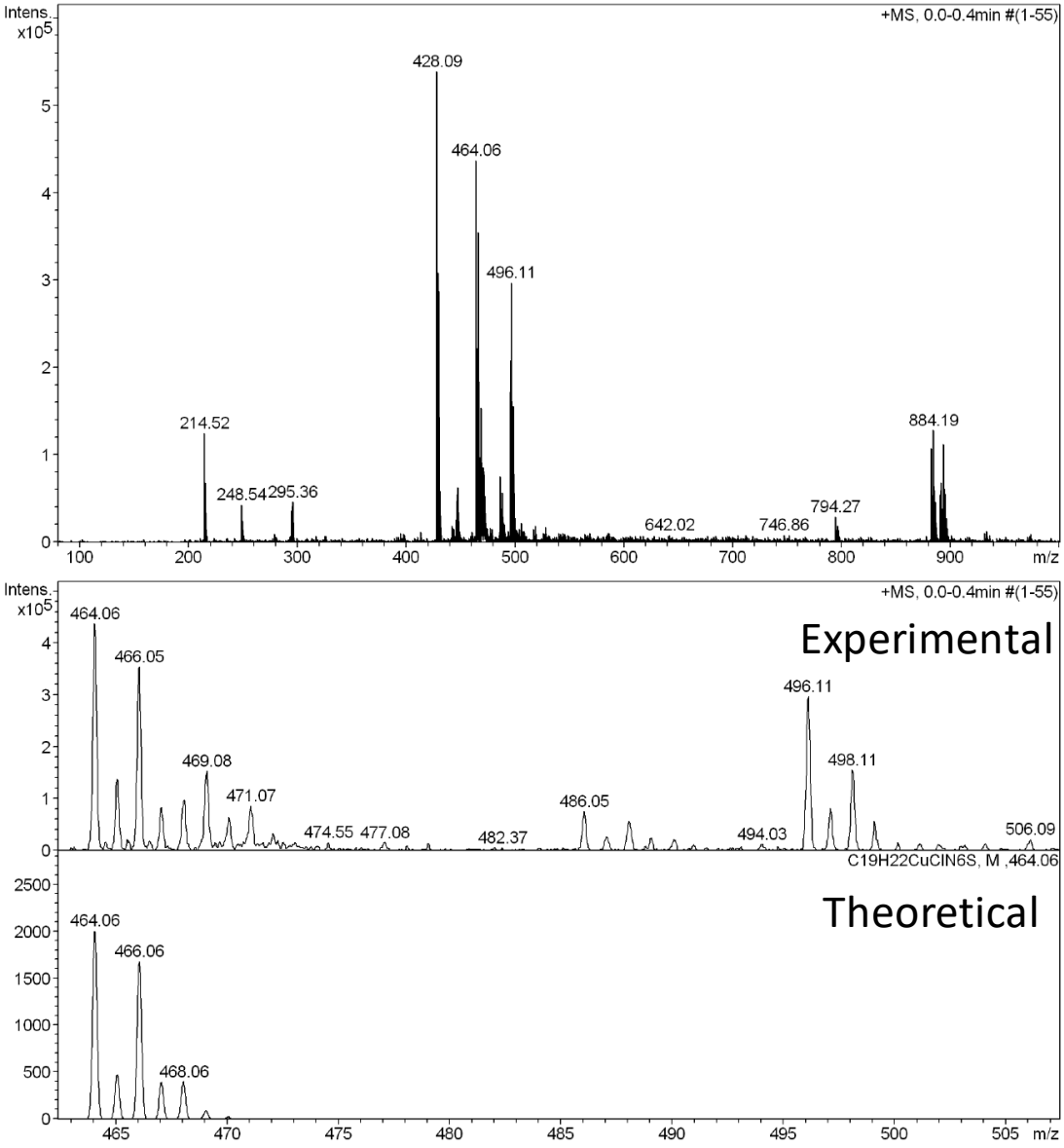

Figure A25. Mass spectrum of Cu-COTI-2.

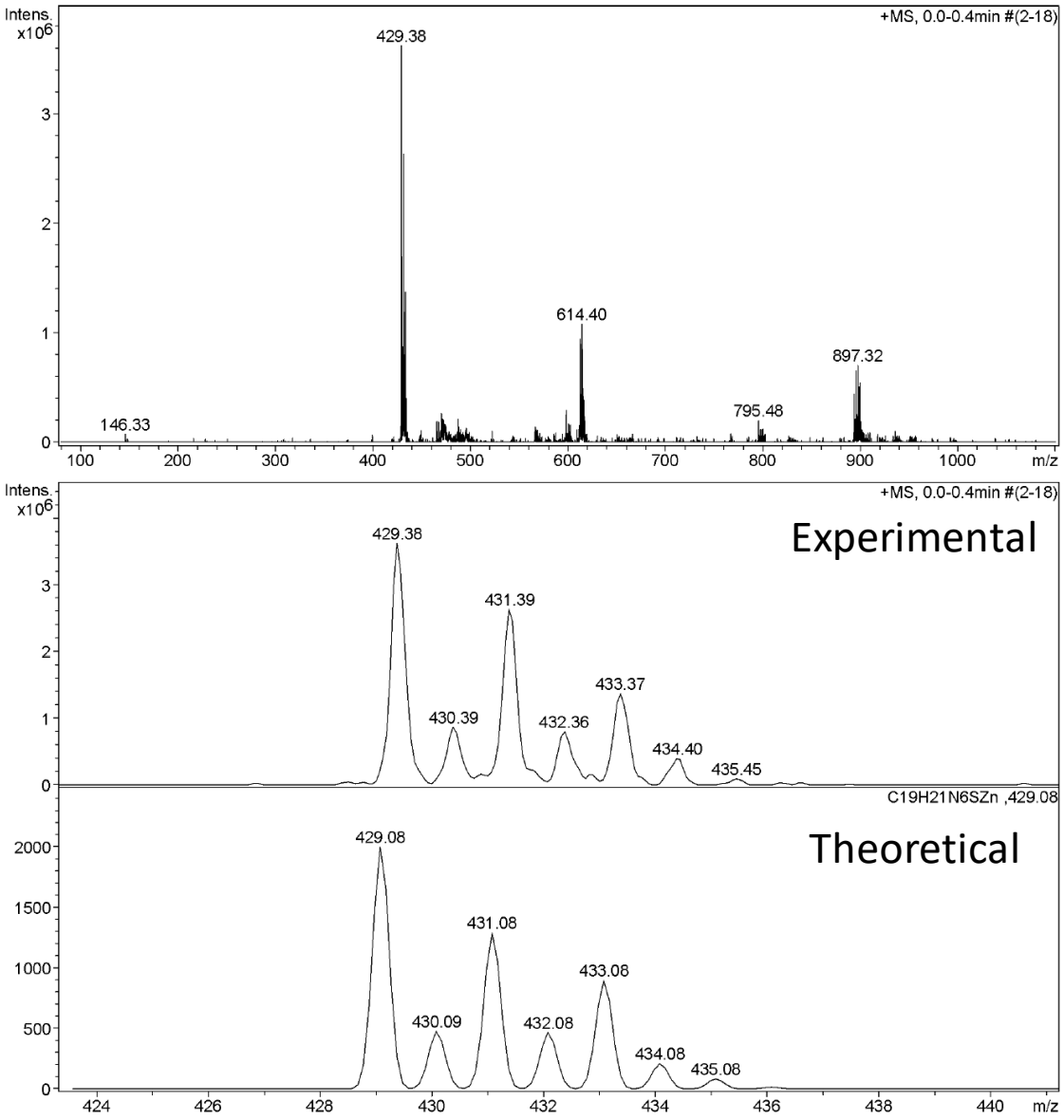

Figure A26. Mass spectrum of Zn-COTI-2.

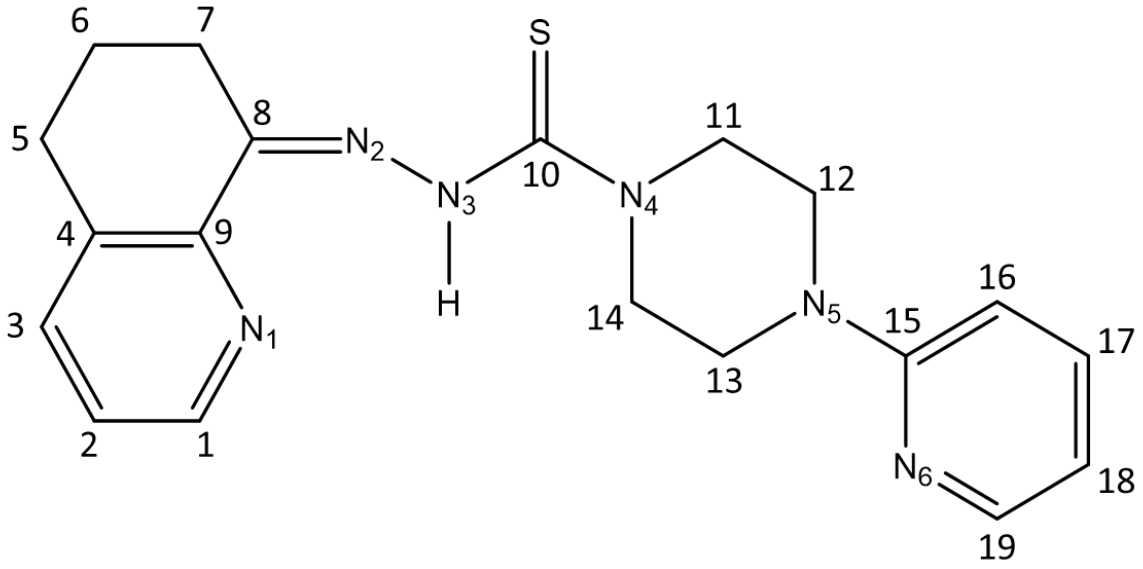

Figure A27. COTI-2 numbering for NMR.

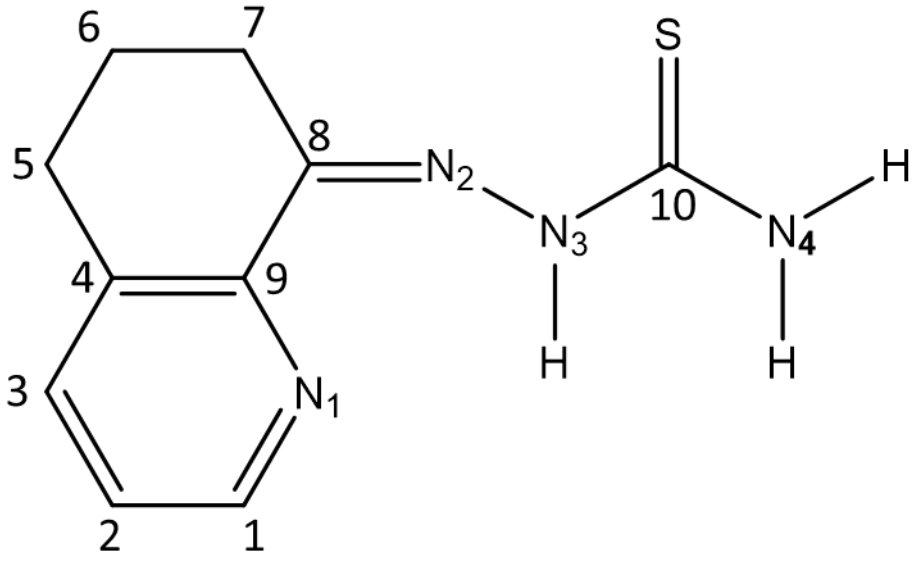

Figure A28. COTI-NH_2 numbering for NMR.

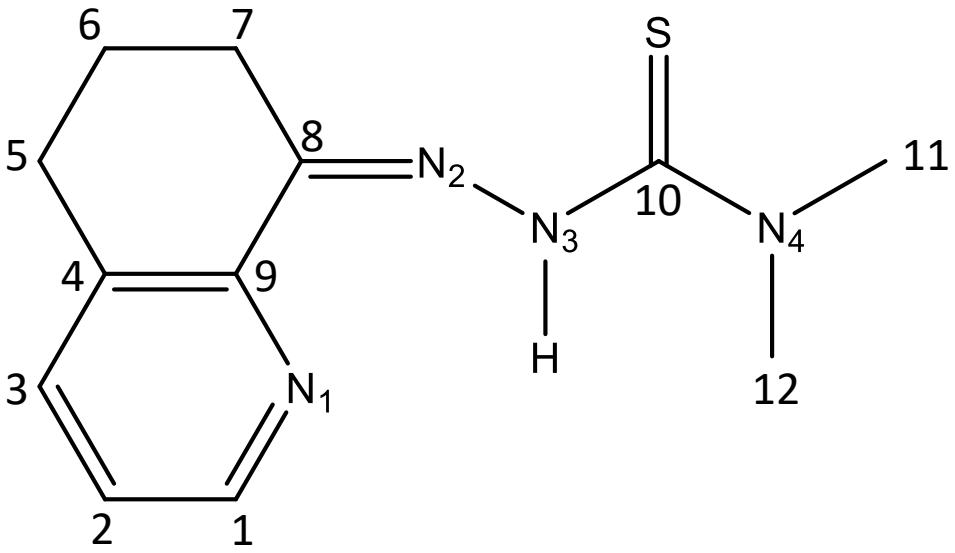

Figure A29. COTI-NMe_2 numbering for NMR.

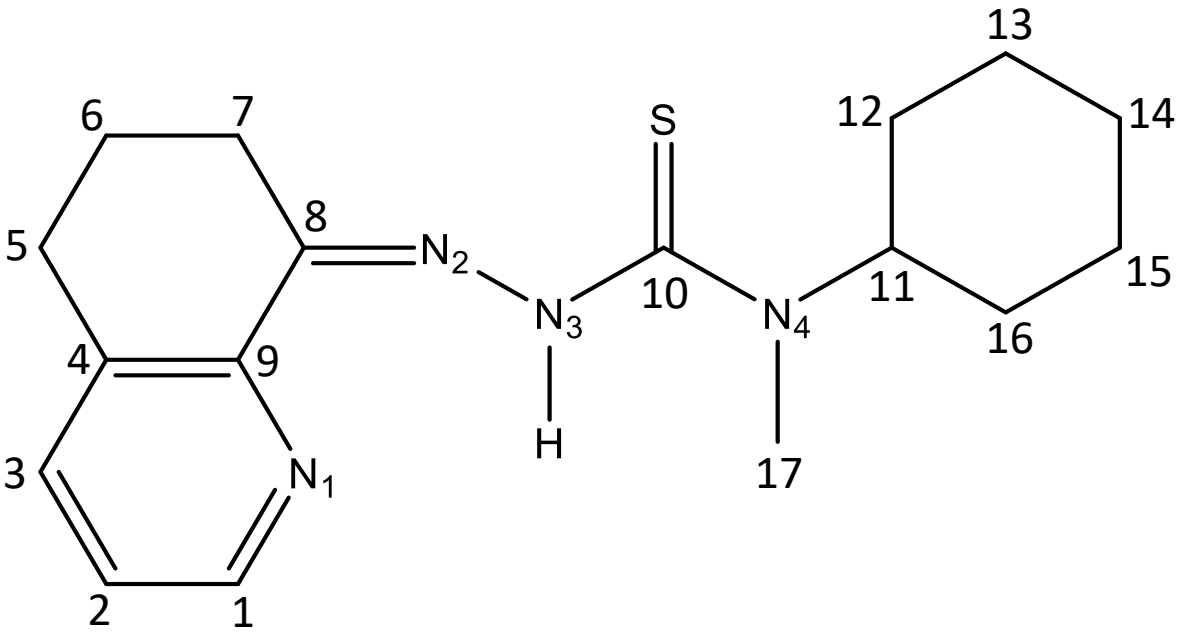

Figure A30. COTI-Nchexyl numbering for NMR.

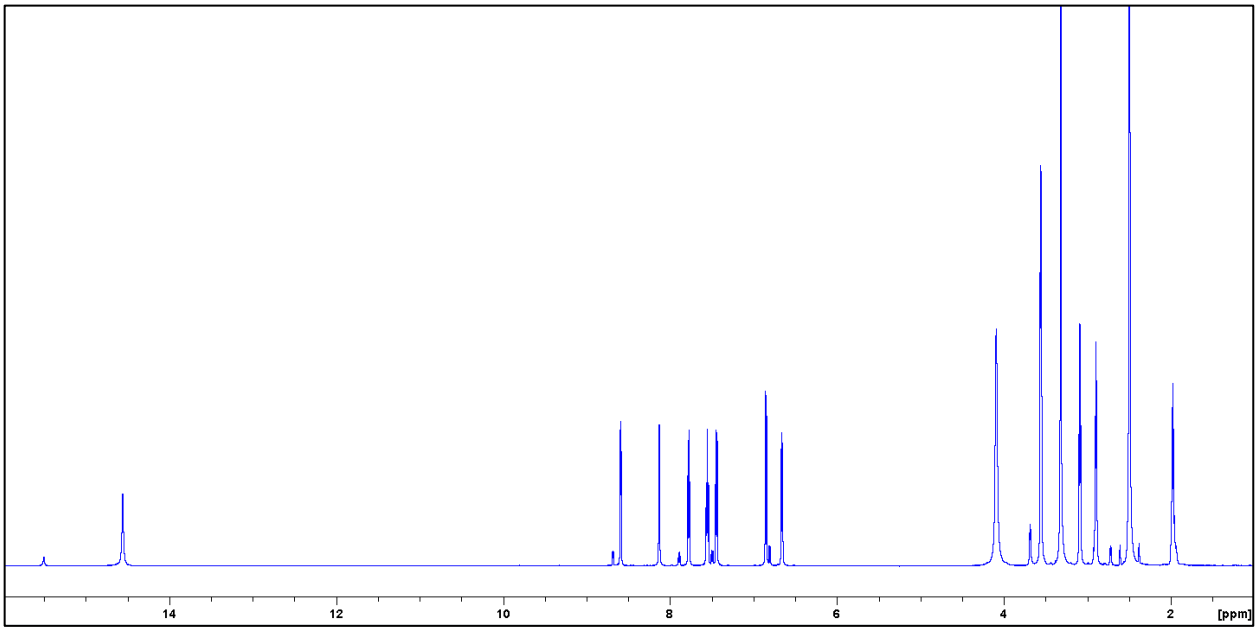

Figure A31. ^{1}H-NMR spectrum in DMSO-d6 of COTI-2.

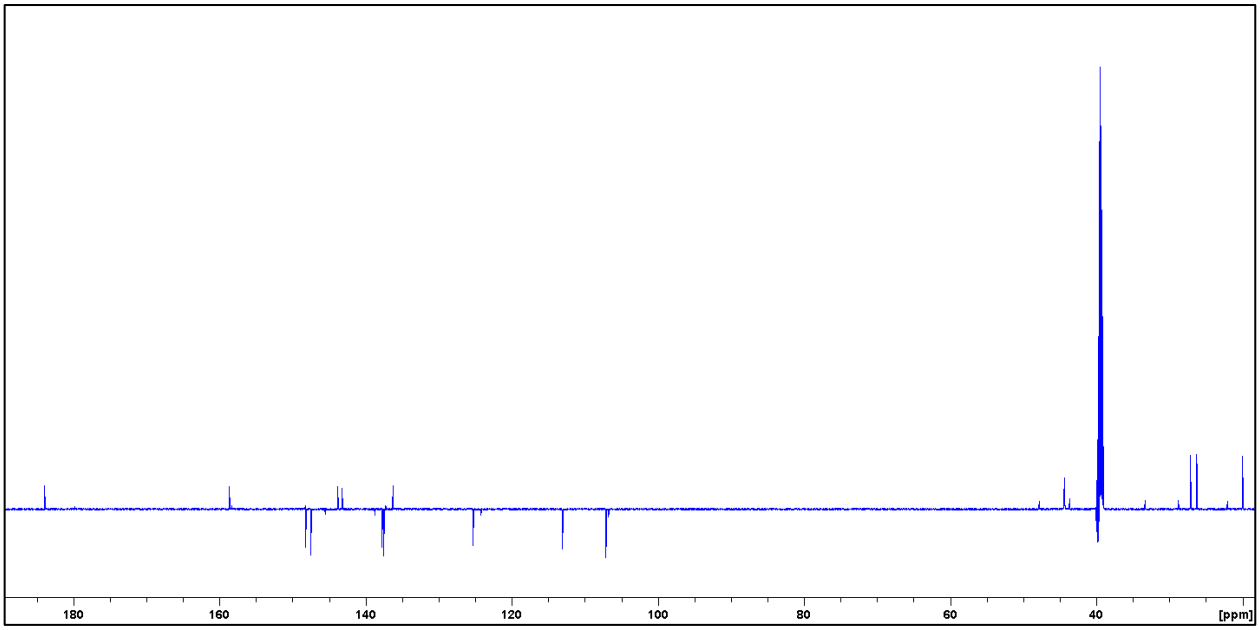

Figure A32. Q-DEPT ^{13}C-NMR spectrum in DMSO-d6 of COTI-2.

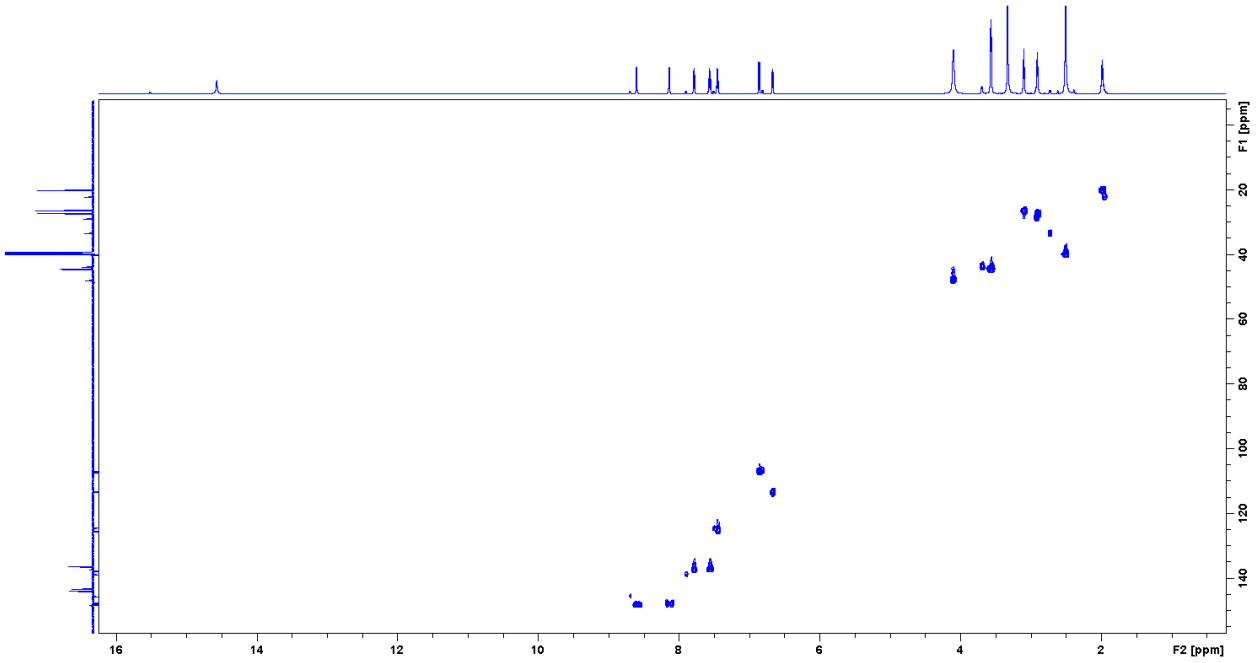

Figure A33. HSQC ^{1}H-^{13}C NMR in DMSO-d6 of COTI-2.

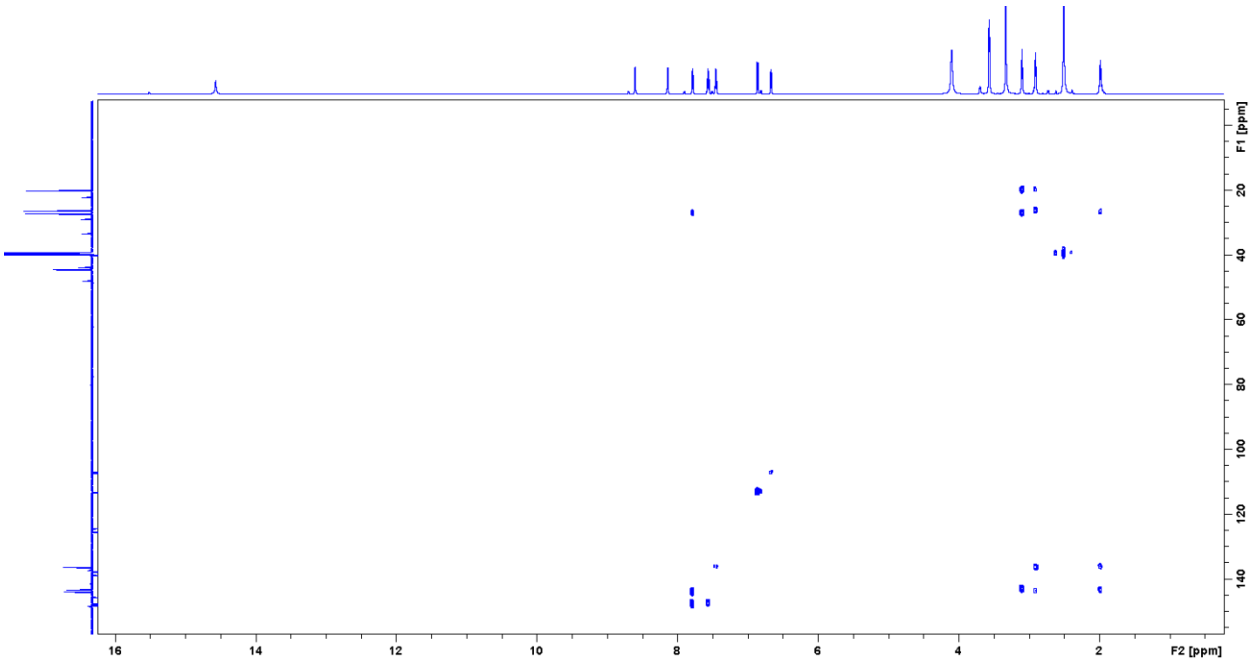

Figure A34. HMBC ^{1}H-^{13}C NMR in DMSO-d6 of COTI-2.

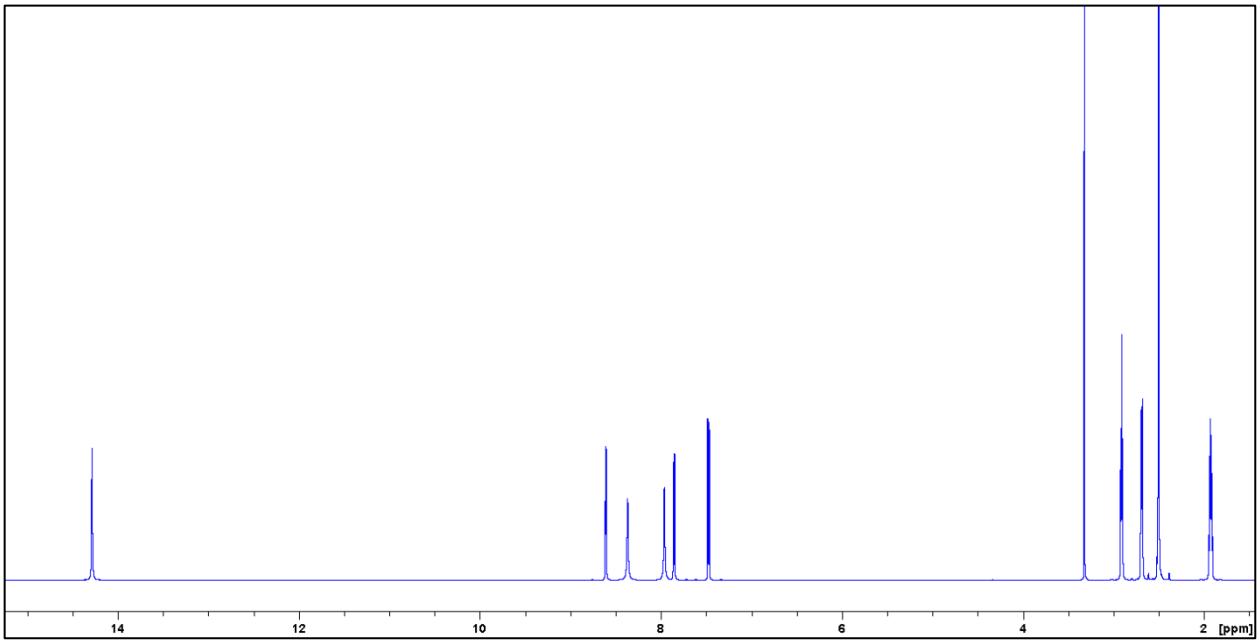

Figure A35. ^{1}H-NMR spectrum in DMSO-d6 of COTI-NH_2.

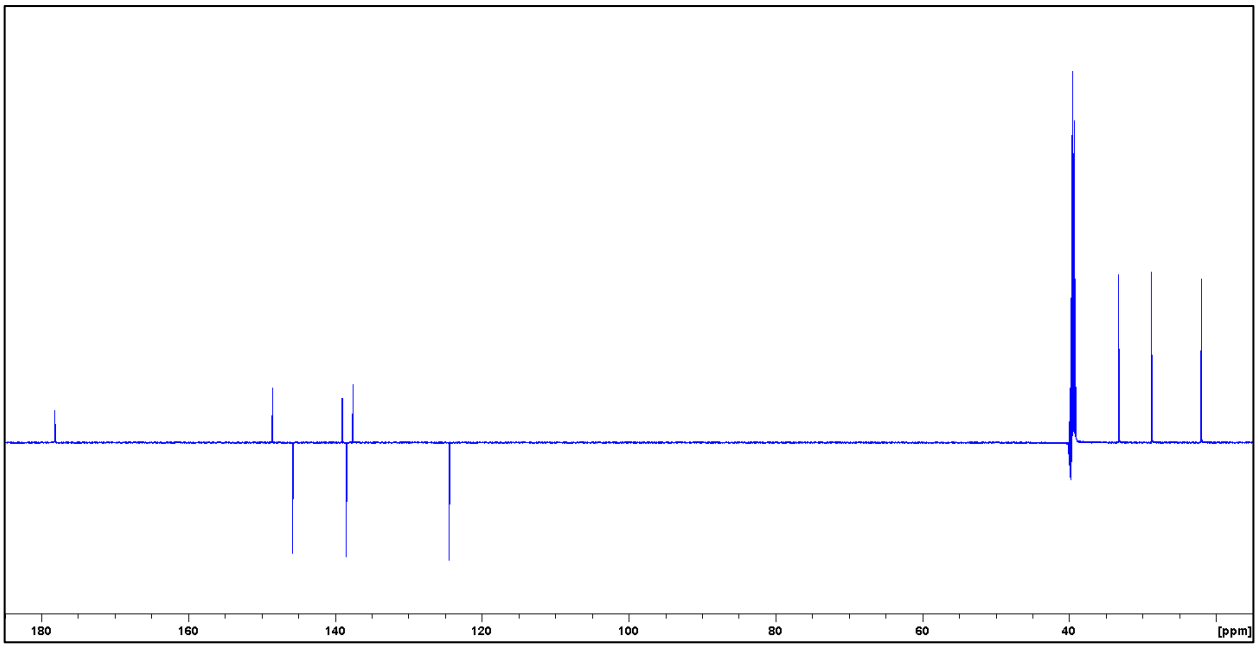

Figure A36. Q-DEPT ^{13}C-NMR spectrum in DMSO-d6 of COTI-NH_2.

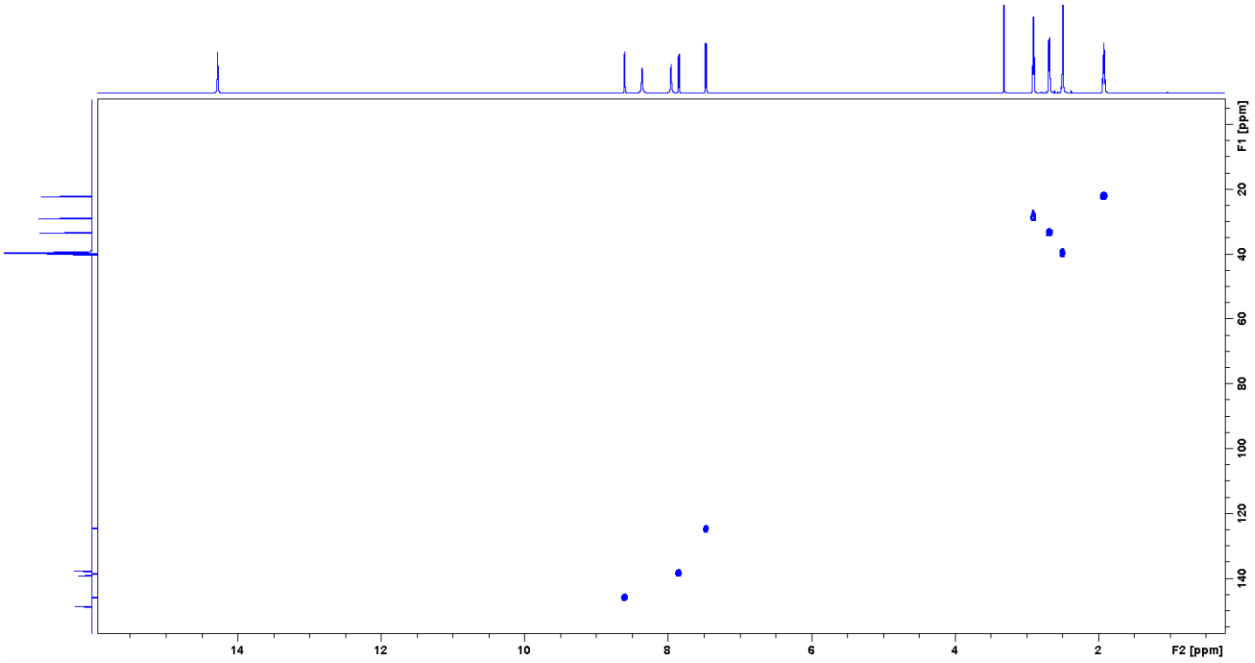

Figure A37. HSQC ^{1}H-^{13}C NMR in DMSO-d6 of COTI-NH_2.

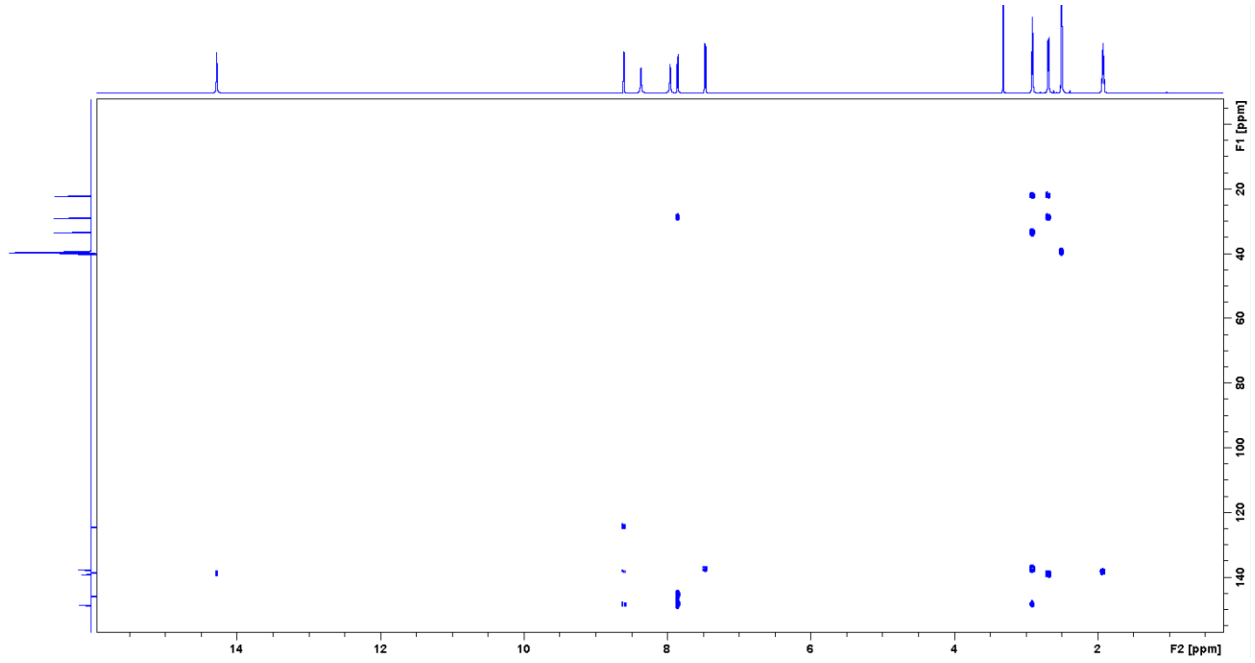

Figure A38. HMBC ^{1}H-^{13}C NMR in DMSO-d6 of COTI-NH_2.

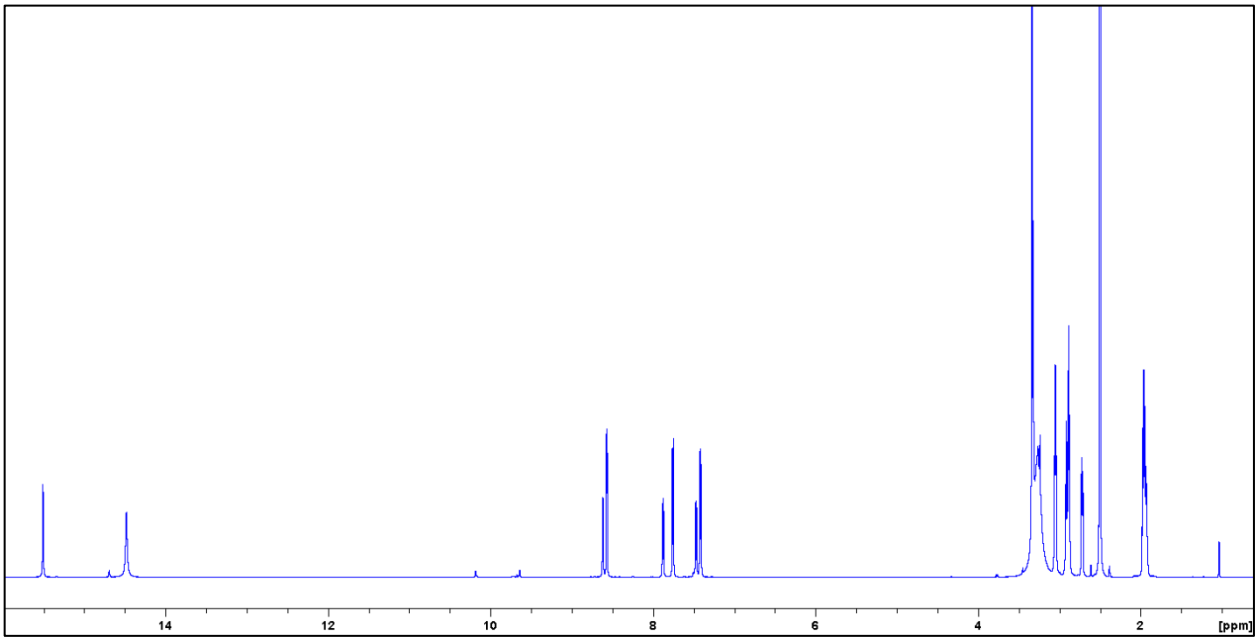

Figure A39. ^{1}H-NMR spectrum in DMSO-d6 of COTI-NMe_2.

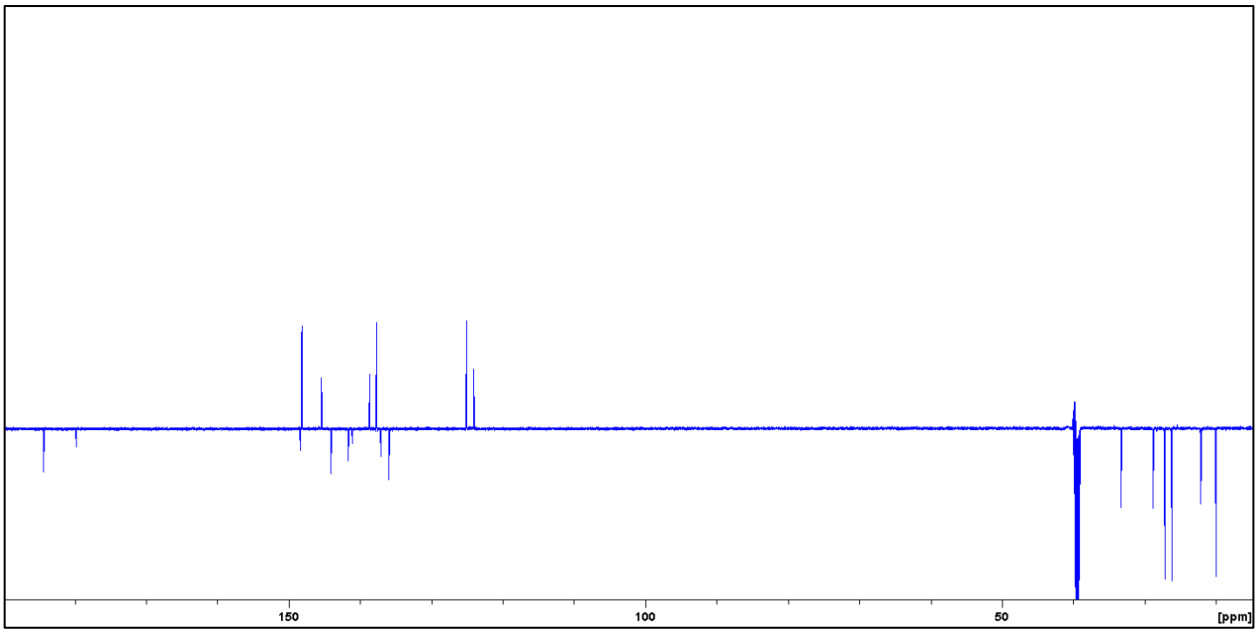

Figure A40. Q-DEPT ^{13}C-NMR spectrum in DMSO-d6 of COTI-NMe_2.

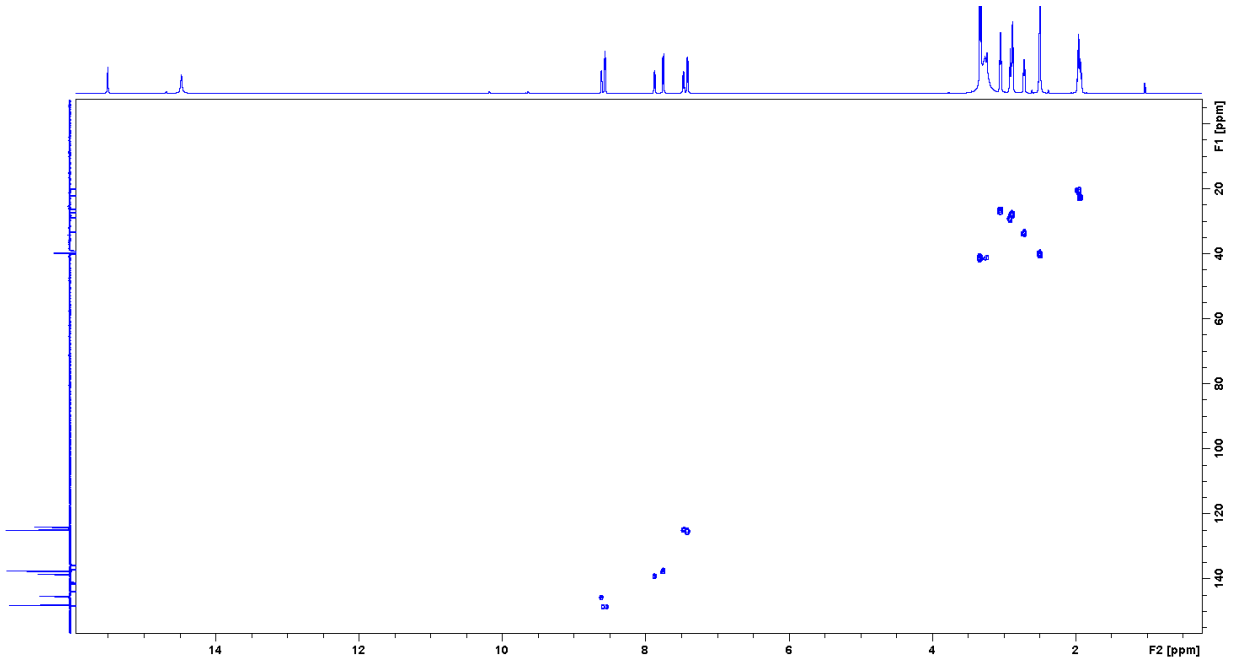

Figure A41. HSQC ^{1}H-^{13}C NMR in DMSO-d6 of COTI-NMe_2.

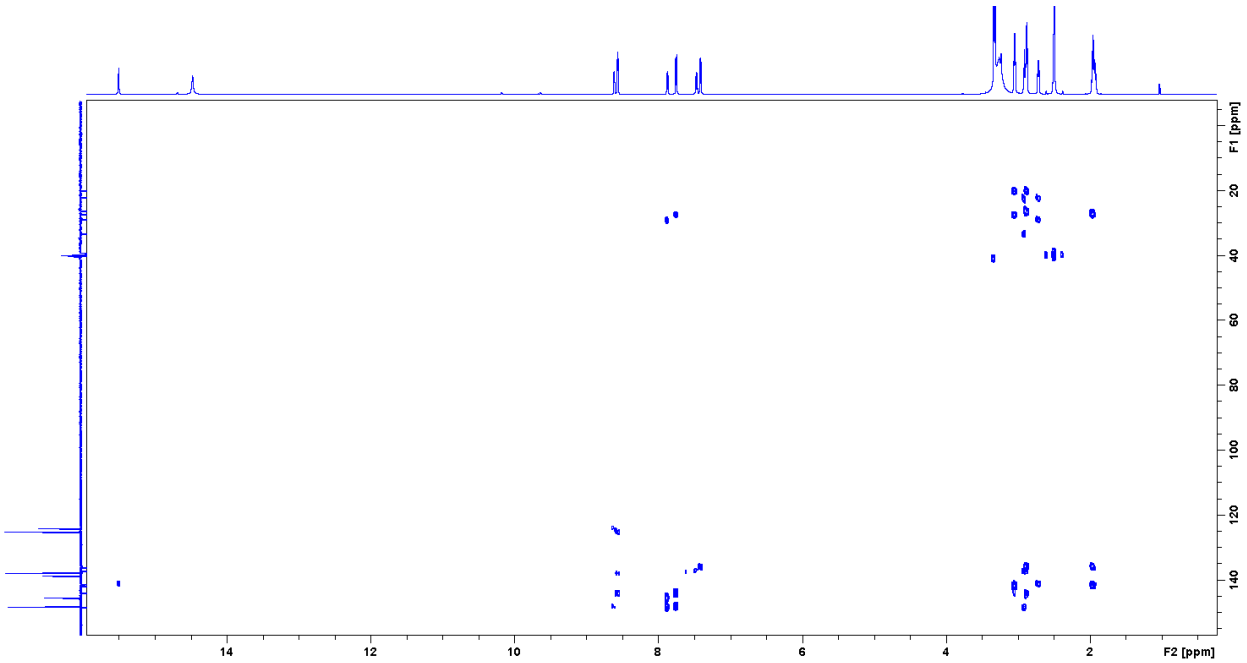

Figure A42. HMBC ^{1}H-^{13}C NMR in DMSO-d6 of COTI-NMe_2.

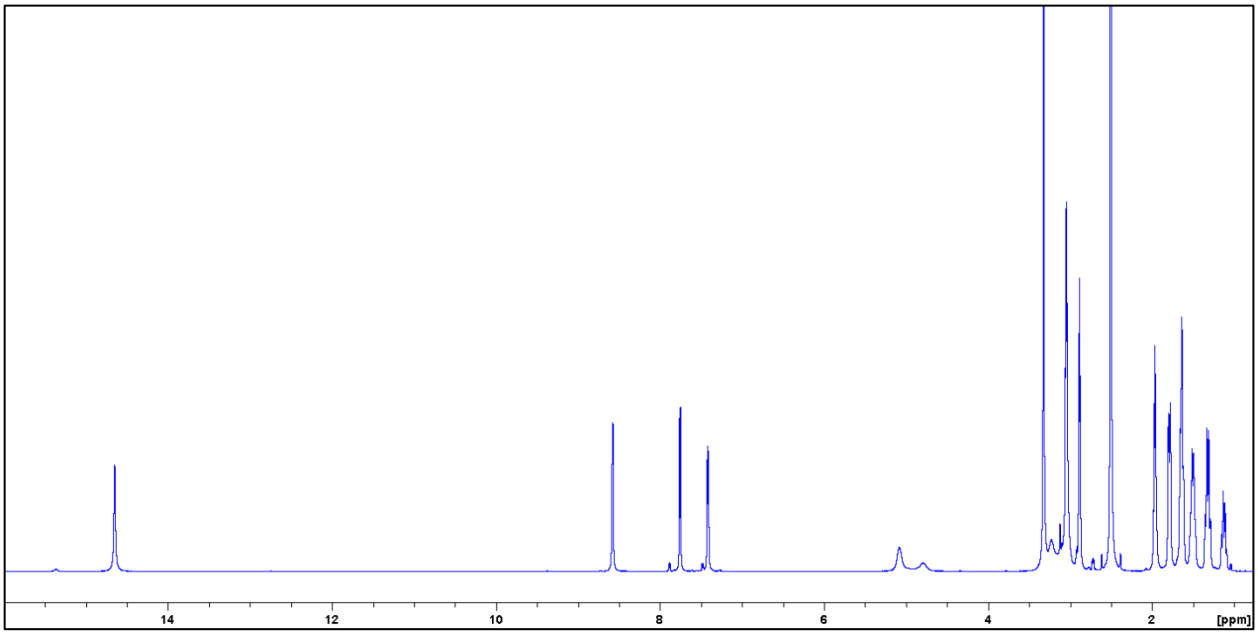

Figure A43. ^{1}H-NMR spectrum in DMSO-d6 of COTI-Nchexyl.

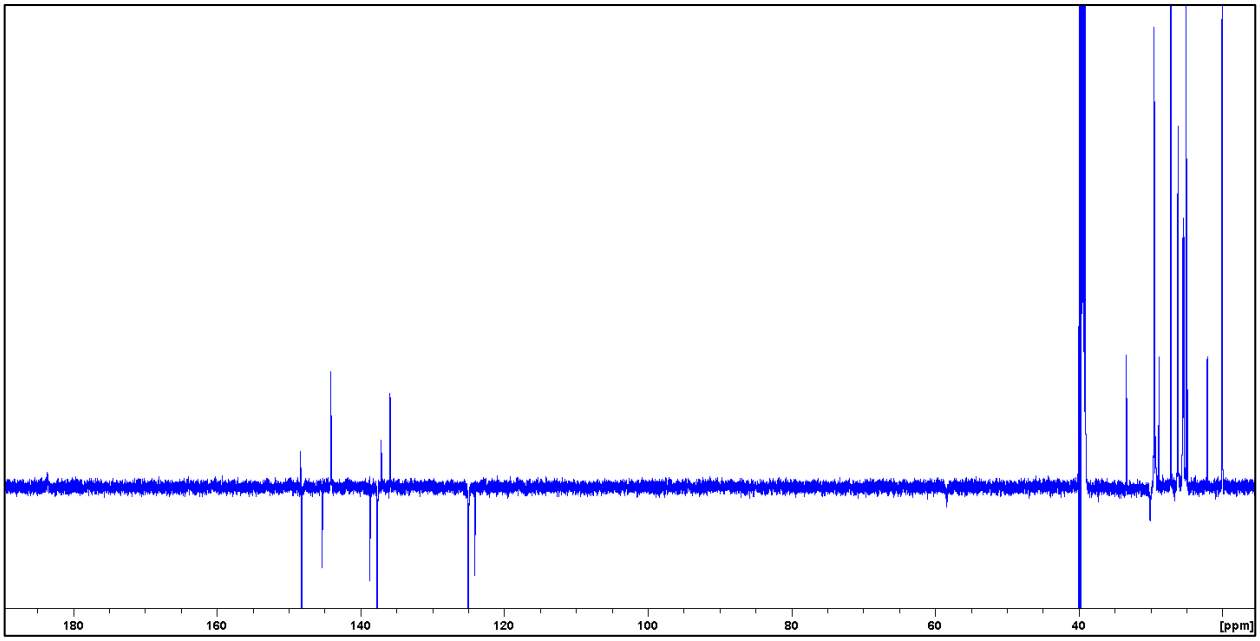

Figure A44. Q-DEPT ^{13}C-NMR spectrum in DMSO-d6 of COTI-Nchexyl.

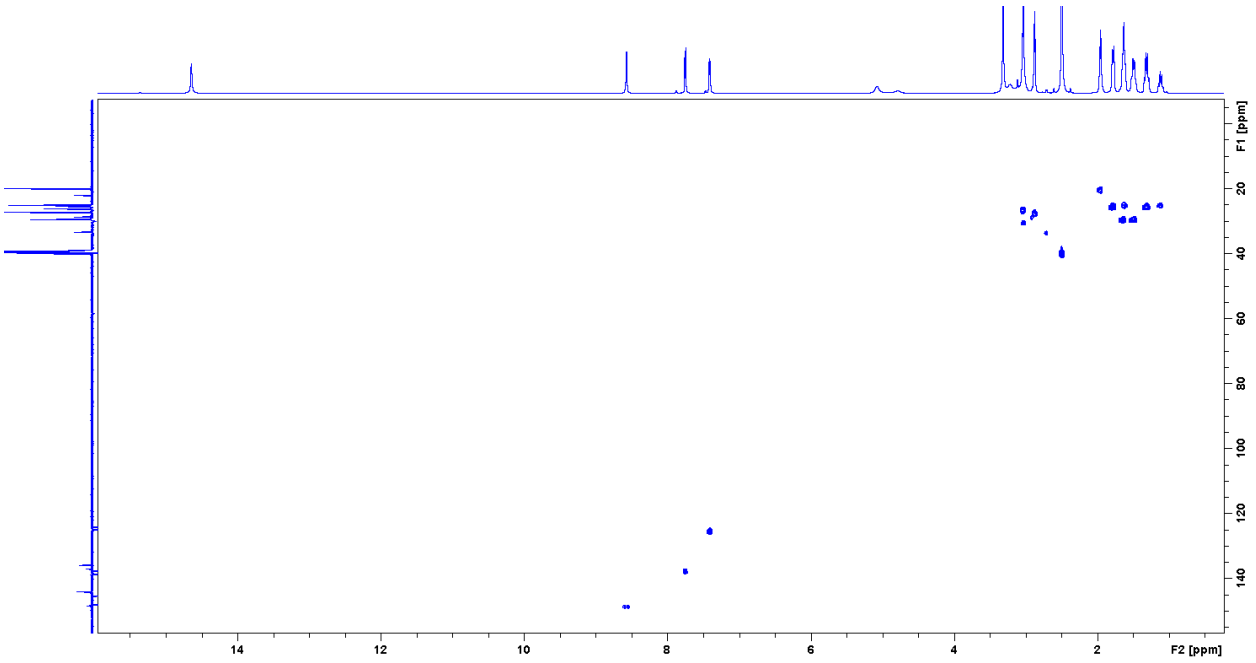

Figure A45. HSQC ^{1}H-^{13}C NMR in DMSO-d6 of COTI-Nchexyl.

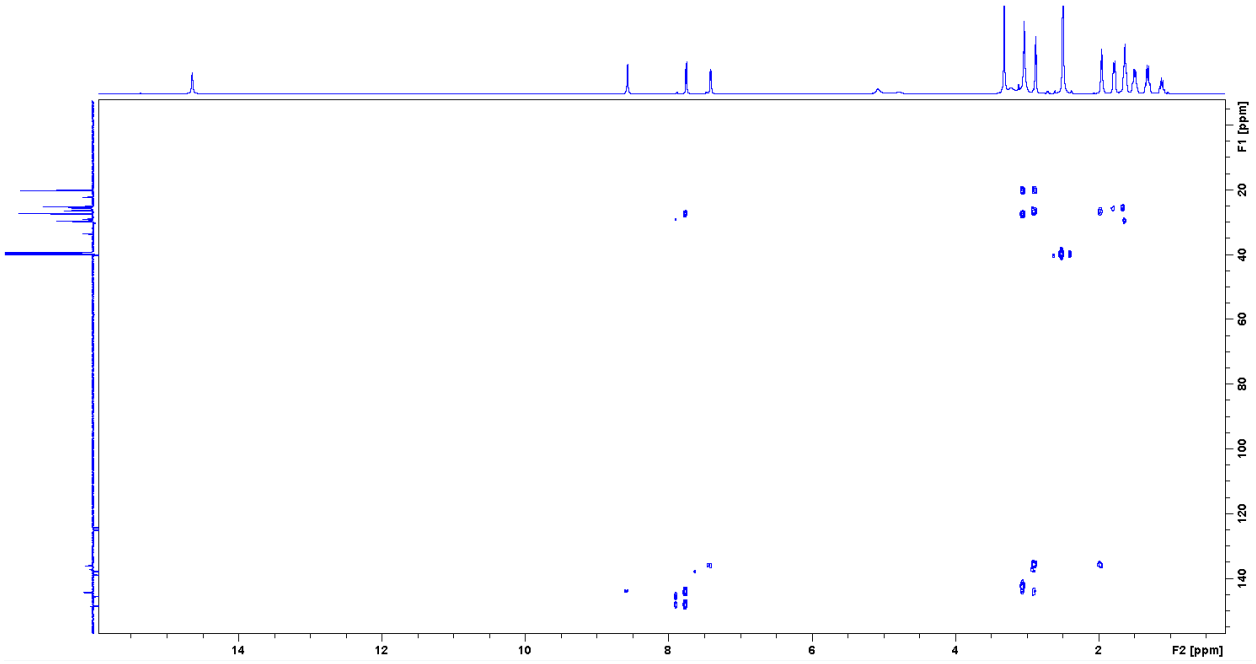

Figure A46. HMBC ^{1}H-^{13}C NMR in DMSO-d6 of COTI-Nchexyl.

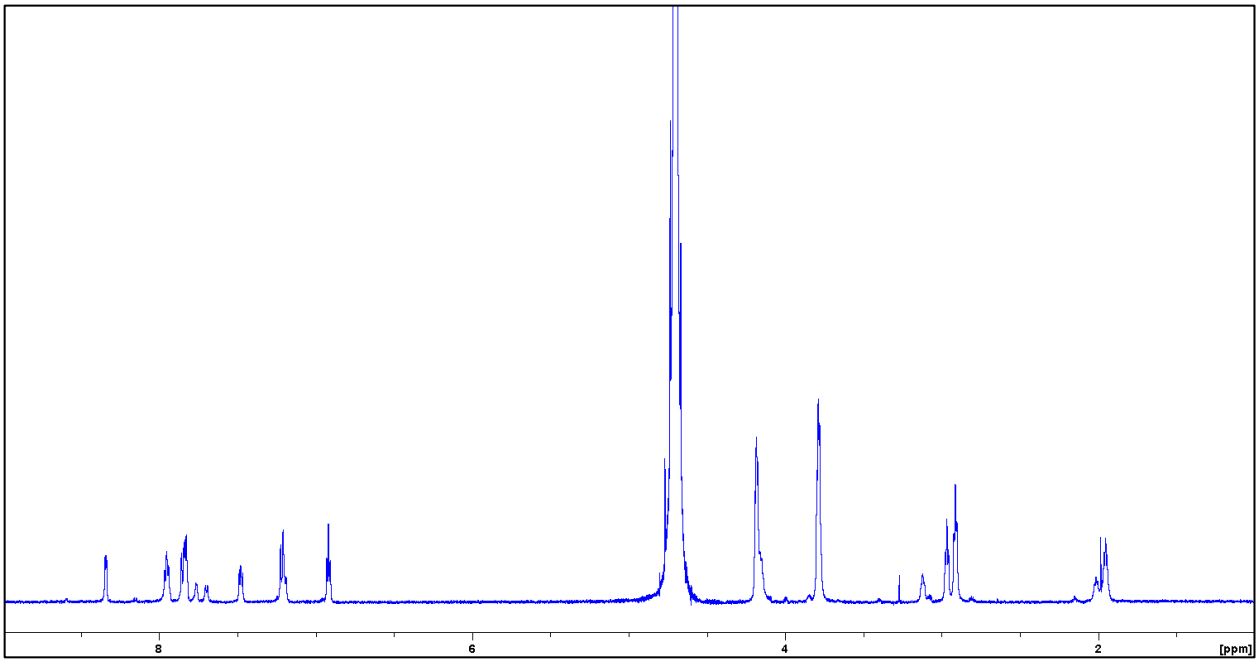

Figure A47. ^{1}H-NMR spectrum in D_2O of Zn-COTI-2.

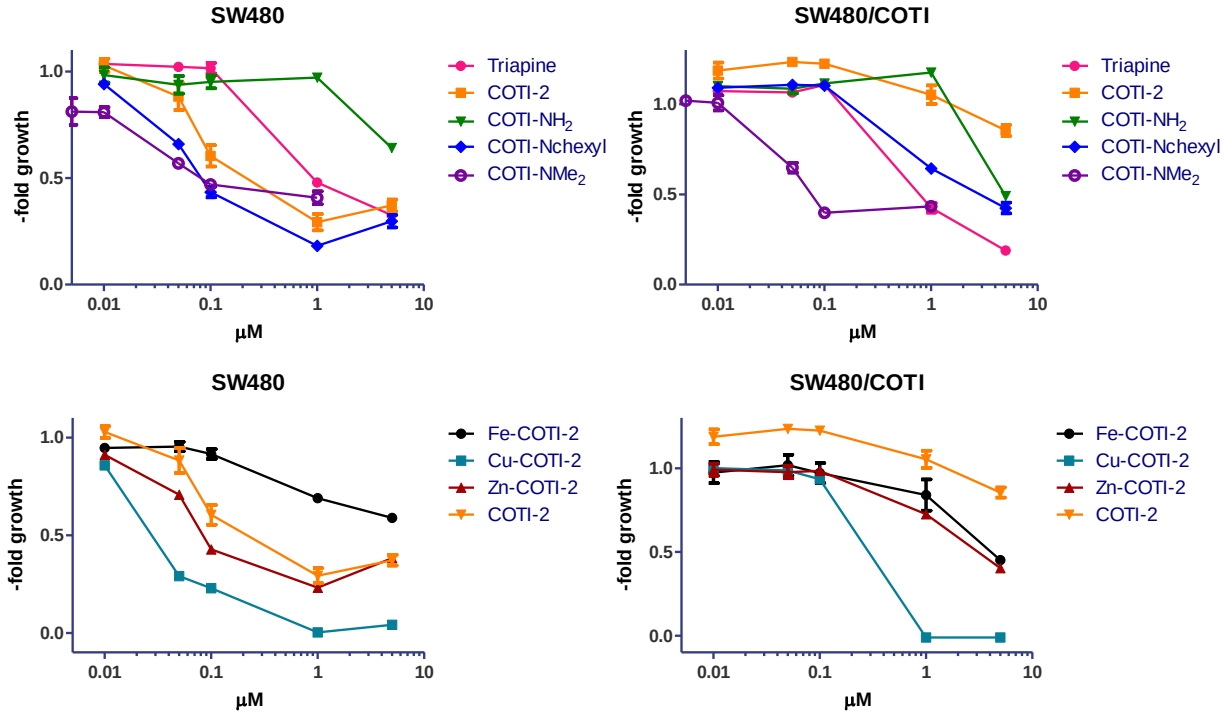

Figure A48. Concentration-response curves for Triapine, COTI-2, COTI-NH_2, COTI-NMe_2, COTI-Nchexyl, Fe-COTI-2, Cu-COTI-2 and Zn-COTI2 over the SW480 line and the chemoresistant line SW480/COTI.

TABLES

PART 1: Metal complexes with uracil derivatives

Table A1. GI_{50} values in μmol L^{-1} of the *in vitro* antiproliferative activity of free 5fu, Ag-5fu, Pd-5fu, Pt-5fu, $K_2[PdCl_4]$, $K_2[PtCl_4]$.

Compounds	MM (g mol^{-1})	Cell lines*									
		2	M	A	7	4	P	O	H	K	Cat
5fu	130.08	6.00	0.47	17.68	1.31	0.65	3.92	0.70	3.23	1.46	0.67
Ag-5fu	580.73	1.95	<0.43	0.62	0.50	0.79	3.93	0.67	0.59	0.43	0.43
Pd-5fu	457.12	7.04	0.24	54.69	1.60	0.96	4.48	2.52	5.62	54.69	0.90
Pt-5fu	602.32	41.51	13.51	41.51	41.51	9.45	41.51	8.28	36.86	41.51	16.60
$AgNO_3$	169.87	19.84	9.77	18.90	20.96	33.85	17.60	16.95	16.90	2.83	15.89
$K_2[PdCl_4]$	326.43	76.59	76.59	76.59	76.59	76.59	76.59	76.59	76.59	76.59	76.59
$K_2[PtCl_4]$	415.09	17.59	11.42	14.43	12.21	13.80	7.44	13.92	13.71	6.02	8.43
Cisplatin	300.05	4.27	7.23	8.30	3.73	0.60	8.70	10.70	17.03	8.07	3.80

*Human tumor cell lines: 2: U251 (glioma); M = MCF-7 (breast); A = NCI/ADR-RES (ovarian multidrug resistant); 7 = 786-0 (renal); 4 = NCI-H460 (lung, non-small cells); P = PC-3 (prostate); O = OVCAR-3 (ovarian); H = HT29 (colon); K = K562 (leukemia); Non-tumor human line: Cat = HaCat (immortal keratinocyte).

Table A2. TGI values in µmol L^{-1} of the *in vitro* antiproliferative activity of $dtuH_2$, $[Ag_2(dtu)]$, $AgNO_3$, tuH_2, Ph_3P-Au-tuH, Ph_3P-Au-Cl, and doxorubicin.

Compounds		Cell lines*								
	MM (g mol^{-1})	2	M	A	7	4	O	H	K	Cat
$dtuH_2$	144.22	980	1733	1733	1733	1733	1733	1733	1733	1733
$[Ag_2(dtu)]$	357.94	698	698	698	698	698	698	698	698	698
$AgNO_3$	169.87	42.39	17.66	198.4	134.2	140.1	35.91	80.06	6.48	226.1
tuH_2	128.15	1951	1951	1951	1951	1951	1951	1951	1951	1951
Ph_3P-Au-tuH	586.4	2.56	8.70	18.76	3.92	45.53	17.74	48.60	0.43	10.40
Ph_3P-Au-Cl	494.7	4.65	9.50	21.22	8.09	505	11.93	505	6.67	29.31
Doxorubicin	543.52	1.49	1.05	46.00	2.02	46.00	3.31	46.00	2.21	1.07

*Human tumor cell lines: 2: U251 (glioma); M = MCF-7 (breast); A = NCI-ADR/RES (multidrug resistant ovarian); 7 = 786-0 (renal); 4 = NCI-H460 (lung, non-small cells); O = OVCAR-3 (ovarian); H = HT29 (colon); K = K562 (leukemia); Non-tumor human line: Cat = HaCat (immortal keratinocyte).

Table A3. Number of counted colonies of NCI/ADR-RES cells after 12 days of growth from 200 cells previously treated with Ag-5fu, 5fu and $AgNO_3$.

Treatment	Triplicate 1	Triplicate 2	Triplicate 3
Control	121	115	113
Ag-5fu 1.5 µg/mL	5	9	9
Ag-5fu 3.0 µg/mL	0	0	0
5fu 0.75 µg/mL	48	60	35
5fu 1.5 µg/mL	1	1	2
$AgNO_3$ 0.75 µg/mL	47	72	62
$AgNO_3$ 1.5 µg/mL	58	32	22

Table A4. Number of counted colonies of NCI/ADR-RES cells after 6 days of growth from 100 cells previously treated with Ph_3P-Au-tuH and Ph_3P-Au-Cl.

Treatment	Triplicate 1	Triplicate 2	Triplicate 3
Control	137	140	140
Ph_3P-Au-tuH 12 µg/mL	47	45	40
Ph_3P-Au-tuH 24 µg/mL	2	1	2
Ph_3P-Au-Cl 10.1 µg/mL	34	20	20
Ph_3P-Au-Cl 20.2 µg/mL	4	4	1

PART 2: Thiosemicarbazones and their metal complexes

Table A5. Experimental parameters for COTI-2 and Cu-COTI-2.

Sample	Machine	Source	Temp.	Detector Distance	Time/ Frame	#Frames	Frame width
	Bruker		[K]	[mm]	[s]		[°]
COTI-2	D8	Mo	100	30	5	5110	0.200
Cu-COTI-2	D8	Mo	100	30	1	3502	0.500

Table A6. Concentration range for MTT assays.

Compound	Conc. SW480 (µM)	Conc. SW480/COTI (µM)	Conc. SW480/tria (µM)
COTI-2	0.01; 0.05; 0.1; 1; 5	0.1; 1; 5; 10; 20	0.01; 0.05; 0.1; 1; 5
COTI-NH_2	0.01; 0.05; 0.1; 1; 5	0.05; 0.1; 1; 5; 10	0.1; 1; 5; 10; 20
COTI-NMe_2	0.005; 0.01; 0.05; 0.1; 1	0.005; 0.01; 0.05; 0.1; 1	0.005; 0.01; 0.05; 0.1; 1
COTI-Nchexyl	0.01; 0.05; 0.1; 1; 5	0.01; 0.05; 0.1; 1; 5	0.01; 0.05; 0.1; 1; 5
Fe-COTI-2	0.1; 1; 5; 10; 20	0.1; 1; 5; 10; 20	0.1; 1; 5; 10; 20
Cu-COTI-2	0.01; 0.05; 0.1; 1; 5	0.01; 0.05; 0.1; 1; 5	0.01; 0.05; 0.1; 1; 5
Zn-COTI-2	0.01; 0.05; 0.1; 1; 5	0.01; 0.05; 0.1; 1; 5	0.01; 0.05; 0.1; 1; 5
Triapine	0.01; 0.05; 0.1; 1; 5	0.01; 0.05; 0.1; 1; 5	0.1; 1; 5; 10; 20